

Archive ouverte UNIGE

https://archive-ouverte.unige.ch

Thèse 2016

Open Access

This version of the publication is provided by the author(s) and made available in accordance with the copyright holder(s).

Anti-angiogenic strategies for chemoembolization of liver tumors

Fuchs, Katrin

How to cite

FUCHS, Katrin. Anti-angiogenic strategies for chemoembolization of liver tumors. Doctoral Thesis, 2016. doi: 10.13097/archive-ouverte/unige:90809

This publication URL: https://archive-ouverte.unige.ch/unige:90809

Publication DOI: <u>10.13097/archive-ouverte/unige:90809</u>

© This document is protected by copyright. Please refer to copyright holder(s) for terms of use.

UNIVERSITÉ DE GENÈVE

FACULTÉ DES SCIENCES

Section des Sciences Pharmaceutiques

Professeur Gerrit Borchard

Laboratoire de Biopharmacie

Docteur Olivier Jordan

Anti-Angiogenic Strategies for Chemoembolization of Liver Tumors

THÈSE

présentée à la Faculté des sciences de l'Université de Genève pour obtenir le grade de Docteur ès sciences, mention sciences pharmaceutiques

par

Katrin Beatrice Fuchs

de

Neumarkt i. d. OPf. (Allemagne)

Thèse N°: 5010

Genève

Atelier de reproduction Repromail 2016



Doctorat ès sciences Mention sciences pharmaceutiques

Thèse de Madame Katrin FUCHS

intitulée:

"Anti-Angiogenic Strategies for Chemoembolization of Liver Tumors"

La Faculté des sciences, sur le préavis de Monsieur G. BORCHARD, professeur ordinaire et directeur de thèse (Section des sciences pharmaceutiques), Monsieur O. JORDAN, docteur et codirecteur de thèse (Section des sciences pharmaceutiques), Monsieur E. ALLÉMANN, professeur ordinaire (Section des sciences pharmaceutiques), Madame P. NOWAK-SLIWINSKA, professeure assistante (Section des sciences pharmaceutiques), Monsieur A. LEWIS, professeur (Biocompatibles UK Ltd, Camberley, Surrey, United Kingdom) et Monsieur H. TIEMESSEN, docteur (Novartis Pharma AG, Basel, Switzerland), autorise l'impression de la présente thèse, sans exprimer d'opinion sur les propositions qui y sont énoncées.

Genève, le 31 octobre 2016

Thèse - 5010 -

Le Doyen

Cette thèse a donné lieu aux publications aux pages 143-147.

Preface i

To my parents, Gerti and Hans

To my brother, Andreas

ii Preface

"Peut-être peut-on affirmer avec philosophie que, pour vivre pleinement, l'humanité aura certainement toujours besoin de... l'incertitude."

Auteur inconnu. Citation dans le hall du CMU Genève.

Table of Contents

| Table of Contents | iii |
|---|-----------------------------------|
| List of Abbreviations | vii |
| Foreword | 1 |
| Chapter One | 9 |
| Drug-Eluting Embolic Microspheres for Local Drug Delivery – Sta | ate of the Art9 |
| 1 Drug Delivery in Transarterial Chemoembolization (TACE) | 10 |
| 2 State of the Art of Drug-Eluting Microspheres | 11 |
| 2.1 Non-Biodegradable Beads for Drug Delivery and In Vitr | o Drug Release11 |
| 2.2 Biodegradable Beads for Drug Delivery and In Vitro Drug | ıg Release15 |
| 3 Drug Pharmacokinetics after DEB-TACE | 21 |
| 3.1 Pharmacokinetic Profiles in the Target Tissue | 21 |
| 3.2 Drug Tissue Distribution | 22 |
| 4 Conclusions on Controlled Drug Release from Drug-Elutin | g Beads and Qualitative In Vitro- |
| In Vivo Comparison | 26 |
| 5 References | 28 |
| Chapter Two | 41 |
| Drug-Eluting Beads Loaded with Anti-Angiogenic Agents for Che | emoembolization: In Vitro |
| Sunitinib Loading, Release and In Vivo Pharmacokinetics in an A | Animal Model41 |
| 1 Introduction | 42 |
| 2 Materials and Methods | 43 |
| 2.1 Materials | 43 |
| 2.2 Methods | 43 |
| 3 Results | 47 |
| 3.1 Loading of Sunitinib into Beads | 47 |
| 3.2 Bead Size Changes with Sunitinib Loading | 47 |
| 3.3 Release of Sunitinib from Loaded Beads | 49 |
| 3.4 Biological Efficacy in Cell Culture | 49 |

| | 3.5 Preclinical <i>In Vivo</i> Studies with Healthy New Zealand White Rabbits | 52 |
|-----------------|--|------|
| 4 | Discussion | 54 |
| 5 | Acknowledgment | 57 |
| 6 | References | 58 |
| 7 | Supplementary Material | 62 |
| | 7.1 Appendix A: DEBs Characterization | 65 |
| | 7.2 Appendix B: Preparation of Sunitinib-Loaded Beads and Oral Solution | 66 |
| Chapt | er Three | 67 |
| Sun | itinib-Eluting Beads for Chemoembolization: Methods for <i>In Vitro</i> Evaluation of Drug | |
| Rele | ease | 67 |
| 1 | Introduction | 69 |
| 2 | Materials and Methods | 70 |
| | 2.1 Loading of Sunitinib into DC Beads | 70 |
| | 2.2 Release Testing | 71 |
| | 2.3 In Vitro-In Vivo Correlation | 73 |
| 3 | Results and Discussion | 74 |
| | 3.1 Drug Release in an Orbital Shaker | 74 |
| | 3.2 Drug Release in Flow-Through Implant Cells | 75 |
| | 3.3 Drug Release in Dialysis Cylinder Inserts | 77 |
| | 3.4 Comparison of Release Profiles in Different Set-ups | 78 |
| | 3.5 Drug Release Fitting with Release Models | 78 |
| | 3.6 In Vitro-In Vivo Correlation (IVIVC) | 80 |
| 4 | Conclusions | 84 |
| 5 | Acknowledgements | 84 |
| 6 | References | 85 |
| Chapt | er Four | 91 |
| Ma _l | pping of Drug Distribution in the Rabbit VX2 Liver Tumor Model after Chemoembolizati | on |
| witl | n Sunitinib-Eluting Beads by Complementary Fluorescence and Mass Spectrometry Image | ging |
| •••• | | 91 |
| 1 | Introduction | 93 |
| 2 | Materials and Methods | 94 |
| | 2.1 Animal Model | 94 |

| | 2 | 2.2 | Sunitinib Biodistribution by Fluorescence Imaging | 94 |
|------------------|------|------|---|------|
| | 2 | 2.3 | Sunitinib Biodistribution by Mass Spectrometry Imaging | 96 |
| | 3 | R | esults | 97 |
| | 3 | 3.1 | Sunitinib Biodistribution in Tumor and Contralateral Liver Tissue by Fluorescence | |
| | I | lma | ging | 97 |
| | 3 | 3.2 | Biodistribution of Sunitinib and Its Metabolites in Liver and Tumor Tissue by Mass | |
| | 9 | Spe | ctrometry Imaging | .100 |
| | 4 | D | iscussion | .104 |
| | 5 | Α | cknowledgements | .106 |
| | 6 | R | eferences | .107 |
| | 7 | Sı | upplementary Material | .111 |
| | 7 | 7.1 | Tissue Sampling | .116 |
| | 7 | 7.2 | Tissue Cryosectioning | .116 |
| | 7 | 7.3 | Correlation of Sunitinib Fluorescence in Tissue and in DC Bead $^{\circ}$ with Its Distribution | .116 |
| | 7 | 7.4 | MALDI-SRM Mass Spectrometry Imaging Technique | .117 |
| Cha _l | oter | Fiv | e | .119 |
| D | evel | lopr | ment of Sunitinib-Loaded Biodegradable Hydrogel Microspheres for Transarterial | |
| Cł | nem | oer | nbolization | .119 |
| | 1 | In | troduction | .121 |
| | 2 | M | laterials and Methods | .122 |
| | 2 | 2.1 | Microsphere Synthesis and Characterization | .122 |
| | 2 | 2.2 | Loading and Release of Microspheres with Sunitinib | .124 |
| | 2 | 2.3 | Microsphere Biodegradation Studies | .124 |
| | 3 | R | esults | .127 |
| | 3 | 3.1 | Microsphere Synthesis and Characterization | .127 |
| | 3 | 3.2 | Loading and Release of Microspheres with Sunitinib | .128 |
| | 3 | 3.3 | Microsphere Biodegradation Studies | .129 |
| | 4 | D | iscussion | .132 |
| | 4 | 4.1 | Microsphere Synthesis and Characterization | .132 |
| | 4 | 4.2 | Loading and Release of Microspheres with Sunitinib | .133 |
| | 4 | 4.3 | Microsphere Biodegradation Studies | .133 |
| | 5 | C | onclusions | .135 |

| 6 | Δ | scknowledgements | 135 |
|---------|-------|--|-----|
| 7 | R | leferences | 136 |
| Summ | ary a | and Conclusions | 143 |
| Résun | né et | Conclusions | 147 |
| List of | Dist | inctions and Publications | 151 |
| Ackno | wled | lgements | 157 |
| Annex | · | | 159 |
| Ant | itum | oral Effect of Sunitinib-Eluting Beads in the Rabbit VX2 Tumor Model | 159 |
| 1 | li | ntroduction | 161 |
| 2 | N | Naterials and Methods | 162 |
| | 2.1 | Animal Model and Tumor Implantation | 162 |
| | 2.2 | First Experiment: Proof of Concept | 163 |
| | 2.3 | Second Experiment: Comparative Study | 163 |
| | 2.4 | Sunitinib-eluting Beads and Oral Sunitinib Preparation | 164 |
| | 2.5 | Interventional Technique | 164 |
| | 2.6 | Monitoring Tumor Volume | 165 |
| | 2.7 | Animal Sacrifice and Tissue Sample Harvesting | 165 |
| | 2.8 | Measurement of Sunitinib Concentrations in Plasma and Liver Tissue | 165 |
| | 2.9 | Immunoprecipitation and Western Blot Analysis | 166 |
| | 2.10 | O Histopathologic Evaluation | 166 |
| | 2.1 | 1 Statistical Analysis | 166 |
| 3 | R | lesults | 167 |
| | 3.1 | First Experiment: Proof of Concept | 167 |
| | 3.2 | Second Experiment: Comparative Study | 170 |
| 4 | | Discussion | 175 |
| 5 | Δ | acknowledgments | 177 |
| 6 | R | eferences | 178 |

Preface vii

List of Abbreviations

ACMs: acetylated chitosan microspheres

ALP: alkaline phosphatase

ALT: alanine aminotransferase

APTA: (3-acrylamidopropyl)trimethylammonium chloride

APS: ammonium persulfate

ASR: age-standardized rate

AST: aspartate aminotransferase

AUC: area under the curve

BAE: bronchial artery embolization

BCLC: Barcelona Clinic Liver Cancer (algorithm)

CMs: chitosan microspheres

CT: computed tomography

cTACE: conventional transarterial chemoembolization

DC Bead: drug-capable bead (Biocompatibles, BTG Ltd., UK)

DEB(s): drug-eluting beads

DEB-TACE: drug-eluting beads transarterial chemoembolization

DMA: N,N-dimethylacetamide

DMEM: Dulbecco's modified Eagle medium

DPBS: Dulbecco's phosphate buffered saline

DOX: Doxorubicin

viii Preface

DSM: degradable starch microspheres

EtOH: ethanol

ECOG: Eastern Cooperative Oncology Group

FDA: Food and Drug Administration

FITC: Fluorescein isothiocyanate

HCI: hydrochloric acid

HCC: hepatocellular carcinoma

HCV: hepatitis C virus

HEMA: hydroxyethyl methacrylate

HIF-1 α : hypoxia-inducible factor-1 α

HUVEC(s): human umbilical vein endothelial cell(s)

IC₅₀: half maximal inhibitory concentration

IQR: interquartile range

IRI: Irinotecan

ITSC: intratumoral sunitinib concentration

IVIVC: in vitro-in vivo correlation

LC-MS/MS: liquid chromatography with tandem mass spectrometry detection

LLOQ: lower limit of quantification

LOD: limit of detection

MA: methacrylate

MALDI-SRM/MSI: matrix-assisted laser desorption ionization with selected reaction monitoring mass spectrometry imaging

Preface ix

MDCK cells: Martin-Darby Canine Kidney cells

MRI: magnetic resonance imaging

MS: microspheres

MSI: mass spectrometry imaging

MW: molecular weight

n. a.: not available

NaCl: sodium chloride

NaN₃: sodium azide

PAE: pulmonary artery embolization

PBS: phosphate buffered saline

PEG: poly(ethylene glycol)

PEG DA: poly(ethylene glycol) diacrylate

PEGMA: poly(ethylene glycol) methacrylate

PLA: poly(D,L-lactic acid)

PLE: porcine liver esterase

PLGA: poly(lactide-co-glycolide) or poly(lactic-co-glycolic acid)

PSC: plasmatic sunitinib concentration

pVEGFR2: phosphorylated vascular endothelial growth factor receptor 2

ROI: region of interest

SDS: sodium dodecyl sulfate

SEB(s): sunitinib-eluting bead(s)

SEC: size exclusion chromatography

x Preface

SEM: scanning electron microscopy

SN38: primary irinotecan metabolite

SPMA: 3-sulfopropyl methacrylate potassium salt

TACE: transarterial chemoembolization

TAE: transarterial embolization

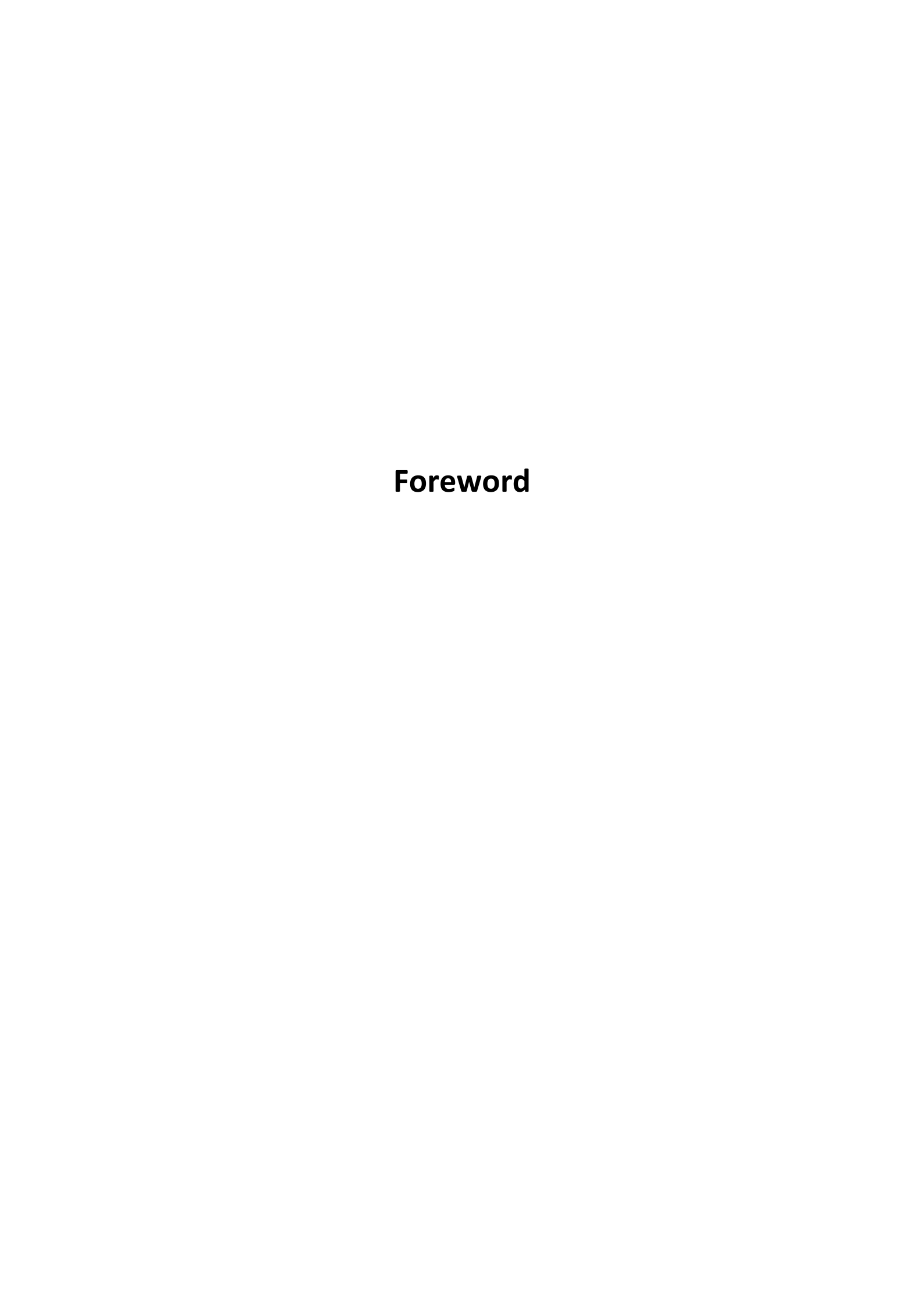
TEMED: N,N,N',N'-tetramethylethylenediamine

US: ultrasonography

USP: US Pharmacopeia

VEGF: vascular endothelial growth factor

VEGFR2: vascular endothelial growth factor receptor 2



Recently, the American Cancer Society predicted an estimate of 39,230 new liver cancer cases and 27,170 deaths in 2016. In contrast to the decline in overall cancer incidence in the United States, liver cancer incidence rate did not follow this trend between 2003 and 2012 [1, 2]. At the same time, mortality rates increased significantly for both men and women since 1992. Among men, liver cancer was the fifth most common cancer in 2012, with Asians, Pacific Islanders, American Indians, Alaska Natives, and Hispanics at higher risk compared to the rest of the US population. [1]

Figure 1 shows that worldwide incidences in 2012 were pronounced in (South-)Eastern Asia and (North-)Western Africa.

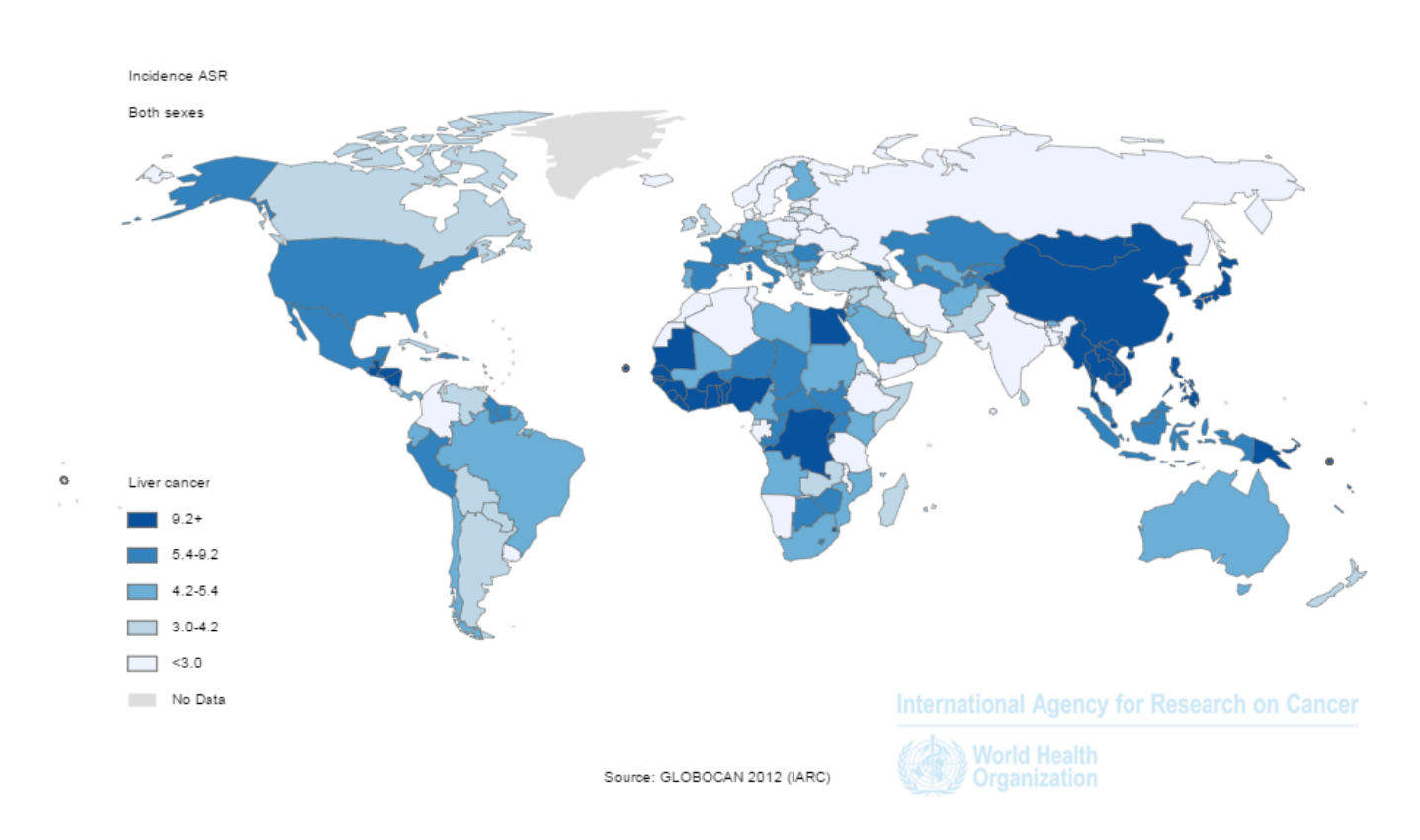


Figure 1. Incidence of Liver Cancer by age-standardized rate (ASR*) in 2012 was higher in less developed than in developed regions [3].

About 80% of the liver cancer cases are derived from hepatocytes, progressing into hepatocellular carcinoma (HCC) [4]. The primary etiological factor worldwide is hepatitis B virus infection,

^{*}An age-standardized rate (ASR) is a summary measure of the rate that a population would have if it had a standard age structure. Standardization is necessary when comparing several populations that differ with respect to age because age has a powerful influence on the risk of cancer. [3]

particularly in high-incidence areas [5]. Hepatitis C virus-associated cirrhosis is the most common etiological factor in Europe and the United States, accounting for approximately 60% of HCC cases [5]. Other risk factors are nonalcoholic steatohepatitis cirrhosis, and environmental factors such as exposure to aflatoxin A and chronic alcohol consumption [4, 5].

Remarkable advances were accomplished in the past decade in prevention, detection, and treatment of hepatocellular carcinoma [6]. This was reflected in the 5-year survival rates, which improved in the US from 4.7% between 1983 and 1992 to 18.9% between 2003 and 2012 [7]. Besides molecular pathogenesis, surveillance and diagnosis, the disease is managed by prognosis assessment [6]. The classification of all stages of disease with the Barcelona Clinic Liver Cancer (BCLC) algorithm allowed for patient stratification according to outcome and treatment planning [6]. The system takes into account tumor size, extrahepatic spread and vascular invasion, together with liver function (Child-Pugh score from A = well-preserved to C = impaired), and the patients' general health status [8]. Curative treatments like ablation, resection, and transplantation are reserved to very early (BCLC 0) and early (BCLC A) stage, whereas transarterial chemoembolization (TACE), which is indicated for intermediate stage (BCLC B), and peroral sorafenib for advanced HCC (BCLC C) are palliative options. Terminal stage (BCLC D) patients are treated with best supportive care. [8]

TACE in particular is the only treatment strategy that has shown survival benefit for intermediate stage-patients in some studies, i.e. for patients with multinodular tumors with preserved liver function [8]. TACE is a minimally invasive intervention, aiming to restrict the highly vascularized tumor's blood supply. Access is gained by means of a catheter in the patient's femoral artery, which is advanced to the hepatic artery under radiologic guidance (Figure 2). Ultimately, the selectively injected microspheres block the arterial blood flow toward the hepatic lesion and lead to ischemic tumor necrosis. The clinical rationale behind intra-arterial catheter-based therapies is the dual vascular supply of the liver. Whereas hepatic malignancies are vascularized by the hepatic artery, the portal vein is predominantly responsible for the liver parenchyma's blood supply. Thus, the liver function is maintained by blood flow from the hepatic portal vein during arterial embolization. [9]

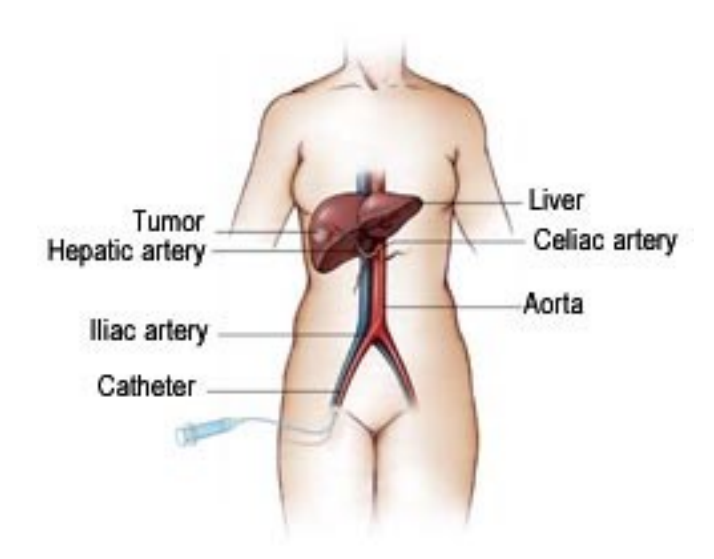


Figure 2. For the transarterial chemoembolization intervention, a catheter is positioned into the femoral artery and guided to the proper hepatic artery in order to inject microspheres locally into the tumor. Image adapted from http://www.cpmc.org.

Transcatheter arterial embolization (TAE) is the embolization of the tumor with unloaded bland microspheres (also called beads). Chemoembolization, i.e. combination of embolization with a chemotherapeutic drug, was introduced around 35 years ago. Conventional TACE (cTACE) describes the injection of an emulsified cytotoxic drug in Lipiodol, an ethiodized oil and embolizing and contrast agent, followed by embolizing particles. When significant delays in tumor progression, vascular invasion, in addition to survival benefits for patients were first demonstrated in two Randomized Controlled Trials, cTACE was included in the official guidelines for HCC treatment. In order to reduce systemic toxicity due to drug washout from the target lesion and in order to achieve controlled drug release into the tumor, the chemotherapeutic drug, typically doxorubicin, was combined with the microspheres to form the so-called drug-eluting beads (DEB). [9, 10]

Many clinical studies have since then been conducted to compare conventional TACE (cTACE) with drug-eluting beads transarterial chemoembolization (DEB-TACE), most of which concluded less severe toxicity for DEB-TACE and equivalence of the two methods in terms of patient survival [11-18].

In this context, we explored options to possibly take beads, as drug delivery devices for the treatment of HCC, a step further.

The first chapter of this thesis reviews the 2016 state of the art in the field of designing and developing embolic drug-eluting beads. Initially, we briefly refer to recent literature giving an overview on drug-eluting beads, which have been established in clinical practice since several years. Then, we move on to display the latest advances with a focus on the beads as drug delivery systems. Drug loading and release of clinically established and novel drugs for HCC treatment, eluted from established or novel bead formulations, are discussed. We tackle the question of the need for biodegradable beads, and how their loading, release mechanisms and kinetics differ from commercialized drug-eluting beads – which are so far all non-biodegradable. We specifically ask the question "Is controlled or sustained release required to achieve long-term tumor exposure to the drug?", and then we try to propose an answer by summarizing local *in vivo* tissue pharmacokinetics and drug tumor distribution.

In the frame of this thesis, we propose a novel combination of DC Bead®, the most used drugeluting beads in DEB-TACE interventions, with the anti-angiogenic drug sunitinib, since angiogenesis after embolization is a major reason for tumor recurrence. Sunitinib (SUTENT®, Pfizer Canada Inc., Quebec, Canada) is a multitargeted tyrosine kinase inhibitor, which is approved by the Food and Drug Administration (FDA) for gastrointestinal stromal tumors after disease progression on or intolerance to imatinib, advanced pancreatic neuroendocrine tumors and advanced renal cell carcinoma [19]. Besides its main target, vascular growth factor receptor 2 (VEGFR2), sunitinib also inhibits VEGFR1, VEGFR3, platelet-derived growth factor receptors (PDGFRα, PDGFRβ), mast/stemcell growth factor receptor (KIT), fms-related tyrosine kinase 3 (FLT3), glial cell-line derived neurotrophic factor receptor (RET), and macrophage colony-stimulating factor 1 receptor (CSF-1R) [19, 20].

We made use of the drug's physicochemical properties (Chapter 1, Table 4) to load the fully protonated sunitinib in an acidic solution on anionic embolic beads. Thus, the second chapter of this thesis describes for the first time the combination of the anti-angiogenic receptor tyrosine kinase inhibitor sunitinib with embolic beads. We demonstrated the *in vitro* loading and release kinetics of sunitinib using two different sizes of DC Bead microspheres, and evaluated the *in vitro* biological efficacy on cell cultures and the resulting *in vivo* pharmacokinetic profiles in an animal model.

Since high drug concentrations were achieved with sunitinib-eluting beads in healthy rabbits, our group was encouraged to demonstrate antitumor efficacy of sunitinib-eluting beads. This study is displayed in the annex of this thesis. Sunitinib-eluting beads of two different small bead sizes were injected transarterially in tumors of rabbits. Plasmatic and intratumoral sunitinib concentrations, tumor growth, inhibition of VEGFR2 activation, and histopathologic modifications were monitored for 14 days after DEB-TACE.

In the third chapter, we took a closer look at the *in vitro* release of sunitinib from DC Bead and correlation of the kinetics with the *in vivo* data. We had become aware of the influence of *in vitro* release parameters and were eager to check their potential to predict *in vivo* pharmacokinetics. We investigated three different release set-ups which differed from each other mainly in terms of chamber geometry and flow velocity, and we also checked the influence of the medium on *in vitro* release kinetics. The results were then compared to drug plasma and tissue concentrations measured in rabbits from the earlier study described in Chapter 2. An effort was made to compute *in vivo* pharmacokinetic profiles based on *in vitro* data, with an attempt to standardize the appropriate parameters for the *in vitro* assay in order to possibly reduce animal experimentation in the future.

The fourth chapter is an in-depth follow-up of the preclinical study investigating antitumor efficacy of sunitinib-eluting beads. In order to be bioavailable, the drug has to be effectively distributed into the target tissue. We aimed to show the local drug delivery into the tumor compared to normal liver after embolization over time, and more specifically the spatial distribution of sunitinib after release from the beads. For this, we took advantage of the fluorescent properties of sunitinib to image its whereabouts in histologic tissue sections by fluorescence microscopy. In order to confirm drug levels and diffusion distances, we developed an additional method to localize sunitinib and its metabolites by mass spectrometry imaging.

Finally, the fifth chapter switches from non-biodegradable embolic microspheres to in house-synthesized biodegradable microspheres for sunitinib delivery via transarterial embolization. The rationale behind transient embolization is the possible repetition of the injection of embolic microspheres into the same arteries supplying the tumor, and lower degrees of tissue inflammation caused by the continuous presence of foreign material in the tissue. The home-made microspheres were examined for their cell toxicity, compressibility, their ability to degrade under normal and

accelerated stress conditions and most importantly, their capacity to deliver sunitinib. We rounded up the discussion with a short comparison of these microspheres with marketed microspheres in terms of sunitinib release, to underline the suitability of our microspheres as drug delivery system for transcatheter embolization.

References

- [1] Siegel RL, Miller KD, Jemal A. Cancer statistics, 2016. CA: a cancer journal for clinicians 2016;66:7-30.
- [2] Altekruse SF, Henley SJ, Cucinelli JE, McGlynn KA. Changing hepatocellular carcinoma incidence and liver cancer mortality rates in the United States. The American journal of gastroenterology 2014;109:542-53.
- [3] GLOBOCAN. Estimated Cancer Incidence, Mortality and Prevalence Worldwide in 2012. 2012.
- [4] Theise ND. Liver Cancer. In: Stewart BW, Wild, C. P., editor. World Cancer Report 2014. Lyon: IARC Nonserial Publication; 2015.
- [5] Knudsen ES, Gopal P, Singal AG. The Changing Landscape of Hepatocellular Carcinoma: Etiology, Genetics, and Therapy. The American journal of pathology 2014;184:574-83.
- [6] Forner A, Llovet JM, Bruix J. Hepatocellular carcinoma. Lancet 2012;379:1245-55.
- [7] Wang S, Sun H, Xie Z, Li J, Hong G, Li D, et al. Improved survival of patients with hepatocellular carcinoma and disparities by age, race, and socioeconomic status by decade, 1983-2012. Oncotarget 2016.
- [8] Forner A, Gilabert M, Bruix J, Raoul JL. Treatment of intermediate-stage hepatocellular carcinoma. Nature reviews Clinical oncology 2014;11:525-35.
- [9] Duran R, Chapiro J, Schernthaner RE, Geschwind JFH. Systematic review of catheter-based intraarterial therapies in hepatocellular carcinoma: state of the art and future directions. The British journal of radiology 2015;88:20140564.
- [10] Meza-Junco J, Montano-Loza AJ, Liu DM, Sawyer MB, Bain VG, Ma M, et al. Locoregional radiological treatment for hepatocellular carcinoma; Which, when and how? Cancer treatment reviews 2012;38:54-62.
- [11] Gao S, Yang Z, Zheng Z, Yao J, Deng M, Xie H, et al. Doxorubicin-eluting bead versus conventional TACE for unresectable hepatocellular carcinoma: a meta-analysis. Hepatogastroenterology 2013;60:813-20.

[12] Ni JY, Xu LF, Wang WD, Sun HL, Chen YT. Conventional transarterial chemoembolization vs microsphere embolization in hepatocellular carcinoma: a meta-analysis. World journal of gastroenterology: WJG 2014;20:17206-17.

- [13] Golfieri R, Giampalma E, Renzulli M, Cioni R, Bargellini I, Bartolozzi C, et al. Randomised controlled trial of doxorubicin-eluting beads vs conventional chemoembolisation for hepatocellular carcinoma. British journal of cancer 2014;111:255-64.
- [14] Han S, Zhang X, Zou L, Lu C, Zhang J, Li J, et al. Does drug-eluting bead transcatheter arterial chemoembolization improve the management of patients with hepatocellular carcinoma? A meta-analysis. PloS one 2014;9:e102686.
- [15] Zhou X, Tang Z, Wang J, Lin P, Chen Z, Lv L, et al. Doxorubicin-eluting beads versus conventional transarterialchemoembolization for the treatment of hepatocellular carcinoma: a meta-analysis. International journal of clinical and experimental medicine 2014;7:3892-903.
- [16] Arabi M, BenMousa A, Bzeizi K, Garad F, Ahmed I, Al-Otaibi M. Doxorubicin-loaded Drugeluting beads Versus Conventional Transarterial Chemoembolization for Nonresectable Hepatocellular Carcinoma. Saudi journal of gastroenterology: official journal of the Saudi Gastroenterology Association 2015;21:175-80.
- [17] Kloeckner R, Weinmann A, Prinz F, Pinto dos Santos D, Ruckes C, Dueber C, et al. Conventional transarterial chemoembolization versus drug-eluting bead transarterial chemoembolization for the treatment of hepatocellular carcinoma. BMC cancer 2015;15:465.
- [18] Xie ZB, Wang XB, Peng YC, Zhu SL, Ma L, Xiang BD, et al. Systematic review comparing the safety and efficacy of conventional and drug-eluting bead transarterial chemoembolization for inoperable hepatocellular carcinoma. Hepatology research: the official journal of the Japan Society of Hepatology 2015;45:190-200.
- [19] Pr SUTENT® Sunitinib capsules. Pfizer Canada Inc.; 2014.
- [20] Faivre S, Demetri G, Sargent W, Raymond E. Molecular basis for sunitinib efficacy and future clinical development. Nature reviews Drug discovery 2007;6:734-45.

Drug-Eluting Embolic Microspheres for Local Drug Delivery – State of the Art

Katrin Fuchs^a, Pierre E. Bize^b, Alban Denys^b, Rafael Duran^b, Gerrit Borchard^a, Olivier Jordan^a

Review Article

To be submitted to:

Journal of Controlled Release

^a School of Pharmaceutical Sciences, University of Geneva, University of Lausanne, Centre Médical Universitaire (CMU), Rue Michel-Servet 1, 1211 Geneva 4, Switzerland

^b Departments of Radiology and Interventional Radiology, Centre Hospitalier Universitaire Vaudois (CHUV), Rue du Bugnon 46, 1011 Lausanne, Switzerland

Abstract

Embolic microspheres or beads are an established treatment method for hepatocellular carcinoma patients. The occlusion of the tumor-feeding vessels by intra-arterial injection of the beads results in tumor necrosis and shrinkage. In this short review, we describe the utility to use these beads as devices for local drug delivery. We review the latest advances in the development of non-biodegradable and biodegradable drug-eluting beads for transarterial chemoembolization. Their capability to load different drugs, such as chemotherapeutics and anti-angiogenic compounds with different physicochemical properties, like charge and hydrophilicity/hydrophobicity, are discussed. We specifically address controlled and sustained drug release from the microspheres, and the resulting *in vivo* pharmacokinetics in the plasma vs drug distribution in the target tissue.

Keywords:

Drug-eluting beads, microspheres, transarterial chemoembolization, hepatocellular carcinoma, biodegradable, degradable, antiangiogenic, controlled release, local delivery, pharmacokinetics

1 Drug Delivery in Transarterial Chemoembolization (TACE)

Liver cancer accounts for 6% of the global cancer incidence. A fatality of 95% resulted in an estimate of 746 000 deaths worldwide in 2012. The most common primary malignancy of the liver is hepatocellular carcinoma (HCC), followed by biliary duct derived cholangiocarcinoma [1].

For patients with multinodular tumors with preserved liver function (intermediate stage), transarterial chemoembolization (TACE) is standard of care [2-4]. During the TACE procedure, which is guided by radiologic imaging, the tumor-feeding arteries are selectively occluded by embolic beads. Conventional TACE (cTACE) is carried out by infusion of a mixture of chemotherapeutic agent with or without iodized oil, followed by unloaded beads. TACE with drug-eluting beads (DEB-TACE), where the beads function as drug-loaded carriers, is considered a more standardized methodology in terms of delivered drug dose when compared to cTACE [3, 5-7]. DEB-TACE was recently suggested to be favorable for the treatment of more advanced disease (Child-Pugh B, ECOG performance status 1, bilobar or recurrent disease) [8-12], with most studies concluding increased tumor response and/or improved safety profile [3, 6-8, 12-17]. Site-specific drug delivery from the beads to the targeted tumor tissue leads to a controlled pharmacokinetic profile [5, 8, 18, 19]. Al-Abd et al. [20] recently summarized the unique advantages of embolization to increase local drug levels and concomitantly decrease systemic toxicity by entrapping the drug in the tumorfeeding vessels. As such, local delivery is achieved by the synergistic combination of local administration and the prevented wash-out of the drug due to interrupted arterial blood flow [21]. Importantly, delivery of the drug in the tumor proximity was reported to effectively result in drug concentration in the targeted tumor tissues [22].

In case embolization is not indicated for treatment, the specific biological and physicochemical HCC environment can be reached with intra-arterially administered targeted nanocarriers. In an excellent recent review, Zhang et al. [23] described the possible targets and gave an overview over currently developed drug delivery systems to tackle advanced-stage HCC lesions.

This review aims to display the latest advances in the design of embolic drug-eluting beads for DEB-TACE of HCC. With this, it also touches at the need for temporary embolizing agents, which show

less serious post-embolization side effects [24] and therefore, are currently in the research focus [25-35]. Drug loading and release of relevant drugs for HCC treatment from established and novel bead formulations are discussed. Besides chemotherapeutics, anti-angiogenic and immunotherapeutic drugs are beneficial in HCC treatment [11, 20, 36-38], which are not necessarily easy candidates for drug loading on beads by ion-exchange such as doxorubicin [39] or irinotecan [40].

Moreover, different drugs show different release profiles, due to different mechanisms of drug loading or due to different affinities to the bead surface [41]. This translates into unique pharmacokinetic profiles *in vivo*, and little is known about the local drug distribution in the target tissue. We discuss here whether there is an "ideal drug release profile", and whether sustained drug release is required to achieve long-term exposure of the tumor to the drug.

2 State of the Art of Drug-Eluting Microspheres

Embolic beads have been used since the 1970s [11] and were compared in experimental [39, 42, 43], pre-clinical [44-47] and clinical settings [48]. Massmann et al. [49] provided a complete tabular overview of clinically established and more recent FDA-approved embolic agents. Among others, Giunchedi et al. [50] and Wáng et al. [11] summarized in recent reviews the features of clinically established and also of some novel embolic agents. In this section, we focus on advances in drug-eluting bead development, i.e. beads still under preclinical evaluation and which were specifically designed to deliver anti-cancer drugs to tumors. Advances in non-biodegradable and biodegradable embolic beads are summarized in Table 1 and Table 2, respectively.

2.1 Non-Biodegradable Beads for Drug Delivery and *In Vitro*Drug Release

Clinically used DC Bead (BTG, London, UK), HepaSphere (Merit Medical, South Jordan, UT, USA), Embozene TANDEM (CeloNova BioSciences, San Antonio, TX, USA), and LifePearl (Terumo, Tokyo, Japan) are non-biodegradable beads, which are capable of drug loading via an ion-exchange mechanism [39]. This elegant method does not interfere with drug activity, ensures drug release in

contact with physiological fluids [51, 52], and is therefore also mainly employed for bead-drug combinations in development.

Lewis et al. and other groups have recently developed a series of non-biodegradable beads with "special features" for drug delivery (Table 1). Beads for the loading of anionic drugs [53], and X-ray image-able beads with doxorubicin loading capacity [54, 55] were presented. DC Bead were also loaded with two drugs at the same time, e.g., doxorubicin was loaded via ion-exchange and rapamycin via drug precipitation into the bead [56], or DC Bead were combined with different antiangiogenic drugs [57-59].

2.1.1 Non-Biodegradable Beads for Anionic Drug Loading

Until today, post-synthesis drug loading on marketed negatively charged beads was limited to cationic drugs. Heaysman et al. [53] have recently prepared beads containing cationic quaternary (3-acrylamidopropyl)trimethylammonium chloride (APTA), which were efficiently loaded with anionic model dyes. Release time *in vitro* was shown to correlate inversely with the number of charged moieties per dye, i.e. multivalence imparted higher affinity between the dye and the bead polymer matrix. These beads display a platform for combination with negatively charged small molecules, which are most likely to penetrate into the bead hydrogel pores. In addition, bigger biologic entities up to 70-250 kDa (pore size of one type of APTA beads) bearing a global negative charge might be loaded, such as miRNA mimetics or antagonists [60, 61], siRNA [23, 62], or antibody (fragments) [23]. This bead invention might make the delivery of relevant drugs possible, which could not be loaded on anionic drug-eluting beads (DEB) before.

2.1.2 Image-able Non-Biodegradable Beads for Doxorubicin Delivery

The purpose to visualize beads by computed tomography (CT) or magnetic resonance imaging (MRI) in real time during DEB-TACE is to judge the endpoint of tumor embolization and consequently, success of the intervention. Both image-able and doxorubicin-loaded beads have been developed: Lipiodol-loaded DC Bead [54, 63] and DC Bead modified by iodinated moieties (iBeads) [55]. Both radiopaque bead types were similar to classic DC Bead in their doxorubicin loading capacity, but iBeads eluted slightly more drug [55], while Lipidiol-loaded beads release rate was slower [63]. A

study correlating bead attenuation, and with that bead distribution in the tissue, with doxorubicin delivery is currently undertaken [64]. This will enable correlating drug delivery to beads per tissue volume. Similarly, doxorubicin or sunitinib fluorescence also allows for evaluation of the drug diffusion in the tissue, which will be discussed in Section 3.2.

2.1.3 Combination of DC Bead with Anti-Angiogenic Drugs

Embolization of tumors creates ischemia, which results in tumor necrosis. However, at the same time ischemia equally increases hypoxia-inducible factor (HIF- 1α) and vascular endothelial growth factor (VEGF) levels, which leads to neoangiogenesis and eventually tumor recurrence [65-69]. To counteract the formation of new blood vessels, the combination of TACE with anti-angiogenic agents seems rational [49, 70, 71]. For local delivery of anti-angiogenic drugs, DC Bead were loaded with the multitargeted tyrosine kinase inhibitors sunitinib [57] and vandetanib [59], and an anti-VEGF antibody, bevacizumab [58]. Sunitinib is loaded at high levels of 30 mg/g beads and rapidly released with a release half time of 1 h from 100-300 μm beads [41], comparable to doxorubicin and slightly slower than irinotecan release from 500-700 µm sized DC Bead using the same Pharmacopeia flow-through release set-up [42]. While sunitinib and irinotecan were released to full extent, doxorubicin was only 27% released due to the formation of self-assembled drug aggregates [42]. In a different set-up, bevacizumab (loaded at 38 mg/ml beads) release was deliberately extended to 3 days with a 41% release to match the time span of increased growth factor levels after embolization. This was achieved by applying biocompatible polymer layers on the bead surface by the layer-by-layer (LbL) technique [58]. In vivo pharmacokinetics, which is for the time being only available for sunitinib, is discussed in Section 3.

 Table 1. Recently developed non-biodegradable beads.

| Bead matrix (material) | Size (μm) | Drug | Mechanism of loading and/or release | Maximal drug loading | Release rates (in vitro, PBS pH 7.4, 37°C) | Reference |
|---|---------------------|----------------------------------|--|---|--|-----------|
| Cationic quaternary (3- acrylamidopropyl)trimethyl ammonium chloride (APTA) | 100-300 | anionic pyrene model drugs | Ion exchange | Up to 30 mg/ml depending on drug and bead formulation | Monovalent pyrene dye: 80% release, plateau reached at 1 h, for 8.6 µmol/ml loading | [53] |
| Lipiodol-loaded DC Bead | 70-150, 100-300 | DOX | Ion exchange | 37.5 mg/ml | Radiopaque beads eluted DOX slightly more slowly than non-radiopaque beads | [54] |
| DC Bead modified by iodinated moieties (iBeads) | 100-300, 300-500 | DOX | Ion exchange | 40-80 mg/ml | Slightly increased released drug dose compared to noniodinated beads, $t_{50\%}$ =0.5 h (100-300 µm), $t_{50\%}$ =0.8 h (300-500 µm) | [55] |
| DC Bead | 500-700 | DOX + rapamycin | Ion exchange (DOX)+ (non-solvent- induced) rapamycin precipitation | 40 mg/ml DOX + 30 mg/ml rapamycin | Not different from single drug-loaded bead at max. loading: 5% DOX release, 27% rapamycin release | [56] |
| DC Bead | 100-300 | Sunitinib | Ion exchange | 30 mg/g | PBS: $t_{50\%} = 0.8 \text{ h}$, 94% release at plateau; NaCl 0.9%: $t_{50\%} = 1.0 \text{ h}$, 100% release at plateau | [41, 57] |
| DC Bead | 70-150 | Bevacizumab | Ion exchange | 38 mg/ml | Extended by layer-by-layer technique to 3 days with a 41% release at plateau | [58] |
| DC Bead | Not yet published | Vandetanib | Ion exchange | Not yet published | Not yet published | [59] |

DOX: Doxorubicin

2.2 Biodegradable Beads for Drug Delivery and *In Vitro*Drug Release

Advantages of temporary embolizing agents have been shown by the clinical use of gelatin sponge and degradable starch microspheres (DSM) for decades [50, 72]. These advantages include reduced occurrence of post-embolization syndrome [24], reduced tissue inflammation and fibrosis [73], reduced risks arising from non-target embolization [11, 74], and possibility of repeated interventions after vessel recanalization [75, 76]. Transient compared to permanent embolization might also be favorable in terms of avoidance of ischemia-induced neoangiogenesis [49]. While being biodegradable, commercialized microspheres like DSM and OcclusinTM500 from (collagencoated poly(lactide-*co*-glycolide) (PLGA) microspheres, IMBiotechnologies Ltd., Edmonton, AB, Canada), are not compressible to pass easily through catheters.

Most recently developed microspheres were designed to be biodegradable (or resorbable) and compressible (Table 2). To include elastic properties in the spheres, research was inspired by already marketed (bio)polymers, such as compressible hydrogel matrices. While this rational choice should allow for drug loading of hydrosoluble drugs, such as they are used in current DEB-TACE, it however precludes the possibility to load more hydrophobic drugs, like sorafenib. Sorafenib is an anti-angiogenic multikinase inhibitor targeting Raf, affecting tumor signaling and the tumor vasculature. For these reasons, sorafenib is considered standard of care for advanced-stage HCC [4, 77]. The use of the ion-exchange mechanism results in the same limitation. Microsphere formulations with their loading and release characteristics are summarized in Table 2, whereas the most advanced microspheres will be additionally introduced in the following.

2.2.1 Bioresorbable Chitosan-Cellulose Microspheres

Biocompatible microspheres from oxidized carboxymethylchitosan-carboxymethylcellulose are degraded by enzymatic or non-enzymatic hydrolysis over adaptable timeframes [27, 78-80]. The rate of degradation may be modulated by polymer crosslinking density and drug loading, and ranges from less than 10 days for unloaded microspheres *in vivo* to 3 months for doxorubicineluting microspheres *in vitro* [78, 80]. Compared to DC Bead standard loading with doxorubicin of

37.5 mg/ml beads, doxorubicin loading on chitosan-cellulose microspheres was similar with maximally 48-85 mg/g wet spheres depending on the degree of crosslinking. Doxorubicin release was claimed to be more sustained than from DC Beads, differences do however not seem of clinical significance [78]. The total release of 27% of the loaded doxorubicin from the least crosslinked microspheres with the largest hydrogel pores and swelling were comparable to doxorubicin total release from DC Bead [42, 79]. The chitosan-cellulose systems are promising in terms of biocompatibility and timeframe of degradation, and compare *in vitro* to DC Beads doxorubicin delivery. Other chitosan-based microspheres for embolization are summarized in Table 2 [30, 81, 82].

2.2.2 Poly(ethylene glycol) Methacrylate (PEGMA) Microspheres

Several clinically established microspheres are acrylate based hydrogels [11], such as poly(ethylene glycol) (PEG) methacrylate (MA) microspheres (ResMic, Occlugel, Jouy-en-Josas, France) for the treatment of uterine fibroids. Due to the introduction of a hydrolysable PLGA-PEG-PLGA crosslinker, they are completely resorbed in less than 2 days in vitro and during 1 week in vivo [29, 73, 75]. For ionic loading of doxorubicin, irinotecan, and sunitinib, carboxylic functions were added to the microspheres by incorporation of up to 20% methacrylate monomer [83]. High loading capacities of 34, 37, and 40 mg/ml of microspheres, respectively, were achieved for the three drugs. This was comparable to total loading on DC Bead, which can carry 39 mg doxorubicin per ml of beads [84], 49 mg irinotecan per ml of beads [40], and 30 mg sunitinib per g of beads [57] (~33 mg/ml of beads, all: 100-300 μm). Release in phosphate buffered saline (PBS) showed the most sustained release for sunitinib among the three drugs, with 48-62% of sunitinib released at 6 hours and complete release after 24 hours [83, 85]. Direct comparison to the release kinetics from DC Beads is not advised due to the use of different release apparatuses, but does not seem to differ strikingly [41]. PEGMA microspheres were also combined with bevacizumab (20 mg/ml microspheres), which was 83-92% released in vitro after six hours, and completely after 24 hours [85]. Loading and release of both anti-angiogenic drugs depend on ion exchange and salt concentration. Concerning the difference in release kinetics for the two anti-angiogenic drugs, bevacizumab was loaded more superficially due to its bigger molecular size, and was thus released more rapidly. To conclude, PEGMA microspheres are capable to load the same high doses of anti-angiogenic drugs as clinically established beads. Their release profile is similar to ion-exchange based commercial beads. The inclusion of PLGA

monomers assures biocompatibility and degradation, and might enable loading of more hydrophobic drugs mediated by van der Waals interactions.

2.2.3 Poly(D,L-lactic acid) and Poly(lactic-*co*-glycolic acid) Biodegradable Microspheres

Beads presented so far are elastic and are loaded with charged molecules post-synthesis via ion-exchange. In contrast, different types of biodegradable microspheres containing drugs were prepared from poly(D,L-lactic acid) (PLA) and PLGA [31, 32, 34].

PLA microspheres (from Purasorb PDL 20) with sizes between 200 and 400 μm and catheter deliverability (4-Fr catheter) hold high drug loads of up to 16% (w/w) sorafenib, 12% (w/w) cisplatin or both drugs in the same spheres (7% (w/w) sorafenib and 5% (w/w) cisplatin) [34]. Both molecules and the polymer are of hydrophobic nature, allowing for drug incorporation by solvent evaporation, opposed to hydrogels and the more water-soluble, charged drugs. Drug release from the combination microspheres showed an initial burst of superficially bound drug, followed by prolonged drug release over 14 days. At 14 days, 91% of sorafenib and 48% of cisplatin were released at pH 7.4. Compared to the single drug-loaded microspheres, release was faster due to the more porous structure and water swelling of the combination drug-eluting microspheres, precluding subsequent degradation-driven release. The drug combination strategy possibly circumvents tumor drug resistance and in addition, synergic effects were reported both in vitro on cell viability and in vivo on tumor growth by the simultaneous release of the two drugs [86]. Concerning degradability, the three types of microspheres were not degraded after 9 months. The degradation half time was modeled to be 7 weeks for the two single drug-loaded microspheres and around 10 weeks for the combination microspheres. The authors assigned the longer degradation time for the sorafenib+cisplatin microspheres to a more porous structure, outward-diffusion of lactic acid monomers and consequently reduced autocatalytic acidic hydrolysis. The PLA microspheres might be modified in the future for faster degradation, although their relatively long degradation time does not necessarily represent a disadvantage.

More hydrophilic PLGA microspheres result in faster degradation. Magnetic resonance image-able, sorafenib-loaded (19% (w/w)) PLGA microspheres (from 75:25 PLGA Resomer RG 752H) were also

proposed for embolization [31]. Inclusion of iron oxide nanoparticles confers the MRI ability. The microspheres were polydisperse with an average diameter of 13 µm, which was adapted for animal embolization, yet is too small for clinical application due to risk of arteriovenous shunting. Sorafenib was released in a sustained manner into PBS + 1% sodium dodecyl sulfate (SDS), with a release of 21% after 3 days. Microsphere degradation was not assessed in this study, but was assumed to be complete during the course of drug release. In a rabbit VX2 model, normalization of VEGF receptor expression and microvessel density were shown at 24 hours, which were signs of successful sorafenib delivery. Although the size of these microspheres is currently an issue for translation into clinical practice, they combine various features necessary for further development, such as biocompatibility, degradability, combined imaging and efficient entrapment and delivery of sorafenib, the most efficacious drug in HCC treatment.

Doxorubicin-loaded microspheres made from a comparable type of PLGA (75:25) led to similar results [32]. The microspheres showed visible signs of partial degradation in serum after 2 weeks, like decrease in size, loss of sphericity, and pore formation. Their diameter was 26 μ m before degradation with a doxorubicin load of 25 mg/g PLGA microspheres and a release of 35% after 3 days. For these similar types of PLGA microspheres, longer degradation and release studies should be carried out to exclude drug dose dumping at later time points.

 Table 2. Recently developed (bio)degradable beads.

| Bead matrix (material) | Drug | Mechanism of loading and/or release | Maximal drug loading | Release rates (in vitro, PBS pH 7.2-7.4, 37°C) | Degradation time | Reference |
|--|-----------------------|---|---|---|--|---------------------|
| Alginate | Lipo- somal DOX | Loading: drug entrapment during alginate bead crosslinking, Release: Heat- triggered | 1.5 mg/g MS | HEPES: 37°C: 20% at 3 h, 42°C: 75% in 30 s, 85% at plateau at 1 min; 50% FBS: 37°C: 30% at 3 h, 42°C: 100% in 3 min | n.a. | [33] |
| Bovine Serum Albumin (crosslinked) | IRI | Loading: into lyophilized MS, Release: swelling- controlled | 98 mg/g MS | 80.6% at 5 h, 88.4% at plateau | Tyrosine PBS solution (50 µg/mL): almost completely degraded within 4 weeks | [35] |
| Chitosan- cellulose | DOX | Ion exchange | 48-85 mg/g wet MS | t _{50%} at ca. 4 h, 15-27% at plateau | <10 days (unloaded) in vivo | [27, 78-80] |
| | | Loading in lyophilized MS, ion exchange | 300-700 mg/g dry MS within 48 h (depending on size) | n. a. | 14-88 days (unloaded) in vitro, >88 days (drug- loaded) in vitro | |
| Chitosan | DOX | Loading: Drug entrapment during water-in-oil (W/O) emulsion, Release: lysozyme- cleavage | CMs: 115 mg/g MS, ACMs: 107 mg/g MS | CMs: 70% at 20 h (plateau), ACMs: 80% at 28 h (plateau) | 0.5 mg/mL lysozyme at 45°C, gentle shaking: Mass loss: CMs: 4.2%, ACMs: 6.3% at 1 week, 40.7% of CMs, 58.1% of ACMs degraded at 8 weeks | [30] |
| Chitosan | DOX | Loading: "Expanding- loading-shrinking" process, Release: presumably enzymatic hydrolysis | 100 mg/g MS | 22.6% at 7 d | 24 weeks in vivo | [81, 82] |
| Gelatin | Cisplatin | Loading: presumably covalent binding, Release: MS degradation | 11.145 mg/g MS | 12% at 24 h | n. a. | [105] |
| PEG methacrylate | DOX | Ion exchange | 34 mg/ml MS | 49% at 1 h, 64% at 6 h (for MS containing 20% methacrylate) | less than 2 days in vitro, 1 week in vivo | [29, 73, 83, 85] |

| | IRI | Ion exchange | 37 mg/ml MS | 75% at 1 h, 87% at 6 h (for MS containing 20% methacrylate) | | |
|-----------------------------------|--------------------------|--|---|--|---|------|
| | Sunitinib | Ion exchange | 40 mg/ml MS | 48-62% at 6 h, 100% at 24 h | | |
| | Bevaci- zumab | Ion exchange | 20 mg/ml MS | 83-92% at 6 h, 100% at 24 h | | |
| Poly(D,L-lactic acid) | Sorafenib | Loading: entrapment during emulsion/solvent | 160 mg/g MS | 4.2% at 24 h, 9.3% at 14 d | t _{50%} = 7.2 weeks [34, 86] (modeled, not degraded after 9 months) | |
| | Cisplatin | evaporation MS preparation, Release: polymer | 120 mg/g MS | 4.0% at 24 h, 6.9% at 14 d | t _{50%} = 7.2 weeks (modeled, not degraded after 9 months) | |
| | Sorafenib + cisplatin | swelling (not yet degradation) | 70 mg sorafenib + 50 mg cisplatin/g MS | 23% of sorafenib and 20% of cisplatin at 24 h, 91% of sorafenib and 48% of cisplatin at 14 d | t _{50%} = 10.4 weeks (modeled, not degraded after 9 months) | |
| Poly(lactic-co- glycolic acid) | Sorafenib | Loading: double emulsion/solvent evaporation | 190 mg/g MS | 21% at 3 d | n. a. | [31] |
| Poly(lactic-co- glycolic acid) | DOX | Loading: solid-in-oil- in-water emulsion, Release: polymer swelling | 25 mg/g MS | 35% at 3 d | 50% (v/v) FBS in PBS and incubated at 37°C at 50 rpm: visible signs at 2 weeks | [32] |

DOX: Doxorubicin, n. a.: not available, MS: microspheres, IRI: Irinotecan, CMs: chitosan microspheres, ACMs: acetylated CMs

3 Drug Pharmacokinetics after DEB-TACE

DEB-TACE was adopted in clinical practice after evidence of treatment safety had been assured [87]. Varela et al. [18] and Poon et al. [19] had shown the absence of the initial peak in doxorubicin plasma concentration compared to cTACE right after the procedure. One of the apparent advantages of DEB-TACE is the locally controlled or even sustained drug release. Poursaid et al. concluded in a recent review that a weakness of two newly developed systems was their non-linear drug release, inherent to loading by ion-exchange [88]. In a recent study, a strategy of instantaneous release was applied [33]. Rapid release of high doxorubicin doses from liposomes incorporated in embolic microspheres was heat-triggered in order to enhance drug tumor penetration. Lilienberg et al. [89] equally determined intracellular doxorubicin concentrations in healthy pig livers to be higher after cTACE than DEB-TACE, i.e. without sustained release, however, at the cost of safety. The summary in Table 2 confirms that embolic microspheres were developed with different, i.e. very fast to prolonged release rates. We will thus approach the question which drug release profiles are actually sought for successful therapy. Since systemic concentrations are known to be reduced as a result of the DEB procedure, we will focus on the drug target tissue concentrations and distribution, which currently little is known about.

3.1 Pharmacokinetic Profiles in the Target Tissue

The advantage of local administration of DEB as a drug delivery system over intravenous or artery infusion is the resulting locally increased and sustained drug concentrations compared to the non-target tissues [32, 89-92]. Several studies also assess drug pharmacokinetics in the target tissue over time (Table 3). For the time being, these were carried out with non-biodegradable beads eluting drugs by ion exchange. Increased drug tissue levels are seen shortly after administration for all drugs included in Table 3. For example, Hong et al. [93] observed a clear doxorubicin peak 3 days after the embolization, after which levels decreased. Rao et al. [91] determined increasing irinotecan tissue levels until 24 hours. Fuchs et al. found sunitinib levels higher at 6 hours than at 24 hours after embolization [57]. Thus, ion-exchange microspheres result in fast drug availability in the target tissue after fast release. The drug is relatively quickly available first in the tissue compartment and second in the plasma [57]. On the other hand, both physicochemical drug and

tissue properties are decisive for the final drug tissue residence time. Doxorubicin was detected in liver explants until 36 days [94], whereas irinotecan was present at low concentrations in rabbit livers 7 days after administration [95]. 4 days after normal sheep lung embolization, neither irinotecan nor its primary metabolite were detectable [90, 96]. This finding had to be attributed to the specific lung architecture, where blood flow increases and the bronchial arteries enlarge after pulmonary embolization. Thus, drug retention is not only inherent to the drug properties, but also depends on the physiology of the tissue environment. While Namur et al. did not detect differences in doxorubicin levels between tumor and liver parenchyma at 8 hours, doxorubicin retention was significantly evidenced in necrotic tissue compared to non-necrotic tissue at 32-36 days [94, 97, 98]. For sunitinib, levels were retained in tumor tissue until 14 d after rabbit VX2 tumor embolization, more than in normal liver [99]. This was in accordance with a population pharmacokinetic metaanalysis by Houk et al., suggesting that the clearance for both sunitinib and its primary metabolite is reduced in patients relative to healthy adult volunteers [100]. Moreover, anti-angiogenic drugs are known to normalize interstitial pressure and flow in leaky tumor vasculature, eventually leading to enhanced drug tumor penetration and availability [20, 101]. When given orally, low dose regular (metronomic) administration within the therapeutic range is most efficacious [101]. Prolonged release and increased tissue residence time are therefore desired characteristics for anti-angiogenic drug delivery.

These data support that ion-exchange microspheres result in fast drug availability in the target tissue, whereas both drug and tissue properties are critical for drug tissue residence time.

3.2 Drug Tissue Distribution

In order for the drug to yield its pharmacological effect, it has to be released into the tissue. To impregnate wide-spread tumor areas, distant diffusion from the delivering beads is desired. Since tumor necrosis is an indicator for tumor response and is often increased with concomitant drug delivery in addition to the embolization itself, necrotic tumor regions are also an indicator for the spatial drug distribution [92, 93, 102, 103]. Inflammation factors were also used for indirect determination of drug diffusion [104]. Most conclusive results are, however, obtained by direct determination of drug distribution. For example, doxorubicin and sunitinib have been imaged by

means of their inherent drug fluorescence, and sunitinib and its metabolites were recently also determined by mass spectrometry imaging [54, 94, 97, 99].

Doxorubicin was detected at a distance of up to 600 µm from the bead rim and up to 90 days after embolization in healthy pigs and HCC liver explants [54, 94, 97]. The doxorubicin diffusion was farther and thus more homogenous in necrotic tissue, where drug distribution profiles appeared "flatter", possibly due to cellular disorganization [94]. In comparison, sunitinib was detected over at least 1.5 mm away from the beads and still at high drug levels in the tumor 14 days after treatment, when the study ended [92, 99]. Levels were especially high in the necrotic tumor. Sunitinib metabolism was also evidenced in this study, with four major metabolites present at 7 and 13 days. To conclude from the available data, the two drugs doxorubicin and sunitinib seem to have different tissue distribution. Table 4 summarizes that sunitinib's lower molecular weight, higher degree of ionization at physiological pH, higher lipophilicity, higher volume of distribution, and later elimination probably favor farther distribution into the tissue compared to doxorubicin transport.

Table 3. Preclinical and clinical studies investigating drug tissue levels and/or distribution after DEB-TACE.

| Drug | DEB | Size (µm) | Dose | Model | Time | Tissue concentration | Samples for quantification | Reference |
|----------------------|------------|---------------------|---|---------------------------|---|---|---|-----------|
| Doxorubicin (DOX) | DC Bead | 100-300 | 45 mg drug/g wet beads, dose delivered: 11.25 mg | Rabbit VX2 liver tumor | 1 h, 12 h, 24 h, 3d, 7 d, 14 d | Tumor: 413.5 at 3 d, 116.7 at 7 d, 41.76 at 14 d (μM), non-tumorous tissue: 2-17 (μM, range over 14 d) | Homogenized tumor or liver | [93] |
| | DC Bead | 100-300, 700-900 | 37.5 mg/ml beads, mean dose delivered: 103 mg | Porcine normal liver | 28 d, 90 d | 100-300 μm: 3.25 (bead edge)-0.55 (600 μm distance) at 28 d, 1.55-0.60 at 90 d; 700-900 μm: 6.80-0.90 at 28 d, 2.60-0.70 at 90 d (μM) | Microspectrofluorimetry on liver tissue sections | [97] |
| | DC Bead | 100-300 | 37.5 mg/ml beads, mean dose delivered: 98.3 ± 24.4 mg | HCC patients | 8 h, 9-14 d, 32-36 d | 8.45 (bead edge)-3.55 (600 µm distance) at 8 h, 4.50-1.40 at 9-14 d, 1.55 to 0.45 at 32-36 d (µM) | Microspectrofluorimetry on liver tissue sections | [94] |
| | DC Bead | 70-150, 100-300 | 37.5 mg/ml beads, dose delivered: 37.5 mg | Normal swine liver | 0.5 h, 1 h, 2 h, 4 h, 8 h, 24 h, 7 d | Adjacent to bead: 70-150 μm: 30-40 at 0.5 h, 7 at 24 h, 5 at 7 d; 100-300 μm: 30-40 at 0.5 h, 3 at 24 h, close to 0 at 7 d (μΜ) | Epifluorescent microscopy | [54] |
| Ibuprofen | Bead Block | 500-700 | 485 mM-loaded beads, 0.5 mL of beads injected | Sheep uterine tissue | 1 d, 1 week | 8.8 ± 4.8 mM in the vessel wall at 1 d, not detected 100 µm from occluded artery, 1 week: <lloq< td=""><td>Fourier transform infrared microspectroscopy on tissue sections</td><td>[106]</td></lloq<> | Fourier transform infrared microspectroscopy on tissue sections | [106] |
| Irinotecan (IRI) | DC Bead | 100-300 | 10, 20, 50 mg/ml beads, dose delivered: 20, 40, 100 mg | Sheep normal lung | 4 d, 4 weeks | IRI and SN38 < LLOQ for all doses | Infrared microspectroscopy on lung tissue sections | [96] |
| | DC Bead | 300-500 | 0, 10, 25, 50 mg/ml beads, dose delivered: 0, 20, 50, 100 mg | Sheep normal lung | 4 d, 4 weeks | IRI and SN38 < LLOQ for all doses | Homogenized lung | [90] |

| | DC Bead | 300-500 | 50 mg/ml beads, | Sheep normal | 4 d | PAE-50+BAE-0: | Homogenized lung | [103] |
|-----------|--------------|----------|------------------|----------------|-------------|---|------------------------------|-------|
| | | for PAE, | dose delivered: | lung | | IRI: 1122±237, | | |
| | | 100-300 | 100 mg single | | | SN38: 35±21, | | |
| | | for BAE | embolization, | | | PAE-50+BAE-50: | | |
| | | | 200 mg double | | | IRI: 16±1, | | |
| | | | embolization | | | SN38: 3286±2769 (ng/mL) | | |
| | DC Bead | 100-300 | 100 mg/ml beads, | Rabbit VX2 | 1 h, 6 h, | Tumor: | Homogenized tumor, | [91] |
| | | | no fixed dose | liver tumor | 24 h | IRI: 101.1 at 1 h, 210.4 at | normal liver within 2 mm to | |
| | | | administered | | | 6 h, 872.2 at 24 h, | tumor, contralateral liver | |
| | | | | | | SN38: 9.7 at 1 h, 23.1 at | | |
| | | | | | | 6 h, 351.1 at 24 h (ng/g) | | |
| | QuadraSphere | 30-60 | 20 mg/ml beads, | Rabbit VX2 | 7 d | Tumor: | Homogenized tumor, | [95] |
| | | | dose delivered: | liver tumor | | IRI: 32.17, | normal liver adjacent to | |
| | | | 12 mg | | | SN38: 463.33 (ng/g) | tumor, normal liver at least | |
| | | | | | | | 1 cm apart from tumor | |
| Sunitinib | DC Bead | 100-300 | 30 mg/g beads, | Healthy rabbit | 6 h, 24 h | 14.9 μg/g at 6 h, | Homogenized liver | [57] |
| | | | dose delivered: | liver | | 3.4 μg/g at 24 h | | |
| | | | 6 mg | | | | | |
| | DC Bead | 70-150, | 30 mg/g beads, | Rabbit VX2 | 1 d, 14 d | Tumor: | Homogenized tumor or | [92] |
| | | 100-300 | dose delivered: | liver tumor | | 70-150 μm: 40.4 at 1 d, | contralateral liver | |
| | | | 1.5 mg | | | 27.4 at 14 d, | | |
| | | | | | | 100-300 μm: 17.8 at 1 d, | | |
| | | | | | | 0.16 at 14 d (μg/g) | | |
| | DC Bead | 70-150 | | | 1-2 d, 7 d, | Tumor: <lloq 1-2="" 39<="" at="" d,="" td=""><td>Fluorescence microscopy</td><td>[99]</td></lloq> | Fluorescence microscopy | [99] |
| | | | | | 12-14d | (bead edge)-19 (1.5 mm | (also: mass spectrometry | |
| | | | | | | distance) at 7 d, 54-23 at | imaging) | |
| | | | | | | 12-14 d (μg/g) | | |

25

LLOQ: lower limit of quantification, PAE: pulmonary artery embolization, BAE: bronchial artery embolization, IRI: irinotecan, SN38: primary irinotecan metabolite, PAE-50+BAE-0: PAE with DEB-IRI and BAE with bland DEB, PAE-50+BAE-50: PAE with DEB-IRI and BAE with DEB-IRI

Table 4. Physicochemical properties of doxorubicin and sunitinib.

| | Doxorubicin [98, 107] | Sunitinib [107-109] |
|--------------------------|------------------------------|---|
| Molecular structure | HO HO OH O CH ₃ | CH ₃ CH ₃ |
| Molecular weight (g/mol) | 543.52 | 398.47 |
| рКа | 7.34, 8.46, 9.46 | 9.30 |
| Ionized form at pH 7.4 | max. 50% | 98.30% |
| log P | pH 7.5: 2.42 ± 0.08 | 2.47 (XLOGP2), pH 7.4: 5.2 (experimental) |
| Volume of distribution | 809 to 1214 L/m ² | 2230 L |
| V_d | | |
| Protein binding | 74-76% | 95% |
| Oral bioavailability | 0% | 50% or higher in different animal species |
| Half life | 20-48 h | 40-60 h |

4 Conclusions on Controlled Drug Release from Drug-Eluting Beads and Qualitative *In Vitro-In Vivo* Comparison

Initially, we raised the question concerning the "ideal drug release profile", and whether sustained drug release was required to achieve long-term exposure of the tumor to the drug. We elucidated that ion-exchange microspheres — commercialized ones as well as microspheres under development, biodegradable and non-biodegradable ones — yield fast release, which mainly depends on the kinetics of the release mechanism rather than the nature of the drug. The extent of release in contrast is more related to the drug itself, and drug-drug interactions as was seen for doxorubicin. Kinetics is expected to be more prolonged for biodegradable polymer drug delivery systems, in which a drug is physically entrapped. In the latter case, the drug is released as a result of initial polymer swelling, diffusion and degradation mechanism, certainly with differences for

surface or bulk degradation and other factors. Complete release will be achieved upon complete degradation of the delivery system.

However, drug diffusion into the target tissue and drug residence time depend on the drug's physicochemical properties and tissue characteristics like vascular flow and interstitial pressure, presence of proteins, lipids, and cell metabolism. That is, manipulation of a delivery system toward sustained drug release should be considered only if the resulting drug residence time after rapid release is too short to obtain a therapeutic effect. For delivery of classical chemotherapeutic small molecules, which remain in the tissue for several months, such as doxorubicin, sustained release is certainly not required. On top of that, common treatment regimens should be considered. Usual dosing of chemotherapeutics includes a recovery break, which should be taken into account also for local delivery to avoid toxicity or resistance. In contrast, dosing of anti-angiogenic drugs was shown to provide more powerful effects with regular low-dose administration. In this case, prolonged release might yield better treatment outcomes after a single embolization.

Since the data on PK tissue distribution is limited, more studies are needed to quantitatively correlate *in vitro* to *in vivo* data. Especially for the newly designed beads and new compounds, the results will be of value to estimate their success. Recently, a mass spectrometry imaging method has been employed for the first time in embolized liver. This method should be an interesting tool in the future to map a drug's spatial diffusion also for non-fluorescent drugs.

5 References

[1] N.D. Theise, Liver Cancer, in: B.W. Stewart, Wild, C. P. (Ed.), World Cancer Report 2014, IARC Nonserial Publication, Lyon, 2015.

- [2] J.M. Llovet, J. Bruix, Systematic review of randomized trials for unresectable hepatocellular carcinoma: Chemoembolization improves survival, Hepatology 37(2) (2003) 429-42.
- [3] J.L. Raoul, B. Sangro, A. Forner, V. Mazzaferro, F. Piscaglia, L. Bolondi, R. Lencioni, Evolving strategies for the management of intermediate-stage hepatocellular carcinoma: available evidence and expert opinion on the use of transarterial chemoembolization, Cancer treatment reviews 37(3) (2011) 212-20.
- [4] A. Forner, J.M. Llovet, J. Bruix, Hepatocellular carcinoma, Lancet 379(9822) (2012) 1245-55.
- [5] A. Forner, M. Gilabert, J. Bruix, J.L. Raoul, Treatment of intermediate-stage hepatocellular carcinoma, Nature reviews. Clinical oncology 11(9) (2014) 525-35.
- [6] A. Facciorusso, R. Licinio, N. Muscatiello, A. Di Leo, M. Barone, Transarterial chemoembolization: Evidences from the literature and applications in hepatocellular carcinoma patients, World journal of hepatology 7(16) (2015) 2009-2019.
- [7] R. Lencioni, T. de Baere, M. Burrel, J.G. Caridi, J. Lammer, K. Malagari, R.C. Martin, E. O'Grady, M.I. Real, T.J. Vogl, A. Watkinson, J.F. Geschwind, Transcatheter Treatment of Hepatocellular Carcinoma with Doxorubicin-loaded DC Bead (DEBDOX): Technical Recommendations, Cardiovascular and interventional radiology 35(5) (2012) 980-5.
- [8] J. Meza-Junco, A.J. Montano-Loza, D.M. Liu, M.B. Sawyer, V.G. Bain, M. Ma, R. Owen, Locoregional radiological treatment for hepatocellular carcinoma; Which, when and how?, Cancer treatment reviews 38(1) (2012) 54-62.
- [9] S.P. Kalva, M. Pectasides, R. Liu, N. Rachamreddy, S. Surakanti, K. Yeddula, S. Ganguli, S. Wicky, L.S. Blaszkowsky, A.X. Zhu, Safety and effectiveness of chemoembolization with drug-eluting beads for advanced-stage hepatocellular carcinoma, Cardiovascular and interventional radiology 37(2) (2014) 381-7.

[10] C.E. Ray, A.C. Brown, T.J. Green, H. Winston, C. Curran, S.M. Kreidler, D.H. Glueck, P.J. Rochon, Survival Outcomes in Patients With Advanced Hepatocellular Carcinoma Treated With Drug-Eluting Bead Chemoembolization, American Journal of Roentgenology 204(2) (2015) 440-447.

- [11] Y.X. Wang, T. De Baere, J.M. Idee, S. Ballet, Transcatheter embolization therapy in liver cancer: an update of clinical evidences, Chin J Cancer Res 27(2) (2015) 96-121.
- [12] S. Han, X. Zhang, L. Zou, C. Lu, J. Zhang, J. Li, M. Li, Does drug-eluting bead transcatheter arterial chemoembolization improve the management of patients with hepatocellular carcinoma? A meta-analysis, PloS one 9(8) (2014) e102686.
- [13] R. Golfieri, E. Giampalma, M. Renzulli, R. Cioni, I. Bargellini, C. Bartolozzi, A.D. Breatta, G. Gandini, R. Nani, D. Gasparini, A. Cucchetti, L. Bolondi, F. Trevisani, Randomised controlled trial of doxorubicin-eluting beads vs conventional chemoembolisation for hepatocellular carcinoma, British journal of cancer 111(2) (2014) 255-64.
- [14] J.Y. Ni, L.F. Xu, W.D. Wang, H.L. Sun, Y.T. Chen, Conventional transarterial chemoembolization vs microsphere embolization in hepatocellular carcinoma: a meta-analysis, World journal of gastroenterology: WJG 20(45) (2014) 17206-17.
- [15] X. Zhou, Z. Tang, J. Wang, P. Lin, Z. Chen, L. Lv, Z. Quan, Y. Liu, Doxorubicin-eluting beads versus conventional transarterialchemoembolization for the treatment of hepatocellular carcinoma: a meta-analysis, International journal of clinical and experimental medicine 7(11) (2014) 3892-903.
- [16] R. Kloeckner, A. Weinmann, F. Prinz, D. Pinto dos Santos, C. Ruckes, C. Dueber, M.B. Pitton, Conventional transarterial chemoembolization versus drug-eluting bead transarterial chemoembolization for the treatment of hepatocellular carcinoma, BMC cancer 15 (2015) 465.
- [17] Z.B. Xie, X.B. Wang, Y.C. Peng, S.L. Zhu, L. Ma, B.D. Xiang, W.F. Gong, J. Chen, X.M. You, J.H. Jiang, L.Q. Li, J.H. Zhong, Systematic review comparing the safety and efficacy of conventional and drug-eluting bead transarterial chemoembolization for inoperable hepatocellular carcinoma, Hepatology research: the official journal of the Japan Society of Hepatology 45(2) (2015) 190-200.
- [18] M. Varela, M.I. Real, M. Burrel, A. Forner, M. Sala, M. Brunet, C. Ayuso, L. Castells, X. Montana, J.M. Llovet, J. Bruix, Chemoembolization of hepatocellular carcinoma with drug eluting beads: efficacy and doxorubicin pharmacokinetics, Journal of hepatology 46(3) (2007) 474-81.

[19] R.T. Poon, W.K. Tso, R.W. Pang, K.K. Ng, R. Woo, K.S. Tai, S.T. Fan, A phase I/II trial of chemoembolization for hepatocellular carcinoma using a novel intra-arterial drug-eluting bead, Clinical gastroenterology and hepatology: the official clinical practice journal of the American Gastroenterological Association 5(9) (2007) 1100-8.

- [20] A.M. Al-Abd, Z.K. Aljehani, R.W. Gazzaz, S.H. Fakhri, A.H. Jabbad, A.M. Alahdal, V.P. Torchilin, Pharmacokinetic strategies to improve drug penetration and entrapment within solid tumors, Journal of Controlled Release 219 (2015) 269-277.
- [21] S.W. Shin, The Current Practice of Transarterial Chemoembolization for the Treatment of Hepatocellular Carcinoma, Korean journal of radiology: official journal of the Korean Radiological Society 10(5) (2009) 425-434.
- [22] K. Hong, H. Kobeiter, C.S. Georgiades, M.S. Torbenson, J.F. Geschwind, Effects of the type of embolization particles on carboplatin concentration in liver tumors after transcatheter arterial chemoembolization in a rabbit model of liver cancer, Journal of vascular and interventional radiology: JVIR 16(12) (2005) 1711-7.
- [23] X. Zhang, H.L.H. Ng, A.P. Lu, C.C. Lin, L.M. Zhou, G. Lin, Y.B. Zhang, Z.J. Yang, H.Q. Zhang, Drug delivery system targeting advanced hepatocellular carcinoma: Current and future, Nanomed-Nanotechnol 12(4) (2016) 853-869.
- [24] T.J. Vogl, S. Zangos, K. Eichler, D. Yakoub, M. Nabil, Colorectal liver metastases: regional chemotherapy via transarterial chemoembolization (TACE) and hepatic chemoperfusion: an update, European radiology 17(4) (2007) 1025-34.
- [25] A. Schwarz, H. Zhang, A. Metcalfe, I. Salazkin, J. Raymond, Transcatheter embolization using degradable crosslinked hydrogels, Biomaterials 25(21) (2004) 5209-5215.
- [26] R.E.J. Forster, F. Thürmer, C. Wallrapp, A.W. Lloyd, W. Macfarlane, G.J. Phillips, J.-P. Boutrand, A.L. Lewis, Characterisation of physico-mechanical properties and degradation potential of calcium alginate beads for use in embolisation, Journal of Materials Science: Materials in Medicine 21(7) (2010) 2243-2251.

[27] L. Weng, H.C. Le, R. Talaie, J. Golzarian, Bioresorbable hydrogel microspheres for transcatheter embolization: preparation and in vitro evaluation, Journal of vascular and interventional radiology: JVIR 22(10) (2011) 1464-1470 e2.

- [28] T. Toyama, N. Nitta, S. Ohta, T. Tanaka, Y. Nagatani, M. Takahashi, K. Murata, H. Shiomi, S. Naka, Y. Kurumi, T. Tani, Y. Tabata, Clinical trial of cisplatin-conjugated gelatin microspheres for patients with hepatocellular carcinoma, Japanese journal of radiology 30(1) (2012) 62-8.
- [29] S. Louguet, V. Verret, L. Bedouet, E. Servais, F. Pascale, M. Wassef, D. Labarre, A. Laurent, L. Moine, Poly(ethylene glycol) methacrylate hydrolyzable microspheres for transient vascular embolization, Acta Biomater 10(3) (2014) 1194-205.
- [30] X. Zhou, M. Kong, X.J. Cheng, C. Feng, J. Li, J.J. Li, X.G. Chen, In vitro and in vivo evaluation of chitosan microspheres with different deacetylation degree as potential embolic agent, Carbohydrate polymers 113 (2014) 304-313.
- [31] J. Chen, S.B. White, K.R. Harris, W. Li, J.W. Yap, D.H. Kim, R.J. Lewandowski, L.D. Shea, A.C. Larson, Poly(lactide-co-glycolide) microspheres for MRI-monitored delivery of sorafenib in a rabbit VX2 model, Biomaterials 61 (2015) 299-306.
- [32] J.W. Choi, J.-H. Park, S.Y. Baek, D.-D. Kim, H.-C. Kim, H.-J. Cho, Doxorubicin-loaded poly(lactic-co-glycolic acid) microspheres prepared using the solid-in-oil-in-water method for the transarterial chemoembolization of a liver tumor, Colloids and Surfaces B: Biointerfaces 132 (2015) 305-312.
- [33] M. van Elk, B. Ozbakir, A.D. Barten-Rijbroek, G. Storm, F. Nijsen, W.E. Hennink, T. Vermonden, R. Deckers, Alginate Microspheres Containing Temperature Sensitive Liposomes (TSL) for MR-Guided Embolization and Triggered Release of Doxorubicin, PloS one 10(11) (2015) e0141626.
- [34] Y. Wang, A. Benzina, D.G.M. Molin, N.v.d. Akker, M. Gagliardi, L.H. Koole, Preparation and structure of drug-carrying biodegradable microspheres designed for transarterial chemoembolization therapy, Journal of Biomaterials Science, Polymer Edition 26(2) (2015) 77-91.
- [35] J. Yan, F. Wang, J. Chen, T. Liu, T. Zhang, Preparation and Characterization of Irinotecan Loaded Cross-Linked Bovine Serum Albumin Beads for Liver Cancer Chemoembolization Therapy, International Journal of Polymer Science 2016 (2016) 8.

[36] L. Faloppi, M. Scartozzi, E. Maccaroni, M. Di Pietro Paolo, R. Berardi, M. Del Prete, S. Cascinu, Evolving strategies for the treatment of hepatocellular carcinoma: from clinical-guided to

molecularly-tailored therapeutic options, Cancer treatment reviews 37(3) (2011) 169-77.

- [37] A. Villanueva, Rethinking future development of molecular therapies in hepatocellular carcinoma: a bottom-up approach, Journal of hepatology 59(2) (2013) 392-5.
- [38] Z. Wang, W. Zhou, H. Zhang, L. Qiao, Combination of anti-angiogenesis agents and transarterial embolization: Is it a promising approach for the treatment of liver cancer?, Discovery medicine 20(108) (2015) 51-5.
- [39] A.L. Lewis, M.V. Gonzalez, A.W. Lloyd, B. Hall, Y. Tang, S.L. Willis, S.W. Leppard, L.C. Wolfenden, R.R. Palmer, P.W. Stratford, DC bead: in vitro characterization of a drug-delivery device for transarterial chemoembolization, Journal of vascular and interventional radiology: JVIR 17(2 Pt 1) (2006) 335-42.
- [40] R.R. Taylor, Y. Tang, M.V. Gonzalez, P.W. Stratford, A.L. Lewis, Irinotecan drug eluting beads for use in chemoembolization: in vitro and in vivo evaluation of drug release properties, European journal of pharmaceutical sciences: official journal of the European Federation for Pharmaceutical Sciences 30(1) (2007) 7-14.
- [41] K. Fuchs, P.E. Bize, A. Denys, G. Borchard, O. Jordan, Sunitinib-eluting beads for chemoembolization: methods for in vitro evaluation of drug release, International journal of pharmaceutics 482(1-2) (2015) 68-74.
- [42] O. Jordan, A. Denys, T. De Baere, N. Boulens, E. Doelker, Comparative study of chemoembolization loadable beads: in vitro drug release and physical properties of DC bead and hepasphere loaded with doxorubicin and irinotecan, Journal of vascular and interventional radiology: JVIR 21(7) (2010) 1084-90.
- [43] A.L. Lewis, C. Adams, W. Busby, S.A. Jones, L.C. Wolfenden, S.W. Leppard, R.R. Palmer, S. Small, Comparative in vitro evaluation of microspherical embolisation agents, Journal of Materials Science: Materials in Medicine 17(12) (2006) 1193-1204.
- [44] S. Stampfl, N. Bellemann, U. Stampfl, C.M. Sommer, H. Thierjung, R. Lopez-Benitez, B. Radeleff, I. Berger, G.M. Richter, Arterial Distribution Characteristics of Embozene Particles and Comparison

with Other Spherical Embolic Agents in the Porcine Acute Embolization Model, Journal of Vascular and Interventional Radiology 20(12) (2009) 1597-1607.

- [45] V. Verret, S.H. Ghegediban, M. Wassef, J.P. Pelage, J. Golzarian, A. Laurent, The arterial distribution of Embozene and Embosphere microspheres in sheep kidney and uterus embolization models, Journal of vascular and interventional radiology: JVIR 22(2) (2011) 220-8.
- [46] V. Verret, M. Wassef, J.P. Pelage, S.H. Ghegediban, L. Jouneau, L. Moine, D. Labarre, J. Golzarian, I. Schwartz-Cornil, A. Laurent, Influence of degradation on inflammatory profile of polyphosphazene coated PMMA and trisacryl gelatin microspheres in a sheep uterine artery embolization model, Biomaterials 32(2) (2011) 339-51.
- [47] J. Namur, F. Pascale, N. Maeda, M. Sterba, S.H. Ghegediban, V. Verret, A. Paci, A. Seck, K. Osuga, M. Wassef, P. Reb, A. Laurent, Safety and Efficacy Compared between Irinotecan-Loaded Microspheres HepaSphere and DC Bead in a Model of VX2 Liver Metastases in the Rabbit, Journal of Vascular and Interventional Radiology 26(7) (2015) 1067-1075.e3.
- [48] D.B. Brown, T.K. Pilgram, M.D. Darcy, C.E. Fundakowski, M. Lisker-Melman, W.C. Chapman, J.S. Crippin, Hepatic arterial chemoembolization for hepatocellular carcinoma: comparison of survival rates with different embolic agents, Journal of vascular and interventional radiology: JVIR 16(12) (2005) 1661-6.
- [49] A. Massmann, T. Rodt, S. Marquardt, R. Seidel, K. Thomas, F. Wacker, G.M. Richter, H.U. Kauczor, A. Bucker, P.L. Pereira, C.M. Sommer, Transarterial chemoembolization (TACE) for colorectal liver metastases--current status and critical review, Langenbeck's archives of surgery / Deutsche Gesellschaft für Chirurgie 400(6) (2015) 641-59.
- [50] P. Giunchedi, M. Maestri, E. Gavini, P. Dionigi, G. Rassu, Transarterial chemoembolization of hepatocellular carcinoma--agents and drugs: an overview. Part 2, Expert opinion on drug delivery 10(6) (2013) 799-810.
- [51] M.J. Abdekhodaie, X.Y. Wu, Drug loading onto ion-exchange microspheres: Modeling study and experimental verification, Biomaterials 27(19) (2006) 3652-3662.

[52] M.V. Gonzalez, Y. Tang, G.J. Phillips, A.W. Lloyd, B. Hall, P.W. Stratford, A.L. Lewis, Doxorubicin eluting beads-2: methods for evaluating drug elution and in-vitro:in-vivo correlation, Journal of materials science. Materials in medicine 19(2) (2008) 767-75.

- [53] C.L. Heaysman, G.J. Phillips, A.W. Lloyd, A.L. Lewis, Synthesis and characterisation of cationic quaternary ammonium-modified polyvinyl alcohol hydrogel beads as a drug delivery embolisation system, Journal of Materials Science: Materials in Medicine 27(3) (2016) 1-10.
- [54] M.R. Dreher, K.V. Sharma, D.L. Woods, G. Reddy, Y. Tang, W.F. Pritchard, O.A. Chiesa, J.W. Karanian, J.A. Esparza, D. Donahue, E.B. Levy, S.L. Willis, A.L. Lewis, B.J. Wood, Radiopaque drugeluting beads for transcatheter embolotherapy: experimental study of drug penetration and coverage in swine, Journal of vascular and interventional radiology: JVIR 23(2) (2012) 257-64.e4.
- [55] A.H. Negussie, M.R. Dreher, C.G. Johnson, Y. Tang, A.L. Lewis, G. Storm, K.V. Sharma, B.J. Wood, Synthesis and characterization of image-able polyvinyl alcohol microspheres for image-guided chemoembolization, Journal of materials science. Materials in medicine 26(6) (2015) 198.
- [56] R.E. Forster, Y. Tang, C. Bowyer, A.W. Lloyd, W. Macfarlane, G.J. Phillips, A.L. Lewis, Development of a combination drug-eluting bead: towards enhanced efficacy for locoregional tumour therapies, Anti-cancer drugs 23(4) (2012) 355-69.
- [57] K. Fuchs, P.E. Bize, O. Dormond, A. Denys, E. Doelker, G. Borchard, O. Jordan, Drug-eluting beads loaded with antiangiogenic agents for chemoembolization: in vitro sunitinib loading and release and in vivo pharmacokinetics in an animal model, Journal of vascular and interventional radiology: JVIR 25(3) (2014) 379-387 e2.
- [58] O.S. Sakr, S. Berndt, G. Carpentier, M. Cuendet, O. Jordan, G. Borchard, Arming embolic beads with anti-VEGF antibodies and controlling their release using LbL technology, Journal of controlled release: official journal of the Controlled Release Society 224 (2016) 199-207.
- [59] A. Hagan, W. Macfarlane, A. Lloyd, G. Phillips, R. Holden, Z. Bascal, R. Whomsley, H. Kilpatrick, Y. Tang, A. Lewis, J. Namur, F. Pascale, J. Pelage, In vitro and in vivo characterisation of a multiple tyrosine kinase inhibitor drug eluting bead, Journal of Vascular and Interventional Radiology 27(3) 584.

[60] M. D'Anzeo, L. Faloppi, M. Scartozzi, R. Giampieri, M. Bianconi, M. Del Prete, N. Silvestris, S. Cascinu, The role of micro-RNAs in hepatocellular carcinoma: from molecular biology to treatment, Molecules 19(5) (2014) 6393-406.

- [61] M. Zhang, X. Zhou, B. Wang, B.C. Yung, L.J. Lee, K. Ghoshal, R.J. Lee, Lactosylated gramicidin-based lipid nanoparticles (Lac-GLN) for targeted delivery of anti-miR-155 to hepatocellular carcinoma, Journal of controlled release: official journal of the Controlled Release Society 168(3) (2013) 251-61.
- [62] J. Varshosaz, M. Farzan, Nanoparticles for targeted delivery of therapeutics and small interfering RNAs in hepatocellular carcinoma, World journal of gastroenterology: WJG 21(42) (2015) 12022-41.
- [63] C.G. Johnson, Y. Tang, A. Beck, M.R. Dreher, D.L. Woods, A.H. Negussie, D. Donahue, E.B. Levy, S.L. Willis, A.L. Lewis, B.J. Wood, K.V. Sharma, Preparation of Radiopaque Drug-Eluting Beads for Transcatheter Chemoembolization, Journal of vascular and interventional radiology: JVIR 27(1) (2016) 117-126.e3.
- [64] A. Mikhail, E. Levy, V. Krishnasamy, F. Banovac, A. Negussie, W. Pritchard, J. Karanian, I. Bakhutashvili, J. Esparza-Trujillo, D. Woods, Y. Tang, C. Macfarlane, S. Willis, A. Lewis, B. Wood, Mapping drug dose distribution with conventional IR imaging following hepatic DEBTACE with drug-eluting radiopaque beads (DEROB), Journal of Vascular and Interventional Radiology 27(3) S126-S127.
- [65] X. Li, G.S. Feng, C.S. Zheng, C.K. Zhuo, X. Liu, Expression of plasma vascular endothelial growth factor in patients with hepatocellular carcinoma and effect of transcatheter arterial chemoembolization therapy on plasma vascular endothelial growth factor level, World journal of gastroenterology: WJG 10(19) (2004) 2878-82.
- [66] J.H. Shim, J.W. Park, J.H. Kim, M. An, S.Y. Kong, B.H. Nam, J.I. Choi, H.B. Kim, W.J. Lee, C.M. Kim, Association between increment of serum VEGF level and prognosis after transcatheter arterial chemoembolization in hepatocellular carcinoma patients, Cancer science 99(10) (2008) 2037-44.
- [67] A. Sergio, C. Cristofori, R. Cardin, G. Pivetta, R. Ragazzi, A. Baldan, L. Girardi, U. Cillo, P. Burra, A. Giacomin, F. Farinati, Transcatheter arterial chemoembolization (TACE) in hepatocellular carcinoma

(HCC): the role of angiogenesis and invasiveness, The American journal of gastroenterology 103(4) (2008) 914-21.

- [68] B. Wang, H. Xu, Z.Q. Gao, H.F. Ning, Y.Q. Sun, G.W. Cao, Increased expression of vascular endothelial growth factor in hepatocellular carcinoma after transcatheter arterial chemoembolization, Acta Radiol 49(5) (2008) 523-9.
- [69] G. Ranieri, M. Ammendola, I. Marech, A. Laterza, I. Abbate, C. Oakley, A. Vacca, R. Sacco, C.D. Gadaleta, Vascular endothelial growth factor and tryptase changes after chemoembolization in hepatocarcinoma patients, World journal of gastroenterology: WJG 21(19) (2015) 6018-6025.
- [70] G. Ranieri, I. Marech, V. Lorusso, V. Goffredo, A. Paradiso, D. Ribatti, C.D. Gadaleta, Molecular targeting agents associated with transarterial chemoembolization or radiofrequency ablation in hepatocarcinoma treatment, World journal of gastroenterology: WJG 20(2) (2014) 486-97.
- [71] V. Gogineni, S. White, Inhibition of HIF-1 alpha induced survival under hypoxic conditions in liver cancer cells, Journal of Vascular and Interventional Radiology 27(3) S21-S22.
- [72] K.Y. Tam, K.C. Leung, Y.X. Wang, Chemoembolization agents for cancer treatment, European journal of pharmaceutical sciences: official journal of the European Federation for Pharmaceutical Sciences 44(1-2) (2011) 1-10.
- [73] V. Verret, J.P. Pelage, M. Wassef, S. Louguet, E. Servais, L. Bedouet, T. Beaulieu, L. Moine, A. Laurent, A novel resorbable embolization microsphere for transient uterine artery occlusion: a comparative study with trisacryl-gelatin microspheres in the sheep model, Journal of vascular and interventional radiology: JVIR 25(11) (2014) 1759-66.
- [74] J. Golzarian, L. Weng, Particle embolization: factors affecting arterial distribution, Journal of vascular and interventional radiology: JVIR 25(11) (2014) 1773-4.
- [75] N. Maeda, V. Verret, L. Moine, L. Bedouet, S. Louguet, E. Servais, K. Osuga, N. Tomiyama, M. Wassef, A. Laurent, Targeting and recanalization after embolization with calibrated resorbable microspheres versus hand-cut gelatin sponge particles in a porcine kidney model, Journal of vascular and interventional radiology: JVIR 24(9) (2013) 1391-8.
- [76] J. Golzarian, 701.8 Resorbable particles: are they the future? (ID: 46), GEST 2013 Europe, Prague, Czech Republic, 2013.

[77] S. Wilhelm, C. Carter, M. Lynch, T. Lowinger, J. Dumas, R.A. Smith, B. Schwartz, R. Simantov, S. Kelley, Discovery and development of sorafenib: a multikinase inhibitor for treating cancer, Nature reviews. Drug discovery 5(10) (2006) 835-844.

- [78] L. Weng, H.C. Le, J. Lin, J. Golzarian, Doxorubicin loading and eluting characteristics of bioresorbable hydrogel microspheres: in vitro study, International journal of pharmaceutics 409(1-2) (2011) 185-93.
- [79] L. Weng, P. Rostamzadeh, N. Nooryshokry, H.C. Le, J. Golzarian, In vitro and in vivo evaluation of biodegradable embolic microspheres with tunable anticancer drug release, Acta Biomater 9(6) (2013) 6823-33.
- [80] L. Weng, D. Seelig, P. Rostamzadeh, J. Golzarian, Calibrated Bioresorbable Microspheres as an Embolic Agent: An Experimental Study in a Rabbit Renal Model, Journal of vascular and interventional radiology: JVIR 26(12) (2015) 1887-94 e1.
- [81] J.S. Kim, B.K. Kwak, H.J. Shim, Y.C. Lee, H.W. Baik, M.J. Lee, S.M. Han, S.H. Son, Y.B. Kim, S. Tokura, B.M. Lee, Preparation of doxorubicin-containing chitosan microspheres for transcatheter arterial chemoembolization of hepatocellular carcinoma, Journal of microencapsulation 24(5) (2007) 408-19.
- [82] B.K. Kwak, H.J. Shim, S.M. Han, E.S. Park, Chitin-based embolic materials in the renal artery of rabbits: pathologic evaluation of an absorbable particulate agent, Radiology 236(1) (2005) 151-8.
- [83] L. Bedouet, V. Verret, S. Louguet, E. Servais, L. Moine, A. Laurent, Doxorubicin, irinotecan and sunitinib: loading and release with a resorbable embolization microsphere (REM), Journal of Vascular and Interventional Radiology 24(4) S48.
- [84] A.L. Lewis, M.V. Gonzalez, S.W. Leppard, J.E. Brown, P.W. Stratford, G.J. Phillips, A.W. Lloyd, Doxorubicin eluting beads 1: effects of drug loading on bead characteristics and drug distribution, Journal of materials science. Materials in medicine 18(9) (2007) 1691-9.
- [85] L. Bedouet, V. Verret, S. Louguet, E. Servais, F. Pascale, A. Beilvert, M.T. Baylatry, D. Labarre, L. Moine, A. Laurent, Anti-angiogenic drug delivery from hydrophilic resorbable embolization microspheres: an in vitro study with sunitinib and bevacizumab, International journal of pharmaceutics 484(1-2) (2015) 218-27.

[86] Y. Wang, D.G.M. Molin, C. Sevrin, C. Grandfils, N.M.S. van den Akker, M. Gagliardi, M.L. Knetsch, T. Delhaas, L.H. Koole, In vitro and in vivo evaluation of drug-eluting microspheres designed for transarterial chemoembolization therapy, International journal of pharmaceutics 503(1–2) (2016) 150-162.

- [87] J. Lammer, K. Malagari, T. Vogl, F. Pilleul, A. Denys, A. Watkinson, M. Pitton, G. Sergent, T. Pfammatter, S. Terraz, Y. Benhamou, Y. Avajon, T. Gruenberger, M. Pomoni, H. Langenberger, M. Schuchmann, J. Dumortier, C. Mueller, P. Chevallier, R. Lencioni, Prospective randomized study of doxorubicin-eluting-bead embolization in the treatment of hepatocellular carcinoma: results of the PRECISION V study, Cardiovascular and interventional radiology 33(1) (2010) 41-52.
- [88] A. Poursaid, M.M. Jensen, E. Huo, H. Ghandehari, Polymeric materials for embolic and chemoembolic applications, Journal of Controlled Release (2016).
- [89] E. Lilienberg, C. Ebeling Barbier, R. Nyman, M. Hedeland, U. Bondesson, N. Axen, H. Lennernas, Investigation of hepatobiliary disposition of doxorubicin following intrahepatic delivery of different dosage forms, Molecular pharmaceutics 11(1) (2014) 131-44.
- [90] M.T. Baylatry, J.P. Pelage, M. Wassef, H. Ghegediban, A.C. Joly, A. Lewis, P. Lacombe, C. Fernandez, A. Laurent, Pulmonary artery chemoembolization in a sheep model: Evaluation of performance and safety of irinotecan eluting beads (DEB-IRI), Journal of biomedical materials research. Part B, Applied biomaterials 98B(2) (2011) 351-9.
- [91] P.P. Rao, F. Pascale, A. Seck, A. Auperin, L. Drouard-Troalen, F. Deschamps, C. Teriitheau, A. Paci, A. Denys, P. Bize, T. de Baere, Irinotecan Loaded in Eluting Beads: Preclinical Assessment in a Rabbit VX2 Liver Tumor Model, Cardiovascular and interventional radiology (2012).
- [92] P. Bize, R. Duran, K. Fuchs, O. Dormond, J. Namur, L.A. Decosterd, O. Jordan, E. Doelker, A. Denys, Antitumoral Effect of Sunitinib-eluting Beads in the Rabbit VX2 Tumor Model, Radiology 280(2) (2016) 425-35.
- [93] K. Hong, A. Khwaja, E. Liapi, M.S. Torbenson, C.S. Georgiades, J.F. Geschwind, New intraarterial drug delivery system for the treatment of liver cancer: preclinical assessment in a rabbit model of liver cancer, Clinical cancer research: an official journal of the American Association for Cancer Research 12(8) (2006) 2563-7.

[94] J. Namur, S.J. Citron, M.T. Sellers, M.H. Dupuis, M. Wassef, M. Manfait, A. Laurent, Embolization of hepatocellular carcinoma with drug-eluting beads: doxorubicin tissue concentration

and distribution in patient liver explants, Journal of hepatology 55(6) (2011) 1332-8.

[95] K. Tanaka, N. Maeda, K. Osuga, Y. Higashi, A. Hayashi, Y. Hori, K. Kishimoto, E. Morii, F. Ohashi, N. Tomiyama, In Vivo Evaluation of Irinotecan-Loaded QuadraSphere Microspheres for Use in Chemoembolization of VX2 Liver Tumors, Journal of Vascular and Interventional Radiology 25(11) 1727-1735.e1.

- [96] J. Namur, Microsphères d'embolisation pour la vectorisation de principes actifs : étude de la libération in vivo par microspectroscopies optiques, Université de Reims Champagne-Ardenne, 2009.
- [97] J. Namur, M. Wassef, J.M. Millot, A.L. Lewis, M. Manfait, A. Laurent, Drug-eluting beads for liver embolization: concentration of doxorubicin in tissue and in beads in a pig model, Journal of vascular and interventional radiology: JVIR 21(2) (2010) 259-67.
- [98] I.R. Dubbelboer, E. Lilienberg, E. Ahnfelt, E. Sjögren, N. Axén, Lennernäs, Hans, Treatment of intermediate stage hepatocellular carcinoma: a review of intrahepatic doxorubicin drug-delivery systems, Therapeutic delivery 5(4) (2014) 447-466.
- [99] K. Fuchs, A. Kiss, P.E. Bize, R. Duran, A. Denys, G. Hopfgartner, G. Borchard, O. Jordan, Mapping of Antiangiogenic Drug Distribution in a Rabbit Model of Liver Cancer by Fluorescence Microscopy and MALDI-SRM/MS Imaging, Controlled Release Society Annual Meeting and Exposition, Seattle, WA, USA., 2016.
- [100] B.E. Houk, C.L. Bello, D.W. Kang, M. Amantea, A Population Pharmacokinetic Meta-analysis of Sunitinib Malate (SU11248) and Its Primary Metabolite (SU12662) in Healthy Volunteers and Oncology Patients, Clinical Cancer Research 15(7) (2009) 2497-2506.
- [101] J. Folkman, Angiogenesis: an organizing principle for drug discovery?, Nature reviews. Drug discovery 6(4) (2007) 273-286.
- [102] J. Namur, F. Pascale, N. Maeda, M. Sterba, S.H. Ghegediban, V. Verret, A. Paci, A. Seck, K. Osuga, M. Wassef, P. Reb, A. Laurent, Safety and efficacy compared between irinotecan-loaded

microspheres HepaSphere and DC bead in a model of VX2 liver metastases in the rabbit, Journal of vascular and interventional radiology: JVIR 26(7) (2015) 1067-1075 e3.

[103] M.-T. Baylatry, Lung chemoembolization with drug eluting beads : in vivo evaluation of anticancer drug release, Université Paris Sud - Paris XI, 2011.

[104] V. Verret, C. Bevilacqua, I. Schwartz-Cornil, J.P. Pelage, M. Wassef, J. Namur, L. Bedouet, A.L. Lewis, P. Martin, A. Laurent, IL6 and TNF expression in vessels and surrounding tissues after embolization with ibuprofen-loaded beads confirms diffusion of ibuprofen, European journal of pharmaceutical sciences: official journal of the European Federation for Pharmaceutical Sciences 42(5) (2011) 489-95.

[105] S. Ohta, N. Nitta, A. Sonoda, A. Seko, T. Tanaka, M. Takahashi, Y. Kimura, Y. Tabata, K. Murata, Cisplatin-conjugated degradable gelatin microspheres: fundamental study in vitro, The British journal of radiology 82(977) (2009) 380-385.

[106] J. Namur, M. Wassef, J.P. Pelage, A. Lewis, M. Manfait, A. Laurent, Infrared microspectroscopy analysis of ibuprofen release from drug eluting beads in uterine tissue, Journal of controlled release : official journal of the Controlled Release Society 135(3) (2009) 198-202.

[107] D.S. Wishart, C. Knox, A.C. Guo, S. Shrivastava, M. Hassanali, P. Stothard, Z. Chang, J. Woolsey, DrugBank: a comprehensive resource for in silico drug discovery and exploration, Nucleic acids research 34(Database issue) (2006) D668-72.

[108] M. Remko, A. Bohac, L. Kovacikova, Molecular structure, pKa, lipophilicity, solubility, absorption, polar surface area, and blood brain barrier penetration of some antiangiogenic agents, Structural Chemistry 22(3) (2011) 635-648.

[109] Pr SUTENT® Sunitinib capsules. http://www.pfizer.ca/en/our_products/products/ monograph/147>, 2014 (accessed August 26, 2016.).

Drug-Eluting Beads Loaded with Anti-Angiogenic
Agents for Chemoembolization: *In Vitro* Sunitinib
Loading, Release and *In Vivo* Pharmacokinetics in
an Animal Model

Katrin Fuchs^a, Pierre E. Bize^b, Olivier Dormond^c, Alban Denys^b, Eric Doelker^a, Gerrit Borchard^a, Olivier

Jordan^a

^a School of Pharmaceutical Sciences, University of Geneva, University of Lausanne, Switzerland
^b Departments of Radiology and Interventional Radiology, CHUV University of Lausanne, Switzerland
^c Department of Visceral Surgery, CHUV University of Lausanne, Switzerland

Original Research Article

Published in:

Journal of Vascular and Interventional Radiology: JVIR. 2014, 25 (3), p. 379-87 e2.

Abstract

Purpose: The combination of embolic beads with a multi-targeted tyrosine kinase inhibitor that inhibits tumor vessel growth is suggested as an alternative and improvement to the current standard doxorubicin-eluting beads for use in transarterial chemoembolization. This study demonstrates the *in vitro* loading and release kinetics of sunitinib using commercially available embolization microspheres, and evaluates the *in vitro* biological efficacy on cell cultures and the resulting *in vivo* pharmacokinetic profiles in an animal model.

Materials and Methods: DC Bead microspheres, 70-150 μ m and 100-300 μ m (Biocompatibles Ltd., Farnham, United Kingdom), were loaded by immersion in sunitinib solution. Drug release was measured in saline in a USP-approved flow-through apparatus and quantified by spectrophotometry. Activity after release was confirmed in cell culture. For pharmacokinetics and *in vivo* toxicity evaluation, New-Zealand white rabbits received sunitinib either by intra-arterial injection of 100-300 μ m sized beads or per os. Drug concentrations in the plasma and liver tissue were assessed by liquid chromatography—tandem mass spectrometry.

Results: Sunitinib loading on beads was close to complete and homogeneous. A total release of 80% in saline was measured, with similar fast release profiles for both sphere sizes. After embolization, drug plasma levels remained below the therapeutic threshold (< 50 ng/ml), but high concentrations at 6 h (14.9 μ g/g) and 24 h (3.4 μ g/g) were found in the liver tissue.

Conclusions: DC Bead microspheres of two sizes were efficiently loaded with sunitinib and displayed a fast and almost complete release in saline. High liver drug concentrations and low systemic levels indicated the potential of sunitinib-eluting beads for use in embolization.

Keywords:

Hepatocellular carcinoma, transarterial chemoembolization, drug-eluting beads, anti-angiogenic agent, sunitinib

1 Introduction

Embolization techniques are widely used to treat various types of hypervascular liver tumors. Recent studies have discussed the potential benefit of drug eluting beads (DEBs) over conventional transarterial chemoembolization (1, 2). These two options differ by the use of embolic agent, the time span and the amount of drug delivered to the tumor. However, this therapeutic approach suffers from two main drawbacks: first doxorubicin might not be the ideal drug for this application (3-5), second the ischemia induced by the embolization procedure contributes to the formation of new vessel sprouts, particularly in the periphery of the tumor (6-8).

The combination of the (doxorubicin-loaded) spheres with systemic anti-angiogenic therapy has already been reported (9-11), and several phase II and III trials with oral sunitinib (SATURNE) or sorafenib are under way or completed (12, 13). Sunitinib malate (SU11248) is available as an oral formulation from Pfizer (New York, New York) and was approved by the U.S. Food and Drug Administration in 2006 for the treatment of renal cell carcinoma and imatinib-resistant gastrointestinal stromal tumor (14). This drug acts as a potent inhibitor of several tyrosine kinases, mainly vascular endothelial growth factor (VEGF) and platelet-derived growth factor receptors (15).

Its lack of specificity results in numerous side effects, including fatigue, nausea and diarrhea (16-19). Therefore, the local delivery of sunitinib via DEB could be a reasonable means to reduce systemic toxicity compared to oral treatment while maintaining local anti-tumoral efficacy.

In the first part of this investigation, sunitinib loading and release kinetics of small-sized beads and the size effects related to drug loading were examined *in vitro*, resulting in an understanding of the affinity and interaction of the active principle with its carrier.

In the second part of this study, the efficacy of sunitinib-eluting beads on an endothelial cell line and several cancer cell lines compared to unloaded beads and free sunitinib was investigated.

In the third section, we addressed the *in vivo* pharmacokinetics and tolerance of 100-300 μ m sunitinib-eluting beads in healthy New Zealand white rabbits, comparing sunitinib concentrations after given time points in the tissue and in the systemic circulation after local and oral

administration. Toxicity was examined by monitoring the liver enzyme activity and general animal status.

2 Materials and Methods

2.1 Materials

DC Bead samples of 70-150 μm and 100-300 μm diameter range (Biocompatibles Ltd., Farnham, UK) were selected for the study.

Sunitinib was purchased as base from LC Laboratories, Woburn, MA, USA. Other chemicals were of analytical grade and were used as received.

2.2 Methods

2.2.1 **DEBs Characterization**

Loading of Sunitinib into Beads. The beads were loaded by incubation in different amounts of a sunitinib stock solution (10 mg/ml), which was prepared according to a proprietary protocol (20).

The amount of drug loading was determined indirectly by measuring the residual unloaded drug in the supernatant of the beads suspension using UV-Vis spectrophotometry at 430 nm (HP 8453, Agilent Technologies AG, Basel, Switzerland).

Release of Sunitinib from Beads. The flow-through United States Pharmacopeia method IV using a Sotax CE 6 (Sotax, Allschwil, Switzerland) served to quantify the drug released from sunitinib-eluting beads in saline.

The loading and release profiles were compared using the similarity factor f_2 , following FDA guidelines for dissolution profile comparison (21-23).

Microsphere Morphometry. Beads were imaged with a Zeiss Axiovert 200 microscope (Carl Zeiss, Feldbach, Switzerland). The size was measured using the open source image analysis software (ImageJ 1.38 software; NIH, Bethesda, MD, USA), analyzing an average of 150 microspheres in a

monolayer. Statistical analysis was performed using a two-sided Student's t-test, at a significance level P = 0.001. Details of DEB characterization can be found in Appendix A (Section 7 Supplementary Material).

2.2.2 **Proof of Biological Efficacy in a Cell Culture Model**

Cells were exposed to control beads, sunitinib-eluting microspheres and free sunitinib to study the ligand-receptor interactions and cell viability.

Sunitinib-eluting beads, size 70-150 μ m, were prepared under sterile conditions at a concentration of 10 μ mol/l/well (\approx 4 μ g/ml, 40 mg beads/well).

Human umbilical vein endothelial cells (HUVECs) were obtained from Lonza Ltd, Visp, Switzerland and were cultured in endothelial growth medium (EGM; Lonza Ltd). Additionally, 786-0 and Caki-1 (kidney), LS174T and SW480 (colon), MDA-MB-231 (breast) and A549 (NSCLC) were purchased from the American Type Culture Collection and were cultured in Dulbecco's Modified Eagles' medium with 10% fetal calf serum, containing 4.5 g/l glucose, L-glutamine, 100 units/ml penicillin and 100 μg/ml streptomycin (Sigma-Aldrich, Buchs, Switzerland). Cells were plated on the upper side of transwells in triplicate at a density of 10⁴ cells/well. Control beads, sunitinib-eluting beads or sunitinib solution was added to the lower part of the transwell.

Phosphorylation of VEGFR2. After 1 h of treatment and stimulation with VEGF (catalog number 100-20; Pepro-Tech France, Neuilly-Sur-Seine, France) for 30 min, the HUVECs were washed once with phosphate-buffered saline and lysed in RIPA Lysis Buffer (Santa Cruz Biotechnology, Inc, Heidelberg, Germany) containing 1 mmol/l sodium orthovanadate and protease inhibitor cocktail (Sigma-Aldrich). An equal amount of protein (20 μg) was separated on 4-12% polyacrylamide gel and subsequently transferred to a polyvinylidene difluoride membrane (Millipore, Zug, Switzerland). Membranes were blocked with the Odyssey blocking buffer (LI-COR Biosciences, Lincoln, Nebraska) and immunoblotted with primary antibodies (rabbit antihuman VEGF #2479, rabbit antihuman phosphorylated vascular endothelial growth factor receptor 2 [pVEGFR2] #4991, Cell signaling Technology, Inc, Danvers, Massachusetts), followed by infrared secondary antibodies (Alexa fluor 680 goat antirabbit #A21109, Invitrogen AG, Basel, Switzerland). Bands from

immunoreactive proteins were visualized by an Odyssey infrared imaging system (LI-COR Biosciences).

HUVEC Migration. HUVEC migration to the lower surface of the filter in the transwells was determined by counting the cells under light microscopy in three high-power fields. For this, transwells were fixed in 2% paraformaldehyde and stained with 0.5% crystal violet 3 h after the addition of the control, sunitinib-eluting beads or sunitinib.

Proliferation and Survival of Cell Lines. All cell types were evaluated by cell counting using a Neubauer hemocytometer and by a Cell Death Detection ELISA^{plus} kit (Roche Diagnostics, Basel, Switzerland) after 24 h of treatment.

Cell Growth in Three-Dimensional Colonies. The capability of the cells to grow in three-dimensional colonies was examined by mixing five hundred 786-0 or Caki-1 cells into Matrigel (BD Biosciences, Allschwil, Switzerland) and plating them on 12-well plates. After 24 h, control beads, sunitinib beads or sunitinib were added to the wells. The number of colonies was counted after 10 days of culture.

2.2.3 **Preclinical In Vivo Studies**

All *in vivo* experiments were carried out at the Centre de Recherche en Imagerie Interventionnelle CR2i in Jouy-en-Josas, France. They were approved by the institutional animal care and use committee of the Center and were conducted according to European Community rules of animal care (Directive EC 86/609).

Experimental Protocol. Healthy New Zealand white rabbits (n = 15; 3.2 - 3.8 kg) were separated into 3 groups. Group 1 and group 2 received 0.2 ml of sunitinib-eluting beads in the hepatic artery. The animals in group 1 (n=4) were sacrificed 6 h after embolization. Animals in group 2 (n=7) were sacrificed one day after embolization. The third group (n=4) received a single dose of sunitinib (6 mg) per os, which should result in therapeutic plasma concentrations (c_{max}) of 45-55 ng/ml, according to previous pharmacological studies (24, 25). In this third group, 2 animals were sacrificed at 6 h, and 2 animals were sacrificed at 24 h.

Preparation of Sunitinib-Loaded Beads and Oral Solution. Syringes prefilled with sunitinib-loaded 100-300 μm sized beads (6 mg sunitinib per 0.2 ml beads per syringe) were prepared under aseptic laminar air-flow conditions for pharmacokinetic studies in rabbits (details can be found in Appendix B [Section 7 Supplementary Material]). The oral sunitinib solution (1 mg/ml) was prepared by diluting the stock solution (10 mg/ml) with pre-filtered glucose 5% (w/v).

Transarterial Chemoembolization Procedure. Embolization procedures were performed under general anesthesia with isoflurane. Access to the right common femoral artery was obtained via surgical cutdown, where a 4 F vascular sheath (Radifocus®, Terumo, Leuwen, Belgium) was introduced. A 2.1/1.7 F, 45° tip microcatheter (Echelon, ev3, Paris, France) was then advanced and used to engage the celiac trunk followed by common hepatic artery under fluoroscopy. Common hepatic arteriography (Omnipaque 300, GE Healthcare, Aulnay-sous-Bois, France) was performed to demonstrate the arterial anatomy. Sunitinib loaded beads were injected through the microcatheter.

Injections were performed as followed: beads were suspended in a total volume of 1 ml and slowly infused by hand in the common hepatic artery, over a period of 20-30 minutes under careful real time fluoroscopy to prevent non-target embolization. Immediately after completion of embolization procedures post-anesthesia care was provided and the animals were monitored.

Dosage of Sunitinib after Administration. Liver enzymes were measured immediately before embolization or oral administration of the drug and at 6 h in all groups and again at 24 h in group 2 and in 2 animals in group 3. Sunitinib plasma levels were measured immediately before and at the end of the embolization procedure, as well as 1, 2, 3, 4, 5 and 6 h after administration and after 24 h for group 2. Plasma levels were determined in only 3 out of 4 animals of group 3 for technical reasons. Whole blood samples were collected into potassium ethylenediaminetetraacetic acid tubes and centrifuged. Plasma samples were stored at -20°C until analysis by liquid chromatography-tandem mass spectrometry (26). Measurements of sunitinib were performed in 4 tissue samples per animal to limit sampling errors (2 in the right lobe and 2 in the left lobe), using the same mass spectrometry method after sacrifice.

3 Results

3.1 Loading of Sunitinib into Beads

Beads showed close to complete loading with sunitinib (100% for 70-150 μ m and 97% for 100-300 μ m sized beads) after a two-hour incubation under agitation and at a loading concentration of 30 mg sunitinib/g beads. Experiments with 100-300 μ m beads showed a maximal drug loading capacity of 32 mg drug/g beads, though at an inferior loading efficiency (Figure 1). Thus, all of the following tests were carried out at a concentration of 30 mg sunitinib per gram of beads.

Profile comparison of the fraction of sunitinib loaded into 70-150 μ m and 100-300 μ m sized spheres showed initially different profiles until t = 30 min (similarity factor f_2 = 47), converging to complete drug loading with an f_2 = 51 for longer incubation periods, indicating profile equivalence of the loading for the two different bead sizes.

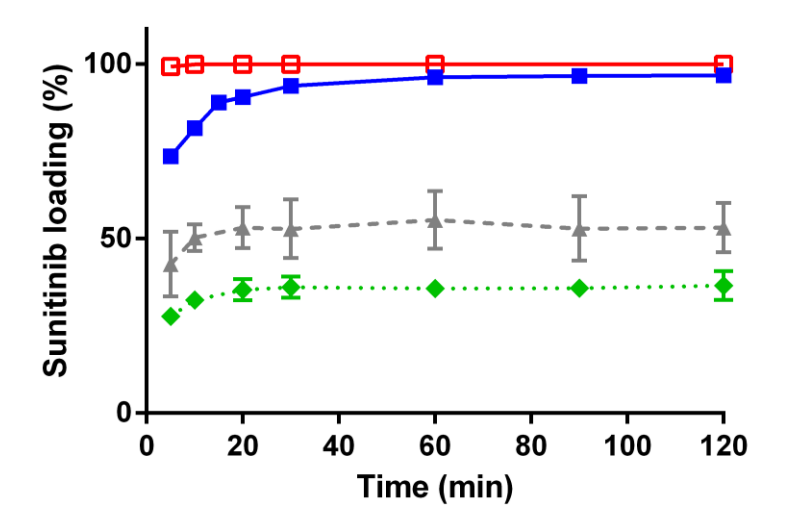


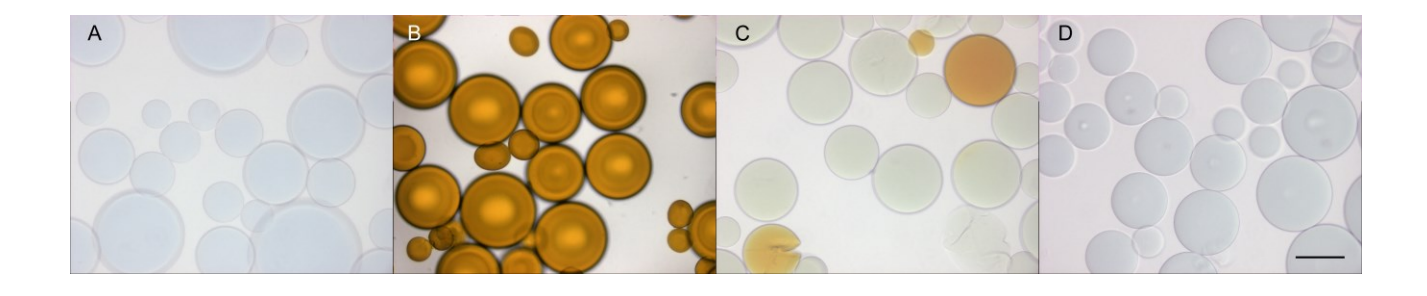
Figure 1. Loading profiles of 70-150 μ m (\square , n=4) and 100-300 μ m (\blacksquare , n=3) beads with a maximal loading of 30 mg sunitinib/g beads and 100-300 μ m sized beads loaded with 60 (\blacktriangle , n=3) and 90 (\blacklozenge , n=3) mg sunitinib/g beads.

3.2 Bead Size Changes with Sunitinib Loading

The microsphere spherical shape was preserved without aggregation or particle damage during loading and after release (Figure 2). Loaded beads were colored an intense orange due to drug

absorption. Beads lost this coloration upon elution by ionic exchange in isotonic NaCl solution. However, Figure 2C shows an inhomogeneous bead discoloration in saline even after several days under flow, which occurs when aggregates form and shield the inner beads from the elution medium. Beads regained the initial blue appearance without any yellow traces upon ethanol addition, thus validating the ethanol wash as an internal standard for 100% drug release.

At 30 mg sunitinib/g beads loading, both sphere sizes shrunk significantly (P < 0.001) by 17% (70-150 μ m) and 15% (100-300 μ m) and in volume by 44% (70-150 μ m) and 39% (100-300 μ m). Initial mean diameters of 126 \pm 17 μ m and 184 \pm 66 μ m decreased to 104 \pm 14 μ m and 156 \pm 50 μ m, respectively. Figure E 1A–D (Section 7 Supplementary Material) elucidates the shift in bead size and the bead size distribution. This phenomenon was found to be reversible after the release of the drug with diameters of 131 \pm 17 μ m vs. 210 \pm 73 μ m in saline and 140 \pm 20 vs. 231 \pm 81 in saline/30% ethanol (V/V).



Solutinion 20 2 4 6 70 75
Time (hours)

Ε

Figure 2. 100-300 μ m beads (A) in saline, (B) after loading (30 mg sunitinib/g beads), (C) after elution in NaCl 0.9% and (D) after elution in NaCl 0.9%/ethanol 30% in a flow-through apparatus. The scale bar indicates 200 μ m. (E) Flow-through release profiles of 70-150 μ m (\square , n=5) and 100-300 μ m (\square , n=3) sunitinib-eluting beads showed equivalence for the two bead sizes. Error bars display standard deviation.

3.3 Release of Sunitinib from Loaded Beads

Similar release profiles for 70-150 μ m and 100-300 μ m sized spheres were obtained (Figure 2E). The drug release half time $t_{50\%}$ was 1.1 h for 70-150 μ m beads and 1.6 h for 100-300 μ m beads, whereas the difference in $t_{75\%}$ was greater (13 h vs 8 h, respectively).

Sink conditions were kept throughout the whole experiment, attaining maximum concentrations of approximately 27.5 mg/l during drug elution, far below the drug solubility of 25 g/L (27).

Profile comparisons showed similarity with f_2 = 81, and no significant differences were found between 70-150 µm and 100-300 µm sized beads. Values within the first 3 h of release were more distinct with f_2 = 67, albeit still indicating a similar initial release profile.

Final release values plateaued at 81% (70-150 μ m beads) and 82% (100-300 μ m beads). A two-tailed unpaired Student's t-test for the average release of the two bead sizes at 1.5, 2 and 3 days when the plateau was reached revealed P = 0.662, 0.546 and 0.594, respectively, indicating similar fractions of sunitinib were released. Overall, sunitinib was released from beads of both sizes in saline in a fast manner and to a large extent.

3.4 Biological Efficacy in Cell Culture

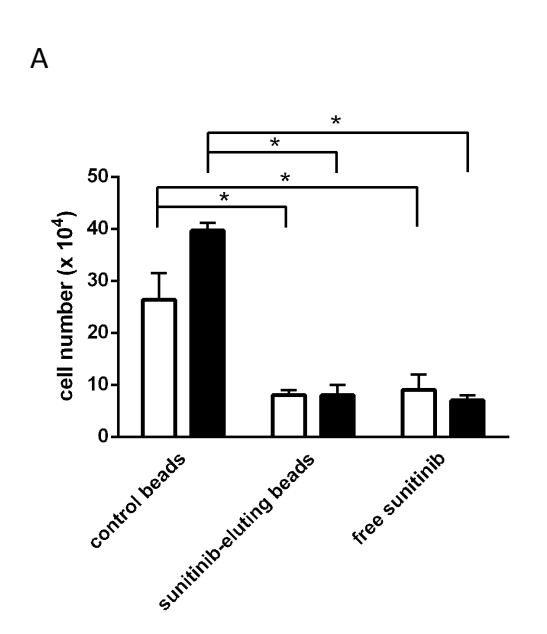
3.4.1 Effects of Sunitinib-Eluting Beads on Endothelial Cell Proliferation, Survival and Migration

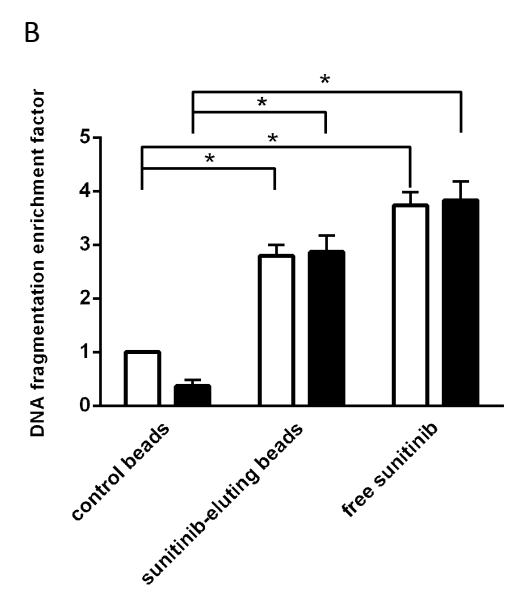
To assess the activity of the anti-angiogenic agent sunitinib, the effects of this drug on human umbilical vein endothelial cells (HUVECs) as an indicator of tumor progression were investigated.

As expected, VEGF increased the phosphorylation of VEGFR2, a growth factor receptor present on endothelial cells, in the presence of control beads. In contrast, sunitinib-eluting beads and sunitinib reduced the baseline phosphorylation of VEGFR2 and blocked VEGF-induced VEGFR2 phosphorylation (Figure E 3 [Section 7 Supplementary Material]).

A nonparametric, paired Friedmann test validated the significant effects of sunitinib on HUVEC proliferation (P = 0.0040), apoptosis (P = 0.0137) and migration (P = 0.0162). Herein, VEGF addition did not significantly affect the activity of sunitinib on the cells, as the nonparametric Wilcoxon test revealed with P > 0.9999 in the three assays. The mean cell numbers (in the proliferation and migration assays) and the mean DNA enrichment factors (in the apoptosis assay) after treatment with sunitinib-eluting beads or free sunitinib were outside of the 95% confidence interval (CI) of the controls, both with and without VEGF addition. This comparison takes into account the standard deviation of the results and reinforces the hypothesis that sunitinib has a significant effect on HUVECs.

To summarize, VEGF-induced HUVEC responses were inhibited by sunitinib-eluting beads (Figure 3A-C, Figure E 2 [Section 7 Supplementary Material]).





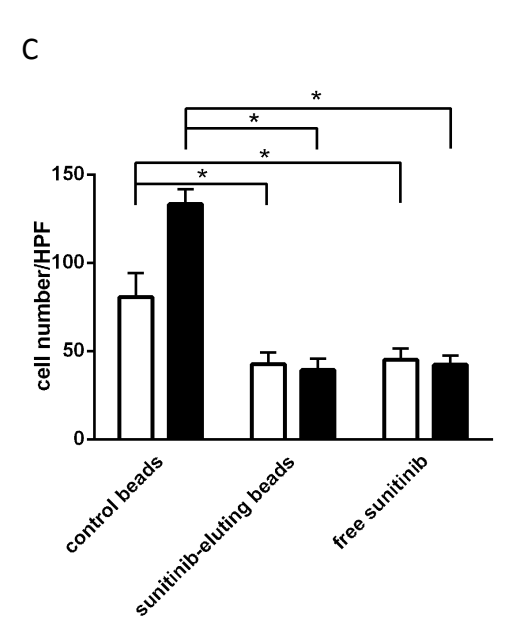


Figure 3. Effects of sunitinib-eluting beads on (A) HUVEC proliferation, (B) HUVEC apoptosis, (C) HUVEC migration. (A) and (B) Endothelial cells were treated with control beads, sunitinib-eluting beads or sunitinib in the presence (black columns) or not (white columns) of VEGF. After 24 h, endothelial cell proliferation was determined by cell counting (± SD) and endothelial cell apoptosis was measured by quantifying DNA fragmentation following the manufacturer's instructions (absorbance of the treated cells/absorbance of the control cells). (C) The migration of endothelial cell stimulated (black columns) or not (white columns) with VEGF was quantified in presence of control beads, sunitinibeluting beads or sunitinib. Significance (*) indicates that the mean cell numbers (A, C) and the mean DNA enrichment factors (B) after treatment with sunitinib-eluting beads or free sunitinib were outside of the 95% confidence interval of the respective controls. VEGF-induced endothelial cell responses were inhibited by sunitinib-eluting beads. HPF = high-power field.

3.4.2 Effects of Sunitinib-Eluting Beads on Cancer Cell Proliferation, Survival and Three-Dimensional Growth

The proliferation assay revealed that sunitinib-eluting beads reduced the proliferation of the renal cancer cell lines 786-0 and Caki-1, LS174T (colon), MDA-MB-231 (breast) and A549 (NSCLC) to a similar extent as sunitinib when compared with control beads (Figure 4, P = 0.009 in nonparametric Friedmann test). No toxicity was observed with the control beads alone. Following treatment with sunitinib-eluting beads or free sunitinib, the mean amounts of cell proliferation for the 786-0 and A-549 cells were located outside of the 95% CI of the control, indicating that these cells showed the most significant reduction in proliferation.

In contrast, sunitinib-eluting beads or free sunitinib did not affect the cancer cell survival. Moreover, they showed no effect on the SW480 colon cancer cell line in either the proliferation

assay or the survival assay. Finally, sunitinib-eluting beads also reduced the growth of 786-0 and Caki-1 cells in Matrigel as observed by a reduction of the number of colonies formed in Matrigel (Figure E 3 [Section 7 Supplementary Material]).

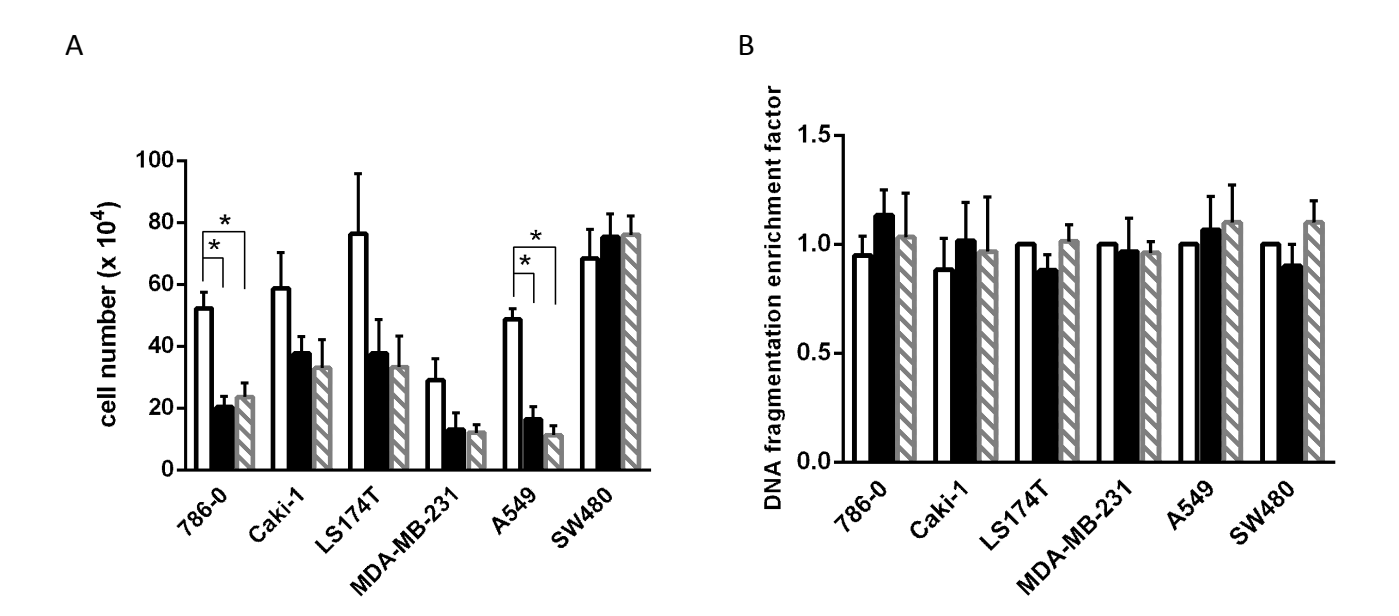


Figure 4. Sunitinib-eluting beads (black columns) and free sunitinib (shaded columns) affected (A) cancer cell proliferation, but not (B) apoptosis compared to control beads (white columns). After 24 h, cell proliferation was determined by cell counting and endothelial cell apoptosis was measured by quantifying DNA fragmentation following the manufacturer's instructions (absorbance of the treated cells/absorbance of the control cells). Significance (*) indicates that the means (± SD) after treatment with sunitinib-eluting beads or free sunitinib were outside of the 95% confidence interval of the respective controls.

3.5 Preclinical *In Vivo* Studies with Healthy New Zealand White Rabbits

Transarterial Chemoembolization Procedure. A total of eleven hepatic artery catheterizations were performed. Three animals in group 2 died from catheterization-related complications (gastric ischemia and perforation), during the 24 h observation period. The injection of the beads was technically not feasible in one animal in this group. Finally, four animals were analysed in group 1 and the three animals that reached the scheduled time of sacrifice in group 2.

Toxicity. Injection of 100-300 μm beads loaded with sunitinib in the common hepatic artery of rabbits resulted in an expected elevation of transaminases (alanine transaminase ALT, aspartate

transaminase AST, Table E 1 [Section 7 Supplementary Material]). Alkaline phosphatase (ALP), another biomarker for liver cytolysis, showed a 3-fold increase from the baseline to 54 ± 54 UI/I. Bilirubin levels were never detected to be higher than 10 μ mol/I after embolization or oral administration of sunitinib and were therefore below the sensitivity limit of the method.

Areas of necrosis were noted at the surface of some livers during necropsy and liver harvesting.

Pharmacokinetics. The tissue concentration of sunitinib in the harvested livers was found to be high at $14.9 \pm 4.7 \,\mu\text{g/g}$ (n=4) and $3.4 \pm 0.8 \,\mu\text{g/g}$ of tissue (n=3) at 6 and 24 h, respectively, when the beads were administered intra-arterially. Lower, but still high, drug levels were achieved by the peroral route (4.2 ± 0.6 $\,\mu\text{g/g}$ after 6 h (n=2) and 2.6 ± 2.6 $\,\mu\text{g/g}$ after 24 h (n=2)). Embolization of the hepatic artery with sunitinib-eluting beads resulted in a local concentration 3.5 times higher after 6 h and 1.3 times higher after 24 h than after oral administration.

In both administration routes, the plasmatic sunitinib levels remained below the theoretical therapeutic threshold of 50 ng/ml, with slightly higher levels after intra-arterial administration (Figure 5). The low 24 h value (p.o.) of 7 ng/ml was determined in an animal whose plasma levels accounted only for 4 ng/ml at 6 h.

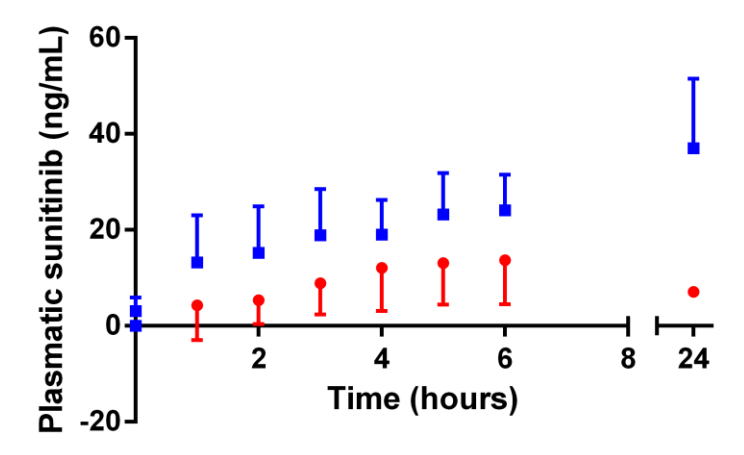


Figure 5. Plasmatic sunitinib levels after oral administration (●) of a single dose of 6 mg of sunitinib and after embolization of the hepatic artery (■) with sunitinib-eluting beads were below the therapeutic threshold of 50 ng/ml.

4 Discussion

The bead consists of poly(vinyl alcohol)-based hydrogel linked to sulfonate groups, resulting in a negatively charged structure (28, 29) that loads the protonated sunitinib with good performance. In accordance with Lewis' investigations, which did not show a significant difference in the loading kinetics for the smallest tested bead size ranges of 100 to 500 μ m (28), the f_2 factor comparison revealed similar loading curves for the tested bead sizes.

As observed for doxorubicin-loaded beads, sunitinib-loaded beads undergo size changes. A similar shrinking was found without major changes in the size distribution profile of the beads. Bead shrinking may have implications *in vivo* because more distal arterioles can be blocked by smaller beads. Padia et al. (30) have recently favored the utilization of smaller (100-300 μ m) beads in hepatocellular carcinoma because fewer side effects and a more complete response was observed when compared with 300-500 μ m beads.

A similar, relatively fast drug release of more than 80% in approximately 3 h was shown for both sizes in saline. In the absence of salts, negligible drug elution occurs (29, 31), as observed during eight-week extraction assays in 5% glucose, which served as an isotonic storage medium in the syringes for the preclinical studies.

Like sunitinib, two other drugs of clinical interest, doxorubicin and irinotecan, can be efficiently loaded into beads, but these drugs display distinct features in terms of elution extent and kinetics (32). In contrast to the complete or almost complete irinotecan and sunitinib elution (100% and 82%, respectively), doxorubicin was partially retained in the beads under saline flow (28% of drug eluted), which could be attributed to stronger ionic interactions with sulfonates or to doxorubicin *in situ* gelation (33). Drug physicochemical properties such as solubility and polarity and sterical ligand hindrance govern binding affinity and, in turn, release kinetics *in vitro* as well as *in vivo*.

Chow et al. (18) stated 20 to 40 mg/kg p.o. as a minimal daily dose to reach the therapeutic *in vivo* concentrations of 50-100 ng/ml in mice plasma to inhibit VEGFR2 and PDGFR phosphorylation over 12 h. With our regimen of approximately 2 mg/kg administered intra-arterially as a single dose, we determined the concentration at the target liver tissue to be above this limit and thereby probably in toxic ranges. In humans, 25-50 mg of sunitinib malate are recommended daily doses for GIST,

metastatic RCC and pancreatic neuroendocrine tumors (34), corresponding to 19-37 mg of pure sunitinib drug per day or only 0.3-0.5 mg/kg/day for a person of 70 kg.

Owing to the first-pass effect, sunitinib is metabolized by CYP450 enzymes in the liver, which is in concordance with a reported accumulation of sunitinib in the tissue (34) and may explain high tissue levels also with oral administration. Comparing the relatively rapid release kinetics obtained in vitro ($t_{50\%} = 1.6$ h) with the retention of the drug in the tissue for at least 6 h points toward sunitinib binding to the surrounding liver tissue. This proposed mechanism is supported by the fact that sunitinib is 95% human plasma protein-bound (18).

The tissue concentrations fell after 6 h, but plasma concentrations continued to increase until 24 h, suggesting that elimination was ongoing in the liver while sunitinib was still transported into the blood circulation for both routes of administration. The drug should be present long enough to cover the early proliferative response to the ischemic effect after the embolization procedure, which is known to peak at day 1 and then gradually decrease (35). In comparison, the Sutent® monography (34) reported a t_{max} between 6 and 12 h after capsule (sunitinib malate) intake and Speed et al. (36) determined an elimination half time of 51 h in humans after an oral dose of 50 mg.

Higher plasmatic levels were expected after oral administration compared to a local delivery. The *in vitro-in vivo* correlation suggested that the drug was accumulating in plasma rather than being eliminated. A direct plotting of the measured plasma concentrations against the cumulative released sunitinib concentration revealed a tendency toward a linear correlation with a coefficient R² = 0.95 (i.a.) and 0.84 (p.o.) until 6 h. This linearity declined at 24 h. The measured plasma concentrations after intra-arterial injection after 24 h exceeded the linear prediction, but remained below therapeutic levels. Presumably, the relatively high administered concentrations led to persistence of the drug in the blood circulation. Superior intra-tissular and plasmatic drug concentrations below therapeutic levels after embolization when compared with an oral administration of the same dose suggested a higher bioavailability from the bead-drug combination. Additionally, no prolonged tissue exposure to the drug was observed when compared with oral uptake. It is still controversial if an extended release is desirable to avoid multiple administrations and plasma peaks or if a permanent exposure to the anticancer drug creates unwanted tumor cell resistance.

Regarding toxicity of sunitinib-eluting beads, transaminase levels, which indicate acute liver injury and cell disruption, increased following the embolization procedure of the hepatic artery, whereas ALP levels augmented only slightly. In contrast, sunitinib given perorally did not result in a change in liver enzymes, indicating that there was no drug-related change in enzyme levels. Recently, a randomized, unblinded phase III trial with oral sunitinib 37.5 mg/d vs. sorafenib 400 mg twice /d has revealed inferior overall survival and more frequent adverse events with sunitinib and was therefore discontinued (19), although sunitinib doses had been lowered compared to earlier phase II trials (37, 38). These issues might be overcome by local drug targeting, for which appropriate doses need to be determined.

Tumor cells are capable of recruiting adjacent supportive cells, enhancing the proliferation of these cells to form vessel walls (15). This effect on the surrounding tissue is hampered by sunitinib and other anti-angiogenic agents. As angiogenesis is not typical for a specific type of cancer, the effects of anti-angiogenic agents are seen in various tumor cell lines and tumor types (18, 25).

The cellular assays in this study confirmed that sunitinib was efficiently released from the spheres and had comparable activity as sunitinib in solution. For primary endothelial cells, the cytotoxic response was based on the mitogenic VEGFR inhibition, which is the major effect of sunitinib. However, the cellular target is less obvious for some cancer cell lines. Because apoptosis was not induced and only cytostatic effects at a concentration of 10 μ mol/l were seen, the drug activity in this study must be based on anti-angiogenic activity by VEGF and PDGF receptor inhibition (25).

The study's scope did not cover the evaluation of the antitumoral effect of sunitinib-eluting beads, this combination is currently assessed in a VX2 tumor model. Although no hepatocellular carcinoma cell lines were tested, we used cell lines that are likely to develop metastases to the liver. Measurement of sunitinib concentrations by liquid chromatography-tandem mass spectrometry in liver samples took into account sunitinib both bound to the tissue and to the beads embedded in the samples. *In vitro* results suggest that 6 hours and 24 h after injection, most of the drug (73% and 81%, respectively) is released.

In conclusion, the VEGFR antagonist sunitinib could be efficiently combined with DC Bead microspheres, consequently qualifying sunitinib as a potential drug candidate for the treatment of hypervascular tumors that suppresses ischemia-triggered angiogenesis and tumor recurrence.

5 Acknowledgment

Animal experiments were supported by a grant from Biocompatibles Ltd., Farnham, United Kingdom to P.E.B., A.D., and O.J.

6 References

1. Varela M, Real MI, Burrel M, et al. Chemoembolization of hepatocellular carcinoma with drug eluting beads: efficacy and doxorubicin pharmacokinetics. J Hepatol 2007; 46:474-481.

- 2. Lammer J, Malagari K, Vogl T, et al. Prospective randomized study of doxorubicin-eluting-bead embolization in the treatment of hepatocellular carcinoma: results of the PRECISION V study. Cardiovasc Intervent Radiol 2010; 33:41-52.
- 3. Malagari K, Pomoni M, Kelekis A, et al. Prospective randomized comparison of chemoembolization with doxorubicin-eluting beads and bland embolization with BeadBlock for hepatocellular carcinoma. Cardiovasc Intervent Radiol 2010; 33:541-551.
- 4. Brown KT, Gonen M, Do KG, et al., editors. A randomized single blind controlled trial of beads versus doxorubicin-eluting beads for arterial embolization of hepatocellular carcinoma (HCC). 2013 Gastrointestinal Cancers Symposium 2013; San Francisco, California: ASCO American Society of Clinical Oncology.
- 5. Boulin M, Guiu S, Chauffert B, et al. Screening of anticancer drugs for chemoembolization of hepatocellular carcinoma. Anticancer Drugs 2011; 22:741-748.
- 6. Liang B, Zheng CS, Feng GS, et al. Correlation of hypoxia-inducible factor 1alpha with angiogenesis in liver tumors after transcatheter arterial embolization in an animal model. Cardiovasc Intervent Radiol 2010; 33:806-812.
- 7. Gupta S, Kobayashi S, Phongkitkarun S, Broemeling LD, Kan Z. Effect of transcatheter hepatic arterial embolization on angiogenesis in an animal model. Invest Radiol 2006; 41:516-521.
- 8. Rhee TK, Young JY, Larson AC, et al. Effect of transcatheter arterial embolization on levels of hypoxia-inducible factor-1alpha in rabbit VX2 liver tumors. J Vasc Interv Radiol 2007; 18:639-645.
- 9. Lewis AL, Holden RR. DC Bead embolic drug-eluting bead: clinical application in the locoregional treatment of tumours. Expert Opin Drug Deliv 2011; 8:153-169.
- 10. Dufour JF. TACE with or without systemic therapy? J Hepatol 2012; 56:1224-1225.
- 11. Liapi E, Geschwind J-FH. Novel local therapies in hepatocellular carcinoma. Clinical Liver Disease 2012; 1:209-211.

12. Qu XD, Chen CS, Wang JH, et al. The efficacy of TACE combined sorafenib in advanced stages hepatocellullar carcinoma. BMC Cancer 2012; 12:263.

- 13. Pawlik TM, Reyes DK, Cosgrove D, Kamel IR, Bhagat N, Geschwind JF. Phase II trial of sorafenib combined with concurrent transarterial chemoembolization with drug-eluting beads for hepatocellular carcinoma. J Clin Oncol 2011; 29:3960-3967.
- 14. Le Tourneau C. Sunitinib: a novel tyrosine kinase inhibitor. A brief review of its therapeutic potential in the treatment of renal carcinoma and gastrointestinal stromal tumors (GIST). Therapeutics and Clinical Risk Management 2007; 3:341–348.
- 15. Faivre S, Demetri G, Sargent W, Raymond E. Molecular basis for sunitinib efficacy and future clinical development. Nat Rev Drug Discov 2007; 6:734-745.
- 16. Theou-Anton N, Faivre S, Dreyer C, Raymond E. Benefit-risk assessment of sunitinib in gastrointestinal stromal tumours and renal cancer. Drug Saf 2009; 32:717-734.
- 17. Demetri GD, van Oosterom AT, Garrett CR, et al. Efficacy and safety of sunitinib in patients with advanced gastrointestinal stromal tumour after failure of imatinib: a randomised controlled trial. Lancet 2006; 368:1329-1338.
- 18. Chow LQM, Eckhardt SG. Sunitinib: From Rational Design to Clinical Efficacy. Journal of Clinical Oncology 2007; 25:884-896.
- 19. Cheng AL, Kang YK, Lin DY, et al. Sunitinib versus sorafenib in advanced hepatocellular cancer: results of a randomized phase III trial. J Clin Oncol 2013; 31:4067-4075.
- 20. Denys A, Bize P, Jordan O, Doelker E, Boulens N, inventors. Chemoembolization composition comprising anti-angiogenic agents. Application number IB2011/055360; publication date June 7, 2012. Available at: http://patentscope.wipo.int/search/en/detail.jsf?docld=WO2012073188&recNum=108&docAn =IB2011055360&queryString=PKC&maxRec=6529. Accessed January 6, 2014.
- 21. FDA Guidance for Industry: Immediate Release Solid Oral Dosage Forms. U.S. Food and Drug Administration; 1995; Available at: http://www.fda.gov/downloads/Drugs/GuidanceComplianceRegulatoryInformation/Guidances/ucm070636.pdf. Accessed June 19, 2012.
- 22. Shah VP, Tsong Y, Sathe P, Liu JP. In vitro dissolution profile comparison--statistics and analysis of the similarity factor, f2. Pharm Res 1998; 15:889-896.

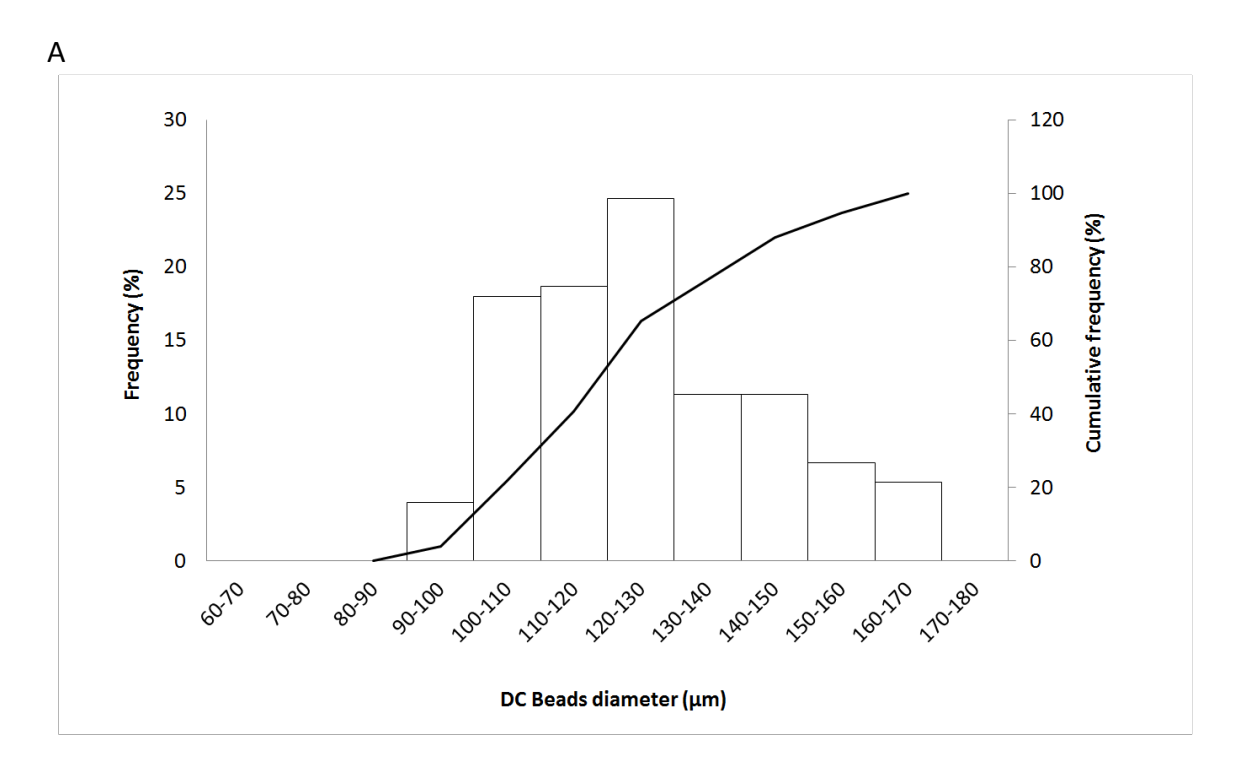
23. <1090> Assessment of drug product performance—bioavailability, bioequivalence, and dissolution.
In: United States Pharmacopeia and National Formulary (USP 36 – NF 31 S2). Rockville, MD: United States
Pharmacopeia Convention; 2013:729–734. Available at: http://www.uspnf.com/uspnf/pub/index?usp=36&nf=31&s=2&officialOn=December%201,%202013. Accessed January 6, 2014.

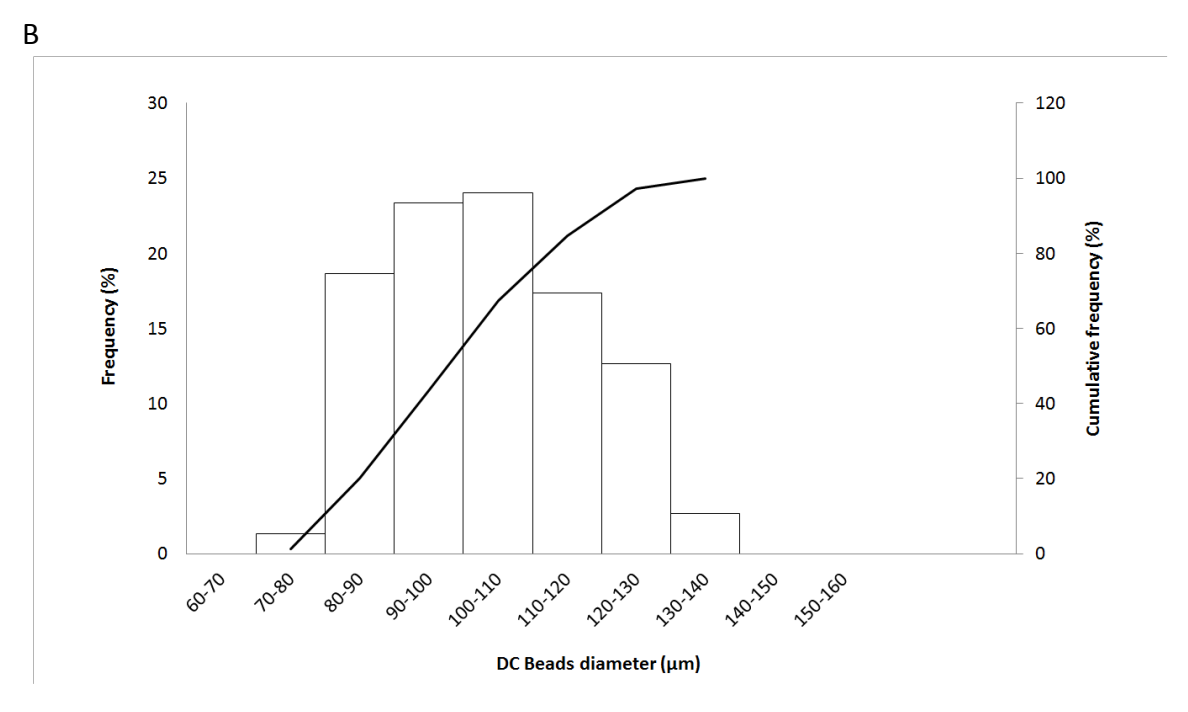
- 24. Verbois SL. Pharmacology/Toxicology Review and Evaluation. U.S. Food and Drug Administration; 2006. Available at: http://www.accessdata.fda.gov/drugsatfda_docs/nda/2006/021938_S000_Sutent_PharmR.pdf. Accessed January 30, 2013.
- 25. Mendel DB, Laird AD, Xin XH, et al. In vivo antitumor activity of SU11248, a novel tyrosine kinase inhibitor targeting vascular endothelial growth factor and platelet-derived growth factor receptors: Determination of a pharmacokinetic/pharmacodynamic relationship. Clinical Cancer Research 2003; 9:327-337.
- 26. Haouala A, Zanolari B, Rochat B, et al. Therapeutic Drug Monitoring of the new targeted anticancer agents imatinib, nilotinib, dasatinib, sunitinib, sorafenib and lapatinib by LC tandem mass spectrometry. J Chromatogr B Analyt Technol Biomed Life Sci 2009; 877:1982-1996.
- 27. Drug Bank Open Data Drug & Drug Target Database. Available at: http://www.drugbank.ca/drugs. Solubility source: FDA label. Accessed September 17, 2013.
- 28. Lewis AL, Gonzalez MV, Leppard SW, et al. Doxorubicin eluting beads 1: effects of drug loading on bead characteristics and drug distribution. J Mater Sci Mater Med 2007; 18:1691-1699.
- 29. Gonzalez MV, Tang Y, Phillips GJ, et al. Doxorubicin eluting beads-2: methods for evaluating drug elution and in-vitro:in-vivo correlation. J Mater Sci Mater Med 2008; 19:767-775.
- 30. Padia SA, Shivaram G, Bastawrous S, et al. Safety and efficacy of drug-eluting bead chemoembolization for hepatocellular carcinoma: comparison of small-versus medium-size particles. J Vasc Interv Radiol 2013; 24:301-306.
- 31. Taylor RR, Tang Y, Gonzalez MV, Stratford PW, Lewis AL. Irinotecan drug eluting beads for use in chemoembolization: in vitro and in vivo evaluation of drug release properties. Eur J Pharm Sci 2007; 30:7-14.
- 32. Jordan O, Denys A, De Baere T, Boulens N, Doelker E. Comparative study of chemoembolization loadable beads: in vitro drug release and physical properties of DC bead and hepasphere loaded with doxorubicin and irinotecan. J Vasc Interv Radiol 2010; 21:1084-1090.
- 33. Hayakawa E, Furuya K, Kuroda T, Moriyama M, Kondo A. Viscosity Study on the Self-Association of Doxorubicin in Aqueous Solution. Chem Pharm Bull (Tokyo) 1991; 39:1282-1286.

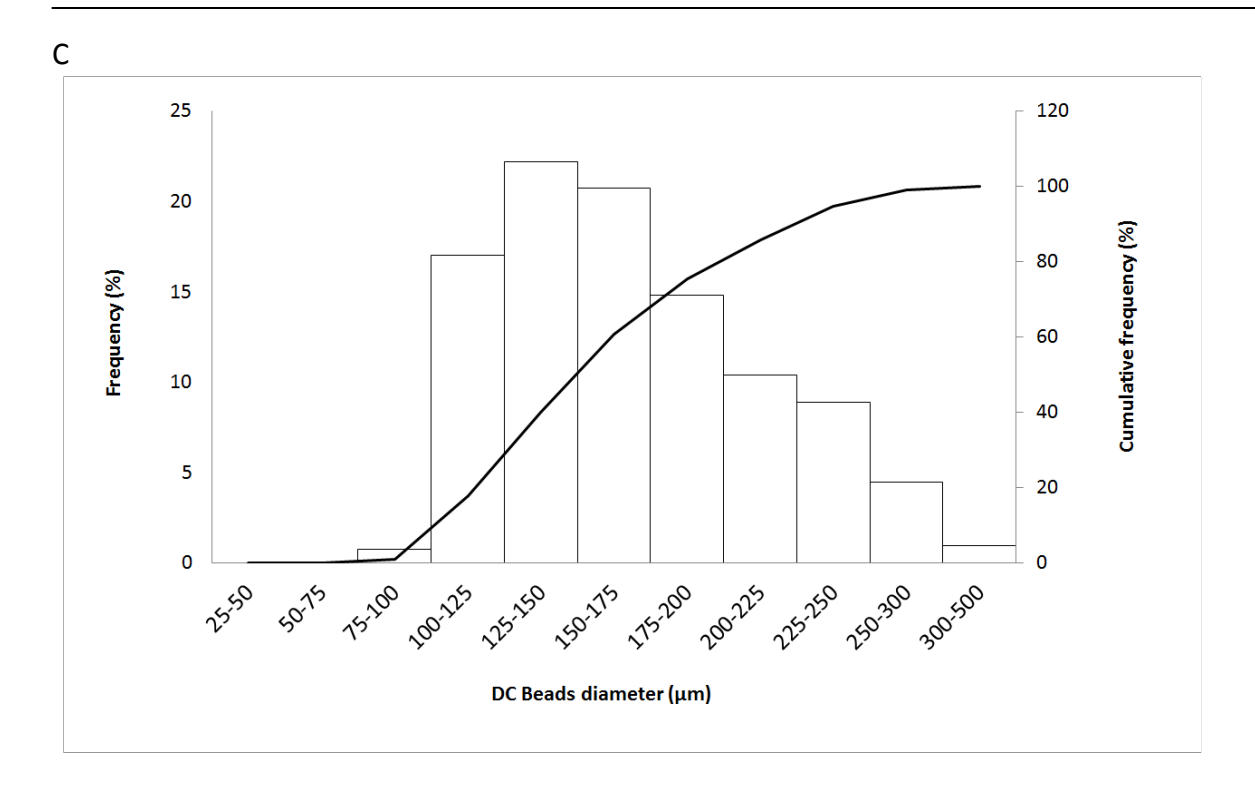
34. Product monograph: Pr SUTENT Sunitinib capsules. 2013. Available at: http://www.pfizer.ca/en/our_products/products/monograph/147. Accessed January 18, 2013.

- 35. Li X, Feng GS, Zheng CS, Zhuo CK, Liu X. Expression of plasma vascular endothelial growth factor in patients with hepatocellular carcinoma and effect of transcatheter arterial chemoembolization therapy on plasma vascular endothelial growth factor level. World J Gastroenterol 2004; 10:2878-2882.
- 36. Speed B, Bu HZ, Pool WF, et al. Pharmacokinetics, distribution, and metabolism of [14C]sunitinib in rats, monkeys, and humans. Drug Metab Dispos 2012; 40:539-555.
- 37. Faivre SJ, Bouattour M, Dreyer C, Raymond E. Sunitinib in Hepatocellular Carcinoma: Redefining Appropriate Dosing, Schedule, and Activity End Points. Journal of Clinical Oncology 2009; 27:E248-E250.
- 38. Faivre S, Raymond E, Boucher E, et al. Safety and efficacy of sunitinib in patients with advanced hepatocellular carcinoma: an open-label, multicentre, phase II study. Lancet Oncology 2009; 10:794-800.

7 Supplementary Material







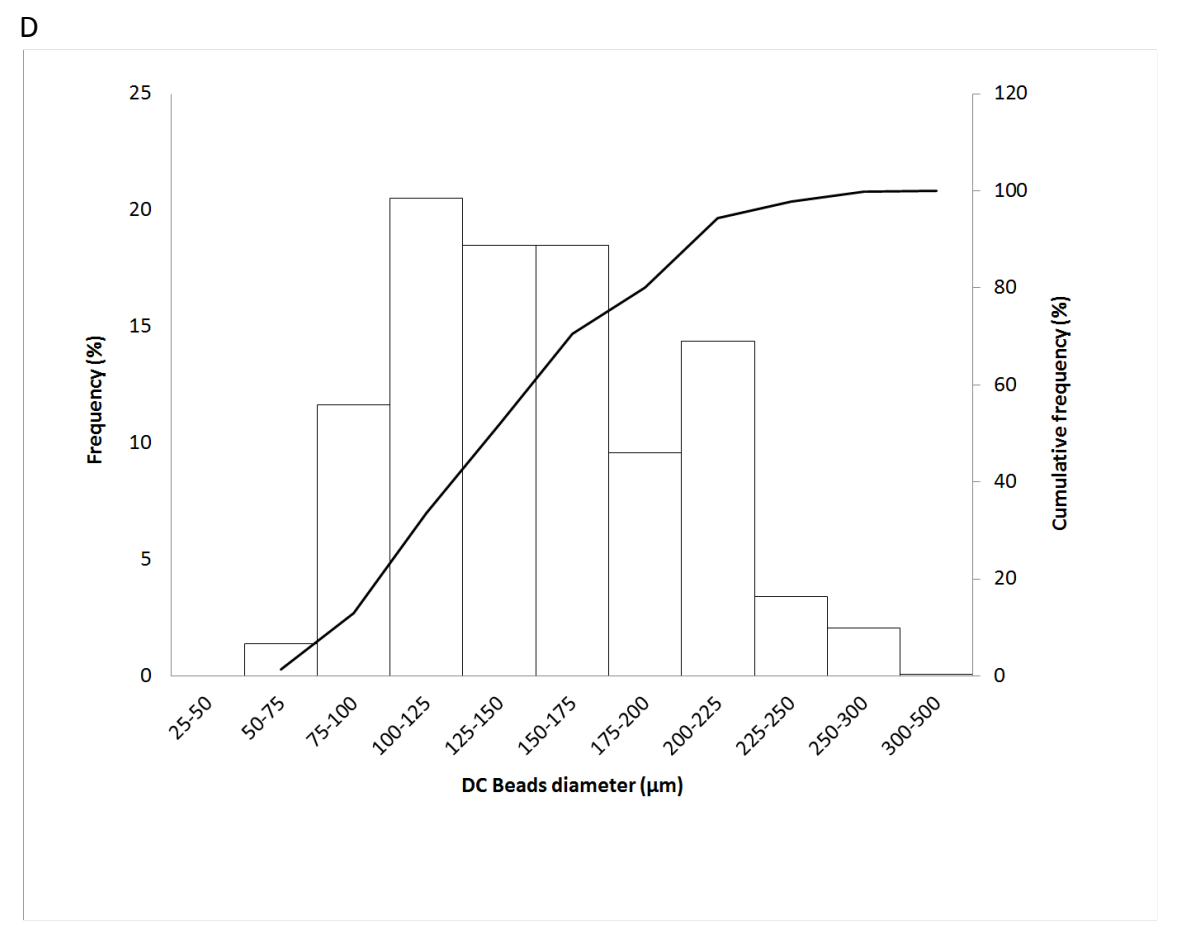


Figure E 1. Size distribution of 70-150 μm beads (A) before and (B) after sunitinib loading and 100-300 μm beads (C) before and (D) after sunitinib loading. A similar shrinking was found without major changes in the size distribution profile of the beads.

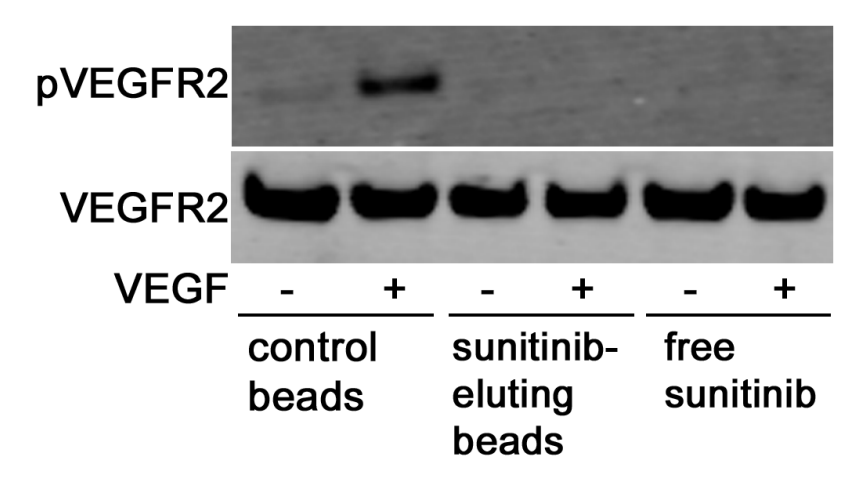


Figure E 2. Sunitinib-eluting beads as well as sunitinib reduced baseline phosphorylation of VEGFR2 and blocked VEGF-induced VEGFR2 phosphorylation. Endothelial cells were exposed to control beads, sunitinib-eluting beads or sunitinib for 1 h. Cells were subsequently stimulated with VEGF for 30 minutes. Cell lysates were prepared and analysed for the phosphorylation of VEGFR2 and the total amount of VEGFR2 by Western blot. pVEGFR2 = phosphorylated vascular endothelial growth factor receptor 2.

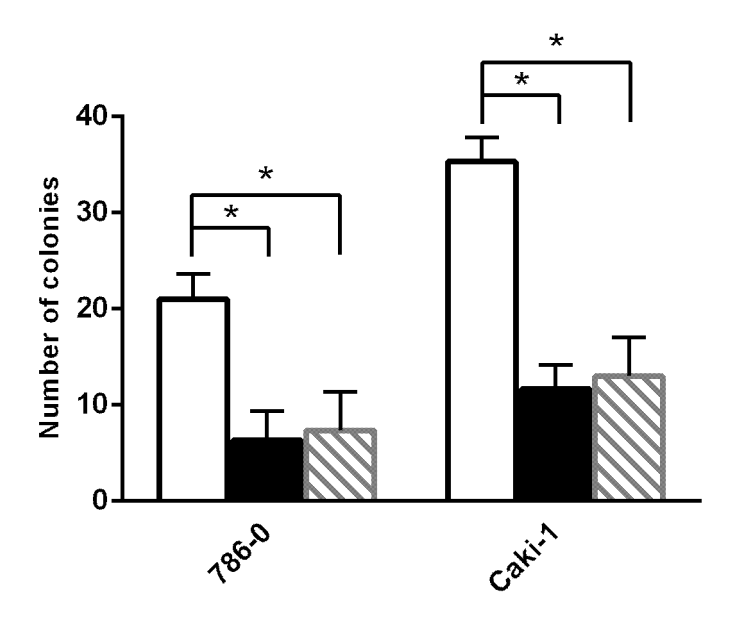


Figure E 3. Effects of control beads (white columns), sunitinib-eluting beads (black columns) and free sunitinib (shaded columns) on three-dimensional growth in Matrigel. Results are represented as the mean number of colonies \pm SD counted in five fields (microscope magnification: 100 x) of three independent experiments. Cell growth in three-dimensional gel matrix, where cell sensitivity to anti-cancer agents may change, allowed for an *in vivo*-like environment where sunitinib inhibited the formation of colonies for the two RCC lines. A nonparametric Friedmann test could not indicate significance (P = 0.1944 for 786-0, P = 0.0556 for Caki-1 three-dimensional growth) due to its low power resulting from the small sample size. Significance (*) indicates that the mean cell numbers after treatment with sunitinib-eluting beads or free sunitinib were outside of the 95% confidence interval of the respective controls.

Table E 1. Mean Serum Alanine Transaminase, Aspartate Transaminase, and Alkaline Phosphatase before and 6 Hours and 24 Hours after Embolization of the Hepatic Artery with Sunitinib-Eluting Beads and after Peroral Administration.

| | Intraarterial Administration [UI/I] | | | Peroral Administration [UI/I] | | | |
|-----|-------------------------------------|-----------|-------------|-------------------------------|-----------|------------|--|
| | Baseline (n=7) | 6 h (n=7) | 24 h (n=3) | Baseline (n=4) | 6 h (n=4) | 24 h (n=2) | |
| ALT | 90 ± 42 | 186 ± 62 | 941 ± 301 | 64 ± 12 | 62 ± 13 | 55 ± 13 | |
| AST | 82 ± 49 | 831 ± 364 | 3010 ± 1403 | 41 ± 17 | 49 ± 21 | 38 ± 8 | |
| ALP | 17 ± 13 | 24 ± 13 | 54 ± 54 | 29 ± 24 | 41 ± 29 | 36 ± 5 | |

ALP = alkaline phosphatase; ALT = alanine aminotransferase; AST = aspartate aminotransferase.

7.1 Appendix A: DEBs Characterization

Loading of Sunitinib into Beads. A sunitinib stock solution (10 mg/ml) was prepared according to a proprietary protocol (19) by acidifying the sunitinib base in 0.1N hydrochloric acid in a 1.1 molar excess to solubilize the drug. Then, a 5% (w/v) glucose solution was added.

The storage saline solution was removed from the vials. Defined volumes of the bead suspensions were incubated with sunitinib solution. Maximum sunitinib loading capacity was tested by adding different volumes of the stock solution. The incubation lasted for 2 h under agitation at ambient temperature.

The loading curves were obtained by a depletion method, i.e., sampling the supernatant at predetermined time points, quantifying sunitinib using UV-Vis spectrophotometry at 430 nm (HP 8453, Agilent Technologies AG, Basel, Switzerland) and subtracting the content from the original known amount of the added drug.

The loading profiles were compared using the similarity factor f_2 , following FDA guidelines for dissolution profile comparison (20-22). Similar curves show f_2 values > 50 in the case of equivalency within a 10% mean profile difference. Loading is based on a similar ion-exchange mechanism as release, which justifies the use of f_2 for the comparison of drug binding kinetics.

Release of Sunitinib from Beads. The flow-through United States Pharmacopeia method IV using a Sotax CE 6 (Sotax, Allschwil, Switzerland) with 6 parallel cells served to quantify the drug released from sunitinib-eluting beads. Each cell was filled with 100 mg of drug-loaded packed beads suspended in equal amounts of 5% glucose.

Each chamber was connected to a reservoir of 200 ml of saline (NaCl 0.9% in purified water, MilliQ academic, Millipore, Zug, Switzerland) by a closed loop, ensuring sink conditions, and a spectrophotometer (HP 8453, Agilent Technologies AG, Basel, Switzerland). The flow rate was set at 5 ml/min (CY 6 pump, Sotax). Chambers with loaded beads were kept at a temperature of 37°C.

As an internal standard of total drug dissolution and release from the beads, ethanol was added to the Sotax apparatus when the dissolution plateau was reached, to achieve a final concentration of 30% V/V. Absorbance at 3 h after ethanol addition was chosen as a reference. We analyzed the obtained release profiles in terms of the time necessary to reach 50% and 75% of the maximum drug release and compared the profiles by means of the similarity factor f_2 .

Microsphere Morphometry. Beads were imaged with a Zeiss Axiovert 200 microscope (Carl Zeiss, Feldbach, Switzerland). Coloration, homogeneity of loading and size alterations were observed visually. Attention was paid to the white field adjustment to ensure true color rendering. The size was measured using the open source image analysis software (ImageJ 1.38 software; NIH, Bethesda, MD, USA), analyzing an average of 150 microspheres in a monolayer. Statistical analysis was performed using a two-sided Student's t-test, at a significance level P = 0.001.

7.2 Appendix B: Preparation of Sunitinib-Loaded Beads and Oral Solution

Syringes prefilled with sunitinib-loaded 100-300 μm sized beads were prepared under aseptic laminar air-flow conditions for pharmacokinetic studies in rabbits.

All consumables were autoclaved according European Pharmacopeia requirements. Sunitinib stock solution and 5% glucose solution were filter sterilized. Sunitinib-loaded beads, obtained as described in Appendix A, were resuspended in 5% glucose, aliquoted volumetrically and distributed in the syringes, resulting in a drug content of 6 mg per 0.2 ml beads per syringe. Beads were allowed to sediment to remove excess supernatant, and the syringes were capped and packed under sterile conditions. Blank beads were aliquoted similarly.

The oral sunitinib solution (1 mg/ml) was prepared by diluting the stock solution (10 mg/ml) with pre-filtered glucose 5% (w/v).

Sunitinib-Eluting Beads for Chemoembolization:

Methods for *In Vitro* Evaluation of Drug Release

Katrin Fuchs^a, Pierre E. Bize^b, Alban Denys^b, Gerrit Borchard^a, Olivier Jordan^a

^a School of Pharmaceutical Sciences, University of Geneva, University of Lausanne, Quai Ernest Ansermet 30, 1211 Geneva 4, Switzerland

^b Departments of Radiology and Interventional Radiology, CHUV Centre Hospitalier Universitaire Vaudois, Rue du Bugnon 46, 1011 Lausanne, Switzerland

Original Research Article

Published in:

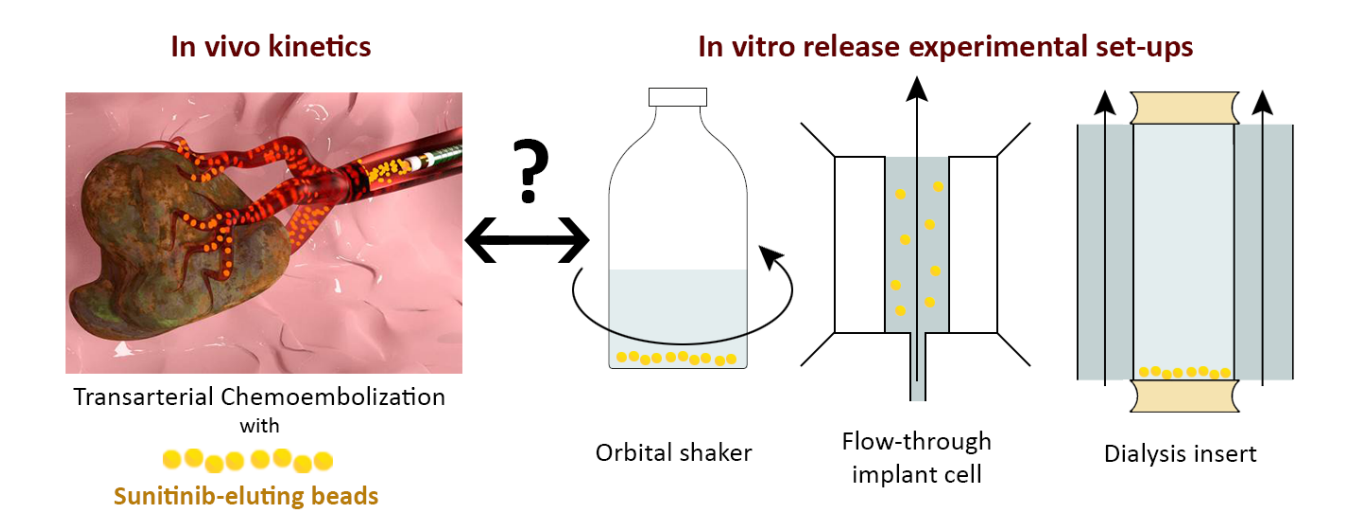
International Journal of Pharmaceutics: IJP. 2015, 482 (1-2), p. 68-74

Abstract

Drug-eluting microspheres are used for embolization of hypervascular tumors and allow for local controlled drug release. Although the drug release from the microspheres relies on fast ion-exchange, so far only slow-releasing *in vitro* dissolution methods have been correlated to *in vivo* data. Three *in vitro* release methods are assessed in this study for their potential to predict slow *in vivo* release of sunitinib from chemoembolization spheres to the plasma, and fast local *in vivo* release obtained in an earlier study in rabbits.

Release in an orbital shaker was slow ($t_{50\%}$ = 4.5 h, 84% release) compared to fast release in USP 4 flow-through implant cells ($t_{50\%}$ = 1 h, 100% release). Release of sunitinib from microspheres in saline in dialysis inserts was prolonged and incomplete ($t_{50\%}$ = 9 d, 68% release) due to low drug diffusion through the dialysis membrane. The slow-release profile fitted best to low sunitinib plasma AUC following injection of sunitinib-eluting spheres. Although limited by lack of standardization, release in the orbital shaker fitted best to local *in vivo* sunitinib concentrations. Drug release in USP flow-through implant cells was too fast to correlate with local concentrations, although this method is preferred to discriminate between different sphere types.

Graphical Abstract:



Keywords:

In vitro drug release, sunitinib, drug-eluting beads, USP dissolution apparatus 4, chemoembolization, *in vitro-in vivo* correlation

1 Introduction

Transarterial chemoembolization (TACE) is the standard of care for patients with hepatocellular carcinoma at an intermediate stage of disease. This treatment involves gel particles that radiologists inject under image guidance through a catheter into the patient's hepatic artery (Bruix et al., 1998) and has been developed over the last decade (Laurent, 2007). The microspheres embolize the artery and block the blood flow toward tumor tissue, suffocating the malignant hypervascular tumor tissue by inducing ischemia and eventually necrosis (Bruix et al., 2004; Li et al., 2004).

In addition, microspheres can serve as carriers of an anti-cancer or anti-angiogenic drug to be released on site. As an alternative to simple injection of the drug solution mixed with the contrast agent, ethiodized oil, followed by injection of blank microspheres (TACE), the use of drug-eluting microspheres (DEB-TACE) has found acceptance in current clinical practice. Efficacy and safety are increased due to locally defined drug administration and therefore reduced side effects (Lammer et al., 2010; Malagari et al., 2012). Moreover, the drug is not administered as a bolus injection, but is claimed to be released in a controlled manner over extended time periods.

The drug release from the microspheres is based on ion-exchange. The influx of small cations (Biondi et al., 2013; Liu et al., 2001) from biological fluids causes immediate release of the positively charged drug from the negatively charged sphere matrix. However so far, *in vitro* dissolution methods resulting in slow drug release have been employed and validated for simulation of the *in vivo* environment, as the blood flow in embolized vessels is supposed to be reduced (Cheung et al., 2004; Gonzalez et al., 2008; Lewis et al., 2006). Among them, the T-apparatus (Gonzalez et al., 2008) and incubation of drug-eluting beads in vials (Biondi et al., 2013) led to differing diffusion mechanisms for the currently used drugs doxorubicin and irinotecan.

We have earlier shown DC Bead microspheres (Biocompatibles Ltd.), a widely used commercial type of embolic microspheres, to be an adequate carrier for a new drug, the anti-angiogenic agent sunitinib (Fuchs et al., 2014).

In this investigation, we compared different *in vitro* methods to measure the drug released from sunitinib-eluting beads, focusing on the influence of different hydrodynamic conditions. The

question to be answered was which release set-up represents the best biorelevant conditions for microsphere release testing.

2 Materials and Methods

2.1 Loading of Sunitinib into DC Beads

DC Bead microspheres (Biocompatibles Ltd., Farnham, UK) consist of a poly(vinyl alcohol)-based hydrogel whose crosslinker contains sulfonate groups, bearing an overall negatively charged structure (Gonzalez et al., 2008; Lewis et al., 2007). The protonation of the tertiary amine of the anti-angiogenic drug, sunitinib and consequent incubation with the concentrated spheres results in high capacity of sunitinib loading into the spheres by ionic interaction (Denys et al., 07.06.2012; Fuchs et al., 2014).

Sunitinib base (LC Laboratories, Woburn, MA, USA) was acidified in 0.1N HCl in a 1.1 molar excess to solubilize the drug. A 5% (w/v) glucose solution was added to obtain the stock solution (10 mg/ml). The content of a DC Bead vial was transferred to a separate vial and the storage saline solution removed to obtain the net weight of spheres. After addition of a defined volume of saline, 30 or 100 mg spheres were sampled by volume under agitation into separate vials, the saline was withdrawn and the spheres' weight was controlled. Spheres were incubated with sunitinib solution (10 mg/ml) for optimal loading of 30 mg sunitinib/g spheres. The sunitinib-free supernatant was withdrawn after at least 2 h of incubation under agitation at ambient temperature and light protection.

The loaded spheres were transferred into the USP release apparatus chambers by suspension in 0.5 ml pure Milli Q water or into glass vials in the orbital shaker by suspension in the release medium.

2.2 Release Testing

The dissolution set-ups were (Figure 1):

1. Release experiment in an orbital shaker. 30 mg sunitinib-eluting spheres (100-300 μ m, n=3) were incubated in glass vials filled with 25 ml 0.9% saline, shaken at 80 rpm, 37°C.

- 2. *Release* of 100 mg sunitinib-eluting spheres (100-300 μm, n=3) was done *in a flow-through apparatus Sotax CE 6 USP Type 4* (Allschwil, Switzerland), in implant cells (diameter 6 mm). 200 μm grids (product n° 2970-4, d = 14.8 mm) and 5 μm nylon filters were inserted at the bottom and the top of the cell to retain the microspheres. The implant cells containing the microspheres were coupled to 200 ml medium reservoirs, a Sotax CY 6 pump at a flow rate of 5 ml/min at 37°C in a closed loop ensuring sink conditions, and a spectrophotometer (HP 8453, Agilent Technologies AG, Basel, Switzerland). Release tests were carried out in NaCl 0.9% (in purified Milli Q water) (n=3) and Dulbecco's phosphate buffered saline (DPBS, LifeTechnologies, Zug, Switzerland, catalogue n° 14190) (n=3). In a separate experiment, the implant chambers were filled with a bed of 1 mm glass beads at a height of 7 mm and release was tested in saline (n=3).
- 3. Flow-through testing in the same Sotax CE 6 apparatus was carried out under the same flow conditions as described above in 0.9% saline (n=3) or DPBS (n=3), while retaining the spheres in a 22.6 mm flow-through cell in a *dialysis cylinder insert* (Bhardwaj and Burgess, 2010) equipped with a 25 kDa MWCO regenerated cellulose membrane (Spectra/Por RC Biotech Membrane, product n° 128626, Spectrum Laboratories Inc., Breda, The Netherlands).

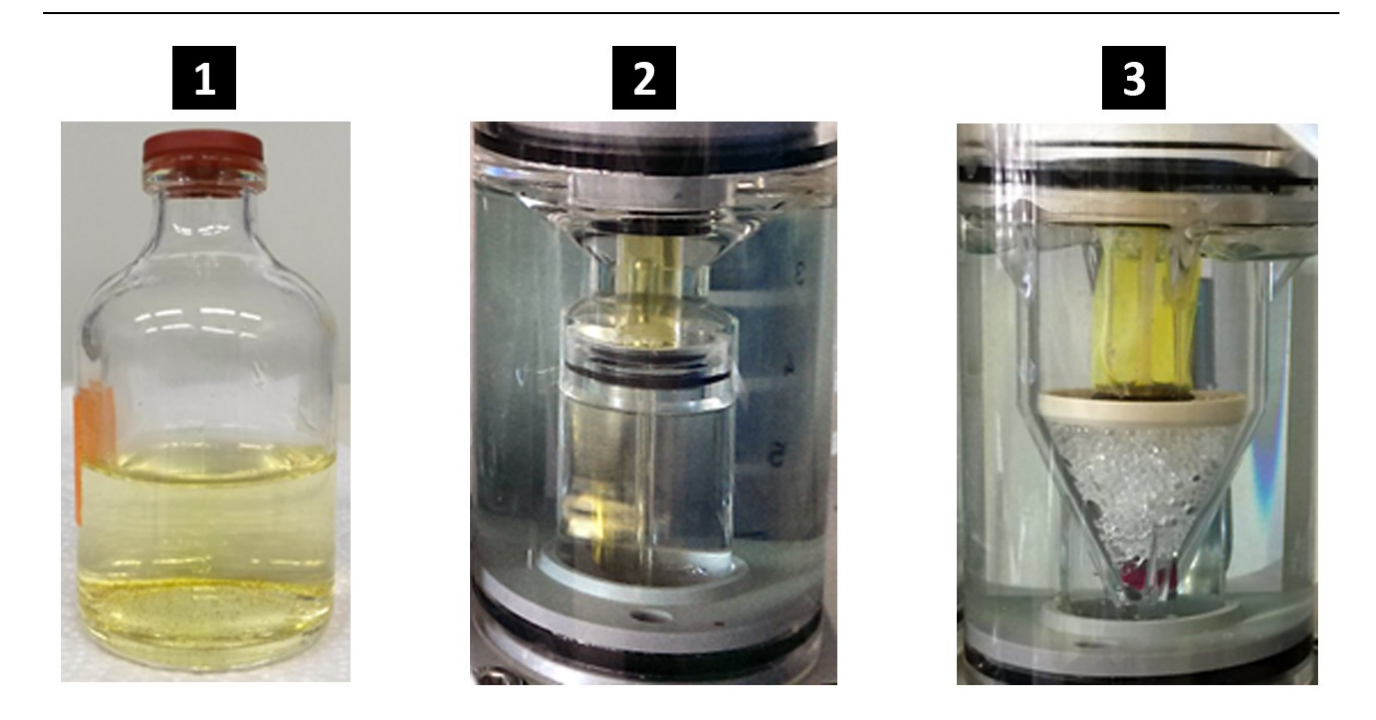


Figure 1. Dissolution set-ups used in this investigation were 1. Orbital shaking, 2. Release in implant cells in a Sotax USP Type 4 apparatus, and 3. Release in dialysis inserts in flow-through cells in the same Sotax USP 4 apparatus.

The drug release was quantified by spectrophotometry at a wavelength of 430 nm (Agilent HP 8453) under light protection (Haouala et al., 2009). At the end of the release, absolute ethanol (EtOH) was added to the media to achieve a final concentration of 30% (V/V) with the purpose to extract all sunitinib from the spheres. The obtained release plateau after EtOH addition served as reference for 100% drug release.

Release profiles were compared by computing the FDA similarity factor f₂

$$f_2 = 50 \cdot \log \left\{ \left[1 + \left(\frac{1}{n} \right) \sum_{t=1}^{n} (R_t - T_t)^2 \right]^{-0.5} \cdot 100 \right\}$$

where R_t and T_t are the cumulative percentage of the drug dissolved at each of the selected n time points in the reference and the test set-up, respectively. An f_2 value between 50 and 100 ensures profile equivalence. This approach is commonly used to compare the performance of two products (USP36-NF31, 2013). The release profiles were also fitted into different kinetic equations (zero order, first order, Higuchi, Peppas, and Boyd (Boyd et al., 1947; Chretien et al., 2004; Gonzalez et

al., 2008; Reichenberg, 1953; Taylor et al., 2007)) to determine the governing release mechanism (Table 1).

Table 1. Kinetic equations to determine sunitinib release kinetics from microspheres.

| Release Kinetic Model | Mathematical equation |
|---------------------------|---|
| Zero order | $M_t = M_0 + k_0 t$ |
| First order | $M_t = M_0 + k_0 t$ $M_t = M_0 \cdot (1 - e^{k_1 t})$ $M_t = k_H t^{0.5}$ |
| Higuchi | $M_t = k_H t^{0.5}$ |
| Peppas (power law) | $\frac{M_t}{M_{\infty}} = kt^n$ |
| Boyd (particle diffusion) | $Bt = -\ln\left(\frac{\pi^2}{6}\right) \cdot \left(1 - \frac{M_t}{M_{\infty}}\right) \qquad \text{for } \frac{M_t}{M_{\infty}} > 0.85$ |
| | $Bt = 2\pi - \left(\frac{\pi^2 \cdot \frac{M_t}{M_{\infty}}}{3}\right) - 2\pi \left(1 - \frac{\pi \cdot \frac{M_t}{M_{\infty}}}{3}\right)^{0.5} \text{ for } \frac{M_t}{M_{\infty}} \le 0.85$ |
| | where $D^i = B \cdot r^2/\pi^2$ |

 M_0 , M_t , and M_∞ are the absolute cumulative amount of drug released at time 0, t, and infinite time, respectively, k_0 the zero-order kinetic constant, k_1 the first-order kinetic constant, k_H the Higuchi rate constant, k_1 a constant incorporating structural and geometric characteristics of the system and n the release exponent. In the Boyd model, B is the exchange rate constant, from which the diffusion coefficient D^i of two exchanging ions inside the microsphere (radius $r = 156 \mu m$ in sunitinib-loaded state (Fuchs et al., 2014)) was calculated.

2.3 In Vitro-In Vivo Correlation

To evaluate which set-up represented *in vivo* conditions best, the obtained release kinetics from the three set-ups were related to *in vivo* concentrations obtained from previously conducted studies (Fuchs et al., 2014). Briefly, seven healthy New Zealand white rabbits were embolized with $100-300~\mu m$ microspheres loaded with 6 mg sunitinib. Four animals were sacrificed 6 h and three animals 24 h after embolization. Plasma concentrations were monitored until 6 h (n=7) and at 24 h (n=3).

The AUC (area under the curve), calculated by the trapezoidal method from *in vivo* plasma concentrations, was correlated to the cumulative release *in vitro*. An alternative approach for an *in vitro-in vivo* correlation is the convolution of *in vitro* dissolution data to predict plasma concentrations *in vivo* according to the FDA guidelines (FDA, 1997), which are accepted for parenteral formulations (Uppoor, 2001). As described by Qureshi (2010), the amount of drug

released *in vitro* between two sampling times (amt.) was calculated. By use of the elimination constant $k_e = 0.693/t_{1/2}$, the first order elimination rate for each drug amount released between two sampling times was determined. The plasma profiles were consequently predicted by the formula concentration (ng/ml) = amt.*1000/(V_d*body weight), where the bioavailability was considered 100% after i.a. administration. Half-life of sunitinib of 50 h and its apparent volume of distribution V_d of 2230 L in humans were retrieved from the product monograph for oral sunitinib (Pfizer, 2014). Given the average body weight of 70 kg for a human, V_d was approximated to the body weight of 3.5 kg for a rabbit by division by 20. The convoluted plasma profiles from *in vitro* data until 50 h from the three set-ups were then compared to the *in vivo* plasma concentrations measured in rabbits.

The ratio of the mean tissue concentrations at 6 h (n=4) and 24 h (n=3) was compared with the ratio of cumulative and differential release *in vitro* at the same time points.

3 Results and Discussion

Several attempts for standardizing microsphere release testing methods have been reported (Amyot et al., 2002; Carugo et al., 2012; Cheung et al., 2004), if possible by modifying compendial methods (Siewert et al., 2003). The method should be able to distinguish different formulations and to mimic *in vivo* conditions after injection of a suspension of embolic microspheres.

3.1 Drug Release in an Orbital Shaker

A simple release method (Figure 1) consists in incubating the microspheres in the release medium while stirring or shaking. However, inter-laboratory standardization is difficult, and the method is not included in pharmacopeia. Thus, this practicable set-up was used for preliminary experiments. Microspheres in saline medium in the orbital shaker showed a relatively sustained ($t_{50\%}$ = 4.5 h) and incomplete drug release (84%) for sunitinib (Figure 2), as for doxorubicin (Jordan et al., 2010). This was attributed to the low shear stress in the dissolution flask.

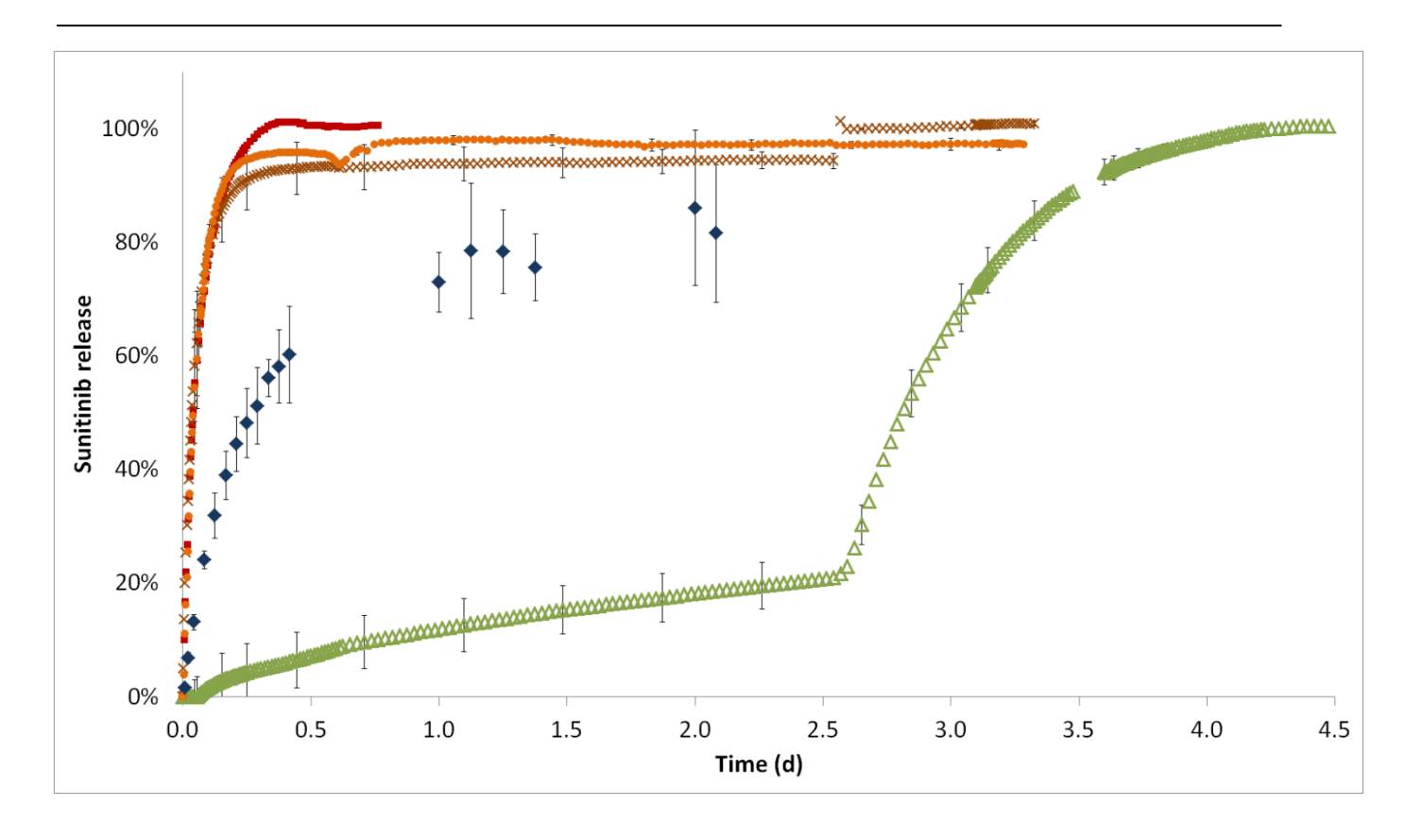


Figure 2. Fast release kinetics of sunitinib-eluting beads in an orbital shaker in NaCl 0.9% (\spadesuit), in implant cells in NaCl 0.9% (\blacksquare), with glass beads (\bullet), in DPBS (X), compared to prolonged kinetics in dialysis inserts (\triangle) in DPBS. After 2.6 days: 30% EtOH addition to (X) and (\triangle). All release experiments were done in triplicate, error bars indicate standard deviation (S.D.).

3.2 Drug Release in Flow-Through Implant Cells

Drug release in flow-through implant cells (Figure 1) was fast and complete in saline and in Dulbecco's PBS. Half of the sunitinib loaded onto the spheres was eluted within 1 h from 100-300 μ m DC Beads in NaCl 0.9%, with a final release of 100%. However, when the sunitinib-eluting spheres suspension was dense and spheres closely packed in the implant cells, the saline medium did not access all single spheres and only 80% instead of 100% of the initial sunitinib content was released. Some spheres were still colored by sunitinib as seen in Figure 2c in (Fuchs et al., 2014). In the present study, filling half of the implant cell chamber with a bed of glass beads to homogenize the speed profile and prevent agglomeration (Zolnik, 2005) did not significantly change the final release or the release profile (f_2 similarity factor = 72, similar profiles, Figure 2) because spheres were able to float.

The composition of the release medium influenced the release kinetics. The drug-ion exchange as a mechanism of loading and release has been demonstrated for other clinically used drugs like irinotecan and doxorubicin (Biondi et al., 2013; Gonzalez et al., 2008; Jordan et al., 2010). Thus, we found isotonic NaCl 0.9% (ionic strength: 154 mM) to be an appropriate release medium for drug-eluting hydrogel spheres. The medium pH value was modestly different after complete (pH = 6.51 ± 0.55 , n=3) or partial (30% released, pH = 6.85 ± 0.20 , n=3) release of sunitinib in saline due to the presence of the conjugated acid form of the drug. Phosphate buffer saline (PBS) might also be used as a release medium, although some drugs (e.g. doxorubicin) may tend to precipitate at high concentration (>5 mg/ml). Release in implant cells in Dulbecco's PBS with a sufficient ionic strength of 333 mM resulted in similar fast dissolution kinetics (f₂ similarity factor for dissolution profile comparison = 78) compared to release in saline, although with a slightly, but significantly lower final release at the plateau (94 vs. 100 %, P=0.01, two-tailed t-test).

When using cell culture medium, the drug release pattern might be influenced by the presence of serum proteins and thus might be enhanced (Cheung et al., 2004; Gonzalez et al., 2008), causing precipitation. This would require a more complicated analysis method than simple and fast UV/vis spectroscopy.

USP Sotax implant cells were used in this study because of their suitability to retain microspheres with thin filters in a small cylindrical compartment, maybe even similar to a vessel, without creating resistance to flow. The method with implant cells is discriminative for different ion-exchange formulations and drugs despite the instantaneous release, such as sunitinib, doxorubicin, and irinotecan release from different sphere types (Jordan et al., 2010). The Reynolds number, which is a measure for the flow stress in the implant chambers, is defined as $Re = F \cdot I / (v \cdot A)$ with F = volumetric flow rate, I = length of the chamber, v = kinematic viscosity, A = chamber cross-sectional area, and indicates a laminar flow for values of Re < 2000. Implant cells have a Re = Velue = 100 for a flow rate of 5 ml/min with water at 37°C, showing laminar flow conditions. For comparison Carugo et al. (2012) have developed a microfluidic device for embolic sphere partitioning with physiological Reynold numbers in the same range between 14 and 72.

3.3 Drug Release in Dialysis Cylinder Inserts

To potentially rule out the aforementioned important effects of flow rate, we carried out flowthrough testing in the same Sotax CE 6 apparatus while retaining the spheres in a dialysis cylinder (Figure 1) (Bhardwaj and Burgess, 2010). This adapter for dispersed systems had been claimed to be flow rate and sample volume independent, discriminative between different formulations and to enable high final release (Bhardwaj and Burgess, 2010). We obtained prolonged, in contrast to Bhardwaj and Burgess (2010) incomplete elution kinetics that continued up to 27 days (Figure 3). In this dialysis set-up, the sample was packed at the bottom of the insert and only bathed by a tangential laminar flow (Reynolds number = 27). Despite the high membrane molecular weight cutoff (Gao and Westenberger, 2012), sunitinib diffusion through the dialysis membrane was the limiting step, thus slowing down sunitinib diffusion out of the spheres due to violation of sink conditions inside the dialysis cylinder. Similar observations were reported by Cipolla et al. (2014), for whom the dialysis system was not suitable, as the rate of drug release from the spheres exceeded the transport of free drug through the dialysis membrane. Accordingly, 100% sunitinib release, detected in implant cells immediately upon addition of EtOH, was reached in dialysis inserts only after 1 day (Figure 2 and Figure 3). Pure sunitinib solution from dialysis inserts had a release half time of 1.8 h (data not shown) due to retention by the membrane.

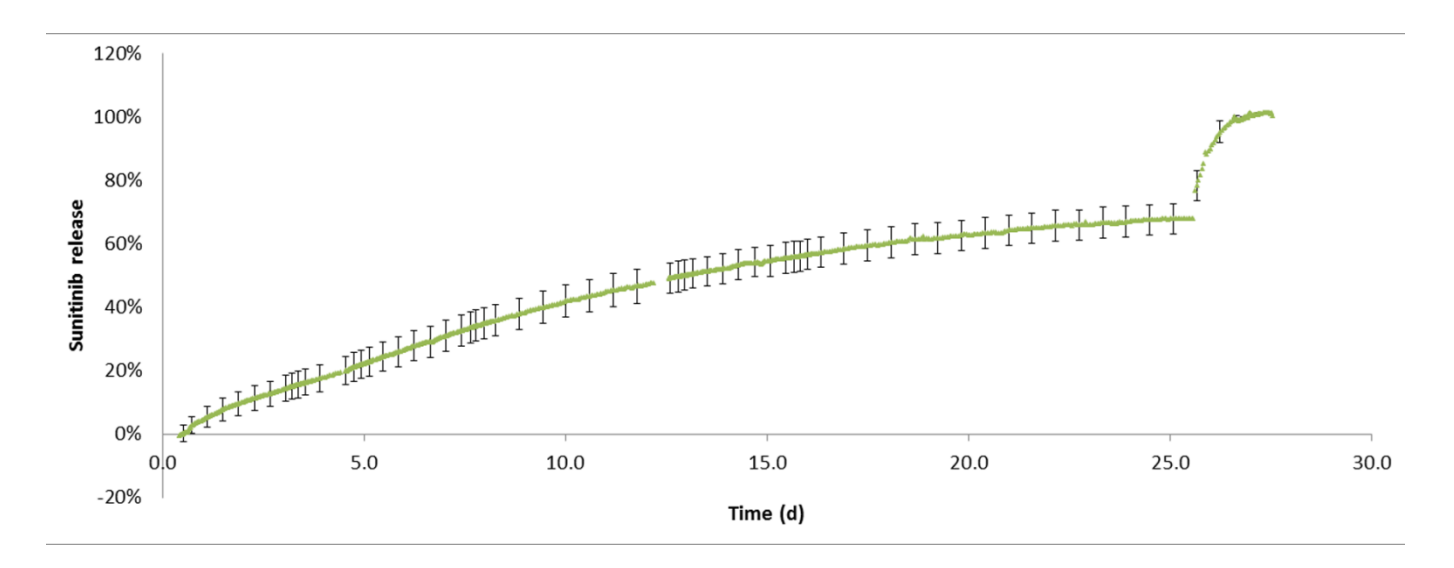


Figure 3. Prolonged release kinetics of sunitinib-eluting beads in NaCl 0.9% in dialysis inserts in flow-through cells over 28 days. After 25 days: 30% EtOH addition. Mean values +/- S.D. (n=3).

3.4 Comparison of Release Profiles in Different Set-ups

Table 2 and Figure 2 summarize the tested set-ups and conditions, and the time to reach 50% and 75% of the final release.

The FDA similarity factor f_2 showed the differences between the release profiles of a single formulation in the three different set-ups, demonstrating the influence of the flow conditions.

Sunitinib release from microspheres in saline in the orbital shaker compared to Sotax implant cells was slower and resulted in different release profiles (f_2 similarity factor for dissolution profile comparison = 22). Fast release in the implant cells compared to the very slow release in dialysis inserts in saline (f_2 = 10) and in DPBS (f_2 = 12), respectively, clearly indicated different profiles due to different agitation of the spheres depending on the chamber. The similarity factor f_2 also showed difference between sunitinib release from the microspheres in saline, whether in the orbital shaker or contained in dialysis inserts (f_2 = 15). Similarity factors were calculated by omitting the lag phase at the beginning of the elution in the dialysis inserts. Given that only a single formulation was tested, these differences pointed out the different responses obtained according to the method used.

3.5 Drug Release Fitting with Release Models

In order to evaluate the kinetics of the drug release process from a single formulation under different hydrodynamic conditions, the experimental data were fitted to different release equations. We retained the model that described best the order of release with a determination coefficient close to 1. Thus, influence of the shear stress during release should be confirmed if the mechanism changed as a function of the set-up. Among zero order, first order, Higuchi and Peppas models, all release profiles were represented well by the Peppas power law fitting up to 60% of release, with two of the release profiles fitting better with Higuchi (sunitinib-eluting microspheres in implant cells or dialysis inserts, suspended in saline). Table 2 displays the determination coefficients R², all greater than 0.9 for Peppas, and the release exponent n obtained in the different set-ups. The release exponent n was determined to be greater than 0.43 (Siepmann and Siepmann,

2008) for all experiments, surprisingly indicating non-Fickian anomalous transport and polymer swelling to be the rate-controlling steps. However, release in the dialysis inserts in saline could as well be fitted to the first order and Higuchi equations with determination coefficients of R^2 =0.99 indicating diffusion control, thus being non-conclusive for the slow-release profile. Slow-release profiles from ion-exchange resins had earlier been successfully correlated (Chretien et al., 2004; Taylor et al., 2007) with the Boyd model (Boyd et al., 1947), which describes particle diffusion to be rate controlling over chemical ion exchange and film diffusion mechanisms. Particle diffusion was assumed due to sufficiently high ion concentration in the medium (Gonzalez et al., 2008), but not confirmed for doxorubicin release from DC Beads (Biondi et al., 2013). Only for the set-ups yielding prolonged sunitinib release from DC Beads, the release profile could be fitted to the Boyd model with a determination coefficient >0.9. Release in the orbital shaker (R^2 =0.94) and in dialysis inserts (R^2 =0.98) returned a low diffusion coefficient D^i of 4.9·10⁻¹¹ cm²/s and 1.9·10⁻¹² cm²/s, respectively (doxorubicin-eluting DC Beads: D^i = 3.0·10⁻⁸ cm²/s (Gonzalez et al., 2008)). Whether the diffusion of sodium ions into the sphere could be described as particle diffusion was consequently also dependent on the choice of release set-up.

Table 2. Kinetic parameters (release time until 50% or 75% of the release plateau reached) of 30 mg/g sunitinib-eluting beads in different set-ups. The determination coefficient R² close to 1 of the release models pointed either toward diffusion control (Higuchi) or polymer swelling (Peppas, release exponent n>0.85).

| | Release conditions | t _{50%} | t _{75%} | Percentage of drug released at | Modeling of release ^a | |
|--|---|------------------|------------------|---------------------------------|----------------------------------|-----------------------|
| | | | | plateau | Peppas | Higuchi |
| Orbital shaking release experiments | Spheres suspended in saline | 4.5 h | 29.1 h | 84 ± 13% | $R^2 = 0.97$ n = 0.85 | $R^2 = 0.89$ |
| Sotax CE6 apparatus: flow-through implant cell | Spheres suspended in saline | 1.0 h | 2.3 h | 100 ± 1% | $R^2 = 0.90$ n = 1.12 | R ² = 0.94 |
| | Spheres over glass bead support in saline | 1.0 h | 2.0 h | 97 ± 1% | $R^2 = 0.96$ n = 1.12 | $R^2 = 0.82$ |
| | Spheres suspended in DPBS | 0.8 h | 1.8 h | 94 ± 1% | $R^2 = 0.99$ n = 0.76 | $R^2 = 0.79$ |
| Sotax CE6 apparatus: dialysis insert cell | Spheres suspended in saline | 8.8 d | 15.7 d | 68 ± 5% | $R^2 = 0.90$ n = 1.01 | $R^2 = 0.99$ |
| 2 2 | Spheres suspended in DPBS | n. a. | n.a. | Plateau not reached in 2.5 d | | |

^a R² = determination coefficient, n = release exponent

3.6 *In Vitro-In Vivo* Correlation (IVIVC)

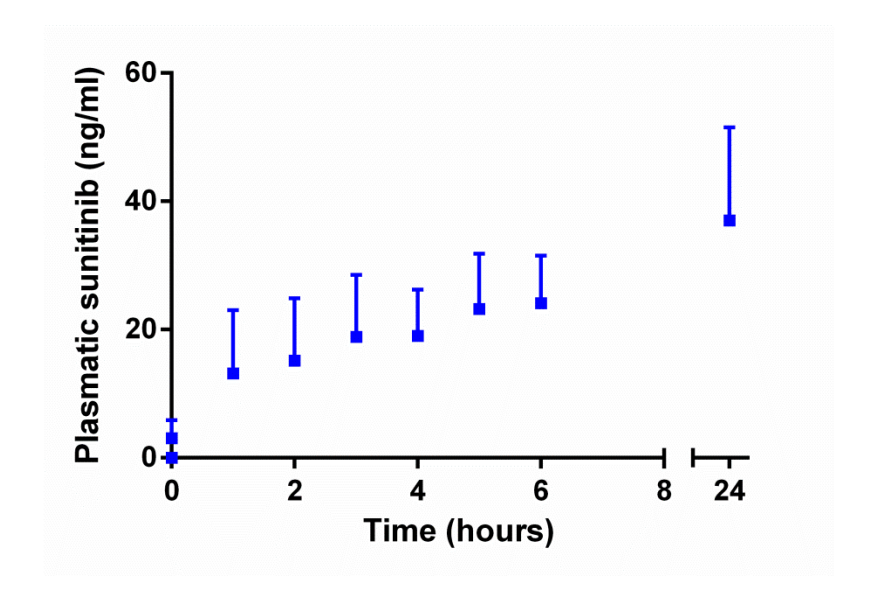
Hydrodynamic stress influence on release was previously reported for doxorubicin-loaded spheres (Cheung et al., 2004; Gonzalez et al., 2008), and *in vitro* release was related to drug concentrations in patients. Gonzalez et al. (2008) correlated the prolonged doxorubicin release in the T-apparatus with patients' plasma AUC until 24 h after administration of doxorubicin. In the T-apparatus, the drug is eluted from spheres in a well by diffusion and then transported by a tangential flux (Amyot et al., 2002). However, drug plasma concentrations following chemoembolization – which should preferably be as low as possible to avoid adverse systemic effects – are not representative for effects within the tumor and are time-shifted after local administration due to distribution in body compartments. Comparison with tissue concentrations is more representative of local drug activity, although more complicated to realize. Namur et al. (2011) found doxorubicin concentrations in liver explants of patients after 8 h of embolization with doxorubicin-eluting beads to be approximately

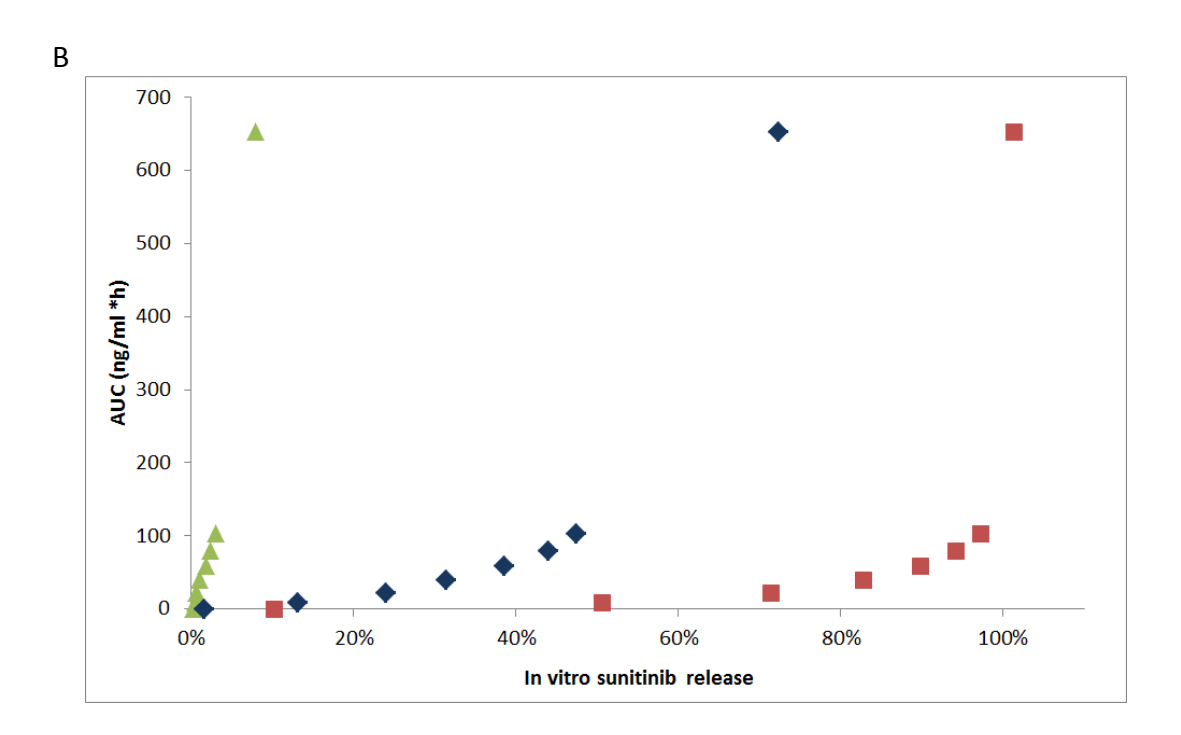
twice as high as after 9-14 days, indicating a drug concentration peak in the tissue shortly after embolization.

The release profiles of sunitinib from microspheres obtained in saline under different hydrodynamic conditions were compared with *in vivo* area under the curve (AUC) and tissue concentrations. First, plasma sunitinib concentrations in rabbits embolized with sunitinib-eluting spheres (Figure 4A) (Fuchs et al., 2014) were used. The area under the curve (AUC) of sunitinib *in vivo* was only related to the *in vitro*-released cumulative drug amounts in the dialysis insert set-up in a Level A (point-by-point) IVIVC (FDA, 1997) until 24 h (Figure 4B). Release *in vitro* in the orbital shaker or implant cells was faster than appearance of the drug in plasma over time. Correlation over a longer period would give better insights, as the drug levels in the systemic circulation might increase more after one day of administration.

Following the description for *in vitro-in vivo* correlation by Qureshi (2010), *in vitro* release data were convoluted with a first order elimination model, leading to predicted plasma profiles (Figure 4C) to be compared with *in vivo* plasma concentrations. All three *in vitro* set-ups predicted too low plasma concentrations because of the lower initial dose used for *in vitro* experiments (0.9 mg or 3 mg sunitinib) compared to 6 mg which had been injected into rabbits. Focusing on the profiles' shape, t_{max} should be at 7 h (implant cells), 27 h (orbital shaking), or should not be reached at 50 h (dialysis inserts). Elimination was visible as a decrease in predicted drug plasma levels after 7 h, when fast release occurred in implant cells. For comparison, drug plasma levels measured *in vivo* were higher after 24 h than after 6 h. Similarly to the AUC correlation, the slow-releasing *in vitro* profile seemed to fit better to the sunitinib plasma concentrations found in rabbits. However, the convolution method took into account elimination, but not distribution into other compartments. The late appearance of the drug in the blood might actually be due to the initial drug distribution into the tissue, before redistribution into the circulation at later time points.

Α





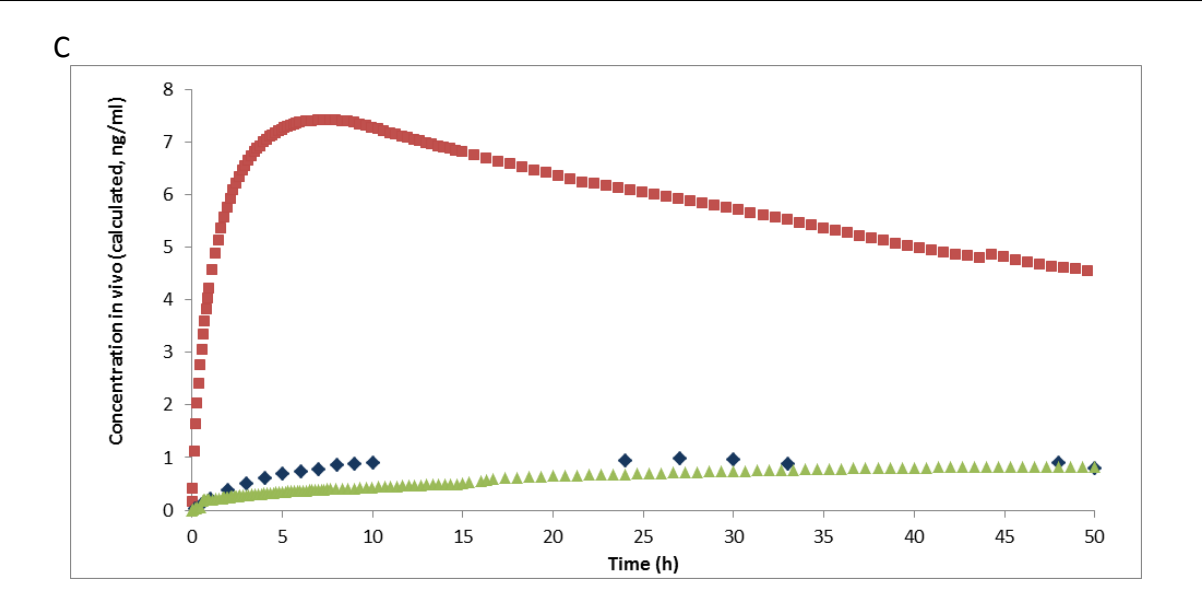


Figure 4.

A. Sunitinib plasma levels after intra-arterial administration of sunitinib-eluting microspheres (6 mg sunitinib loaded on 0.2 g spheres) in healthy New Zealand white rabbits (n=7 until 6 h, n=3 at 24 h) (Fuchs et al., 2014).

B. IVIVC until 24 h from plasma AUC of healthy New Zealand white rabbits after intra-arterial administration of sunitinib-eluting beads (Fuchs et al., 2014) with *in vitro* cumulative release of sunitinib-eluting beads.

Release in the orbital shaker (♠) and in implant cells (■) in NaCl 0.9% was faster than the appearance of sunitinib in rabbit plasma, whereas slow release in dialysis inserts in saline (▲) correlated linearly with AUC until 24 h (R²=0.95).

C. Convoluted plasma concentrations from mean release of *in vitro* experiments (n=3) in the orbital shaker (\diamond), in implant cells (\blacksquare), or dialysis inserts (\blacktriangle) in NaCl 0.9%.

Local drug tissue concentrations were 4.4 times higher at 6 h than at 24 h after intra-arterial injection of sunitinib-eluting spheres, thus clearly favoring a relatively fast sunitinib release model for the representation of drug concentrations at the tumor site. Considering the rate of drug released rather than the cumulated values, the ratio of the differential drug amounts released in saline until 6 h and 24 h in the three tested set-ups was 4.6 in the orbital shaker, 70.6 in the Sotax flow-through implant cells, and 1.8 in the Sotax dialysis inserts. Thus, local concentrations in rabbits were well represented by the simple orbital shaking method, which is however not standardized and whose Reynolds number varies especially depending on vial dimensions and amount of medium used. Among the pharmacopeia-approved methods, the flow-through implant cells, although overestimating the relation of two available tissue concentrations *in vivo*, represented the actual fast drug wash-out off the spheres, which might be of interest to compare different types of microspheres used for liver chemoembolization.

4 Conclusions

The hydrodynamic stress, flow rate and the drug's physicochemical properties play crucial roles in the rate and extent of drug elution. Among three different set-ups, slow drug release correlated better with *in vivo* drug plasma levels, whereas fast release represented tissue drug levels. Flow-through implant cells detected the immediate release of sunitinib from ion-exchange microspheres in a small vessel-like chamber, and would be best suited to discriminate between different types of drug-eluting spheres. Slow release in dialysis cylinder inserts only correlated because of drug redistribution mechanisms between tissue and plasma *in vivo* and was not the method of choice for fast-eluting microspheres due to low drug diffusion (Wacker, 2013; Wacker, 2014). A flow-through set-up with relatively low shear without a membrane barrier might be envisaged.

5 Acknowledgements

The authors acknowledge Adam Wilson and Omar Sakr for their contribution to the design of the graphical abstract.

6 References

Amyot, F., Jurski, K., Dufaux, J., Guiffant, G., 2002. An experimental and theoretical study of mass transfer from loaded embolisation microbeads: Possible optimisation. Int Commun Heat Mass 29, 623-632.

Bhardwaj, U., Burgess, D.J., 2010. A novel USP apparatus 4 based release testing method for dispersed systems. International journal of pharmaceutics 388, 287-294.

Biondi, M., Fusco, S., Lewis, A.L., Netti, P.A., 2013. Investigation of the mechanisms governing doxorubicin and irinotecan release from drug-eluting beads: mathematical modeling and experimental verification. Journal of materials science. Materials in medicine 24, 2359-2370.

Boyd, G.E., Adamson, A.W., Myers, L.S., 1947. The Exchange Adsorption of Ions from Aqueous Solutions by Organic Zeolites .2. Journal of the American Chemical Society 69, 2836-2848.

Bruix, J., Llovet, J.M., Castells, A., Montana, X., Bru, C., Ayuso, M.C., Vilana, R., Rodes, J., 1998. Transarterial embolization versus symptomatic treatment in patients with advanced hepatocellular carcinoma: results of a randomized, controlled trial in a single institution. Hepatology 27, 1578-1583.

Bruix, J., Sala, M., Llovet, J.M., 2004. Chemoembolization for hepatocellular carcinoma. Gastroenterology 127, S179-188.

Carugo, D., Capretto, L., Willis, S., Lewis, A.L., Grey, D., Hill, M., Zhang, X.L., 2012. A microfluidic device for the characterisation of embolisation with polyvinyl alcohol beads through biomimetic bifurcations. Biomed Microdevices 14, 153-163.

Cheung, R.Y., Kuba, R., Rauth, A.M., Wu, X.Y., 2004. A new approach to the in vivo and in vitro investigation of drug release from locoregionally delivered microspheres. Journal of controlled release: official journal of the Controlled Release Society 100, 121-133.

Chretien, C., Boudy, V., Allain, P., Chaumeil, J.C., 2004. Indomethacin release from ion-exchange microspheres: impregnation with alginate reduces release rate. Journal of controlled release: official journal of the Controlled Release Society 96, 369-378.

Cipolla, D., Wu, H., Eastman, S., Redelmeier, T., Gonda, I., Chan, H.-K., 2014. Development and Characterization of an In Vitro Release Assay for Liposomal Ciprofloxacin for Inhalation. Journal of pharmaceutical sciences 103, 314-327.

Denys, A., Bize, P., Jordan, O., Doelker, E., Boulens, N., 07.06.2012. Chemoembolization Composition Comprising Anti-Angiogenic Agents. WO/2012/073188.

Guidance for Industry. Extended Release Oral Dosage Forms: Development, Evaluation, and Application of In Vitro/In Vivo Correlations. Available at: http://www.fda.gov/cder/guidance/index.htm. Accessed 03.10.2014.

Fuchs, K., Bize, P.E., Dormond, O., Denys, A., Doelker, E., Borchard, G., Jordan, O., 2014. Drug-eluting beads loaded with antiangiogenic agents for chemoembolization: in vitro sunitinib loading and release and in vivo pharmacokinetics in an animal model. Journal of vascular and interventional radiology: JVIR 25, 379-387 e372.

Gao, Z., Westenberger, B., 2012. Dissolution testing of acetaminophen suspension using dialysis adapter in flow-through apparatus: a technical note. AAPS PharmSciTech 13, 944-948.

Gonzalez, M.V., Tang, Y., Phillips, G.J., Lloyd, A.W., Hall, B., Stratford, P.W., Lewis, A.L., 2008. Doxorubicin eluting beads-2: methods for evaluating drug elution and in-vitro:in-vivo correlation. Journal of materials science. Materials in medicine 19, 767-775.

Haouala, A., Zanolari, B., Rochat, B., Montemurro, M., Zaman, K., Duchosal, M.A., Ris, H.B., Leyvraz, S., Widmer, N., Decosterd, L.A., 2009. Therapeutic Drug Monitoring of the new targeted anticancer agents imatinib, nilotinib, dasatinib, sunitinib, sorafenib and lapatinib by LC tandem mass spectrometry. Journal of chromatography. B, Analytical technologies in the biomedical and life sciences 877, 1982-1996.

Jordan, O., Denys, A., De Baere, T., Boulens, N., Doelker, E., 2010. Comparative study of chemoembolization loadable beads: in vitro drug release and physical properties of DC bead and hepasphere loaded with doxorubicin and irinotecan. Journal of vascular and interventional radiology: JVIR 21, 1084-1090.

Lammer, J., Malagari, K., Vogl, T., Pilleul, F., Denys, A., Watkinson, A., Pitton, M., Sergent, G., Pfammatter, T., Terraz, S., Benhamou, Y., Avajon, Y., Gruenberger, T., Pomoni, M., Langenberger,

H., Schuchmann, M., Dumortier, J., Mueller, C., Chevallier, P., Lencioni, R., 2010. Prospective randomized study of doxorubicin-eluting-bead embolization in the treatment of hepatocellular carcinoma: results of the PRECISION V study. Cardiovascular and interventional radiology 33, 41-52.

Laurent, A., 2007. Microspheres and nonspherical particles for embolization. Techniques in vascular and interventional radiology 10, 248-256.

Lewis, A.L., Gonzalez, M.V., Leppard, S.W., Brown, J.E., Stratford, P.W., Phillips, G.J., Lloyd, A.W., 2007. Doxorubicin eluting beads - 1: effects of drug loading on bead characteristics and drug distribution. Journal of materials science. Materials in medicine 18, 1691-1699.

Lewis, A.L., Gonzalez, M.V., Lloyd, A.W., Hall, B., Tang, Y., Willis, S.L., Leppard, S.W., Wolfenden, L.C., Palmer, R.R., Stratford, P.W., 2006. DC bead: in vitro characterization of a drug-delivery device for transarterial chemoembolization. Journal of vascular and interventional radiology: JVIR 17, 335-342.

Li, X., Feng, G.S., Zheng, C.S., Zhuo, C.K., Liu, X., 2004. Expression of plasma vascular endothelial growth factor in patients with hepatocellular carcinoma and effect of transcatheter arterial chemoembolization therapy on plasma vascular endothelial growth factor level. World journal of gastroenterology: WJG 10, 2878-2882.

Liu, Z., Cheung, R., Wu, X.Y., Ballinger, J.R., Bendayan, R., Rauth, A.M., 2001. A study of doxorubicin loading onto and release from sulfopropyl dextran ion-exchange microspheres. Journal of controlled release: official journal of the Controlled Release Society 77, 213-224.

Malagari, K., Pomoni, M., Moschouris, H., Bouma, E., Koskinas, J., Stefaniotou, A., Marinis, A., Kelekis, A., Alexopoulou, E., Chatziioannou, A., Chatzimichael, K., Dourakis, S., Kelekis, N., Rizos, S., Kelekis, D., 2012. Chemoembolization with Doxorubicin-eluting beads for unresectable hepatocellular carcinoma: five-year survival analysis. Cardiovascular and interventional radiology 35, 1119-1128.

Namur, J., Citron, S.J., Sellers, M.T., Dupuis, M.H., Wassef, M., Manfait, M., Laurent, A., 2011. Embolization of hepatocellular carcinoma with drug-eluting beads: doxorubicin tissue concentration and distribution in patient liver explants. Journal of hepatology 55, 1332-1338.

88 Chapter Three

Pr SUTENT® Sunitinib capsules. Pfizer Canada Inc. Available at: http://www.pfizer.ca/en/our_products/products/monograph/147. Accessed 20.10.2014.

Qureshi, S.A., 2010. In Vitro-In Vivo Correlation (IVIVC) and Determining Drug Concentrations in Blood from Dissolution Testing – A Simple and Practical Approach. The Open Drug Delivery Journal 4, 38-47.

Reichenberg, D., 1953. Properties of Ion-Exchange Resins in Relation to Their Structure .3. Kinetics of Exchange. Journal of the American Chemical Society 75, 589-597.

Siepmann, J., Siepmann, F., 2008. Mathematical modeling of drug delivery. International journal of pharmaceutics 364, 328-343.

Siewert, M., Dressman, J., Brown, C.K., Shah, V.P., Fip, Aaps, 2003. FIP/AAPS guidelines to dissolution/in vitro release testing of novel/special dosage forms. AAPS PharmSciTech 4, E7.

Taylor, R.R., Tang, Y., Gonzalez, M.V., Stratford, P.W., Lewis, A.L., 2007. Irinotecan drug eluting beads for use in chemoembolization: in vitro and in vivo evaluation of drug release properties. European journal of pharmaceutical sciences: official journal of the European Federation for Pharmaceutical Sciences 30, 7-14.

Uppoor, V.R.S., 2001. Regulatory perspectives on in vitro (dissolution)/in vivo (bioavailability) correlations. Journal of Controlled Release 72, 127-132.

United States Pharmacopeia and National Formulary (USP 36-NF 31). <1090> Assessment of Drug Product Performance - Bioavailability, Bioequivalence, and Dissolution. United States Pharmacopeia Convention, Rockville, MD, pp. 729-734. Available at: http://www.uspnf.com/uspnf/pub/index?usp=37&nf=32&s=1&officialOn=August%201,%202014. Accessed 08.08.2014.

Wacker, M., 2013. Nanocarriers for intravenous injection—The long hard road to the market. International journal of pharmaceutics 457, 50-62.

Wacker, M.G., 2014. Nanotherapeutics—Product Development Along the "Nanomaterial" Discussion. Journal of pharmaceutical sciences 103, 777-784.

Chapter Three 89

Zolnik, B.S., Raton, J.-L., Burgess D.J., 2005. Application of USP Apparatus 4 and In Situ Fiber Optic Analysis to Microsphere Release Testing. Dissolution Technologies 12, 11-14.

Mapping of Drug Distribution in the Rabbit VX2

Liver Tumor Model after Chemoembolization with

Sunitinib-Eluting Beads by Complementary

Fluorescence and Mass Spectrometry Imaging

Katrin Fuchs^a, Andras Kiss^b, Pierre E. Bize^c, Rafael Duran^c, Alban Denys^c, Gérard Hopfgartner^b, Gerrit

Borchard^a, Olivier Jordan^a

^a School of Pharmaceutical Sciences, University of Geneva, University of Lausanne, Geneva, Switzerland

^b Life Sciences Mass Spectrometry, Department of Analytical and Inorganic Chemistry, University of Geneva, Geneva, Switzerland

^c Departments of Radiology and Interventional Radiology, CHUV Centre Hospitalier Universitaire Vaudois, Lausanne, Switzerland

Original Research Article

Submitted to:

Radiology

Abstract

Purpose: Drug-eluting beads are used for transarterial embolization of hepatocellular carcinoma. Sunitinib-eluting beads were developed with the aim to locally inhibit embolization-induced neoangiogenesis in the tumor. We studied the local delivery into the tumor and liver tissue and spatial distribution of the anti-angiogenic sunitinib and its metabolites over time.

Materials and Methods: Eight VX2-tumor bearing New Zealand rabbits were embolized with 70-150 μ m DC Bead (total dose of 1.5 mg sunitinib). In adjacent sections of tumor and non-targeted contralateral liver tissue, sunitinib distribution was mapped around occluded vessels 1, 2, 7, 12, 13 and 14 days after embolization by complementary fluorescence and mass spectrometry imaging (MSI). Sunitinib metabolites were also assessed by MSI.

Results: Sunitinib was found localized around beads both in tumor and contralateral liver at 1 day. At 12-14 days, the drug was still retained by the necrotic tumor tissue, resulting in homogeneously distributed, high levels of 25-40 μ g/g in a 1.5 mm radius around the beads, but almost completely eliminated from the contralateral liver tissue. Several of the drug's metabolites, including its primary active metabolite SU12662, were detected in the tumor tissue over 14 days.

Conclusion: Sunitinib was selectively delivered to the tumor by drug-eluting beads at high, therapeutic levels. The drug was distributed at far distances from the beads, possibly reaching most of the VX2 tumor, during at least 14 days. This matches the time span of vascular endothelial growth factor overexpression after embolization.

Keywords:

Transarterial chemoembolization, hepatocellular carcinoma, sunitinib, drug-eluting beads, drug tissue distribution, biodistribution, fluorescence drug mapping, MALDI-SRM mass spectrometry imaging

Advance(s) in Knowledge:

1. In the rabbit VX2 liver tumor model, sunitinib eluted from embolic beads was found localized in the tumor 1-7 days after embolization and distributed farther from the beads after 12-14 days due to diffusion.

- 2. Necrotic tumors were impregnated with high drug levels of 25-40 $\mu g/g$ up to a radius of 1.5 mm around the occluded vessel at 7-14 days.
- 3. Sunitinib was retained by the necrotic tissue to a larger extent than by the non-tumor or viable tumor tissue.
- 4. The four most abundant metabolites of sunitinib, among them the active metabolite SU12662, followed the same distribution pattern as sunitinib and were mainly detected between 7 and 13 days.
- 5. Sunitinib was at least 99.5% eluted from beads both in the tumor and in the contralateral liver already at 1 day.

Implication(s) for Patient Care:

The combination of an embolic device with an anti-angiogenic agent could help overcome TACE-induced neoangiogenesis.

Summary Statement:

After a single embolization of VX2 tumor tissue with sunitinib-eluting beads, sunitinib diffused up to 1.5 mm around the occluded vessel, allowing for coverage of wide tumor areas over at least 14 days, during which its anti-angiogenic activity was required.

1 Introduction

Patients with multinodular tumors and preserved liver function (intermediate stage) are eligible for transarterial chemoembolization (TACE) according to the Barcelona Clinic Liver Cancer (BCLC) guidelines (1). TACE implies the selective injection of a cytostatic agent followed by occlusion of the tumor feeding arteries by some embolic agent. Drug-eluting beads (DEBs) allow for more site-specific and consistent drug delivery to the targeted tumor tissue, resulting in a controlled pharmacokinetic profile (2).

Ischemia caused by TACE is the main trigger of cancer cell death. However, ischemia has been shown to lead to detrimental effects such as the promotion of angiogenesis and tumor recurrence (3-5). The expression of numerous hypoxia-response genes translates into vascular endothelial growth factor (VEGF) expression one day after the intervention, possibly persisting until almost thirty days (6, 7). Prognosis after TACE intervention is more favorable when plasma levels of proangiogenic factors are low (7). To suppress embolization-induced angiogenesis, a therapy combining TACE with anti-angiogenic drugs was proposed (8-10). However, association of TACE with an orally given tyrosine kinase inhibitor failed to demonstrate clinical benefit (11). In contrast, the anti-angiogenic sunitinib loaded on drug-eluting beads showed anticancer efficacy in a preclinical rabbit model for liver tumors with a tolerable safety profile, maintaining therapeutic local drug concentrations with VEGF receptor 2 inhibition during at least fourteen days (12).

The scope of this study was to further investigate the suitability of sunitinib to be delivered via DEBs, investigating the spatial distribution of the drug into the tissue over time. The targeted delivery to the tumor over the time frame of peaking VEGF levels is of utmost importance for the efficacy of the treatment. In addition, a complete, homogeneous impregnation of the tumor with the drug is desired in order to limit tumor relapse. The typical drug quantification technique based on liver homogenization cannot discriminate between eluted and bead-bound drug, the latter providing no anti-angiogenic effect. Moreover, the tissue by itself might influence the drug diffusion and its metabolism, so that drug diffusion distances, distribution and kinetics might differ between tumor and healthy liver tissue, which has not been elucidated for sunitinib yet (13). Fluorescence and mass spectrometry imaging were developed and employed in this study in order to visualize sunitinib and its metabolites around the beads. These methods allowed for checking the efficacy of

sunitinib delivery via drug-eluting beads and determination of drug distribution in the tissue over fourteen days. In addition, therapeutic drug levels could be mapped relative to their distance to the beads in the tumor and liver tissue.

2 Materials and Methods

2.1 Animal Model

Tissues were retrieved from a previous animal study, described as "second comparative study" (12). The protocol was approved by the French Ethics Committee for Animal Experiments (COMETHEA approval number 11/028).

Briefly, adult New Zealand white rabbits (n=13, age 6-7 months, body weight 3.0-3.8 kg) were implanted with VX2 tumors in the left liver lobe. Treatment was administered 14 days later, when the VX2 tumor growth was confirmed by ultrasound imaging (Voluson E8 Expert, GE Healthcare, Velizy, France).

Eight animals were embolized by 0.05 ml 70-150 μm sunitinib-eluting DC Bead® (SEB, Biocompatibles/BTG, Farnham, UK) resulting in a total dose of 1.5 mg sunitinib. Details regarding the SEB loading and the interventional technique are described elsewhere (12, 14, 15). Briefly, tumor-bearing liver lobes were embolized using superselective catheterization, leaving non-targeted contralateral lobes as controls. Four animals were administered orally with 6 mg sunitinib (sunitinib base, LC Laboratories, Woburn, MA, USA) solution per day. One untreated rabbit served as control.

Details regarding tissue sampling and cryosectioning are supplied in the Appendix.

2.2 Sunitinib Biodistribution by Fluorescence Imaging

2.2.1 Fluorescence Imaging Technique

Tissue sections were imaged by an AxioZ1 Imager (Zeiss, Feldbach, Switzerland) with a Fluar 5x/0.25 (magnification/numerical aperture) objective equipped with a cooled, sensitive monochrome

camera (Zeiss Axiocam MRm). Fluorescence of sunitinib (16) was acquired using a fluorescent filter (FITC, 50 ms exposure, 16-bit image resolution), together with bright field images. To visualize the amount of sunitinib around beads in the tissue, fluorescent image heatmaps were generated using ImageJ (v1.50a, NIH, Bethesda, MD, USA) Lookup Table "Thermal" by adjusting images to 650-2000 pixel brightness (650 pixel and lower: violet, 2000 pixel and higher: red). Within this brightness, both low and high sunitinib levels were visualized optimally, avoiding picture saturation, and fluorescence and sunitinib amounts per tissue represented a linear relationship.

2.2.2 Correlation of Sunitinib Fluorescence in Tissue and in DC Bead® with Its Distribution

Linear correlations between fluorescence intensity in tissue sections or bead sections and sunitinib levels were developed (17). The techniques are described in the Appendix.

2.2.3 Sunitinib Distribution Profile around Beads and Non-Eluted Sunitinib

Images of tissue sections taken with the fluorescent filter were analyzed by an ImageJ plugin allowing for concentric measurements around the beads in a vessel. Specifically, the sunitinib fluorescence intensity mean was measured in bands of 10 μ m width until 1.5 mm distance from the bead(s). The mean fluorescence intensity per band was then converted to amount of sunitinib per amount of tissue.

The amount of non-eluted drug remaining in the beads was calculated on the same images by the fluorescence mean intensity per bead. The fluorescence signal of the same bead appearing on several consecutive sections was averaged before calculation of the mean of all beads per animal.

2.2.4 **Statistics**

Sunitinib spatial distribution profiles over time were compared in GraphPad Prism 6.01, using ordinary two-way ANOVA and multiple comparison correction (Tukey post-test), and with paired two-sided student t-test.

2.3 Sunitinib Biodistribution by Mass Spectrometry Imaging

2.3.1 Correlation of Sunitinib Signal in Tissue with Its Distribution

A linear calibration between MSI signal intensity and sunitinib amount per tissue was developed by homogenizing control tissue with sunitinib solution of ascending concentrations. Rabbit liver tissue frozen at -80°C from a control animal embolized with saline 0.9% from the proof of concept study described by (12) was diluted 1:1 with ascending aqueous sunitinib solutions (0-1.5 mg/ml) and homogenized in a FastPrep[®]-24 (MP Biomedicals, Illkirch, France) tissue homogenizer. 0.5 μl of each concentration was deposited on the same steel slide as the tissue sections to be analyzed, and were left to dry.

The resulting calibration curve was measured in the range of 0 to 1500 μ g sunitinib/g tissue (Supplementary Figure 2). The method had a limit of detection of 10.89 μ g sunitinib/g tissue and a limit of quantification of 36.29 μ g/g tissue.

2.3.2 MALDI-SRM Mass Spectrometry Imaging Technique

For the quantitative MALDI-SRM/MS imaging of the sunitinib distribution the slides were coated with d10-sunitinib (Alsachim, Illkirch, France) as internal standard by an iMatrixSpray (18) apparatus. After drying, α -cyano-4-hydroxycinnamic acid in acetonitrile:H₂O 1:1 + 0.1% trifluoroacetic acid were deposited, and slides were frozen at -20°C before further analysis. For the imaging of sunitinib metabolites no internal standard was used.

The MALDI-SRM/MSI measurements were performed on a MALDI-triple quadrupole linear ion trap mass spectrometer (Sciex, Concord, ON, Canada). All the datasets were recorded in positive ionization mode in combination with selected reaction monitoring (SRM). The SRM transitions used for the quantitative imaging of sunitinib, the internal standard and for the metabolites can be found in the Appendix.

The MSI datasets were analyzed using the BioMap software (Novartis, Basel, Switzerland). The sunitinib images were normalized to the internal standard image pixel by pixel using the divide function in BioMap. The metabolite images were used without normalization.

3 Results

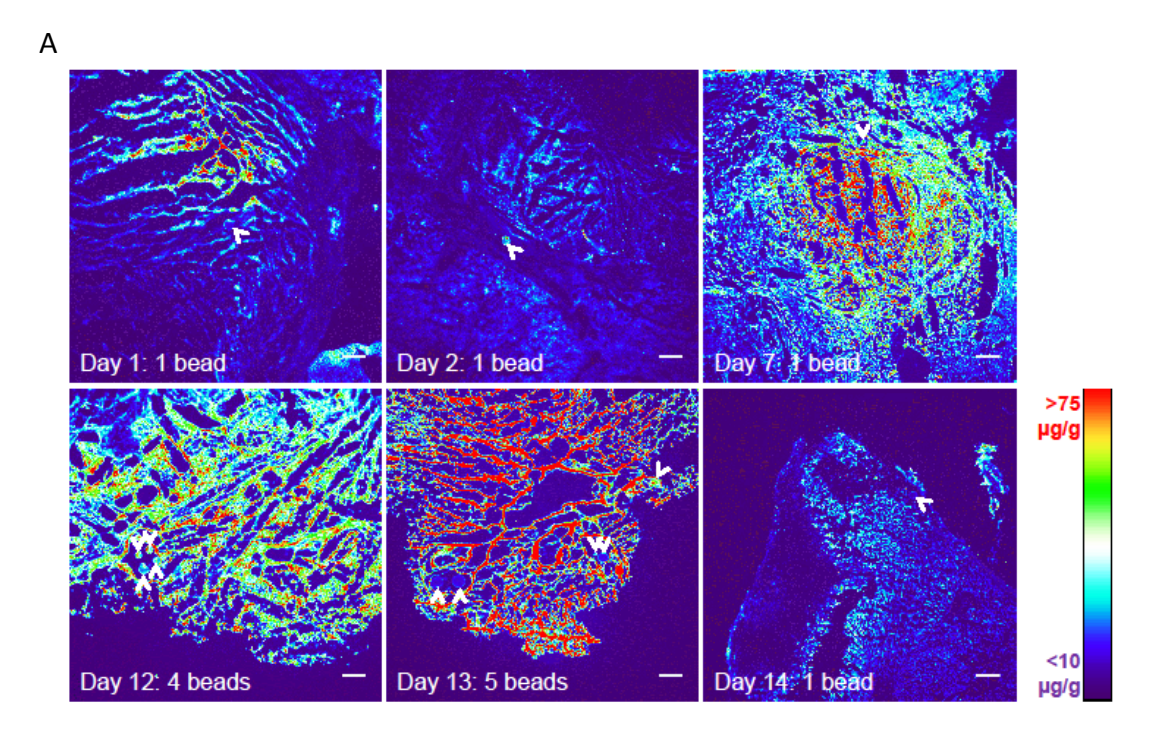
3.1 Sunitinib Biodistribution in Tumor and Contralateral Liver Tissue by Fluorescence Imaging

Sunitinib diffusion from 70-150 μ m drug-eluting beads was imaged in tumor tissue and contralateral liver lobe from eight embolized rabbits, taking advantage of sunitinib fluorescence. Figure 1 shows representative regions of interest (ROIs) from six animals at each time point from day 1 to 14, color-weighted by the intensity of fluorescence and thus sunitinib levels.

Beads had reached the tumor tissue in all eight animals. In the contralateral liver lobe, beads were found only in three of eight animals due to non-target embolization (Table 1). Figure 2 demonstrates the drug diffusion distances and kinetics in the tumor tissue (A) and the contralateral liver lobe (B) 1 to 14 days after embolization.

Table 1. Rabbit tumor and contralateral liver samples from the SEB group. Number of analyzed sections for fluorescence varied by the presence of beads.

| Days after embolization | Analyzed samples of tumor (T) and/or | Number of sections with beads for fluorescence acquisition | | |
|-------------------------|--------------------------------------|--|----------------------------|--|
| | contralateral liver (L) | Tumor | Contralateral liver tissue | |
| 1 d | T+L | 3 | 22 | |
| 2 d | T+L | 3 | 0 | |
| 7 d | T+L | 13 | 11 | |
| 12 d | T+L | 15 | 0 | |
| 12 d | Т | 8 | - | |
| 13 d | T+L | 28 | 8 | |
| 13 d | T+L | 10 | 0 | |
| 14 d | T+L | 9 | 0 | |



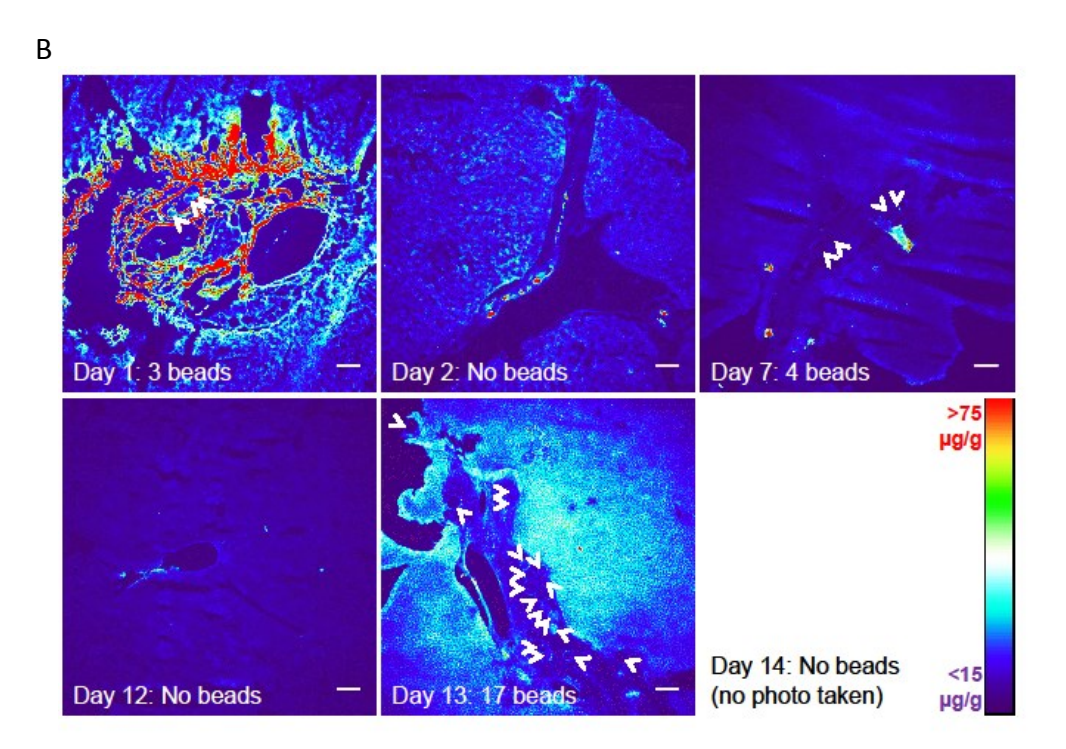
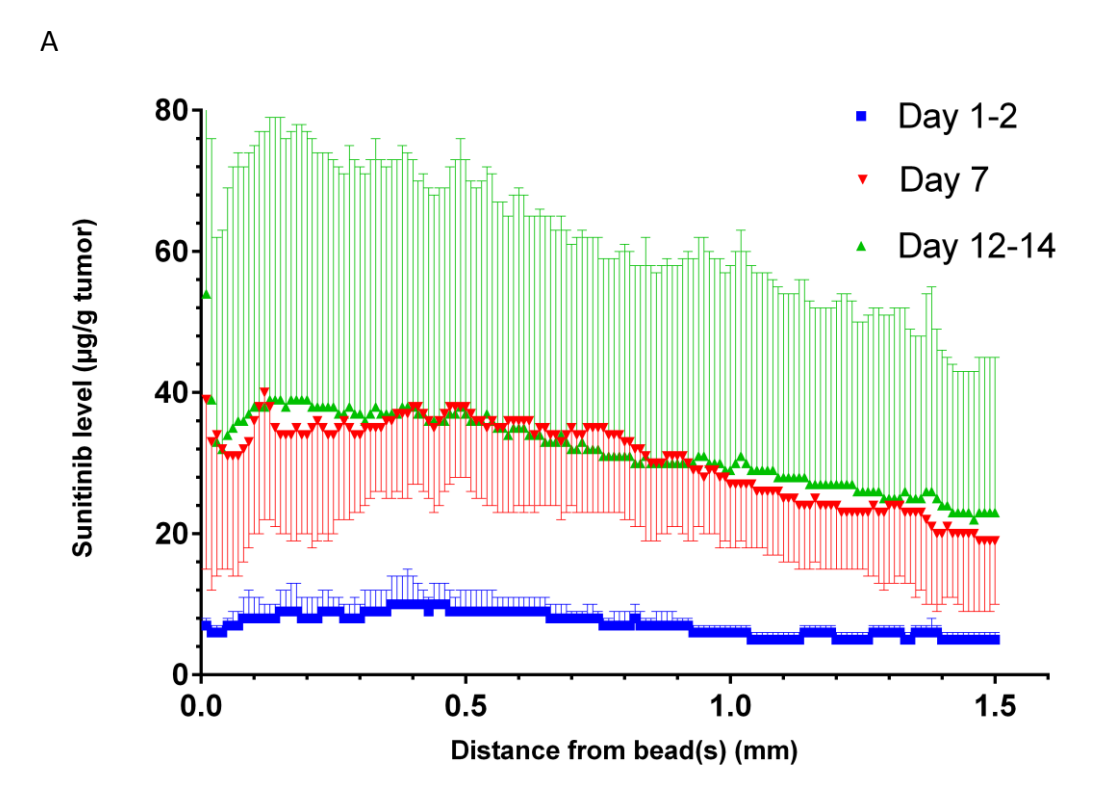


Figure 1. Fluorescence maps of sunitinib eluted from embolic beads in (A) tumor and (B) contralateral liver lobe sections from day 1 to 14 after embolization. Drug levels are color-weighted (color bar). Number of beads is stated for the displayed section. Arrowhead pointing toward bead, scale bar = $200 \, \mu m$.



В

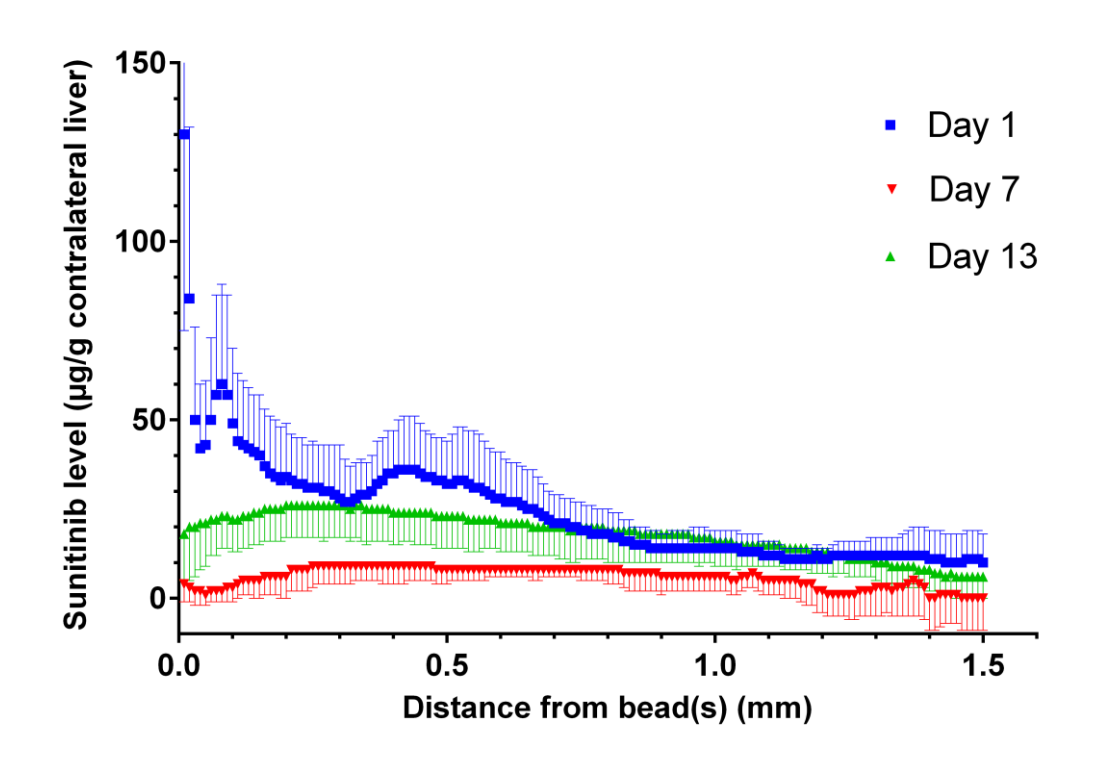


Figure 2. Sunitinib levels around beads in (A) the tumor and (B) the contralateral liver lobe from day 1 until day 14 after embolization with sunitinib-eluting beads.

In the tumor (Figure 1A), sunitinib was found localized 1-7 days after embolization and distributed farther from the beads with time. The necrotic tumor was impregnated with high drug levels of 25-40 μ g/g up to a radius of 1.5 mm around the occluded vessel at 7-14 days (Figure 2A). Ordinary two-way ANOVA comparing sunitinib distribution profiles showed statistical difference of the drug level with regard to time after embolization (P<0.0001, Figure 2A), but not with regard to distance from the bead (P=0.9992).

In the contralateral liver lobe, the drug was concentrated around beads at early time points, whereas amounts were lower at 13 days (Figure 1B, Figure 2B). Sunitinib levels of $60 \mu g/g$ in a $100 \mu m$ radius around the beads were reached at 1 day with a sharp and fast decrease with increasing distance from the bead (Figure 2B). At later time points, sunitinib was barely detectable. Two-way ANOVA with post-hoc correction comparing sunitinib distribution profiles in the contralateral liver tissue showed statistical difference until diffusion distances of 0.85 mm from the bead at 1, 7 and 13 days after embolization.

Sunitinib diffusion profiles around the bead(s) were different at every time point between tumor and contralateral liver lobe (paired t-test, P<0.0001, Figure 2A and B).

Sunitinib was at least 99.5% eluted from the beads both in the tumor and in the contralateral liver at every measured time point (Supplementary Figure 3).

3.2 Biodistribution of Sunitinib and Its Metabolites in Liver and Tumor Tissue by Mass Spectrometry Imaging

Quantitative MSI was used to complement the data obtained by fluorescence imaging. While fluorescence might measure the totality of the parent drug (sunitinib) and its metabolites, MSI is posed to discern between these species, quantifying the analyte and its metabolites. Figure 3 shows the distribution of sunitinib in tumor sections at different treatment time points obtained by MSI. Similar to the fluorescence imaging datasets, the drug was mainly localized in a restricted tissue region close to the beads' location at earlier time points, whereas its distribution became more homogeneous at later time points due to drug diffusion.

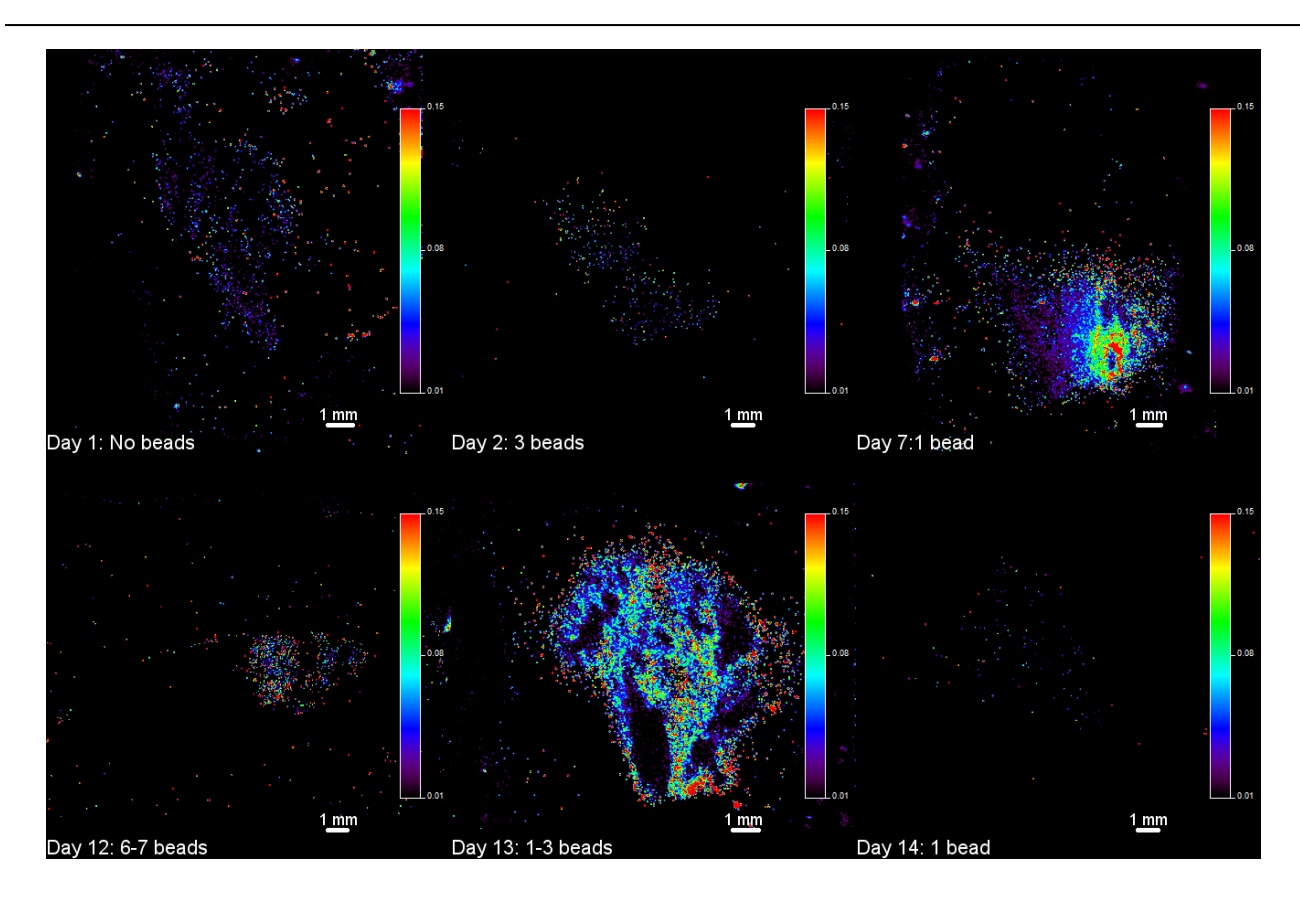


Figure 3. MSI images showing sunitinib diffusion in the tumor at different time points after treatment. Color bar shows the intensity of the sunitinib signal normalized pixel-by-pixel to the internal standard signal.

The qualitative observations were confirmed by sunitinib quantification. Pixel-by-pixel quantification in MSI is currently still unreliable (19). To overcome this issue, two different approaches were applied. In the first approach, 6 regions of interests were randomly selected on each tissue sample (Supplementary Figure 4) and the drug quantity was calculated in these ROIs. The quantitative results (Table 2) confirmed the qualitative assessment of the drug diffusion in the day 7 and day 13 tumor samples. In the day 7 sample, half of the selected ROIs were in the high intensity area ($^{\sim}160~\mu\text{g/g}$) and had 4-5 times higher drug levels than the other three ROIs. The drug level in the ROIs in the tumor sample 13 days after embolization had low variability confirming the more homogeneous sunitinib distribution. Interestingly after 12 days, several of the ROIs showed relatively high sunitinib levels (50-70 $\mu\text{g/g}$), although the average drug level was below the limit of quantification.

Table 2. Sunitinib levels (µg/g tissue) in selected ROIs of the tumor samples measured by MSI.

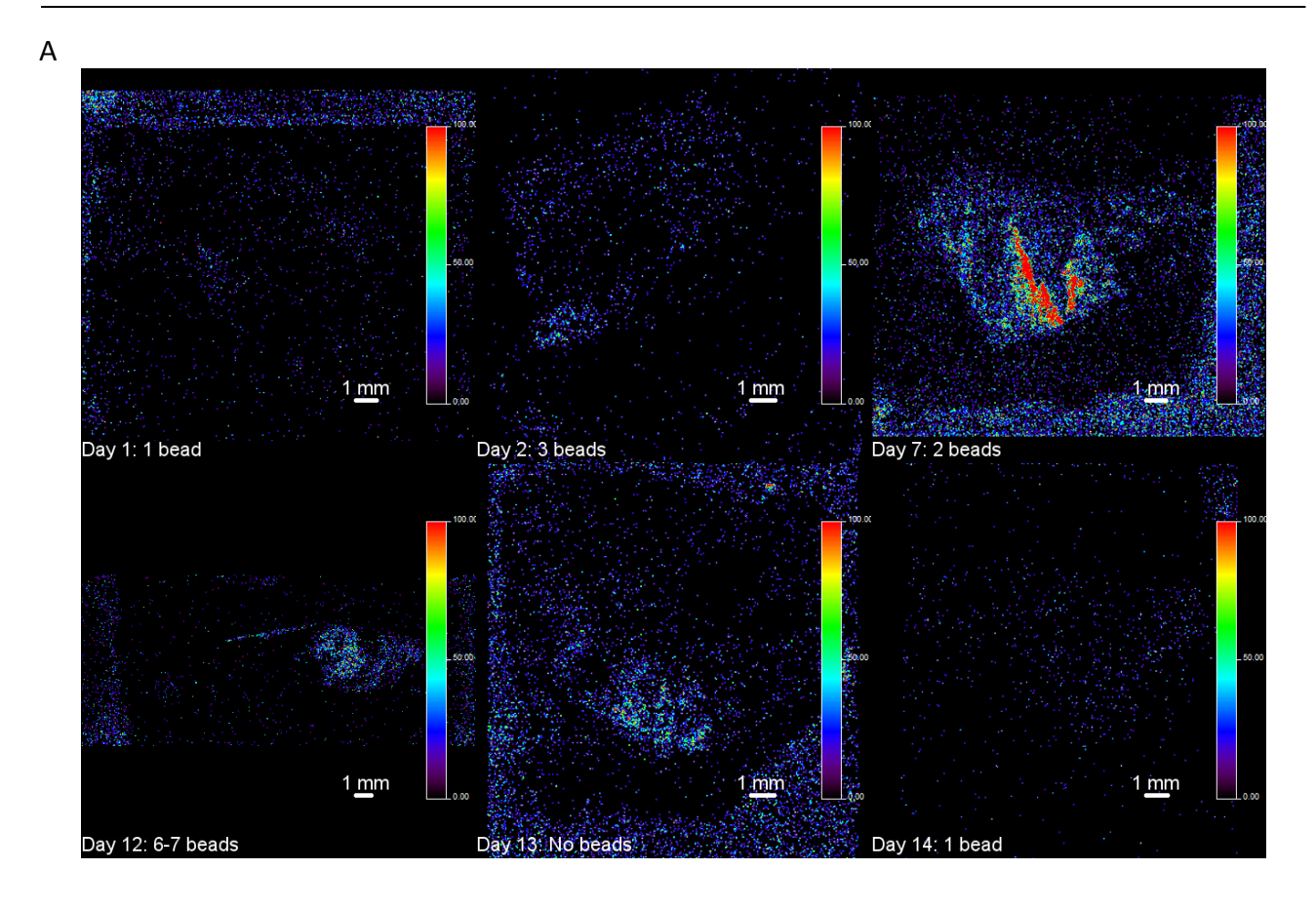
| | 1 day | 2 days | 7 days | 12 days | 13 days | 14 days |
|-------|-------|--------|--------|---------|---------|---------|
| ROI 1 | < LOD | < LOD | 164.5 | 73.5 | 105.3 | < LOD |
| ROI 2 | < LOD | < LOD | 157.4 | < LOD | 112.8 | < LOD |
| ROI 3 | 20.32 | < LOD | 152.5 | 58.5 | 133.8 | < LOD |
| ROI 4 | < LOD | < LOD | 33.2 | 16.0 | 98.8 | < LOD |
| ROI 5 | < LOD | < LOD | 40.1 | 52.4 | 60.4 | < LOD |
| ROI 6 | < LOD | < LOD | 19.4 | < LOD | 138.6 | < LOD |

LOD = limit of detection

In the second method, the average signal intensity from the whole tissue was used to calculate the sunitinib level (Supplementary Table 1). The sunitinib level was above the limit of quantification for all of the day 7 and day 13 tumor samples and the measured levels were close to those obtained by LC-MS/MS measurements (12). Additionally, in one tumor sample at day 12 the signal was above the limit of detection, but below the limit of quantification. As a result, no reliable quantitative information was obtained.

In the contralateral liver lobe, sunitinib levels were below the limit of detection of the MALDI-SRM/MS imaging method. No drug was visible in any of the images (data not shown), despite the presence of beads in the contralateral livers of some animals.

MALDI-SRM/MSI also enabled the detection of the four most frequent sunitinib metabolites (20), among them the active metabolite SU12662 (Figure 4, Supplementary Figure 5). Their distribution followed the one of the parent drug with a high concentration region in the tissue 7 days after treatment and a much more homogenous distribution at later time points. All of the metabolites were still present in the tumor tissue up to 14 days after treatment. Similar to sunitinib itself, their level was below the limit of detection in the contralateral liver samples and 1 day after treatment.



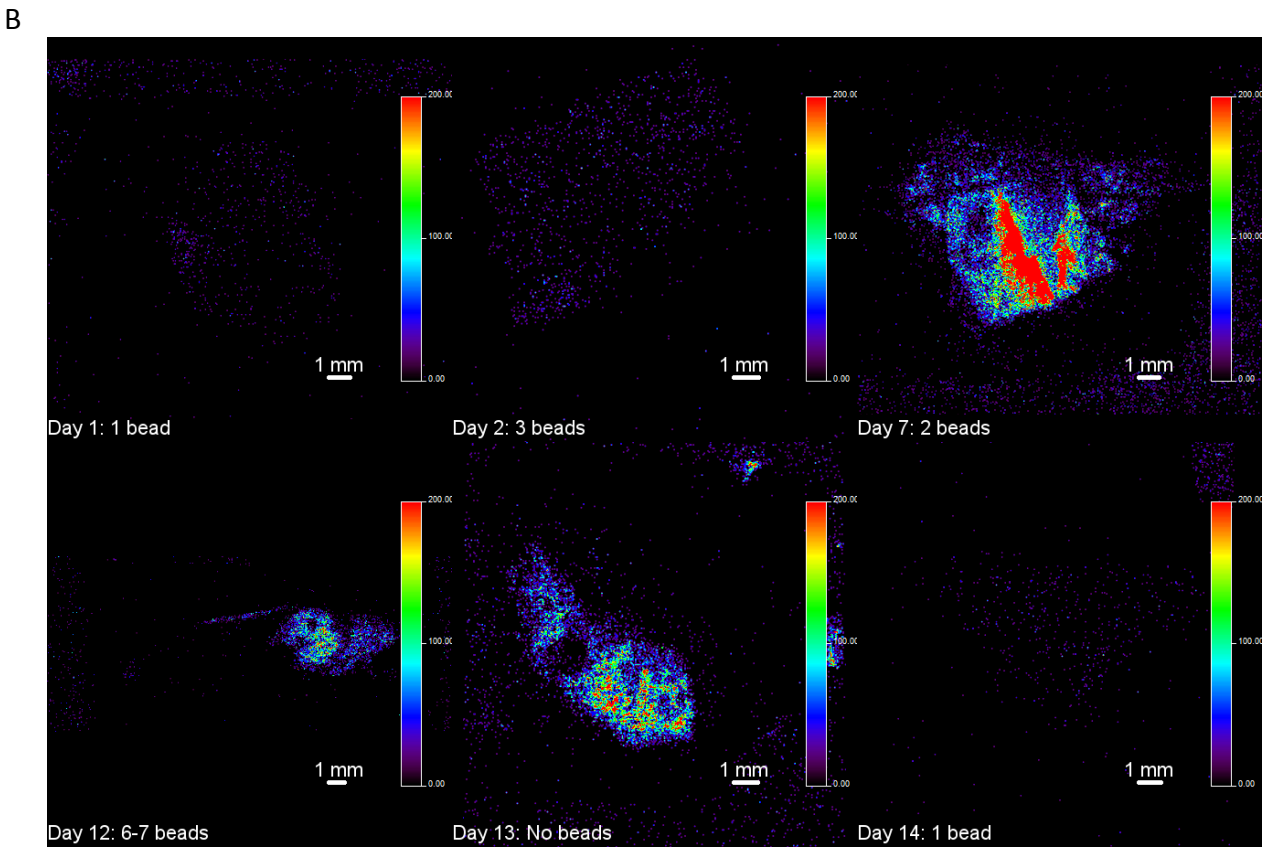


Figure 4. Diffusion of N-desethyl sunitinib (A) and N-desaturated sunitinib (B) in the tumor over time. Color bar shows the absolute intensity of the SRM transition of the respective compound.

4 Discussion

Local delivery of sunitinib by embolic beads was performed with the intent to counteract the undesired onset of neoangiogenesis caused by embolization-induced hypoxia, resulting in tumor recurrence and poor outcomes (3-5, 14). This technique would limit systemic toxicity as compared to the oral route (21), while increasing its efficacy by high intratumoral concentration. Even if this combination seemed to be efficient in the VX2 model (12), questions remained concerning the drug distribution and metabolism within the tumor and at the periphery of beads.

Imaging methods applied in this study confirmed the complete sunitinib elution from embolization beads and delivery into rabbit liver tumors. Sunitinib elution from beads into the tumor was localized at early time points after embolization, while diffusion led to wide-spread distribution at fourteen days. In contrast to doxorubicin elution, sunitinib elution from DC Beads *in vivo* was found to be faster and complete 1 day after embolization in both tumor and liver tissues, as predicted from data obtained *in vitro* (14, 15, 22). In the present study, sunitinib was found to diffuse farther around embolized vessels with diffusion distances over at least 1.5 mm vs. 0.6 mm for doxorubicin (22). Thus, sunitinib attained more extended tissue areas over a shorter time period compared to doxorubicin. The early, but sustainably high sunitinib levels coincided with the secretion of VEGF, which was inhibited by sunitinib (6, 7). The far diffusion of sunitinib into the tissue with time allowed reaching more distant tumor areas and thus resulted in higher probabilities to reach all tumor cells and complete anti-angiogenesis, with a cut-off of the malignancy from blood supply.

Sunitinib was retained by the necrotic tissue to a larger extent than by the non-tumor or viable tumor tissue. This resulted in significantly higher levels in the tumor than in the contralateral liver in the same animals at 7 days and 12-14 days after embolization, as confirmed equally by the two employed methods. Similarly to doxorubicin, sunitinib diffusion into the non-tumor liver tissue was facilitated and elimination occurred quickly, whereas fibrotic barriers or loss of functioning cellular mechanisms resulted in higher drug levels retained in necrotic tissue (22, 23). Thus, the drug diffusion, metabolism and elimination were inherent to the type of tissue, and were slowed down in cancer cells compared to contralateral liver.

The drug-tissue binding allowed for attaining therapeutic or supra-therapeutic sunitinib levels of 25-40 μ g/g specifically in the tumor core at 7-14 days. For comparison, the target effective concentration of sunitinib in plasma was determined to be as low as 50-100 ng/ml (24), IC₅₀ for VEGF receptor 2 inhibition is 2-21 ng/ml in endothelial cells and 20-37 ng/ml for platelet-derived growth factor receptor β (PDGFR β) inhibition (25). Sunitinib IC₅₀ in HCC cultures lies in the 1-2 μ M (0.5-1 μ g/ml) range (26). The maintenance of the therapeutic margin together with the treatment regimen display a pivotal factor for outcome (27, 28), because pharmacological effects of sunitinib were seen to be related to toxicity and drug resistance (29, 30). To compare to doxorubicin-eluting beads, Namur et al. (22) found doxorubicin levels after bead elution to be in similar ranges as the IC₅₀, hence doses of sunitinib loaded on DEBs might be lowered for the use in clinics. Sunitinib maximum loading of 30 mg/g beads was used for the present study (14).

Fluorescence imaging does not only determine sunitinib itself, but includes fluorescent metabolites, like its major, pharmacologically active N-desethyl metabolite SU12662 (31). For this reason, the complementary mass spectrometry imaging technique was added to unequivocally identify sunitinib in the tumor. It confirmed the sunitinib spatial diffusion over time and sunitinib levels in the tumor samples. Distribution of the studied metabolites also followed closely the distribution of sunitinib itself. Additionally, the active SU12662 was still present two weeks after treatment, evidencing successful sustained drug exposure coinciding with the time span of intra-tissular VEGF release (3, 4, 6, 7, 10).

In conclusion, beads administered during TACE were shown to effectively elute sunitinib into the tumor at therapeutic levels. Sunitinib diffused over large distances around the occluded vessel, allowing for coverage of wide tumor zones. Due to tissue binding of sunitinib, the drug persisted in the necrotic environment after a single embolization over at least 14 days, during which its antiangiogenic activity was required. Selective local delivery of sunitinib might be considered as means for efficient local inhibition of angiogenesis and prevention of tumor rebound.

5 Acknowledgements

The authors acknowledge Dr. Hesham Ismail, Dr. Olivier Dorchies and Ophélie Patthey for their competent advice with the use of the cryotome, the Bioimaging platform for the ImageJ plugin "Concentric measurements", and Sophie Montandon, Dr. Athanasia Tzika and Prof. Michel Milinkovitch for instructions and use of the tissue homogenizer (all from the University of Geneva).

The animal study was partially funded by a research grant from Biocompatibles Ltd./BTG, Farnham, UK to AD, PEB and OJ.

6 References

1. Forner A, Gilabert M, Bruix J, Raoul JL. Treatment of intermediate-stage hepatocellular carcinoma. Nat Rev Clin Oncol. 2014;11(9):525-535.

- 2. Varela M, Real MI, Burrel M, et al. Chemoembolization of hepatocellular carcinoma with drug eluting beads: efficacy and doxorubicin pharmacokinetics. J Hepatol. 2007;46(3):474-481.
- 3. Shim JH, Park JW, Kim JH, et al. Association between increment of serum VEGF level and prognosis after transcatheter arterial chemoembolization in hepatocellular carcinoma patients. Cancer Sci. 2008;99(10):2037-2044.
- 4. Sergio A, Cristofori C, Cardin R, et al. Transcatheter arterial chemoembolization (TACE) in hepatocellular carcinoma (HCC): the role of angiogenesis and invasiveness. Am J Gastroenterol. 2008;103(4):914-921.
- 5. Wang B, Xu H, Gao ZQ, Ning HF, Sun YQ, Cao GW. Increased expression of vascular endothelial growth factor in hepatocellular carcinoma after transcatheter arterial chemoembolization. Acta Radiol. 2008;49(5):523-529.
- 6. Britten CD, Gomes AS, Wainberg ZA, et al. Transarterial chemoembolization plus or minus intravenous bevacizumab in the treatment of hepatocellular cancer: a pilot study. BMC Cancer. 2012;12:16.
- 7. Li X, Feng GS, Zheng CS, Zhuo CK, Liu X. Expression of plasma vascular endothelial growth factor in patients with hepatocellular carcinoma and effect of transcatheter arterial chemoembolization therapy on plasma vascular endothelial growth factor level. World J Gastroenterol. 2004;10(19):2878-2882.
- 8. Gadaleta CD, Ranieri G. Trans-arterial chemoembolization as a therapy for liver tumours: New clinical developments and suggestions for combination with angiogenesis inhibitors. Crit Rev Oncol Hematol. 2011;80(1):40-53.

9. Ranieri G, Marech I, Lorusso V, et al. Molecular targeting agents associated with transarterial chemoembolization or radiofrequency ablation in hepatocarcinoma treatment. World J Gastroenterol. 2014;20(2):486-497.

- 10. Xiong ZP, Yang SR, Liang ZY, et al. Association between vascular endothelial growth factor and metastasis after transcatheter arterial chemoembolization in patients with hepatocellular carcinoma. Hepatobiliary Pancreat Dis Int. 2004;3(3):386-390.
- 11. Lencioni R, Llovet JM, Han G, et al. Sorafenib or placebo plus TACE with doxorubicin-eluting beads for intermediate stage HCC: The SPACE trial. J Hepatol. 2016.
- 12. Bize P, Duran R, Fuchs K, et al. Antitumoral Effect of Sunitinib-eluting Beads in the Rabbit VX2 Tumor Model. Radiology. 2016;280(2):425-435.
- 13. Weinberg BD, Blanco E, Lempka SF, Anderson JM, Exner AA, Gao J. Combined radiofrequency ablation and doxorubicin-eluting polymer implants for liver cancer treatment. J Biomed Mater Res A. 2007;81(1):205-213.
- 14. Fuchs K, Bize PE, Dormond O, et al. Drug-eluting beads loaded with antiangiogenic agents for chemoembolization: in vitro sunitinib loading and release and in vivo pharmacokinetics in an animal model. J Vasc Interv Radiol. 2014;25(3):379-387 e372.
- 15. Fuchs K, Bize PE, Denys A, Borchard G, Jordan O. Sunitinib-eluting beads for chemoembolization: methods for in vitro evaluation of drug release. Int J Pharm. 2015;482(1-2):68-74.
- 16. Gotink KJ, Broxterman HJ, Labots M, et al. Lysosomal sequestration of sunitinib: a novel mechanism of drug resistance. Clin Cancer Res. 2011;17(23):7337-7346.
- 17. Gao J, Qian F, Szymanski-Exner A, Stowe N, Haaga J. In vivo drug distribution dynamics in thermoablated and normal rabbit livers from biodegradable polymers. J Biomed Mater Res. 2002;62(2):308-314.
- 18. Stoeckli M, Staab D. Reproducible Matrix Deposition for MALDI MSI Based on Open-Source Software and Hardware. J Am Soc Mass Spectrom. 2015;26(6):911-914.

19. Porta T, Lesur A, Varesio E, Hopfgartner G. Quantification in MALDI-MS imaging: what can we learn from MALDI-selected reaction monitoring and what can we expect for imaging? Anal Bioanal Chem. 2015;407(8):2177-2187.

- 20. Torok S, Vegvari A, Rezeli M, et al. Localization of sunitinib, its metabolites and its target receptors in tumour-bearing mice: a MALDI-MS imaging study. Br J Pharmacol. 2015;172(4):1148-1163.
- 21. Cheng AL, Kang YK, Lin DY, et al. Sunitinib versus sorafenib in advanced hepatocellular cancer: results of a randomized phase III trial. J Clin Oncol. 2013;31(32):4067-4075.
- 22. Namur J, Citron SJ, Sellers MT, et al. Embolization of hepatocellular carcinoma with drugeluting beads: doxorubicin tissue concentration and distribution in patient liver explants. J Hepatol. 2011;55(6):1332-1338.
- 23. Blanco E, Qian F, Weinberg B, Stowe N, Anderson JM, Gao JM. Effect of fibrous capsule formation on doxorubicin distribution in radiofrequency ablated rat livers. Journal of Biomedical Materials Research Part A. 2004;69a(3):398-406.
- 24. Mendel DB, Laird AD, Xin XH, et al. In vivo antitumor activity of SU11248, a novel tyrosine kinase inhibitor targeting vascular endothelial growth factor and platelet-derived growth factor receptors: Determination of a pharmacokinetic/pharmacodynamic relationship. Clinical Cancer Research. 2003;9(1):327-337.
- 25. Chow LQM, Eckhardt SG. Sunitinib: From Rational Design to Clinical Efficacy. Journal of Clinical Oncology. 2007;25(7):884-896.
- 26. Bagi CM, Gebhard DF, Andresen CJ. Antitumor effect of vascular endothelial growth factor inhibitor sunitinib in preclinical models of hepatocellular carcinoma. Eur J Gastroenterol Hepatol. 2012;24(5):563-574.
- 27. Faivre SJ, Bouattour M, Dreyer C, Raymond E. Sunitinib in Hepatocellular Carcinoma: Redefining Appropriate Dosing, Schedule, and Activity End Points. Journal of Clinical Oncology. 2009;27(35):E248-E250.

28. Lee JL, Kim MK, Park I, et al. RandomizEd phase II trial of Sunitinib four weeks on and two weeks off versus Two weeks on and One week off in metastatic clear-cell type REnal cell carcinoma: RESTORE trial. Ann Oncol. 2015.

- 29. Huang L, Hu C, Di Benedetto M, et al. Induction of multiple drug resistance in HMEC-1 endothelial cells after long-term exposure to sunitinib. Onco Targets Ther. 2014;7:2249-2255.
- 30. Zhu AX, Duda DG, Ancukiewicz M, et al. Exploratory analysis of early toxicity of sunitinib in advanced hepatocellular carcinoma patients: kinetics and potential biomarker value. Clin Cancer Res. 2011;17(4):918-927.
- 31. Speed B, Bu HZ, Pool WF, et al. Pharmacokinetics, distribution, and metabolism of [14C]sunitinib in rats, monkeys, and humans. Drug Metab Dispos. 2012;40(3):539-555.

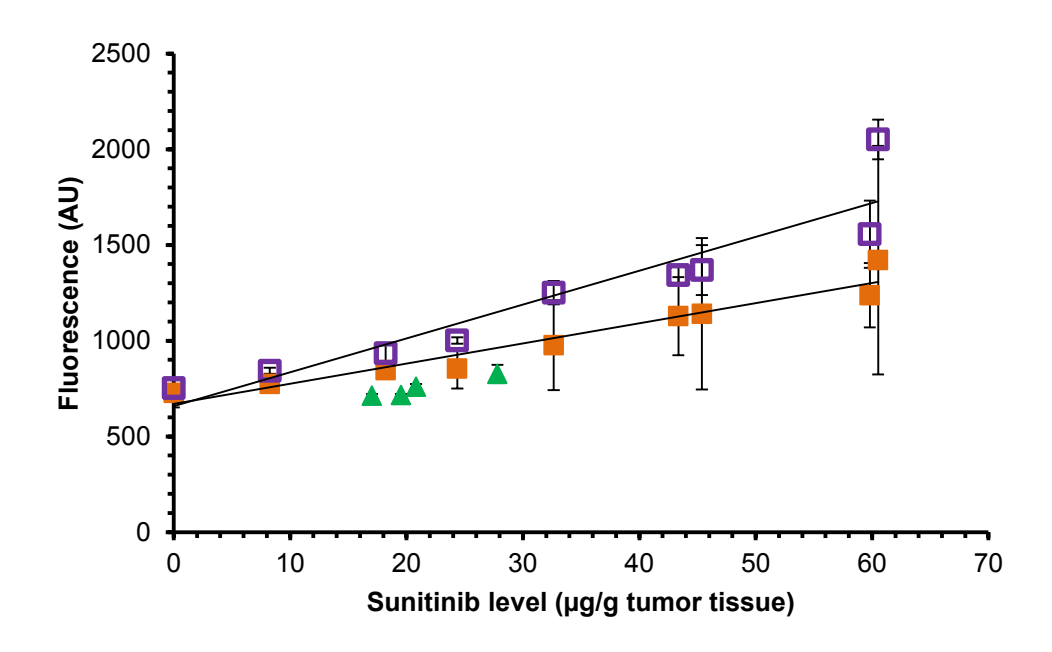
7 Supplementary Material

Supplementary Table 1. Sunitinib levels ($\mu g/g$ tissue) measured by MSI in the tumor, averaged over complete tumor sections from the SEB group.

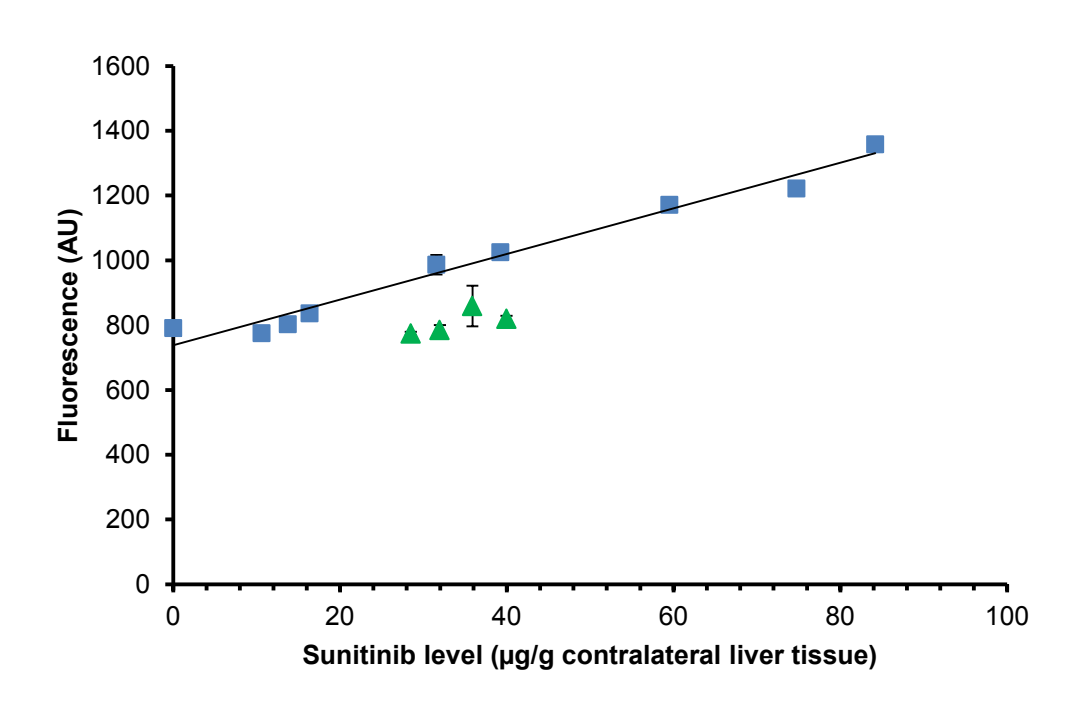
| Tumor section | 1 day | 2 days | 7 days | 12 days | 13 days | 14 days |
|------------------|-------|--------|----------|---------|----------|---------|
| 1 | < LOD | < LOD | 52.3 | 12.5 | 63.5 | < LOD |
| 2 | < LOD | < LOD | 50.4 | < LOD | 68.2 | < LOD |
| 3 | < LOD | < LOD | 46.3 | < LOD | 62.4 | < LOD |
| average | < LOD | < LOD | 49.7±7.7 | 12.5 | 64.7±7.7 | < LOD |

LOD = limit of detection

Α

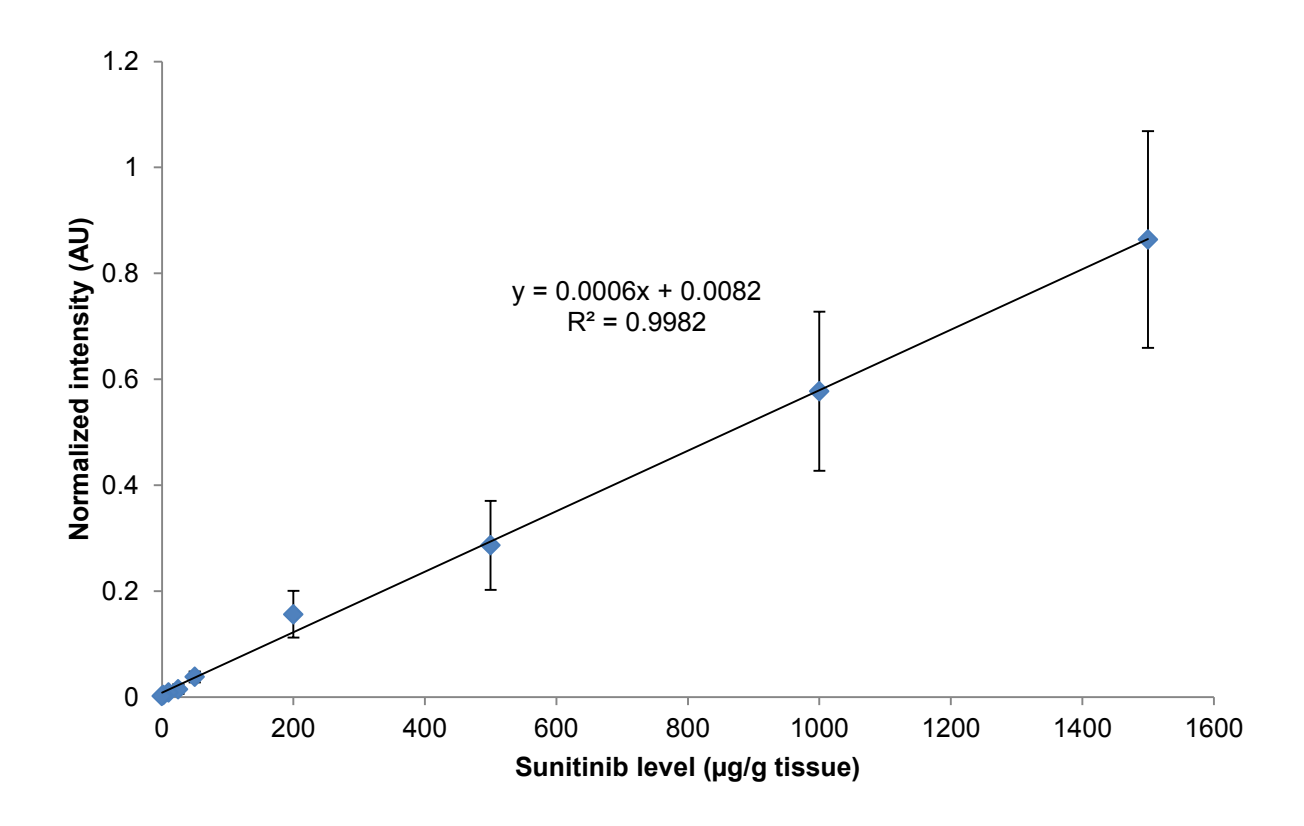


В

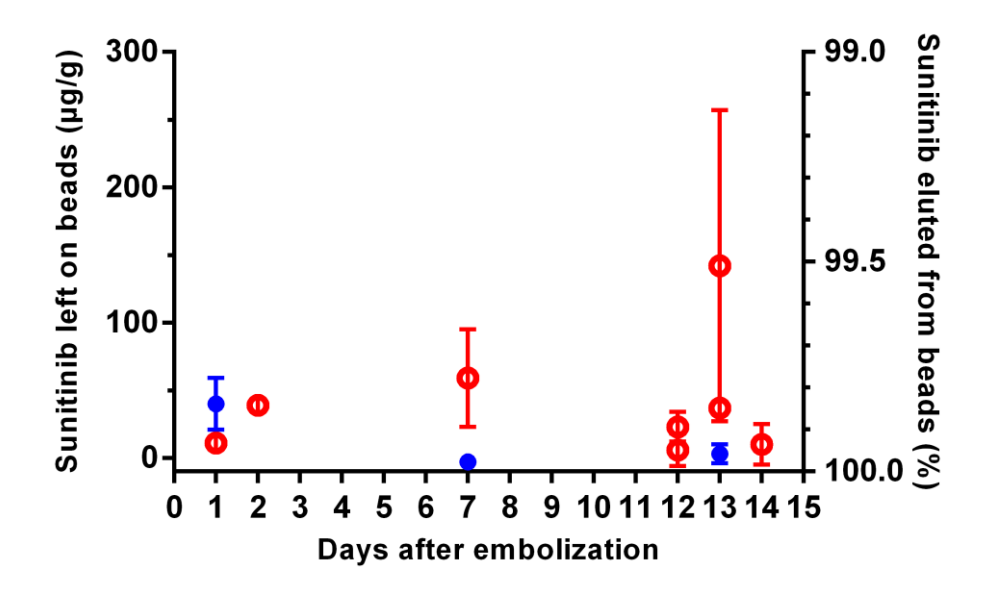


Supplementary Figure 1. Calibration lines for sunitinib levels by fluorescence in (A) the viable (\blacksquare) and the necrotic (\square) tumor tissue and in (B) the contralateral liver lobe, and comparison with p.o. tumor and liver samples (\blacktriangle).

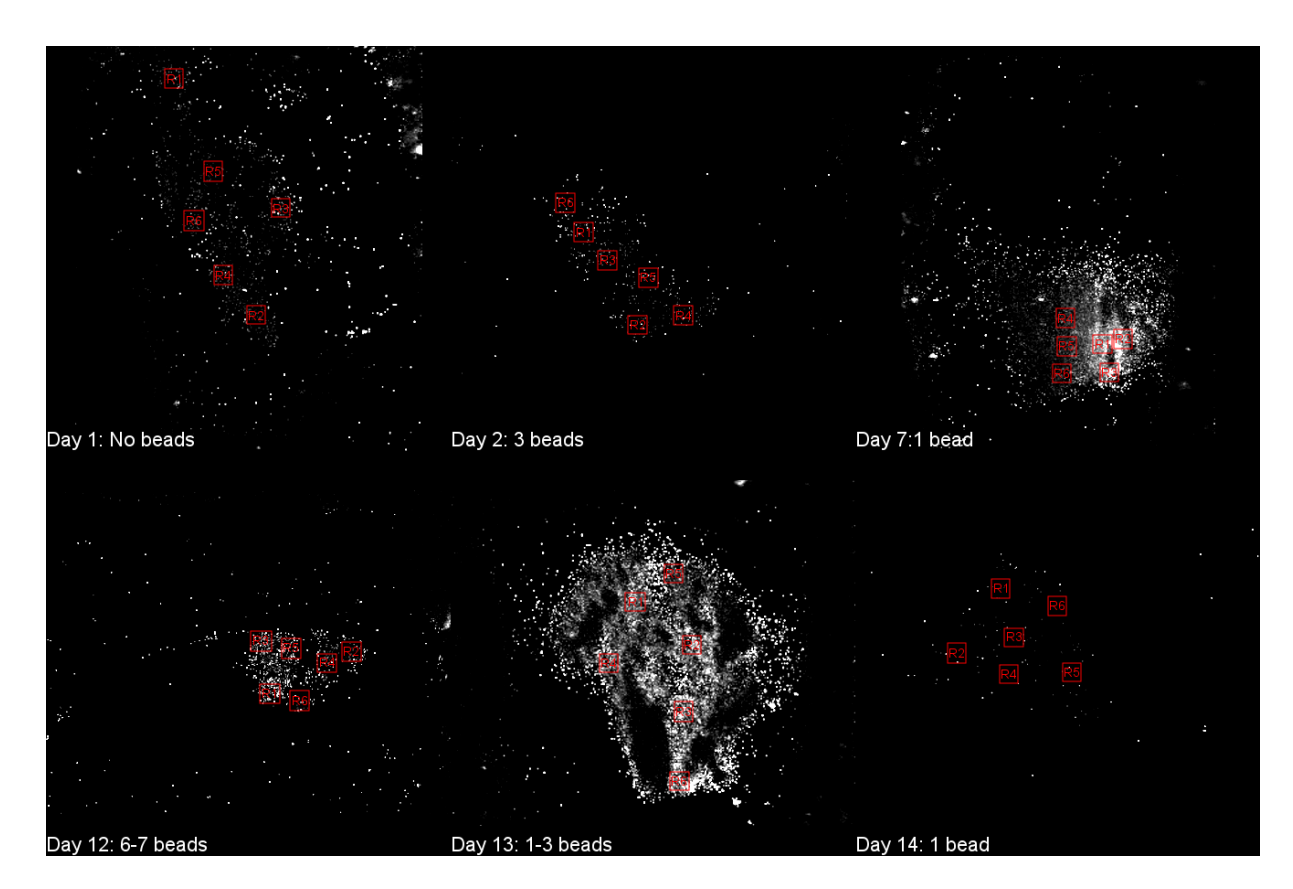
Fluorescence intensity in tissue sections with known sunitinib levels from animals treated perorally were used to check and validate the calibration. Sunitinib levels after a single peroral administration of 6 mg of sunitinib had been previously defined by LC-MS/MS measurements (14). A displays sunitinib fluorescence related to the sunitinib tissue levels measured by LC-MS/MS in (A) the viable tumor tissue and (B) the liver in four animals (12). There was no necrotic tissue in animals administered via the peroral route. AU = Arbitrary Units.



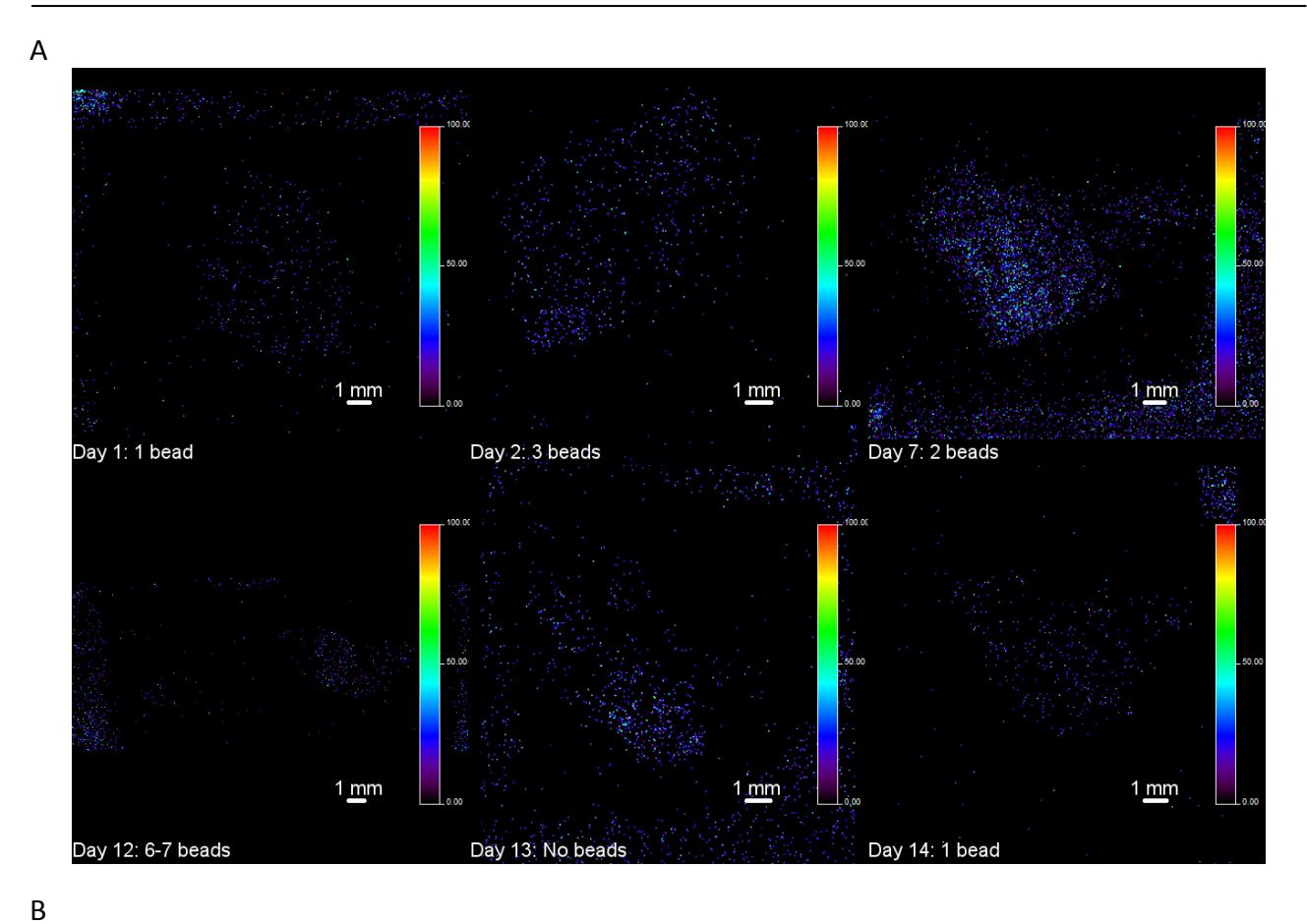
Supplementary Figure 2. Calibration curve for determination of sunitinib levels in the tissue by MSI. AU = Arbitrary Units.

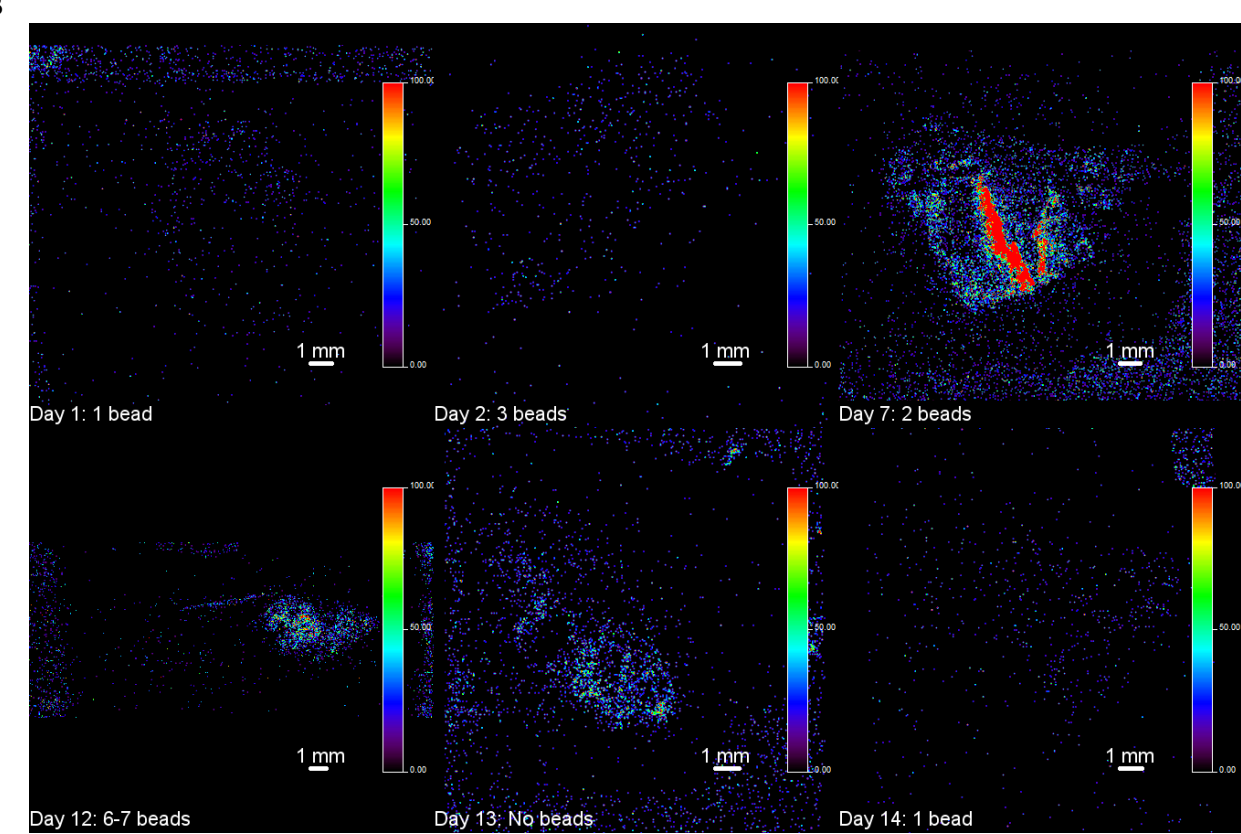


Supplementary Figure 3. Sunitinib amount left on beads 1-14 days after embolization in tumor tissue (○, 1 d: n=3, 2 d: n=2, 7 d: n=27, 12 d: n=8+48 (2 animals), 13 d: n=10+71 (2 animals), 14 d: n=10) and contralateral liver (○, 1 d: n=71, 7 d: n=65, 13 d: n=73). N stands for the number of sectioned beads measured.



Supplementary Figure 4. Selected regions of interest in the tumor over time used for quantification of sunitinib by MSI.





Supplementary Figure 5. MSI images of the distribution of N,N-didesethyl-sunitinib (A) and sunitinib N-oxide (B) in the tumor over time. Color bar shows the absolute intensity of the SRM transitions of the respective compound.

7.1 Tissue Sampling

On day 14, all surviving animals were euthanized with an intracardiac injection of pentobarbital (Dolethal, Vetoquinol, Paris, France) under general anesthesia.

Tumor samples were harvested in the solid part of the tumor. Tumor and contralateral liver lobe samples (approximately 1 x 1 x 1 cm) were snap-frozen, embedded in OCT cryosectioning medium (Tissue Tek OCT compound, Sakura Finetek, Torrance, CA, USA) and stored at -80°C for cryosectioning.

7.2 Tissue Cryosectioning

At least 24 hours prior to cryosectioning, the tumor or contralateral liver samples were stored at - 20° C. Tissues were sectioned at a thickness of $10~\mu m$ at - 15° C in a CryoStar NX70 (Thermo Fisher Scientific, Walldorf, Germany). Consecutive sections containing beads were taken for fluorescence microscopy, histology (Haematoxylin-Eosin staining) on glass slides, and for mass spectrometry imaging (MSI) on stainless steel slides.

7.3 Correlation of Sunitinib Fluorescence in Tissue and in DC Bead[®] with Its Distribution

A linear calibration correlating fluorescence intensity in tissue sections with sunitinib levels was developed (17).

Tumor and contralateral liver sections from the untreated rabbit were spiked with 10 μ l of increasing concentrations of sunitinib solution (0.3-2.5 μ g/ml). After drying, fluorescence microscopy images were acquired in at least three different tissue sections. Calibration lines were developed separately for viable and necrotic tumor, and contralateral liver tissues (R²= 0.94, 0.88, and 0.98, respectively) by normalizing the mean fluorescence signal of the tissue in ImageJ to the tissue volume (area x section thickness) covered. Tissue autofluorescence was included in the calibration line. Lower limit of sunitinib quantification was 10 μ g/g. The calibration line for sunitinib

in necrotic tissue was used for all tumors and one contralateral liver tissue (at 1 day), where non-target embolization induced tissue necrosis. For all other calculations, the calibration for contralateral liver tissue was used.

The correlation method described above was challenged by comparison with a quantitative orthogonal technique, LC-MS/MS (Supplementary Figure 1). Sunitinib levels in tumor tissue and contralateral liver of the same animals were known from previous LC-MS/MS measurements (12, 14). The correlation method predicted sunitinib amounts in the tissue comparable to values found by LC-MS/MS (-35% for the tumor, -29% for the contralateral liver lobe) in animals which had received sunitinib perorally.

For measurement of sunitinib contained in the beads, fluorescence of sunitinib-loaded beads sections was correlated to their drug loading. 70-150 μ m DC Bead were loaded with ascending amounts of drug (0-150 μ g/g) as per usual loading protocol (14). Beads were vortexed after complete drug loading and aliquots were embedded with OCT in liquid nitrogen on cork squares. The beads were then cryosectioned at 10 μ m thickness before fluorescence imaging. The average bead fluorescence was obtained for five images per loading, which served as calibration line (R²= 0.82) for quantification of non-eluted sunitinib remaining in beads.

7.4 MALDI-SRM Mass Spectrometry Imaging Technique

For the quantitative MALDI-SRM/MS imaging of the sunitinib distribution the slides were first coated with 3 cycles of 70 μ M d10-sunitinib (Alsachim, Illkirch, France) internal standard dissolved in methanol:H₂O 1:1 by an iMatrixSpray (18) apparatus. After drying, 6 cycles of 10 mg/mL α -cyano-4-hydroxycinnamic acid dissolved in acetonitrile:H₂O 1:1 + 0.1% trifluoroacetic acid were deposited, and slides were frozen at -20°C before further analysis. For the imaging of sunitinib metabolites no internal standard was used.

The MALDI-SRM/MSI measurements were performed on a MALDI-triple quadrupole linear ion trap mass spectrometer (Sciex, Concord, ON, Canada) equipped with a high repetition rate Nd-YAG laser (355 nm wavelength, 100 by 200 μ m laser spot size). All the datasets were recorded in positive ionization mode in combination with selected reaction monitoring (SRM). The SRM transitions used for the quantitative sunitinib imaging were m/z 399>283 and 399>326 for the sunitinib (dwell time:

20 ms) and m/z 409>283 and 409>326 (dwell time: 20 ms) for the d10-sunitinib. The measurement parameters were the following: laser repetition rate=1000 Hz, laser energy=100 μ J, stage speed in horizontal rastering mode=0.5 mm/s, which results in 50 μ m pixel size in the x dimension with 100 ms total scan time, step size in y dimension=50 μ m. For the metabolite measurements the SRM transitions were m/z 371>283 for N-desethyl sunitinib, m/z 343>283 for N,N-didesethyl sunitinib, m/z 397>283 for N-desaturated sunitinib and m/z 415>283 for sunitinib N-oxide.

Chapter Five

Development of Sunitinib-Loaded Biodegradable Hydrogel Microspheres for Transarterial Chemoembolization

Katrin Fuchs, Omar Sakr, Tayeb Jbilou, Van N. Nguyen, Gerrit Borchard, Olivier Jordan

School of Pharmaceutical Sciences, University of Geneva, University of Lausanne, Quai Ernest Ansermet 30, 1211 Geneva 4, Switzerland

Original Research Article

To be submitted to:

European Journal of Pharmaceutics and Biopharmaceutics

Chapter Five 119

Abstract

Embolic hydrogel microspheres are used for the treatment of liver tumor patients by occlusion of the tumor-feeding arteries. Desired features of these microspheres are the ability to degrade in order to avoid long-term presence of foreign materials in the body, and the ability to load and release drugs for enhanced local tumor treatment.

Acrylic microspheres containing a polyethyleneglycol crosslinker and sulfonate moieties for delivery of cationic anti-angiogenic drugs *in situ* were synthesized by an inverse suspension polymerization reaction. Absence of residual organic solvents from the synthesis process was confirmed by gas chromatography.

The anti-angiogenic drug sunitinib was loaded at high loading capacity of 850 mg/g lyophilized microspheres and was released rapidly from the microspheres, in high dose and with a release profile adequate for an antitumoral application.

To evaluate degradation, microspheres were submitted to one of the following conditions: normal aging at 37°C pH 7.4 for 24 weeks, accelerated aging for 8 weeks at higher temperatures (45°C, 60°C), acidic environment (pH 6.2, pH 3), or exposure to liver esterases. While microspheres were not completely degraded after 8 and 24 weeks, surface and bulk degradation of the microspheres were observed by optical microscopy. A significant decrease in elasticity was measured by oscillatory rheology at high temperatures and at pH 6.2 at 8 weeks, indicating hydrolysis of the crosslinks. In contrast, leached polymers were only detected at low concentrations in the degradation media by size exclusion chromatography, and did not reveal toxic effects on renal epithelial cells.

Keywords:

Transarterial chemoembolization, hepatocellular carcinoma, degradable microspheres, drug-eluting beads, sunitinib

Statement of Significance:

Embolic microspheres are an established treatment method for liver tumor patients. The microspheres are injected into tumor-feeding arteries in order to cut off the tumor of its blood supply, resulting in tumor shrinkage. Despite successful clinical intervention, this may cause the growth of vessels toward the tumor, which can lead to tumor recurrence. Therefore, microspheres should be loaded with a drug that is able to locally inhibit vascular growth. Currently used microspheres either persist in the tumor arteries provoking inflammation and tissue infarction, or cannot be loaded with drugs. In this study, we present hydrogel microspheres, which degrade slowly enough to provide the needed occlusion of tumor arteries, and can be loaded with a drug preventing vascular growth.

1 Introduction

Embolic microspheres are considered a standard treatment for intermediate hepatocellular carcinoma. Occlusion of the tumor-feeding arteries leads to necrosis and eventually tumor shrinkage [1, 2]. In addition, combining embolic microspheres with a chemotherapeutic drug allows for localized drug delivery to the tumor, and therefore a lower dose compared to peroral route avoiding systemic toxicity [3].

While non-degradable microspheres are in clinical use for embolization, there is a medical rationale for degradable (or resorbable) microspheres [4]: Foreign body reactions such as tissue inflammation and infarction are transitory compared to non-degradable microspheres, and risks arising from non-target embolization are reduced [5]. In addition, degradable microspheres allow for repeated interventions after vessel recanalization [6-9].

Several degradable microsphere types have been commercialized or are under development. Examples for FDA-approved degradable embolization microspheres for hepatocellular carcinoma (HCC) treatment are degradable starch microspheres (DSM) [10, 11], and collagen-coated poly(lactide-co-glycolide) (PLGA) microspheres [12]. Both are however not compressible to pass easily through catheters and avoid catheter clogging, and are used without a loaded drug.

Other elastic and drug-eluting embolic spheres are currently in development. An example is the biocompatible carboxymethylchitosan-cellulose microspheres, which degrade by enzymatic or non-enzymatic hydrolysis over adaptable timeframes ranging from 1 week to 4 weeks *in vitro* and *in vivo* showing only mild inflammatory tissue reactions [9, 13-15].

Another example is microspheres containing acrylate monomers. Acrylate hydrogels are widely used as diffusion- and swelling-controlled drug delivery devices [5, 16, 17], provide elasticity, high swelling capacities and biocompatibility due to the inclusion of water soluble monomers [18]. For embolization, microsphere elasticity ensures easy catheter passage and delivery to distal tumor arteries. Upon degradation, resulting hydrophilic fractions are cleared by glomerular filtration, provided they are of sufficiently low molecular weight (below 30 kDa) [19]. Methacrylate hydrogel microspheres containing a hydrolysable PLGA-poly(ethylene glycol) (PEG)-PLGA crosslinker are completely resorbed during 1 week *in vivo* without inflammatory response and complete vessel

recanalization [7, 8]. These microspheres were designed to degrade rapidly for the treatment of leiomyoma, whereas slower degradation might be required for the treatment of HCC [20, 21].

In addition to elasticity and biodegradability as requirements for the microspheres in development, ability to carry anti-tumor drugs is a necessity. Local delivery of anti-angiogenic drugs in particular is intended to prevent neovascularization and tumor rebound induced by embolization [22-24]. Small molecules like sunitinib and sorafenib, and antibodies like bevacizumab have been combined with embolic spheres at therapeutically relevant concentrations [21, 25-27]. Sunitinib loading on chitosan-cellulose microspheres is feasible, but presumably only at moderate doses [28]. Cellulose is not sufficiently negatively charged for cationic drugs like sunitinib to be loaded at high ratios. Due to the presence of carboxylate groups, methacrylate microspheres can be loaded with a high sunitinib dose up to 50 mg per ml of spheres. However, their quick degradation rate might not be suitable to induce effective occlusion for the treatment of HCC [20, 21].

The scope of this research work is to design and prepare elastic embolic microspheres for the treatment of HCC, bearing sulfonates as negative moieties to achieve high loading of cationic drugs, which degrade within a timeframe of 8 weeks. We describe the synthesis of acrylic microspheres for transarterial chemoembolization (TACE), sunitinib loading and release *in vitro*, and a biodegradation study over 8 weeks with elements of microspheres innocuity *in vitro*.

2 Materials and Methods

2.1 Microsphere Synthesis and Characterization

2.1.1 Microsphere Preparation

Microspheres (MS) were synthesized using an inverse suspension polymerization reaction (water-in-oil) [29]. The organic phase was prepared by adding Span 60 (1% w/w, Sigma-Aldrich, Buchs, Switzerland) into 25 ml of cyclohexane (Fluka Chemika, Buchs, Switzerland) in a 50 ml 3-neck flask, which was heated to 30°C in an oil bath. The mixture was stirred at 100 rpm using a Eurostar digital rotor (IKA, Staufen, Germany) connected to a 30 cm agitator (Schmizo AG, Oftringen, Switzerland) and Schmizo ZRS 10 adaptive piece for the flask, and degassed by nitrogen bubbling.

The aqueous phase was prepared from 1779 mg of 3-sulfopropyl methacrylate potassium salt (98% SPMA, 47 mol%, Sigma-Aldrich) in 2 ml H_2O milliQ (Millipore, Zug, Switzerland) and 1000 mg of 2-hydroxyethyl methacrylate (HEMA, 50 mol%, Sigma-Aldrich) as the two monomers, and 323 mg of poly(ethylene glycol) diacrylate (PEGDA, M_n =700, 3 mol%, Sigma-Aldrich) in 2 ml H_2O milliQ as crosslinking agent. The aqueous phase was completed to 8 ml H_2O milliQ, the initiator 71.4 mg of ammonium persulfate (APS, 98%, 2 mol% of solids, Acros Organics, Geel, Belgium) was added, and then heated to 30°C. Aqueous and organic phase were mixed at 250 rpm, while temperature was increased to 70°C. The polymerization reaction was started by addition of the catalyst N,N,N',N'-tetramethylethylenediamine (TEMED 99%, 20.75 mg, Sigma-Aldrich, ratio of 1:1.75 of APS:TEMED) in 2.4 ml H_2O milliQ and left to react for 2 hours.

MS were collected by vacuum filtration over a G4 Büchner filter and washed extensively with ethanol and milliQ water. Consequent lyophilization was performed with 10% sucrose solution as cryoprotector, in an Edwards Modulyo K40 (Oberwil, Switzerland) lyophilizer at -40°C. MS were rehydrated in water and their swelling ratio was determined as described by Nguyen et al. [30].

Before lyophilization, microspheres size was measured with a Mastersizer S Long Bench (n=6, Malvern Instruments, Orsay, France), analyzed using the Polydisperse Model, presented with the Standard – Wet Model, and interpreted by volume distribution.

2.1.2 Residual Solvent Detection by Gas Chromatography

Residual organic solvents (cyclohexane, ethanol) in MS from the synthesis process before and after lyophilization were monitored by gas chromatography (Agilent 6850 GC, Agilent Technologies, Basel, Switzerland) equipped with a flame ionization detector with limits of detection in the low picogram range. Agilent 7694 Headspace sampler was used to load and inject the samples into the Agilent DB-624 column with Helium gas as carrier according to Ph. Eur. 8 specifications. Reference solvents were absolute ethanol (Fisher Scientific 99.99%), cyclohexane HPLC grade (Sigma-Aldrich), N,N-dimethylacetamide (DMA) HPLC grade (Sigma-Aldrich) was used as a diluent for cyclohexane, and purified milliQ water for both cyclohexane and ethanol. Quantitative analysis was performed by external linear calibration: Ethanol standards with known amounts over the quantification range of 200 to 1500 mg/L of ethanol were measured (R²=0.99967) to determine the amount of ethanol

contained in wet (0.1 g MS/ml) or lyophilized MS (0.01 g MS/ml), incubated in water overnight. MS in the same concentrations were also incubated both in DMA and water for cyclohexane detection.

2.2 Loading and Release of Microspheres with Sunitinib

Lyophilized MS were immersed in sunitinib (LC Laboratories, Woburn, MA, USA) hydrochloride solution (10 mg/ml) [25, 31] to achieve a nominal loading of 500 mg or 1000 mg sunitinib per g of lyophilized MS, corresponding to 3 mg or 6 mg sunitinib per ml of wet MS (swelling factor 167, see section 3.1). Drug loading was quantified indirectly by absorbance measurement of the residual unloaded drug in the supernatant at a wavelength of 425 nm (BioTek Synergy Mx plate reader).

To assess release kinetics, 500 and 850 mg/g sunitinib-loaded MS were submitted to 5 ml/min 0.9% NaCl medium flow-through in a USP 4 apparatus (Sotax, Allschwil, Switzerland) and released drug was quantified in-line by an HP 8453 spectrophotometer (Agilent). Ethanol addition to achieve a final concentration of 30% V/V served as a control for complete drug elution [32].

Release profiles of MS with two different sunitinib loads were compared by computing the FDA similarity factor f_2 (Eq. 1):

$$f_2 = 50 \cdot \log \left\{ \left[1 + \left(\frac{1}{n} \right) \sum_{t=1}^{n} (R_t - T_t)^2 \right]^{-0.5} \cdot 100 \right\}$$
 Eq. 1

where R_t and T_t are the cumulative percentage of the drug dissolved at each of the selected time points (n) of the reference and test product, respectively. An f_2 value between 50 and 100 ensures profile equivalence. This approach is used to compare the dissolution profile between two strengths of products [33].

2.3 Microsphere Biodegradation Studies

MS were left to degrade in PBS over 24 weeks and additionally under five stress conditions supposed to accelerate the degradation over 8 weeks. The *in vitro* degradation of 0.1 g lyophilized MS was followed in 15 ml sterile-filtered PBS pH 7.4, 58 mM (n=3) [34]. The experiment was carried out in a horizontally incubated, 50 ml Falcon tube rotating at 80 rpm. Samples were measured each week for 12 weeks and at 16, 20 and 24 weeks. In the accelerated study, MS from one master batch

were used to study degradation under accelerated conditions and were analyzed at 2, 4 and 8 weeks (n=3 vials per condition and time point). The medium was modified by adding 0.95% NaN₃ and by either increasing temperature (45°C or 60°C), decreasing pH (PBS pH 3 or PBS pH 6.2), or adding porcine liver esterase (PLE, EC 3.1.1.1, Sigma-Aldrich E 3019) 30 U/ml [35]. To test degradation in the presence of esterase from porcine liver (PLE), the PLE crude powder was first diluted in 10 ml H₂O and added to MS in PBS pH 7.4 at 30 U/ml. Aliquots of the enzyme in anti-protein adhesion vials were frozen at -20°C until further use. Enzyme activity was routinely checked each week by ethyl butyrate hydrolysis test according to the supplier's protocol [36], and fresh enzyme was added to complete to 30 U/ml.

The 3 vials of MS for each condition and time point and at t_0 were submitted to optical microscopy (Nikon Optiphot-2 equipped with Infinity-2 camera, Egg, Switzerland), scanning electron microscopy (SEM, JEOL JSM-7001F, Tokyo, Japan), and viscoelasticity measurements. After MS in the accelerated degradation study had settled down, supernatants were sampled and tested for leachables using size exclusion chromatography (SEC). Renal epithelial cells were incubated with supernatants to reveal potential cytotoxicity.

2.3.1 **Viscoelasticity of Microspheres**

MS viscoelasticity before and after lyophilization and rehydration, and during degradation was evaluated using oscillatory rheology. The rheometer (Haake Rheostress 1, Tracomme AG, Bonstetten, Switzerland) was equipped with a 35 mm plate-plate geometry at 25°C and a solvent trap [30]. A monolayer of MS was deposited in the 100 μ m gap between the plates and shear sweeping from 0.0001 Pa to 0.1 Pa at constant frequency of 1 Hz determined the linear strain regime of G' (elastic modulus) and G'' (viscous modulus). Consequently, frequency sweeps between 0.1 Hz to 14 Hz at a constant imposed strain γ of 0.2% in the linear region allowed for measurement of the moduli and the phase angle δ = tan(G''/G'). MS elasticity modulus and storage modulus at 10 Hz over time (n=9 from 3 vials per condition per time point) were compared to the value measured at t_{0 weeks} (n=9) by one-sided t-test with 95% confidence level.

2.3.2 **Characterization of Degradation Products**

2.3.2.1 Detection of Leaching Polymers by Size Exclusion Chromatography (SEC)

PBS supernatants from degrading MS of each accelerated condition at 0, 2, 4 and 8 weeks, and porcine liver esterase 30 U/ml were submitted to SEC in triplicate. PLE containing supernatants were centrifuged at 10.000 g for 15 min followed by 5 min at 20.000 g to separate the supernatant from the enzymes [35]. The molecular weight distribution of leached polymers was measured using an injector (Waters Alliance 2790 HPLC system) coupled to a size exclusion chromatography Waters (Milford, USA) Ultrahydrogel linear column. A refractive index detector (Schambeck, Bad Honnef, Germany) and a multi-angle light scattering detector (MiniDawn, Wyatt, USA) (SEC-MALS-RI) were used in series, and data was processed using ASTRA V 5.3.4.20 analysis software. Molecular weight calculation had been validated beforehand by weight calculation of pullulans P-5 to P-200 (Shodex™, Showa Denko Europe, Munich, Germany), using the same system. Chromatographic conditions were: mobile phase of 100% PBS pH 7.4, flow rate of 0.5 ml/min, run time of 30 min and injection volume of 100 µl. The refractive index increment dn/dc used was 0.145, approximated according to previous literature [37].

2.3.2.2 Toxicity on Renal Epithelial MDCK Cells

Cytotoxicity of leachables of degrading MS into the degradation medium was assessed by exposing Martin-Darby Canine Kidney (MDCK) cells (ATCC, Manassas, VA, USA) to aliquots of the degradation medium after 8 weeks (n=9 wells from 3 vials per condition). Cells were cultured in Dulbecco's modified Eagle medium (DMEM, ThermoFisher Scientific, LuBioScience GmbH, Lucerne, Switzerland) enriched with 10% fetal calf serum and 1% streptomycin at 5% CO_2 at 37°C, seeded into two 96-well plates at initial densities of 10^5 cells and 2.5×10^5 cells/well. Negative controls were cells in full DMEM, PBS/DMEM and 0.95% NaN₃/DMEM, and positive controls for cytotoxicity were 0.05% SPMA/DMEM and 0.5% SPMA/DMEM (all 1:1). After 24 hours of incubation, DMEM was removed from the wells and supernatant from the MS accelerated degradation study mixed with full DMEM 1:1 (100 μ l working volume) was added to each well. After 4 hours of incubation, medium was removed and 100 μ l WST-1 metabolic activity reagent/full DMEM 1:9 were added to each well and additionally to three wells without cells as blank. Plate absorbance was read after 30 min of incubation with a BioTek Synergy Mx plate reader (Lucerne, Switzerland) at 450 nm

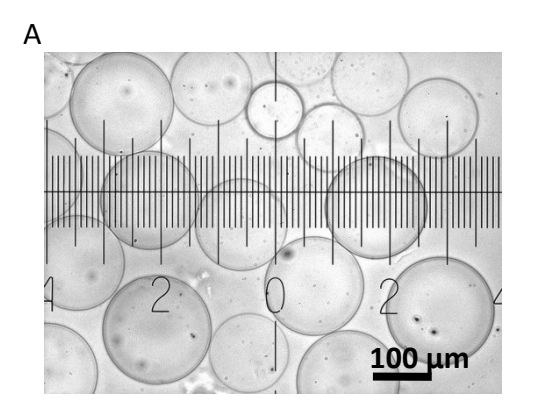
absorbance after 1 min shaking at 37°C, and cell metabolic activity was calculated according to the supplier's protocol.

Conditions were compared to control by GraphPad Prism 6.01 software by one-way ANOVA with Holm's multiple comparisons correction.

3 Results

3.1 Microsphere Synthesis and Characterization

MS were produced by an inverse suspension polymerization reaction. The microsphere yield was 79 \pm 18 % (n=7 reactions), compared to the initially weighed monomers and the crosslinker. Obtained MS were spherical in shape with monomodal size distribution. The volume mean diameter D[4;3] after synthesis for different batches varied between 110 and 230 µm with Span values ranging from 1.1 to 1.6 (data not shown). After lyophilization, MS regained their shape with a swelling ratio of 167 \pm 22 (g/g) after 3 hours (n=3) in water. MS also swelled in PBS (Figure 1). MS were tested for residual solvents from the synthesis or washing processes (cyclohexane and ethanol, respectively). Cyclohexane was neither detected before nor after MS lyophilization. Ethanol was detected at 3588 ppm and 7598 ppm in the wet MS before lyophilization in the two batches used for the following accelerated degradation study, and at 139 ppm for the lyophilized MS after swelling in the combined batch. Ethanol is a class 3 solvent whose concentration should be below <5000 ppm according to Ph. Eur. 8.



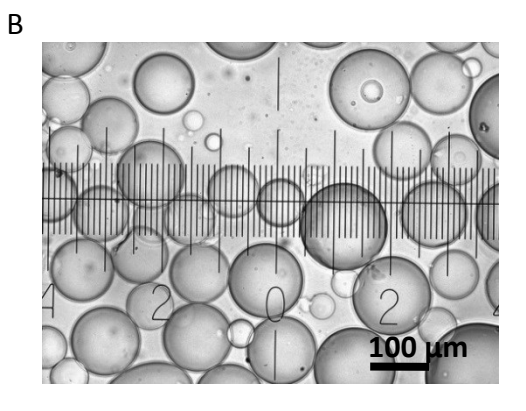


Figure 1. Optical micrographs of smooth, spherical MS (A) before and (B) after lyophilization and rehydration in PBS pH 7.4.1 major unit of the ruler corresponds to $100 \mu m$.

3.2 Loading and Release of Microspheres with Sunitinib

MS were successfully loaded with sunitinib at a maximum capacity of 850 mg per g lyophilized MS, corresponding to 5 mg drug per g wet MS (Figure 2). Maximum loading was attained after 30 minutes, when a plateau was reached and no further drug was uptaken. Since MS showed a tendency to shrink and aggregate at maximum loading, a loading of 500 mg sunitinib per g lyophilized MS (corresponding to 3 mg sunitinib per g wet MS) was selected. The 500 mg/g loading was completed after 5 min and is sufficient for clinical use (Figure 2).

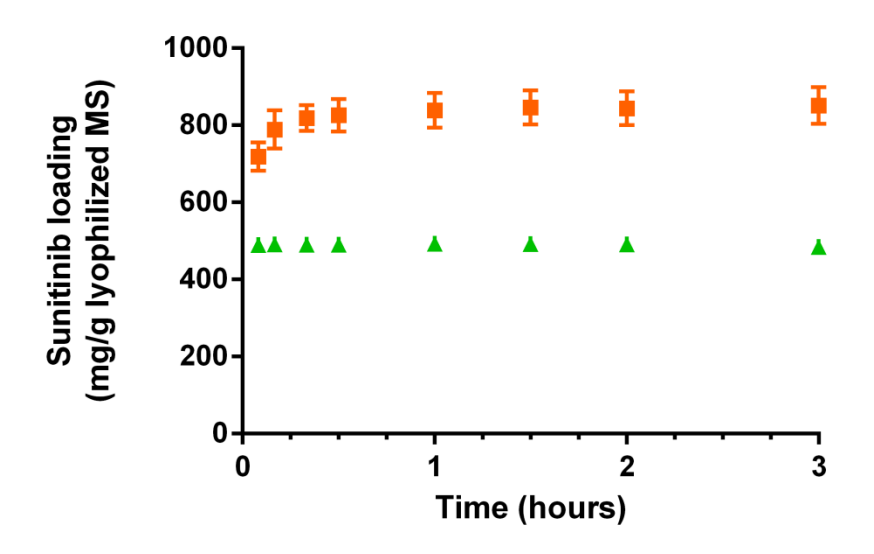


Figure 2. Sunitinib loading at 500 mg (▲) and 1000 mg (■) per g lyophilized MS. Loading is fast up to a capacity of 850 mg/g lyophilized MS, resulting in 100% loading for 500 mg/g and 85% loading efficiency for 1000 mg sunitinib/g lyophilized MS.

Sunitinib-loaded MS showed fast drug release *in vitro* in physiological saline (Figure 3). The release half time $t_{1/2}$ was between 20 and 25 minutes at 500 mg/g loading, and prolonged to 5 hours at 850 mg/g loading with high variation between repetitions for the higher loading due to microsphere aggregation. The FDA similarity factor f_2 = 19 showed different release profiles at different drug payloads. Total release at the plateau was 90±1% and 88±3% of the initial loading of 500 mg/g and 850 mg/g MS, respectively.

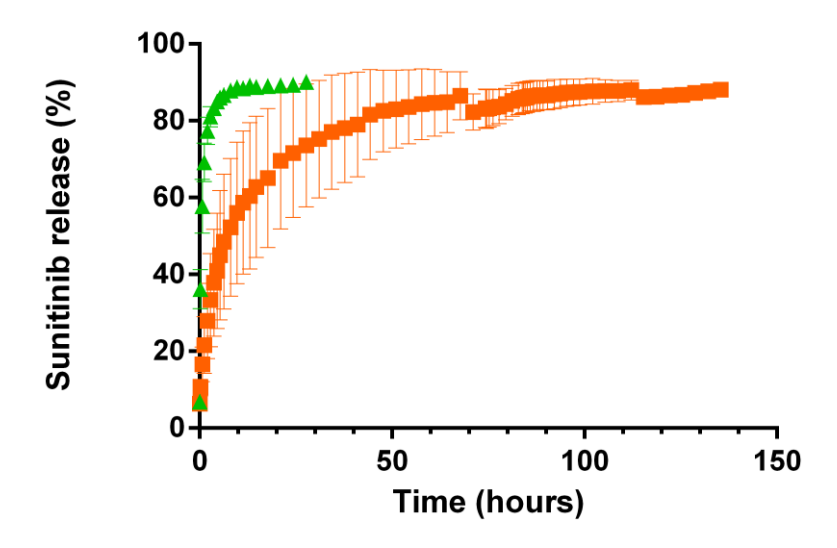


Figure 3. Sunitinib release in NaCl 0.9% from MS loaded with 500 mg (▲, n=6) and 850 mg sunitinib (■, n=6). Fast drug release kinetics was seen for 500 mg sunitinib per g lyophilized MS, whereas MS aggregation slowed down and caused variability in sunitinib release at 850 mg/g loading. For the higher loading, the irregular shape of the release curve was due to different numbers of repetitions displayed: After 70 hours, MS in 3 flow-through cells had reached their plateau, thus release from the residual 3 flow-through cells was reported (n=3) between 70 and 115 hours. At 115 hours, MS in only one cell had not yet reached the release plateau (115-135 hours: n=1).

3.3 Microsphere Biodegradation Studies

MS observed by optical microscopy showed slight signs of surface degradation and possible bulk degradation resulting in breaking or hollowing of some MS for all degradation conditions in PBS between 2 to 8 weeks (Figure 4). Similar observations were made with scanning electron microscopy (data not shown). MS were elastic with an initial elastic modulus (G') of around 4000 Pa, and remained compressible throughout all degradation studies. Meanwhile, the phase angle δ never exceeded 8° at 37°C or under accelerated conditions over 8 and 24 weeks, which is a sign for mainly elastic properties. For the MS in the accelerated study, a tendency toward a decrease of 1000 Pa (25% decrease) in elastic modulus was observed, indicating crosslink hydrolysis (Figure 5) [30]. This tendency was particularly pronounced at high temperatures (45°C and 60°C) and at pH 6.2 (tumor pH), where G' at 8 weeks was significantly different from the value at t_0 . This tendency was not visible at 37°C during 24 weeks (data not shown).

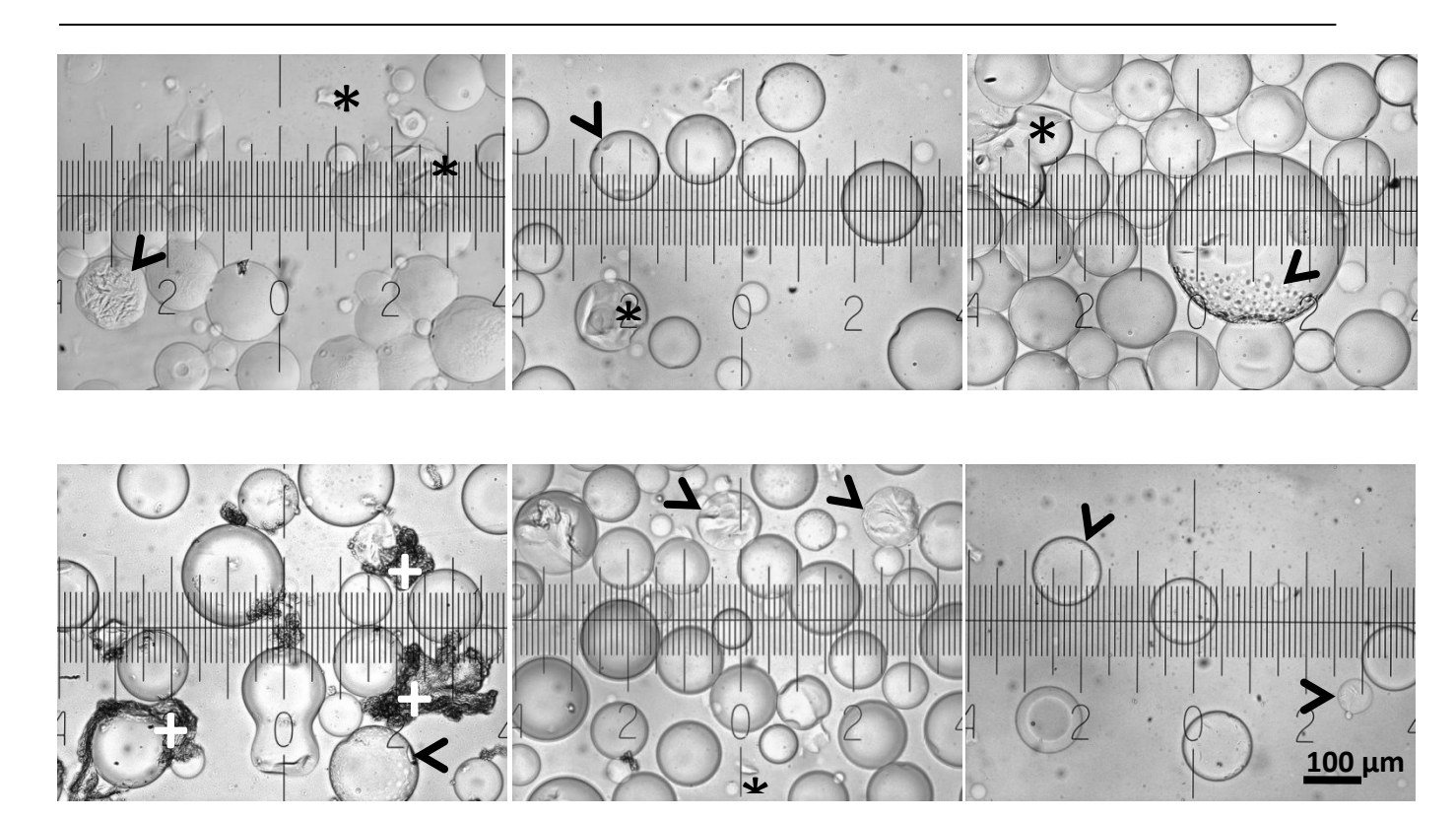


Figure 4. Optical micrographs of MS in PBS at 8 weeks at 37°C, 45°C, 60°C (top row, from left to right), PLE, pH 3 and pH 6.2 (bottom row, from left to right) showed slight signs of surface degradation (arrows) or bulk degradation (broken or eroded MS, stars). Aggregated PLE was marked with a white +.

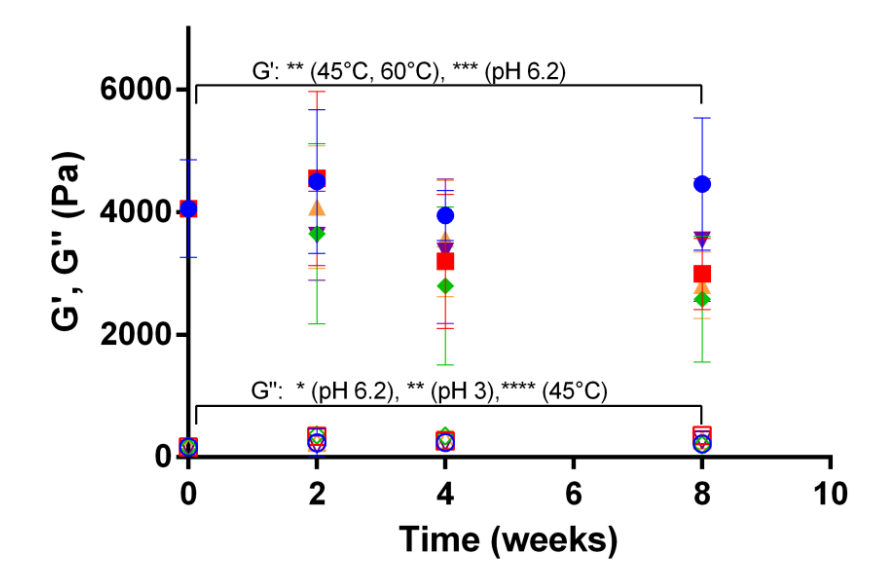


Figure 5. Elastic modulus G' (filled symbol) and viscous modulus G'' (empty symbol) of MS in PBS at 10 Hz over 8 weeks (n=9 per condition per time point). Degradation was modified as a function of temperature (■: 45° C, ◆: 60° C), pH (▼: pH 3, △: pH 6.2), or by addition of porcine liver esterase (•). A tendency for decrease in elastic modulus G' signified decrease in crosslinking of the hydrogel, thus MS degradation by ester hydrolysis. Significance levels: P > 0.05: ns (not significant), P ≤ 0.05: *, P ≤ 0.01: ***, P ≤ 0.001: ****, P ≤ 0.0001: *****.

In the PBS supernatants, in which the MS had been incubated for 2, 4 or 8 weeks under accelerated conditions, leached polymers were only detected at low concentrations (Table 1). The mass fraction, i.e. the recovered mass compared to the initial MS concentration in the degradation medium, was between 0 and 3 %. Polymer mass could not be quantified in presence of PLE due to an overlap of the peaks on the chromatograms, indicating high molecular weight degradation products. Molecular weights were between 80.000 and 300.000 g/mol, with no tendency of decrease in weight with time.

Table 1. Mass fraction and molecular size of leached polymers from the microspheres in PBS at increased temperature, with addition of porcine liver esterase (PLE), and at decreased pH. Polymer release from the microspheres was negligible at any time until 8 weeks, signifying a rather low microsphere degradation rate. Condition with PLE: (Enzyme detected). Reported values are means of three independent experiments.

| | Mass fraction (%) | | | | Mw (g/mol) | | | | | |
|----------------------|-------------------|-------|----------|-------|------------|---------|---------|-----------|---------|---------|
| Condition | 45°C | 60°C | PLE | pH 3 | pH 6.2 | 45°C | 60°C | PLE | pH 3 | pH 6.2 |
| t _{0 weeks} | 0.02% | | | | 238.500 | | | | | |
| t _{2 weeks} | 0.56% | 1.18% | (11.31%) | 0.29% | 0.98% | 240.500 | 142.500 | (148.650) | 178.600 | 79.775 |
| t _{4 weeks} | 0.61% | 1.26% | (15.31%) | n/a | 0.60% | 255.110 | 300.633 | (158.167) | n/a | 137.485 |
| t _{8 weeks} | 0.94% | 2.94% | (13.95%) | 0.91% | 0.51% | 140.000 | 149.773 | (162.533) | 81.063 | 146.340 |

n/a: no polymers detected

Leached polymers from the MS in PBS at 8 weeks did not inhibit the metabolic activity of renal epithelial cells (Figure 6). Cells which were exposed to the MS supernatants at 45°C, pH 3 and pH 6.2, maintained a metabolic activity of at least 88%. The supernatants from MS in presence of esterases and at a temperature of 60°C caused a decrease in cell metabolic activity to 70% and 74%, respectively. Nevertheless, this was comparable to what was observed for cells cultured in full DMEM. Likewise, free sulfopropylmethacrylate (SPMA) at the lower concentration did not significantly interfere with cells' metabolism, nor did aqueous sodium azide, which was present in the degradation medium to inhibit bacterial growth. The exact same tendencies in cell metabolic activity were found for both tested cell densities (data not shown for 2.5x10⁵ cells/well).

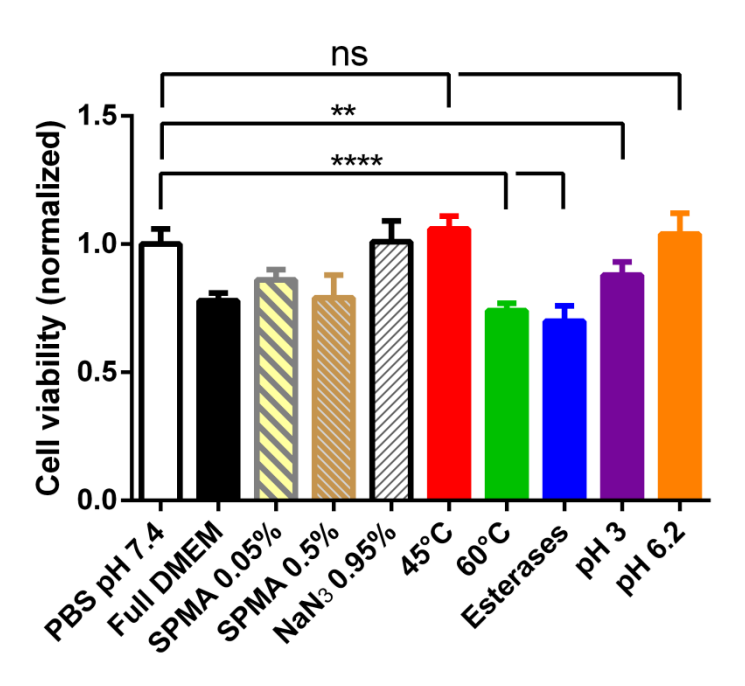


Figure 6. MDCK renal epithelial cell metabolic activity by WST-1 assay (105 cells/well, n=3 for the controls, n=9 for tested conditions) was only marginally influenced by the supernatants of the MS at 8 weeks. Activity was normalized to cells in PBS pH 7.4/DMEM as 100%. Significance levels: P > 0.05: ns (not significant), $P \le 0.05$: **, $P \le 0.01$: ***, $P \le 0.001$: ***, $P \le 0.0001$: ****

4 Discussion

Treatment of HCC by chemoembolization using biodegradable drug-eluting microspheres enables transient vascular occlusion, where drug elution occurs by diffusion and during microsphere degradation.

4.1 Microsphere Synthesis and Characterization

In this study, we have synthesized elastic, non-toxic hydrogel microspheres in the suitable size range for chemoembolization of 100-300 μ m that were ready to be loaded with cationic drugs. The microspheres were composed of hydrophilic hydroxyethylmethacrylate for water swelling and sulfopropylmethacrylate to confer negative charge for post-hoc cationic drug loading. The aforementioned monomers reacted randomly by radical polymerization, while insertion of a short PEGdiacrylate crosslinker allowed for establishment of the 3D gel structure. The low crosslinking density of 3 mol% was intended to allow for fast degradation. The same applies to the composition

from PEG and acrylate monomers, which accelerate degradation by water uptake due to intrinsic hydrophilicity [20, 38]. The formulation showed a high swelling ratio compared to PEG-acrylate microspheres containing PLGA in the crosslinker [30]. This resulted in microsphere elasticity as shown by oscillatory rheology, which ensures catheter passage during radiologic intervention. During the formulation design, hydrolysable bonds were preferred, since moieties requiring enzymatic cleavage for biodegradation might be subjected to inter-individual variation of enzyme expression.

4.2 Loading and Release of Microspheres with Sunitinib

An interesting aspect of the microspheres in this study is their simple composition and ease and efficiency of cationic drug loading. The inverse suspension polymerization allowed for incorporation of high content of water-soluble sulfopropylmethacrylate (here 47 mol%), forming microspheres with high density of negative charges. The anti-angiogenic cationic sunitinib was thus loaded at high amounts of maximally 850 mg sunitinib per g lyophilized microspheres with the same simple procedure as for clinically used non-degradable DC Beads (BTG/Biocompatibles Ltd.), corresponding to approximately 5 mg drug loading per ml wet microspheres. For comparison, maximum capacity of DC Beads for sunitinib is 30 mg/g wet microspheres [25, 32]. However, this payload results even in supra-therapeutic concentrations *in vivo* [23]. Release pharmacokinetics with acrylate microspheres from this study was faster compared to DC Beads (25 min. vs. 60 min.) with almost complete final release [25, 32]. Similar to DC Bead microspheres containing sulfonate moieties, the release mechanism is governed by ionic exchange with the saline medium. Despite the rapid drug release *in vitro*, sunitinib can be expected to be retained in the target lesion *in vivo* for 2 weeks [23], providing the necessary sustained anti-angiogenic effect [39].

4.3 Microsphere Biodegradation Studies

A study examining the degradation of the microspheres over 24 weeks in PBS at body temperature was designed. Since surface degradation or changes in size, elasticity and medium pH were only modestly noticeable (data not shown), the microspheres were also submitted to degradation under accelerated conditions. For this, nonspecific esterases were added to accelerate the hydrolysis of

the ester links forming the gel structure, pH was acidified for the same reason (pH 3) or to mimic the tumor environment (pH 6.2) [40, 41], or temperature was increased to accelerate microsphere aging. Under accelerated conditions, microspheres showed signs of degradation between 2 and 8 weeks. However, all MS did not degrade to the same extent, nor was degradation *in vitro* complete. Over this timeframe, progression of the degradation was not clearly detectable by optical microscopy. Still, the significant decrease in elasticity measurements at 8 weeks under the accelerated stress conditions indicated the hydrolysis of the crosslinks between the acrylate polymers, loosening of the gel structure, and degradation.

In order to undergo more rapid degradation over the 8 weeks period, MS should be designed to be more sensitive to hydrolysis. Crosslinks within acrylate gels might have hindered hydrolysis: Formation of crosslink loops and heterogeneous crosslinking in presence of high amounts of water (50 wt%) was reported previously [17]. Nguyen et al. [34] hypothesized possible self-crosslinks of PEG methylether methacrylates, even in the absence of a crosslinker with two acrylate ends. Their microspheres were insoluble even in organic solvents. The ester bonds were too close to the main chains, resulting in reduced sensitivity to hydrolysis. In our microspheres, only this type of ester bonds existed. Considering modifications of the microsphere formulation, a longer crosslinker would probably allow for higher porosity and increased water penetration into the hydrogel. This would in turn accelerate hydrolysis of the ester bonds between the acrylate polymer chains and the PEG crosslinker [20]. Insertion of ester bonds into the acrylate chains would probably prevent chain entanglement, achieve faster and complete break-down as well as hydrolytic products of shorter polymeric length, such as for PEG-PLGA-acrylate microspheres described by Laurent et al. [7, 8, 20].

The optimal degradation time of microspheres for chemoembolization remains yet to be determined. To our knowledge, there is no scientific evidence determining during which timeframe the anoxic environment created by embolization is definitely required. Fast degradation may lead to hypoxia instead of anoxia like in the case of incomplete embolization, translating into the release of unfavorable pro-angiogenic factors [42-44]. Hypoxia-induced factors (HIF- 1α) upregulate angiogenic factors like vascular endothelial growth factor (VEGF) up to 4 weeks following embolization [45, 46]. Several studies showed ischemia-induced plasma VEGF peaks 1-2 days after TACE followed by decreasing levels until 1 month [43, 44, 47]. Over this timeframe, we suggested that the embolization of the tumor arteries should be maintained.

Safety is a major issue for approval and commercialization of embolic microspheres. The absence of solvents in the microspheres after synthesis and preservation of epithelial cell metabolism during exposure to the microsphere supernatants strongly supports lack of MS toxicity. A renal epithelial cell line was chosen because of the kidneys' role in the elimination of the MS degradation products. Biocompatibility was expected, similar to hydrolysable PEG-PLGA-acrylate microspheres [7, 8, 20]. Low mass fraction of <3% of the initial microspheres concentration was seen by size exclusion chromatography, indicating a relatively slow MS degradation.

5 Conclusions

To summarize, this research broadens the platform of degradable microspheres in development and might contribute valuable information to the design of a first compressible degradable microsphere for the clinical treatment of hepatocellular carcinoma. Non-toxic microspheres with high swelling capacity were synthesized, which can be loaded with sunitinib at therapeutic concentrations due to sulfonate moieties in the microsphere composition. Drug release pharmacokinetics *in vitro* was similar to non-degradable microspheres in clinical use. In the future, the microsphere gel composition will be adjusted by introduction of a higher number of ester bonds to accelerate hydrolytic degradation, which will require an *in vivo* assessment in addition to biocompatibility and safety checks.

6 Acknowledgements

The authors acknowledge Prof. Alban Denys and Dr. Pierre Bize from the Centre Hospitalier Universitaire Vaudois (CHUV, Lausanne, Switzerland) for the fruitful collaboration on the project. During their master theses, Yassine Dhif, Malika Lebbar, and François Loeliger contributed valuable information to the studies of biodegradable microspheres and the techniques used. Authors also thank Emmanuelle Sublet for her advice and assistance with cell culture experiments.

7 References

[1] J.M. Llovet, A.M. Di Bisceglie, J. Bruix, B.S. Kramer, R. Lencioni, A.X. Zhu, M. Sherman, M. Schwartz, M. Lotze, J. Talwalkar, G.J. Gores, H.C.C.D.C.T. for the Panel of Experts in, Design and Endpoints of Clinical Trials in Hepatocellular Carcinoma, Journal of the National Cancer Institute 100(10) (2008) 698-711.

- [2] A. Forner, M. Gilabert, J. Bruix, J.L. Raoul, Treatment of intermediate-stage hepatocellular carcinoma, Nature reviews. Clinical oncology 11(9) (2014) 525-35.
- [3] M. Varela, M.I. Real, M. Burrel, A. Forner, M. Sala, M. Brunet, C. Ayuso, L. Castells, X. Montana, J.M. Llovet, J. Bruix, Chemoembolization of hepatocellular carcinoma with drug eluting beads: efficacy and doxorubicin pharmacokinetics, Journal of hepatology 46(3) (2007) 474-81.
- [4] J. Golzarian, 701.8 Resorbable particles: are they the future? (ID: 46), GEST 2013 Europe, Prague, Czech Republic, 2013.
- [5] Y.X. Wang, T. De Baere, J.M. Idee, S. Ballet, Transcatheter embolization therapy in liver cancer: an update of clinical evidences, Chin J Cancer Res 27(2) (2015) 96-121.
- [6] A. Schwarz, H. Zhang, A. Metcalfe, I. Salazkin, J. Raymond, Transcatheter embolization using degradable crosslinked hydrogels, Biomaterials 25(21) (2004) 5209-5215.
- [7] N. Maeda, V. Verret, L. Moine, L. Bedouet, S. Louguet, E. Servais, K. Osuga, N. Tomiyama, M. Wassef, A. Laurent, Targeting and recanalization after embolization with calibrated resorbable microspheres versus hand-cut gelatin sponge particles in a porcine kidney model, Journal of vascular and interventional radiology: JVIR 24(9) (2013) 1391-8.
- [8] V. Verret, J.P. Pelage, M. Wassef, S. Louguet, E. Servais, L. Bedouet, T. Beaulieu, L. Moine, A. Laurent, A novel resorbable embolization microsphere for transient uterine artery occlusion: a comparative study with trisacryl-gelatin microspheres in the sheep model, Journal of vascular and interventional radiology: JVIR 25(11) (2014) 1759-66.

[9] L. Weng, D. Seelig, P. Rostamzadeh, J. Golzarian, Calibrated Bioresorbable Microspheres as an Embolic Agent: An Experimental Study in a Rabbit Renal Model, Journal of vascular and interventional radiology: JVIR 26(12) (2015) 1887-94 e1.

- [10] C.C. Pieper, C. Meyer, B. Vollmar, K. Hauenstein, H.H. Schild, K.E. Wilhelm, Temporary Arterial Embolization of Liver Parenchyma with Degradable Starch Microspheres (EmboCept®S) in a Swine Model, Cardiovascular and interventional radiology 38(2) (2015) 435-441.
- [11] C. Niessen, E. Unterpaintner, H. Goessmann, H.J. Schlitt, M. Mueller-Schilling, W.A. Wohlgemuth, C. Stroszczynski, P. Wiggermann, Degradable Starch Microspheres versus Ethiodol and Doxorubicin in Transarterial Chemoembolization of Hepatocellular Carcinoma, Journal of Vascular and Interventional Radiology 25(2) (2014) 240-247.
- [12] R.J. Owen, P.N. Nation, R. Polakowski, J.A. Biliske, P.B. Tiege, I.J. Griffith, A Preclinical Study of the Safety and Efficacy of Occlusin™ 500 Artificial Embolization Device in Sheep, Cardiovascular and interventional radiology 35(3) (2012) 636-644.
- [13] L. Weng, H.C. Le, J. Lin, J. Golzarian, Doxorubicin loading and eluting characteristics of bioresorbable hydrogel microspheres: in vitro study, International journal of pharmaceutics 409(1-2) (2011) 185-93.
- [14] L. Weng, H.C. Le, R. Talaie, J. Golzarian, Bioresorbable hydrogel microspheres for transcatheter embolization: preparation and in vitro evaluation, Journal of vascular and interventional radiology: JVIR 22(10) (2011) 1464-1470 e2.
- [15] L. Weng, M. Rusten, R. Talaie, M. Hairani, N.K. Rosener, J. Golzarian, Calibrated bioresorbable microspheres: a preliminary study on the level of occlusion and arterial distribution in a rabbit kidney model, Journal of vascular and interventional radiology: JVIR 24(10) (2013) 1567-75.
- [16] N.A. Peppas, P. Bures, W. Leobandung, H. Ichikawa, Hydrogels in pharmaceutical formulations, European Journal of Pharmaceutics and Biopharmaceutics 50(1) (2000) 27-46.
- [17] L. Serra, J. Doménech, N.A. Peppas, Drug transport mechanisms and release kinetics from molecularly designed poly(acrylic acid-g-ethylene glycol) hydrogels, Biomaterials 27(31) (2006) 5440-5451.

[18] A.S. Hoffman, Hydrogels for biomedical applications, Advanced drug delivery reviews 54(1) (2002) 3-12.

- [19] B. Chen, K. Jerger, J.M.J. Fréchet, F.C. Szoka Jr, The influence of polymer topology on pharmacokinetics: Differences between cyclic and linear PEGylated poly(acrylic acid) comb polymers, Journal of Controlled Release 140(3) (2009) 203-209.
- [20] S. Louguet, V. Verret, L. Bedouet, E. Servais, F. Pascale, M. Wassef, D. Labarre, A. Laurent, L. Moine, Poly(ethylene glycol) methacrylate hydrolyzable microspheres for transient vascular embolization, Acta Biomater 10(3) (2014) 1194-205.
- [21] L. Bedouet, V. Verret, S. Louguet, E. Servais, F. Pascale, A. Beilvert, M.T. Baylatry, D. Labarre, L. Moine, A. Laurent, Anti-angiogenic drug delivery from hydrophilic resorbable embolization microspheres: an in vitro study with sunitinib and bevacizumab, International journal of pharmaceutics 484(1-2) (2015) 218-27.
- [22] C.D. Gadaleta, G. Ranieri, Trans-arterial chemoembolization as a therapy for liver tumours: New clinical developments and suggestions for combination with angiogenesis inhibitors, Critical reviews in oncology/hematology 80(1) (2011) 40-53.
- [23] P. Bize, R. Duran, K. Fuchs, O. Dormond, J. Namur, L.A. Decosterd, O. Jordan, E. Doelker, A. Denys, Antitumoral Effect of Sunitinib-eluting Beads in the Rabbit VX2 Tumor Model, Radiology 280(2) (2016) 425-35.
- [24] B. Wang, H. Xu, Z.Q. Gao, H.F. Ning, Y.Q. Sun, G.W. Cao, Increased expression of vascular endothelial growth factor in hepatocellular carcinoma after transcatheter arterial chemoembolization, Acta Radiol 49(5) (2008) 523-9.
- [25] K. Fuchs, P.E. Bize, O. Dormond, A. Denys, E. Doelker, G. Borchard, O. Jordan, Drug-eluting beads loaded with antiangiogenic agents for chemoembolization: in vitro sunitinib loading and release and in vivo pharmacokinetics in an animal model, Journal of vascular and interventional radiology: JVIR 25(3) (2014) 379-387 e2.
- [26] O.S. Sakr, S. Berndt, G. Carpentier, M. Cuendet, O. Jordan, G. Borchard, Arming embolic beads with anti-VEGF antibodies and controlling their release using LbL technology, Journal of controlled release: official journal of the Controlled Release Society 224 (2016) 199-207.

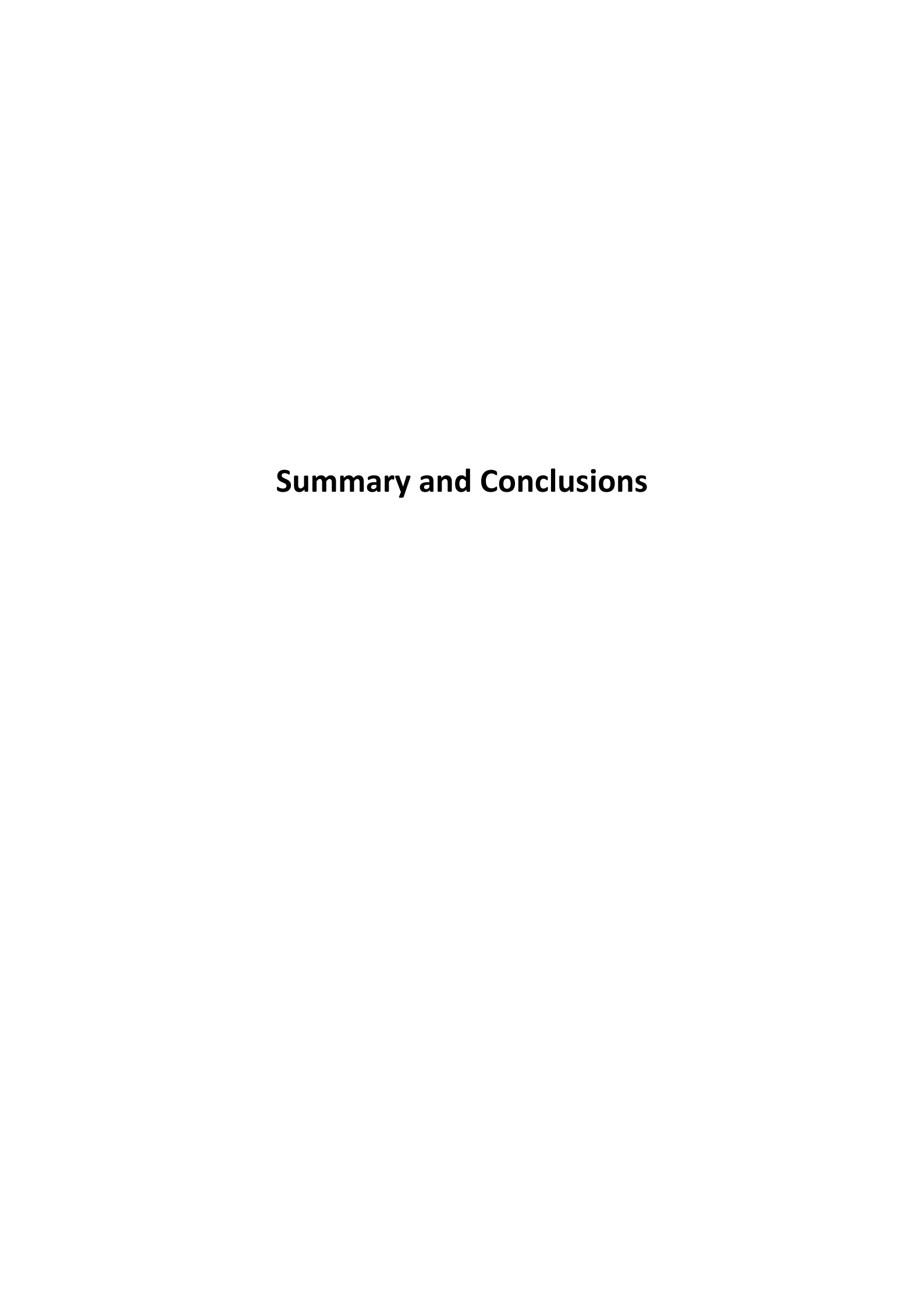
[27] Y. Wang, A. Benzina, D.G.M. Molin, N.v.d. Akker, M. Gagliardi, L.H. Koole, Preparation and structure of drug-carrying biodegradable microspheres designed for transarterial chemoembolization therapy, Journal of Biomaterials Science, Polymer Edition 26(2) (2015) 77-91.

- [28] L. Weng, S. Akurati, P. Rostamzadeh, J. Golzarian, In vitro evaluation of sunitinib loading and release of bioresorbable microspheres, Journal of Vascular and Interventional Radiology 25(3) S27.
- [29] D.L. Elbert, Liquid–liquid two-phase systems for the production of porous hydrogels and hydrogel microspheres for biomedical applications: A tutorial review, Acta Biomaterialia 7(1) (2011) 31-56.
- [30] V.N. Nguyen, N. Huang, J.-L. Grossiord, L. Moine, F. Agnely, C. Vauthier, Rheological characterization of mechanical properties of chemically crosslinked microspheres, Journal of Applied Polymer Science 128(5) (2013) 3113-3121.
- [31] A. Denys, P. Bize, O. Jordan, E. Doelker, N. Boulens, Chemoembolization Composition Comprising Anti-Angiogenic Agents, in: C.H.U.V. (CH), R.d.B.C.-L.C.F.A.D.S.E. US). (Eds.) Switzerland, 07.06.2012.
- [32] K. Fuchs, P.E. Bize, A. Denys, G. Borchard, O. Jordan, Sunitinib-eluting beads for chemoembolization: methods for in vitro evaluation of drug release, International journal of pharmaceutics 482(1-2) (2015) 68-74.
- [33] USP36-NF31, United States Pharmacopeia and National Formulary (USP 36-NF 31). <1090> Assessment of Drug Product Performance Bioavailability, Bioequivalence, and Dissolution. http://www.uspnf.com/uspnf/pub/index?usp=37&nf=32&s=1&officialOn=August%201,%202014>, 2013 (accessed 28.08.2016.).
- [34] V.N. Nguyen, C. Vauthier, N. Huang, J.-L. Grossiord, L. Moine, F. Agnely, Degradation of hydrolyzable hydrogel microspheres, Soft Matter 9(6) (2013) 1929-1936.
- [35] E.L. Kostoryz, K. Dharmala, Q. Ye, Y. Wang, J. Huber, J.G. Park, G. Snider, J.L. Katz, P. Spencer, Enzymatic biodegradation of HEMA/bisGMA adhesives formulated with different water content, Journal of biomedical materials research. Part B, Applied biomaterials 88(2) (2009) 394-401.
- [36] Sigma-Aldrich Co. LLC, Enzymatic Assay of Esterase. http://www.sigmaaldrich.com/technical-documents/protocols/biology/enzymatic-assay-of-esterase.html, 2016 (accessed 29.05.2016.).

[37] D. Reith, B. Müller, F. Müller-Plathe, S. Wiegand, How does the chain extension of poly (acrylic acid) scale in aqueous solution? A combined study with light scattering and computer simulation, The Journal of Chemical Physics 116(20) (2002) 9100-9106.

- [38] V.N. Nguyen, Microsphères résorbables pour embolisation et chimio embolisation., Université Paris Sud, Paris XI, 2013.
- [39] J. Folkman, Angiogenesis: an organizing principle for drug discovery?, Nature reviews. Drug discovery 6(4) (2007) 273-286.
- [40] L. Wang, C. Li, pH responsive fluorescence nanoprobe imaging of tumors by sensing the acidic microenvironment, Journal of Materials Chemistry 21(40) (2011) 15862-15871.
- [41] X. Zhang, Y. Lin, R.J. Gillies, Tumor pH and its measurement, Journal of nuclear medicine: official publication, Society of Nuclear Medicine 51(8) (2010) 1167-1170.
- [42] Z.P. Xiong, S.R. Yang, Z.Y. Liang, E.H. Xiao, X.P. Yu, S.K. Zhou, Z.S. Zhang, Association between vascular endothelial growth factor and metastasis after transcatheter arterial chemoembolization in patients with hepatocellular carcinoma, Hepatobiliary & pancreatic diseases international: HBPD INT 3(3) (2004) 386-90.
- [43] J.H. Shim, J.W. Park, J.H. Kim, M. An, S.Y. Kong, B.H. Nam, J.I. Choi, H.B. Kim, W.J. Lee, C.M. Kim, Association between increment of serum VEGF level and prognosis after transcatheter arterial chemoembolization in hepatocellular carcinoma patients, Cancer science 99(10) (2008) 2037-44.
- [44] G. Ranieri, M. Ammendola, I. Marech, A. Laterza, I. Abbate, C. Oakley, A. Vacca, R. Sacco, C.D. Gadaleta, Vascular endothelial growth factor and tryptase changes after chemoembolization in hepatocarcinoma patients, World journal of gastroenterology: WJG 21(19) (2015) 6018-6025.
- [45] C.D. Britten, A.S. Gomes, Z.A. Wainberg, D. Elashoff, R. Amado, Y. Xin, R.W. Busuttil, D.J. Slamon, R.S. Finn, Transarterial chemoembolization plus or minus intravenous bevacizumab in the treatment of hepatocellular cancer: a pilot study, BMC cancer 12 (2012) 16.
- [46] A. Sergio, C. Cristofori, R. Cardin, G. Pivetta, R. Ragazzi, A. Baldan, L. Girardi, U. Cillo, P. Burra, A. Giacomin, F. Farinati, Transcatheter arterial chemoembolization (TACE) in hepatocellular carcinoma (HCC): the role of angiogenesis and invasiveness, The American journal of gastroenterology 103(4) (2008) 914-21.

[47] X. Li, G.S. Feng, C.S. Zheng, C.K. Zhuo, X. Liu, Expression of plasma vascular endothelial growth factor in patients with hepatocellular carcinoma and effect of transcatheter arterial chemoembolization therapy on plasma vascular endothelial growth factor level, World journal of gastroenterology: WJG 10(19) (2004) 2878-82.



In this thesis, we explore a novel anti-angiogenic strategy for the treatment of intermediate hepatocellular carcinoma. Patients suffering from this stage of the disease are usually treated by transarterial chemoembolization, which has proven clinical benefit. Nevertheless, ischemia created by the embolization leads to post-interventional neoangiogenesis, and may eventually result in tumor rebound. Therefore, the idea evolved to combine marketed drug-capable embolic beads, which are successfully established in this technique, with an anti-angiogenic drug. An additional advantage of the beads is the possibility to deliver the drug locally and in a controlled manner, while possibly reducing undesired drug-related systemic toxicity.

The first chapter of this thesis reviews the 2016 state of the art of novel embolic drug-eluting beads. Drug loading and release characteristics of newly developed embolic microspheres are presented. Whereas ion-exchange based systems lead to rapid drug release, diffusion- and/or degradation-based systems may be tailored to yield prolonged release. We have seen that once administered, long-term tumor exposure to the drug is not only drug-dependent, but the local tissue architecture and the tissue integrity play a crucial role for the pharmacokinetics.

In the second chapter, we describe for the first time the combination of the anti-angiogenic receptor tyrosine kinase inhibitor sunitinib with embolic beads. We have demonstrated the fast loading and *in vitro* release kinetics of sunitinib using two different sizes of DC Bead microspheres, and have confirmed their potential to suppress ischemia-triggered proliferative cell responses and vascular growth factor activation *in vitro* and *in vivo*. In the pilot study with healthy rabbits, efficacious sunitinib delivery with high liver concentrations and infra-therapeutic systemic exposure over one day is illustrated.

We continue with a more in-depth comparison of *in vitro* release of sunitinib from DC Bead microspheres with the pharmacokinetics *in vivo*, which is described in the third chapter. We have demonstrated the influence of the hydrodynamic stress, flow rate and the drug's physicochemical properties on the rate and extent of drug elution. Among three different set-ups, slow drug release correlated better with *in vivo* drug plasma levels, whereas fast release represented more adequately drug tissue levels after local drug delivery. Meaningful *in vitro-in vivo* correlation is rendered difficult by the fact that drug residence time in the tissue is both inherent to the particular drug properties and the tissue environment. For sunitinib delivery via embolic beads, we have

suggested a flow-through set-up with relatively low shear without a membrane barrier to mimic *in vivo* kinetics.

Following a preclinical study showing the anti-tumoral activity of sunitinib-eluting beads in a VX2 tumor rabbit model, the liver tumor samples were submitted to an imaging study. In the fourth chapter, we report the investigation of the spatial distribution of sunitinib in the tumor tissue after elution from beads. For this, specific fluorescence microscopy and mass spectrometry imaging methods have been developed. Images clearly displayed the effective local drug delivery in the necrotic tumor compared to normal liver over 2 weeks. Sunitinib was retained by the necrotic tissue to a larger extent than by the non-tumor tissue. More specifically, sunitinib was transported in a radius of up to 1.5 mm around the beads, which is necessary to possibly reach tumor coverage by the drug.

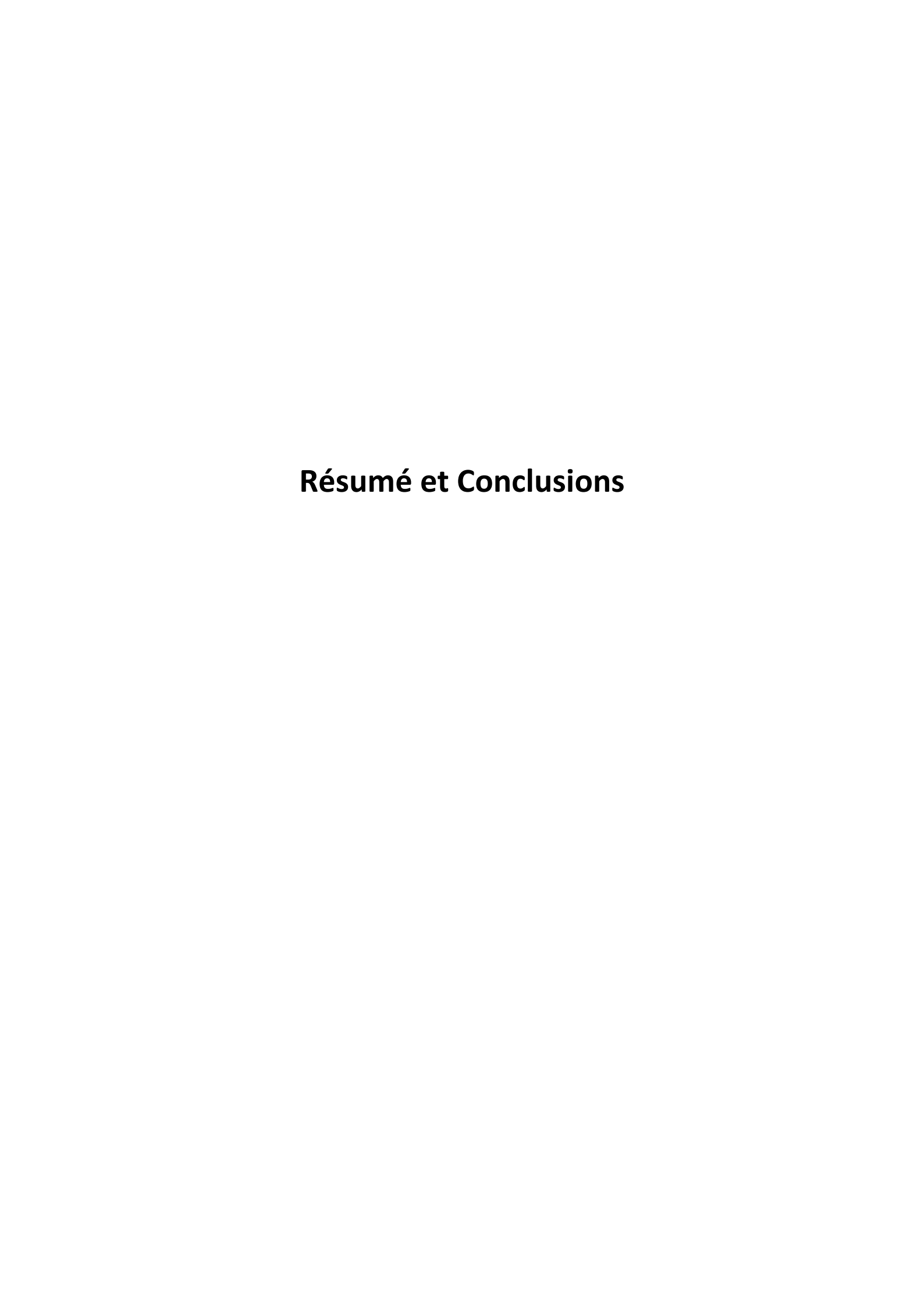
Finally in the fifth chapter, the development of biodegradable microspheres for sunitinib delivery via transarterial embolization is described. Sulfopropylmethacrylate microspheres were in the size range to be employed for embolization, were shown to be non-toxic to renal epithelial cells, and had a high swelling capacity and consequently elasticity. After eight weeks, decreasing elastic modulus and surface modifications were signs of early biodegradation under accelerating conditions. The lyophilized microspheres took up sunitinib at high loading capacity, sufficient to reach therapeutic concentrations *in vivo*. Sunitinib *in vitro* release was fast and almost complete and was deemed comparable to commercial embolic drug-eluting beads.

As outlined in the review article in chapter one, research is currently directed toward the design of beads which, 1. can be loaded with novel drugs, 2. can be imaged during the radiologic intervention, or 3. are biodegradable or bioresorbable. Sunitinib is definitely an interesting candidate for local delivery after embolization-triggered angiogenesis, since oral delivery led to systemic toxicity and consequently to discontinuation of a randomized phase III trial vs sorafenib. Thus, anti-angiogenic drug-bead combinations have high potential for clinical translation.

From a more general perspective, recent break-through advances in HCV treatment will probably alleviate the global hepatitis C burden in the next years and decades. Gilead Sciences Inc. had introduced sofosbuvir as a single agent under the tradename Sovaldi® in the European Union beginning of 2014. From end of 2014 on, the combination sofosbuvir/ledipasvir (Harvoni®) reached cure rates of close to 100% with minimal side effects in the most prevalent genotypes of HCV

infection. A press release from July 2016¹ reports marketing authorization for Epclusa® (sofosbuvir/velpatasvir) for the treatment of all genotypes of chronic hepatitis C. Provided the world's population will have access to these medicines, hepatitis C cases progressing into cirrhosis and hepatocellular carcinoma will likely decrease.

¹http://www.gilead.com/news/press-releases/2016/7/european-commission-grants-marketing-authorization-for-gileads-epclusa-sofosbuvirvelpatasvir-for-the-treatment-of-all-genotypes-of-chronic-hepatitis-c



Résumé et Conclusions 147

L'objectif de cette thèse est l'exploration d'une stratégie anti-angiogénique pour le traitement du carcinome hépatocellulaire. Les patients au stade intermédiaire de la maladie sont généralement traités par la chimioembolisation transartérielle, qui a fait preuve d'un bénéfice clinique. Cependant, l'ischémie créée par l'embolisation induit une néoangiogénèse post-interventionnelle pouvant aboutir à la récurrence de la tumeur. Pour cette raison il a été proposé de combiner des sphères d'embolisation déjà commercialisées et établies cliniquement, avec un principe actif anti-angiogénique. Un avantage supplémentaire de ces « chimiosphères » est la possibilité de libérer le médicament de manière locale et contrôlée, tout en réduisant la toxicité systémique indésirable liée au principe actif.

Le premier chapitre de cette thèse passe en revue l'état de l'art 2016 des chimiosphères pour embolisation. Les caractéristiques de chargement et de libération des chimiosphères en développement sont présentées. Alors que les systèmes basés sur l'interaction ionique entre les sphères et le principe actif résultent en une libération rapide de celui-ci, des systèmes basés sur la diffusion et/ou la dégradation sont conçus pour une libération prolongée. Nous avons vu qu'après administration, l'exposition de la tumeur au médicament ne dépend pas seulement des propriétés du principe actif, mais aussi de l'architecture locale et de l'intégrité du tissu qui jouent un rôle crucial pour la pharmacocinétique.

Dans le deuxième chapitre, nous décrivons pour la première fois la combinaison du sunitinib, un principe actif anti-angiogénique, avec des sphères destinées à l'embolisation. Nous démontrons un chargement efficace et une cinétique de libération rapide *in vitro* du sunitinib, à l'aide de deux tailles différentes des microsphères DC Bead®, et nous confirmons leur potentiel de suppression des réponses cellulaires prolifératives, déclenchées par l'ischémie, ainsi que de l'activation du facteur de croissance de l'endothélium vasculaire *in vitro* et *in vivo*. Une expérience pilote avec des lapins sains a illustré la libération efficace du sunitinib à des concentrations élevées dans le foie, mais infra-thérapeutiques dans la circulation systémique durant 24 heures.

Nous poursuivons dans le troisième chapitre avec une comparaison plus approfondie de la libération *in vitro* du sunitinib avec la pharmacocinétique *in vivo*. Nous démontrons l'influence prédominante des conditions hydrodynamiques, de la vélocité du flux et des propriétés physicochimiques du principe actif sur la vitesse et le degré d'élution de la drogue. Parmi les trois différentes méthodes testées, menant à des profils de libération distincts, le profil de libération lent

148 Résumé et Conclusions

du principe actif corrèle mieux avec le niveau plasmatique obtenu *in vivo*, tandis que la libération rapide représente de manière plus adéquate le niveau tissulaire du principe actif après administration locale. Une corrélation *in vitro-in vivo* pertinente est rendue difficile par le fait que le temps de résidence du principe actif dans le tissu est inhérent tant aux propriétés spécifiques du principe actif qu'à l'environnement tissulaire. Afin de simuler la cinétique *in vivo*, nous suggérons un appareillage à flux continu avec un cisaillement relativement faible, sans présence d'une membrane faisant office de barrière.

Suite à une étude préclinique qui démontre l'activité antitumorale des chimiosphères de sunitinib dans un modèle de tumeur VX2 chez le lapin, les échantillons de tumeurs de foie ont été examinés par imagerie. Ainsi, dans le quatrième chapitre, nous investiguons la distribution spatiale du sunitinib dans la tumeur après son élution des microsphères. Dans ce but, des méthodes spécifiques de microscopie fluorescente et d'imagerie par spectrométrie de masse ont été développées. Les images ont démontré une libération locale et efficace dans la tumeur nécrotique, comparée au foie normal, pendant deux semaines. Le sunitinib a été retenu davantage par le tissu nécrotique que par le tissu non-tumoral. En outre, le sunitinib a été transporté sur des distances allant jusqu'à 1.5 mm autour des microsphères, atteignant potentiellement la totalité des cellules malignes.

Finalement dans le cinquième chapitre, nous décrivons le développement de microsphères biodégradables pour l'administration de sunitinib par chimioembolisation transartérielle. Des microsphères de méthacrylate de sulfopropyle de taille adéquate pour l'embolisation des vaisseaux de carcinome hépatocellulaire ont été obtenues. Elles se sont montrées non-toxiques pour les cellules épithéliales du rein, ainsi que possédant les propriétés d'élasticité et de capacité de gonflement requises. Après huit semaines, une baisse du module d'élasticité ainsi que des modifications de surface indiquent un début de biodégradation sous conditions accélérées. Les microsphères lyophilisées ont été chargées de sunitinib à des taux élevés, suffisant pour atteindre des concentrations thérapeutiques *in vivo*. La libération du sunitinib *in vitro* a été rapide et presque complète, considérée comparable aux chimiosphères commerciales pour embolisation.

Comme détaillé dans l'article de revue du premier chapitre, les recherches sont actuellement dirigées vers la mise en place de microsphères pouvant être chargées avec de nouveaux principes actifs, visualisées pendant l'intervention radiologique, étant biodégradables ou biorésorbables.

Résumé et Conclusions 149

Parmi les principes actifs, le sunitinib est un candidat de choix pour une administration locale afin de minimiser l'angiogénèse engendrée par l'embolisation. En effet, une étude clinique randomisée de phase III a montré une toxicité systémique intolérable du sunitinib administré per os, menant à la suspension de cet essai. De ce fait, les combinaisons d'agents anti-angiogéniques avec les microsphères d'embolisation possèdent un fort potentiel pour une translation en clinique.



Awards & Distinctions

Katrin Fuchs, Poster Award 9th Swiss Pharma Science Day August 31, 2016, Bern (Switzerland) Third Prize for Mapping of Antiangiogenic Drug Distribution in a Rabbit Model of Liver Cancer Sponsored by Pharmazeutische Gesellschaft Zürich (PharmGZ)

A. Denys, P. Bize, O. Jordan, **K. Fuchs**, G. Borchard Award of Excellence and Innovation in IR Handed over at the Annual Meeting of the Cardiovascular and Interventional Radiological Society of Europe (CIRSE) September 26-30, 2015, Lisbon (Portugal)

Katrin Fuchs, The best IO papers of 2014, Invited for Oral Presentation at the European Conference on Interventional Oncology (ECIO) April 22-25, 2015, Nice (France) For the scientific article:

K. Fuchs, P. E. Bize, A. Denys, G. Borchard, O. Jordan Sunitinib-Eluting Beads for Chemoembolization: Methods for In Vitro Evaluation of Drug Release Int J Pharm. 2015 March;482(1-2):68-74. DOI: 10.1016/j.ijpharm.2014.11.041

Katrin Fuchs, JVIR Editor Award Outstanding Laboratory Investigation for 2014 Handed over at the Annual Scientific Meeting of the Society of Interventional Radiology (SIR)
February 28 - March 5, 2015, Atlanta, GA (US)
For the scientific article:

K. Fuchs, P. E. Bize, O. Dormond, A. Denys, E. Doelker, G. Borchard, O. Jordan Drug-Eluting Beads Loaded with Antiangiogenic Agents for Chemoembolization: In Vitro Sunitinib Loading and Release and In Vivo Pharmacokinetics in an Animal Model J Vasc Interv Radiol. 2014 March;25(3):379-387, 387.e1-2. DOI: 10.1016/j.jvir.2013.11.039

Peer-reviewed Publications

K. Fuchs, R. Duran, A. Denys, P. E. Bize, G. Borchard, O. Jordan *Drug-Eluting Embolic Microspheres for Local Drug Delivery – State of the Art* To be submitted to Journal of Controlled Release, 2016 December

K. Fuchs, A. Kiss, P. E. Bize, R. Duran, A. Denys, G. Hopfgartner, G. Borchard, O. Jordan *Mapping of Drug Distribution in the Rabbit VX2 Liver Tumor Model after Chemoembolization with Sunitinib-Eluting Beads by Complementary Fluorescence and Mass Spectrometry Imaging To be submitted to Radiology, 2016 December*

K. Fuchs, O. Sakr, T. Jbilou, V.N. Nguyen, G. Borchard, O. Jordan Development of Sunitinib-Eluting Hydrogel Microspheres for Transarterial Chemoembolization To be submitted to European Journal of Pharmaceutics and Biopharmaceutics, 2016 December

P. Bize, R. Duran, **K. Fuchs**, O. Dormond, J. Namur, L. A. Decosterd, O. Jordan, E. Doelker, A. Denys *Antitumoral Effect of Sunitinib-eluting Beads in the Rabbit VX2 Tumor Model* Radiology. 2016 August;280(2):425-435. DOI: 10.1148/radiol.2016150361

K. Fuchs, P. E. Bize, A. Denys, G. Borchard, O. Jordan Sunitinib-Eluting Beads for Chemoembolization: Methods for In Vitro Evaluation of Drug Release Int J Pharm. 2015 March;482(1-2):68-74. DOI: 10.1016/j.ijpharm.2014.11.041

K. Fuchs, P. E. Bize, O. Dormond, A. Denys, E. Doelker, G. Borchard, O. Jordan Drug-Eluting Beads Loaded with Antiangiogenic Agents for Chemoembolization: In Vitro Sunitinib Loading and Release and In Vivo Pharmacokinetics in an Animal Model J Vasc Interv Radiol. 2014 March;25(3):379-387, 387.e1-2. DOI: 10.1016/j.jvir.2013.11.039

Not Peer-reviewed Publications

K. Fuchs, O. Jordan

Drug-eluting beads loaded with anti-angiogenic agents for chemoembolization: Interesting findings from the lab for IRs

Interventional News, September 2015

Oral Presentations

A. Kiss, **K. Fuchs**, P. E. Bize, R. Duran, A. Denys, G. Borchard, O. Jordan, G. Hopfgartner *Mapping of anticancer drug distribution in a rabbit model of liver cancer by MALDI-SRM/MS imaging and fluorescence microscopy*European Molecular Imaging Meeting (EMIM) 2016
March 8-10, 2016, Utrecht (The Netherlands)

K. Fuchs, P. E. Bize, R. Duran, A. Denys, O. Dormond, G. Borchard, O. Jordan *Antitumor effect and drug distribution profile of anti-angiogenic sunitinib embolization beads in the rabbit*

Annual Meeting of the European Federation for Pharmaceutical Sciences (EUFEPS) June 15-17, 2015, Geneva (Switzerland)

K. Fuchs, P. E. Bize, A. Denys, G. Borchard, O. Jordan *Sunitinib-Eluting Beads for Chemoembolization: Methods for In Vitro Evaluation of Drug Release* European Conference on Interventional Oncology (ECIO) April 22-25, 2015, Nice (France)

K. Fuchs, P. E. Bize, O. Dormond, A. Denys, G. Borchard, O. Jordan *Anti-Angiogenic Strategies for Chemoembolization of Liver Tumors* Joint Meeting Pharmaceutical Technology of Switzerland January 22, 2015, Basel (Switzerland)

K. Fuchs, P. E. Bize, O. Dormond, A. Denys, E. Doelker, G. Borchard, O. Jordan *Sunitinib-Eluting Beads for Chemoembolization* 9th European Workshop on Particulate Systems March 13-14, 2014, Utrecht (The Netherlands)

P. E. Bize, **K. Fuchs**, O. Jordan, O. Dormond, R. Duran, E. Doelker, T. De Baere, A. Denys *Evaluation of the anti-tumoral effect of 70-150 μm sunitinib eluting beads in VX2 carrying rabbits* 2013 Society of Interventional Radiology (SIR) 38th Annual Scientific Meeting April 13-18, 2013, New Orleans, LA (US)

O. Jordan, **K. Fuchs**, N. Boulens, P. E. Bize, E. Doelker, A. Denys In vitro characterization of sunitinib loaded DC Beads Cardiovascular and Interventional Radiological Society of Europe (CIRSE) September 15-19, 2012, Lisbon (Portugal)

Abstracts and Poster Presentations

K. Fuchs, A. Kiss, P. E. Bize, R. Duran, A. Denys, G. Hopfgartner, G. Borchard, O. Jordan *Mapping of Antiangiogenic Drug Distribution in a Rabbit Model of Liver Cancer* 9th Swiss Pharma Science Day August 31, 2016, Bern (Switzerland)

K. Fuchs, A. Kiss, P. E. Bize, R. Duran, A. Denys, G. Hopfgartner, G. Borchard, O. Jordan *Mapping of Antiangiogenic Drug Distribution in a Rabbit Model of Liver Cancer by Fluorescence Microscopy and MALDI-SRM/MS Imaging*

Controlled Release Society (CRS) Annual Meeting & Exposition July 17-20, 2016, Seattle, Washington (US)

Travel Grant by the Société Académique de Genève (SACAD) over 1600 CHF for K. Fuchs for attendance of the meeting.

A. Kiss, **K. Fuchs**, P. E. Bize, R. Duran, A. Denys, G. Borchard, O. Jordan, G. Hopfgartner *Study of sunitinib elution from hydrogels in rabbit VX2 tumor samples by MALDI-SRM imaging and fluorescence microscopy*

OurConIII: Imaging Mass Spectrometry Conference 2015 October 27-29, 2015, Pisa (Italy)

K. Fuchs, P. E. Bize, R. Duran, A. Denys, O. Dormond, G. Borchard, O. Jordan *Anti-Angiogenic Strategies for Chemoembolization of Liver Tumors* 8th Swiss Pharma Science Day August 19, 2015, Bern (Switzerland)

K. Fuchs, P. E. Bize, R. Duran, A. Denys, O. Dormond, G. Borchard, O. Jordan *Anti-Angiogenic Strategies for Chemoembolization of Liver Tumors*Controlled Release Society (CRS) Annual Meeting & Exposition
July 26-29, 2015, Edinburgh (Scotland)

Y. Dhif, O. Sakr, **K. Fuchs**, V. Nguyen, T. Jbilou, O. Jordan, G. Borchard *Layer-by-Layer (LbL) Coated Biodegradable Microspheres for Chemoembolization of Liver Tumors* 7th Swiss Pharma Science Day August 20, 2014, Bern (Switzerland)

F. Loeliger, **K. Fuchs**, O. Sakr, V. Nguyen, T. Jbilou, G. Borchard, O. Jordan Sunitinib- and Sorafenib-Eluting Biodegradable Microspheres for Transarterial Chemoembolization 7th Swiss Pharma Science Day August 20, 2014, Bern (Switzerland)

K. Fuchs, P. E. Bize, O. Dormond, A. Denys, E. Doelker, G. Borchard, O. Jordan Drug-Eluting Beads Loaded with Anti-Angiogenic Agents for Chemoembolization: In Vitro Sunitinib Loading, Release and Biological Efficacy in a Cell Culture Model 9th World Meeting on Pharmaceutics, Biopharmaceutics and Pharmaceutical Technology March 31-April 4, 2014, Lisbon (Portugal)

- P. E. Bize, O. Jordan, **K. Fuchs**, O. Dormond, R. Duran, E. Doelker, T. De Baere, A. Denys *In vitro and in vivo characterization of sunitinib-eluting beads*American Society of Clinical Oncology (ASCO) Gastrointestinal Cancers Symposium January 24-26, 2013, San Francisco, CA (US)
- P. E. Bize, O. Jordan, **K. Fuchs**, O. Dormond, R. Duran, E. Doelker, T. De Baere, A. Denys Evaluation of the anti-tumoral effect of sunitinib-eluting beads in the VX2 liver tumour model of the rabbit

American Society of Clinical Oncology (ASCO) Gastrointestinal Cancers Symposium January 24-26, 2013, San Francisco, CA (US)

K. Fuchs, C. Siegfried, A. Denys, P. Bize, O. Dormond, E. Doelker, G. Borchard, O. Jordan Drug-eluting beads for transarterial chemoembolization: sunitinib loading, release properties and in vivo pharmacokinetics of DC Bead™ microspheres

5th Swiss Pharma Science Day
August 29, 2012, Bern (Switzerland)

- O. Jordan, **K. Fuchs**, C. Siegfried, N. Boulens, G. Borchard, P. Bize, E. Doelker, A. Denys *In vitro characterization of sunitinib-loaded DC Bead™: Loading and release characteristics* Global Embolization Symposia and Technologies (GEST) May 3-6, 2012, New York (US)
- K. Fuchs, C. Siegfried, A. Denys, P. Bize, O. Dormond, E. Doelker, G. Borchard, O. Jordan Sunitinib-loaded microspheres for transarterial chemoembolization: Study of drug loading, release properties and in vivo pharmacokinetics of DC Bead™ microspheres

 Controlled Release Society German Chapter

 March 29-30, 2012, Würzburg (Germany)

Travel Grant by the Swiss Society of Industrial Pharmacists (SSIP) for K. Fuchs for attendance of the meeting.

O. Jordan, **K. Fuchs**, N. Boulens, P. E. Bize, E. Doelker, A. Denys *In vitro characterization of sunitinib-eluting beads*Society for Interventional Radiology Annual Meeting
March 24-29, 2012, San Francisco (US)



Acknowledgements 157

It is September 1st 2016, that I write these lines, which I feel will make me sentimental. It was exactly five years ago when I started my PhD thesis in Gerrit's lab. Although he insisted that he should not be acknowledged for doing his job, there are of course a lot of things that I am thankful for, and that I could not just take for granted. So, Gerrit, thank you for taking me into the group (or should I say, thanks to Christiane?) and thank you for believing in me (which was not so obvious after the first months?). Thank you for following up in the group meetings, which taught me the importance of scientific communication. Thanks for sending me around the world for various congresses and ensuring networking possibilities in a way, one could not imagine better during a PhD! Thanks for coming to the office for chats – the casual atmosphere made the lab ambiance for me just a pleasure to continue the project day by day.

This PhD would not have been as successful without Olivier's limitless input, ideas, help, interest, presence and patience. We regularly spent hours in your office discussing data and you were the one showing me the priorities of my scientific work, encouraging me to think more independently, directing me and teaching me. You taught me not to lose myself in details and you were always up to date with the scientific field and literature. Thank you so much for your open ear, precious time and words. There was rarely any meeting that I would not come out with a clearer mind and lots of motivation to keep science going! You can ask Omar about that and he will confirm that I often returned to the office after our meetings with a smile on my face.

Thanks to Omar, my office-mate, for our common work! Thanks for transferring your presentation tricks to me and for the scientific and free time discussions we had together. Special thanks to Van for passing on her experience, and to Tayeb for assisting me at the end of my thesis. Thanks go also to the four master students who worked with me, Priscilla, Liridone, François, and Malika, for their great efforts! I believe we have grown together in these projects.

I would like to acknowledge the MDs Pierre Bize, Alban Denys, Olivier Dormond, and Rafael Duran for our fruitful collaboration. You were always very positive about our results, and I was very happy about your believe in me and your encouragement.

I would also like to thank the jury members, including Prof. Eric Allémann, Prof. Andrew Lewis, Prof. Patrycja Nowak-Sliwinska and Dr. Harry Tiemessen for accepting to review my thesis and for their time spent in this process.

158 Acknowledgements

An immense thank you to all my colleagues and friends in FABIO and FATEC! I really enjoyed the lab

atmosphere and meeting you when there was need for a break. I particularly address Viktorija,

Stella, Floriane, Tiziana, and Yanna! We spent gorgeous holidays and plenty of our leisure time

together and became close friends. It was you that made Geneva a special place!

C'est aussi grâce à Patrick que j'ai adoré le temps passé à Genève. Merci, Patrick, de m'avoir

accueillie dans ta maison, et de me considérer comme ta troisième fille! C'était vraiment la belle vie

chez toi et tu es une des personnes qui m'ont appris à ne pas prendre la vie trop au sérieux. J'ai eu

beaucoup de chance de me retrouver chez toi et chez ta famille! En même temps, je voudrais aussi

remercier Florence qui a « arrangé » mon emménagement et que j'apprécie tant sur le niveau

professionnel que personnel.

Danke, Mama und Papa, dass ihr mich immer unterstützt habt in meinen Zielen und mir gezeigt

habt, dass ihr mich dennoch nicht missen wollt. Ihr seid da in allen Lebenslagen und das

bedingungslos und allzeit. Ihr seid mein sicherer Hafen! Ein Dankeschön von Herzen auch an meine

Zwischenstationen auf dem Heimweg nach Buchberg und Genf, bei Andreas und Jana in Freiburg

und bei Rosa und Dieter in Karlsbad. Ich komme unheimlich gerne zu euch und die Stops bei euch

waren ausnahmslos sehr erfrischend! Wir werden das so fortsetzen, keine Frage!

Finally thanks to Djordje, you accompanied me through all sorts of ups and downs and I am

extremely thankful that you were able to shine a different light on some situations during these

years. You always bring up new topics, thoughts and arguments, which makes your company so

special and interesting. I love the time we spend together and I really hope we will be friends for

life.

Katrin Fuchs

Geneva, September 2016

Antitumoral Effect of Sunitinib-Eluting Beads in the Rabbit VX2 Tumor Model

Pierre Bize^a, Rafael Duran^a, **Katrin Fuchs**^b, Olivier Dormond^a, Julien Namur^c, Laurent A. Decosterd^a,

Olivier Jordan^b, Eric Doelker^b, Alban Denys^a

^c Archimmed, 12 Rue Charles de Gaulle, 78350 Jouy-en-Josas, France

Original Research Article

Published in:

Radiology. 2016, 280 (2), p. 425-35.

^a Departments of Radiology (P.B., R.D., A.D.), Surgery (O.D.), and Clinical Pharmacology (L.A.D.), University Hospital of Lausanne, Rue du Bugnon 46, 1011 Lausanne, Switzerland

^b School of Pharmaceutical Sciences, University of Geneva, University of Lausanne, Quai Ernest Ansermet 30, 1211 Geneva 4, Switzerland

Abstract

Purpose: To measure plasmatic (PSC) and intratumoral sunitinb concentrations (ITSC) following transcatheter arterial chemoembolization (TACE) with two different sizes of sunitinib-eluting beads (SEBs) in rabbits with VX2 hepatic allografts and to investigate treatment effects on vascular endothelial growth factor receptor type 2 (VEGFR2) phosphorylation, tumor volume and histopathological changes.

Materials and Methods: The protocol was approved by the French Ethics Committee for Animal Experiments (Comité d'Ethique en Expérimentation Animale du Centre INRA de Jouy-en-Josas et AgroParisTech, or COMETHEA, approval no. 11/028). Two experiments were performed. In the first, seven animals received 0.05 mL of 100-300 μm SEBs (1.5 mg of sunitinib) and six animals received saline injections. In the second, eight animals received 0.05 ml of 70-150 μm SEBs (1.5 mg of sunitinib), seven received 0.05 mL of 70-150 μm unloaded beads, and seven received oral sunitinib (6 mg every day). Tumor size was monitored with ultrasonography. PSC, ITSC, and phosphorylation of VEGFR2 were assessed on days 1 and 14. After the animals were sacrificed, histopathologic analysis was performed. The Kruskal-Wallis test, Mann-Whitney U test, and Fisher exact test were used to look for statistically significant differences between groups.

Results: Maximum PSC following TACE with 100-300 μ m SEBs was 0.002 μ g/mL on day 1. ITSC was 17.8 μ g/g on day 1 and 0.16 μ g/g on day 14. After TACE with 70-150 μ m SEBs, ITSC was 40.4 μ g/g on day 1 and 27.4 μ g/g on day 14. Phosphorylation of VEGFR2 was inhibited until day 14 after TACE with both sizes of SEBs. The size of VX2 tumors treated with 70-150 μ m SEB-TACE increased less (-2%) than that of tumors treated with unloaded beads (+42%) and oral sunitinib (6 mg every day; +1853%; P = .044).

Conclusions: SEB-TACE resulted in minimal PSC, high ITSC, and sustained VEGFR2 phosphorylation inhibition until day 14.

Advances in Knowledge:

1. In this preclinical animal study, we showed that transcatheter arterial chemoembolization (TACE) with 100-300 μ m sunitinib-eluting beads (SEBs) in VX2-carrying rabbits resulted in low (infratherapeutic) plasmatic sunitinib concentrations and high intratumoral sunitinib concentrations until day 14.

- 2. Phosphorylation (i.e. activation) of vascular endothelial growth factor type 2 (VEGFR2) was not detected with the Western blot until day 14 after a single intra-arterial administration of SEBs.
- 3. The size of VX2 tumors treated by transcatheter arterial chemoembolization (TACE) with 70-150 μ m SEBs increased less (-2%) than that of tumors treated with unloaded beads (+42%) and oral sunitinib (6 mg every day; +1853%; P = .044).
- 4. TACE with SEBs in rabbits with VX2 tumors caused more necrotic changes than unloaded beads (P = .024). A complete response was observed in 60% of animals treated with SEBs compared with 42.8% of those treated with unloaded beads, and systemic sunitinib concentrations remained insignificant (maximum median concentration, 0.002 µg/µL).

Implications for Patient Care:

The combination of an embolic device with an antiangiogenic agent could help overcome TACE-induced neoangiogenesis.

Summary Statement:

Our study shows that SEB-TACE was safe resulting in high ITSC with minimal systemic levels. Tumor control was better with SEB-TACE than with oral sunitinib, probably because of sustained inhibition of VEGFR2 phosphorylation and subsequent inhibition of post-embolization tumor angiogenesis rebound.

1 Introduction

Transcatheter arterial chemoembolization (TACE) is a treatment for liver tumors in which a chemotherapeutic agent is administered directly to the hepatic artery. Then, the artery is occluded with an embolic agent to prevent rapid washout of the administered agent and achieve an ischemic insult to induce tumor necrosis. Various treatment regimens have been evaluated in animal models (1-3). TACE with doxorubicin in association with ethiodized oil has been shown to improve survival in humans and is currently the standard treatment in patients with intermediate-stage hepatocellular carcinoma (HCC) (4). Although various cytostatic drugs such as doxorubicin, epirubicin, cisplatine, mitomycin C and 5-fluorouracil have been evaluated in this setting, none of these drugs has been clearly shown to be better than another (5). Drug-eluting beads have been developed to standardize the procedure, but once again, no clear benefit has been demonstrated in overall survival or progression-free survival (6). At present, TACE is considered to result in a partial response in 15%-55% of patients and to increase the median expected survival from 16 months without treatment to 20 months (7). One possible explanation for these poor results is the development of hypoxic stress in the tumor microenvironment, resulting in a strong stimulus for increasing proangiogenic factors (eg, hypoxia-inducible factor 1 and vascular endothelial growth factor) (8, 9). The activation of this angiogenic pathway can be detected as soon as 6 hours after embolization (10, 11) and is associated with a poor prognosis (12).

In two phase III, double-blind, placebo-controlled trials (13, 14), investigators showed that sorafenib, an oral multikinase inhibitor of vascular endothelial growth factor receptor subtypes 1-3), platelet-derived growth factor receptor β , Raf-1, and B-Raf (15), improves survival in patients with intermediate-stage HCC. These modestly positive results were encouraging for a highly chemoresistant cancer such as HCC, and numerous prospective trials have been performed to investigate the combination of TACE with systemic antiangiogenic therapy (16-19). Although combination therapy appears to be safe and well tolerated, preliminary results on effectiveness are controversial, and the improvements in overall survival have not been confirmed (16, 20).

One antiangiogenic drug being evaluated in this setting is sunitinib. Sunitinib is a multikinase inhibitor that acts to inhibit platelet-derived growth factor receptors and vascular endothelial growth factor receptors, which both play a role in tumor angiogenesis and cell proliferation.

Moreover this agent inhibits KIT (CD117), which promotes the proliferation of certain tumor cells (21-23). Although the activity of this drug on tyrosine kinases seemed promising for the systemic treatment of patients with advanced-stage HCC, the use of sunitinib was abandoned because of clinically significant toxicity (24). Drug-eluting beads loaded with sunitinib have recently been described (25). *In vitro*, these sunitinib-eluting beads (SEBs) were found to release sunitinib and inhibit tumor cell growth. SEBs administered to healthy rabbits did not show any sunitinib-related toxicity such as liver failure, cardiotoxicity, diarrhea, emesis or conjunctival irritation (26).

In this article, we report the results of two studies in which the goals were to measure serum plasma sunitinib concentration (PSC) and intratumoral sunitinib concentration (ITSC) after TACE with two different sizes of SEBs in rabbits with VX2 hepatic allografts and to investigate the effects of this treatment on vascular endothelial growth factor receptor type 2 (VEGFR2) phosphorylation and tumors.

2 Materials and Methods

This study was supported in part by Biocompatibles, Farnham, United Kingdom. The composition of a chemoembolization agent loaded with an antiangiogenic agent (sunitinib in this study) is subject to a patent (no. WO/2012/073188) filed by four of the authors (A.D., P.B., O.J., and E.D.) and one of their coworkers (a nonauthor) (26). The patent has been licensed to BTG, London, United Kingdom, who in the meantime had acquired Biocompatibles. One investigator (A.D.) has been a scientific consultant for BTG since the contract was licensed to that company. Other investigators (P.B., R.D., K.F., O.D., J.N., L.A.D., O.J., and E.D.) had full control of the data during the study and the publication of its findings.

2.1 Animal Model and Tumor Implantation

The protocol was approved by the French Ethics Committee for Animal Experiments (Comité d'Ethique en Expérimentation Animale du Centre INRA de Jouy-en-Josas et AgroParisTech, or COMETHEA, approval no. 11/028). Adult New Zealand white rabbits (n = 35; age, 6–7 months; body weight, 3.0–3.8 kg) were used for the study. Briefly, VX2 tumors were grown in the hind limb of a

carrier rabbit, and small fragments (approximately 8 mm²) were implanted surgically in the left liver lobe by using general anesthesia. Tumors were left to grow for 14 days before treatment. Growth of implanted tumors was confirmed by using ultrasonography (US) (Voluson E8 Expert; GE Healthcare, Velizy, France).

2.2 First Experiment: Proof of Concept

Seven animals received 100-300 μ m SEBs, and six animals (the control group) received an injection of 1 mL of saline in the left branch of the hepatic artery (P.B., with 10 years of experience in interventional radiology; and R.D., with 3 years of experience in interventional radiology). In the 100-300 μ m SEB group, one animal was sacrificed on day 1, and the others were followed up for survival until day 14. Blood samples were collected to determine liver enzyme levels and sunitinib concentrations before and after treatment and every day until day 7 and on day 14.

2.3 Second Experiment: Comparative Study

On the basis of the results of the first experiment, a second study was designed to compare the antitumoral effectiveness of SEB-TACE, unloaded beads, and oral sunitinib. Since smaller beads (70-150 μ m) were available at that time and it has been shown that more distal embolization can result in better antitumoral effectiveness, these small beads were chosen for the second experiment (27). Eight animals received 70-150 μ m SEBs, and seven animals received unloaded 70-150 μ m drug-eluting beads (DC Beads; Biocompatibles, Farnham, United Kingdom) in the hepatic artery (P.B., R.D.). Seven animals received 6 mg of oral sunitinib every day. This dose was chosen because preclinical studies have shown that it corresponds to the maximum oral dose that can be administered to rabbits without clinically significant side effects, such as dysrhythmia, diarrhea, emesis, and conjunctival irritation (28). One animal was sacrificed on day 1 in the 70-150 μ m SEB group, and the others were followed up until day 14. Embolization with unloaded beads was performed in separate sessions.

2.4 Sunitinib-eluting Beads and Oral Sunitinib Preparation

Sunitinib was purchased from LC Laboratories (Woburn, Mass). A stock solution of sunitinib (10 mg/mL) was prepared by acidifying the sunitinib base in 0.1 N hydrochloric acid in a 1.1-mol/L excess to solubilize the drug. A 5% (wt/vol) glucose solution was then added. The storage solution was removed from the drug-eluting bead vials, and the beads were incubated with the sunitinib solution, resulting in a drug content of 30 mg per milliliter of beads. SEBs were resuspended in 5% glucose, aliquoted volumetrically to 0.05 mL (1.5 mg of sunitinib), and distributed in sterile ready-to-use 1-mL syringes. This dose was chosen on the basis of the results of a previously published pharmacokinetic study (25), which showed that the administration of 0.2 mL of SEBs (6 mg of sunitinib) to the whole liver was well tolerated and resulted in an intrahepatic sunitinib concentration of 3.4 μ g/g 24 hours after delivery (therapeutic threshold, 50 ng/g). A quarter of this dose was chosen for both experiments, since we were only planning to embolize the left lateral lobe. Unloaded drug-eluting beads were aliquoted similarly. The oral sunitinib solution (1 mg/mL) was prepared by diluting the stock solution (10 mg/mL) with prefiltered glucose 5% (wt/wt) (O.J., K.F.).

2.5 Interventional Technique

Embolization was performed (day 0) by using general anesthesia 2 weeks after tumor implantation (P.B., R.D.). Briefly, the femoral artery was exposed with a surgical cut, and a 4-F introducer sheath (Radifocus; Terumo Europe, Leuwen, Belgium) was placed. A 2.1-F/2.7-F, 45°-tip microcatheter (Echelon; EV3, Paris, France) was used to perform selective angiography of the celiac trunk. Branches of the left hepatic artery were catheterized, and treatment was administered (29). When unloaded drug-eluting beads or SEBs were administered, contrast medium (Omnipaque 300; GE Healthcare, Aulnay-sous-Bois, France) was added to the beads, and the treatment was administered in 20–30 minutes via small boluses under fluoroscopic control, taking care to avoid reflux. The end point of SEB-TACE was considered to be reached when 0.05 mL of SEBs were administered. After bead delivery, the catheter was carefully flushed with saline under fluoroscopic control. No further embolization was performed to reduce blood flow at the end of the SEB-TACE

procedures. Embolization with unloaded beads was performed in the same manner, with the same end point.

2.6 Monitoring Tumor Volume

Tumor growth was monitored with US on days 0, 7, and 14 by using a 5-MHz linear transducer (Voluson E8 Expert; GE Healthcare) (P.B., R.D.). Tumor volume was calculated by using the following modified formula for elliptic volume:

$$\frac{\pi}{6 \times D1 \times D2 \times D3}$$

2.7 Animal Sacrifice and Tissue Sample Harvesting

On day 14, all surviving animals were preanesthesized and euthanized with an intracardiac injection of Dolethal (Vetoquinol, Paris, France). A comprehensive postmortem thoracoabdominal examination was performed. Tumor samples were harvested in the solid part of the tumor, and necrotic areas were avoided (P.B., R.D., J.N.). Liver and tumor tissue samples (approximately 1 x 1 x 1 cm) were snap-frozen and stored at -80°C for sunitinib concentration measurements.

2.8 Measurement of Sunitinib Concentrations in Plasma and Liver Tissue

PSC, ITSC, and sunitinib concentrations in the right (untreated) liver lobe were measured by using liquid chromatography tandem mass spectroscopy (L.A.D.) (30). Tissue samples were obtained on days 1 and 14 from animals that received SEBs (first and second experiments) and on day 14 only from animals that received oral sunitinib (second experiment), because it has been shown that sunitinib concentrations were low in the liver after a single dose of 6 mg (28).

2.9 Immunoprecipitation and Western Blot Analysis

Phosphorylation of VEGFR2 (ie, activation) in the tumor samples was studied by means of Western blot analysis (O.D.). Tumors were lysed in a radioimmunoprecipitation assay lysis buffer. Lysates were centrifuged at 4°C for 15 minutes, and supernatants were collected. Immunoprecipitation was performed with 1 mg of total protein and incubated with an anti-VEGFR2 antibody (2479; Cell Signaling Technology, Danvers, Mass) for 90 minutes at 4°C. Immunocomplexes were captured with Protein A/G Sepharose beads (Amersham Pharmacia Biotech, Marlborough, Mass) and washed four times in radioimmunoprecipitation assay buffer. Finally, immunoprecipitated proteins were separated on a polyacrylamide gel and analyzed by using the Western blot for the phosphorylated form of VEGFR2 (pVEGFR2) (4991; Cell Signaling) and total VEGFR2.

2.10 Histopathologic Evaluation

In the second experiment, a thorough histopathologic analysis was performed after the animals were sacrificed (J.N.). Tumor and liver samples were fixed in formaldehyde 3.6%. The samples were dehydrated, set in xylene, and embedded in paraffin. Sections were cut 3–4 μ m thick and mounted on a slide (n = 79). Sections were stained with hematein-eosin-saffron after rehydration and were digitized with a NanoZoomer 2.0-HT slide scanner (Hamamatsu Photonics, Hamamatsu City, Japan) at x20 enlargement. The presence or absence of necrotic changes in the tissue surrounding the embolic particles was noted. A response was considered to be complete when 100% of the visible tumor tissue was necrotic on histopathologic slides.

2.11 Statistical Analysis

In the first experiment, the Mann-Whitney U test was used to assess differences in tumor growth percentages) during follow-up between the 100-300 μ m SEB group and the control group. In the second experiment, the Mann-Whitney U test was used to assess tumor growth (percentages) during follow-up for each single group, and the Kruskal-Wallis test was used to assess the differences in tumor growth (percentages) during follow-up between the three groups. A two-sided

P value of less than .05 was considered to indicate a statistically significant difference. The x_2 test was used to investigate the difference in pathologic complete response among the three groups of the second study. The Fisher exact test was used for pairwise comparison when the overall test yielded a significant result in both places. The statistical analysis was performed with SPSS software (version 22; SPSS, Chicago, III).

3 Results

Implanted VX2 tumors grew successfully in all animals. Administration of the scheduled treatment was achieved in all animals.

3.1 First Experiment: Proof of Concept

All animals treated with 100-300 μ m SEBs survived until the day of sacrifice. Two animals died in the control group on days 4 and 9 as a result of respiratory failure due to massive metastatic lung involvement. One animal had to be euthanized on day 7 when paraplegia developed, which was thought to be due to spinal trauma from manipulation of the animal. SEB-TACE resulted in an expected transient increase of transaminases; maximum aspartate aminotransferase and alanine aminotransferase levels were reached on day 2, followed by a gradual decrease (Fig 1). Lactate dehydrogenase and bilirubin levels remained within the normal range, compared with baseline values, after the SEB-TACE procedure. Liver enzymes remained within the normal ranges in the control group.

 $\it Tumor\ volume. —$ No significant difference in tumor volume was identified between the 100-300 μm SEB group and the control group.

Sunitinib concentrations in plasma, tumor, and liver.—In the 100-300 μ m SEB group, PSC remained low throughout follow-up and never reached the therapeutic threshold of 0.05 μ g/mL (31) (Fig 2). The highest PSC (median, 0.002 μ g/mL; interquartile range [IQR], 0.001-0.003 μ g/mL) was recorded on day 0, then it rapidly decreased until day 4 (Fig 2). The ITSC was 17.8 μ g/g in the animal sacrificed on day 1. The median ITSC was 0.16 μ g/g (IQR, 0-0.3 μ g/g) in the remaining animals on day 14. The sunitinib concentration was 2.3 μ g/g in the untreated right liver lobe in the animal

sacrificed on day 1. There was no detectable sunitinib in the untreated liver in the remaining animals on day 14 (Table).

Inhibition of VEGFR2 phosphorylation in the tumor.—After a single administration of 100-300 μm SEBs, the phosphorylated (active) form of VEGFR2 could not be detected with Western blot analysis on day 1 or day 14, while phosphorylated VEGFR2 was detectable in the control group (Fig 3).

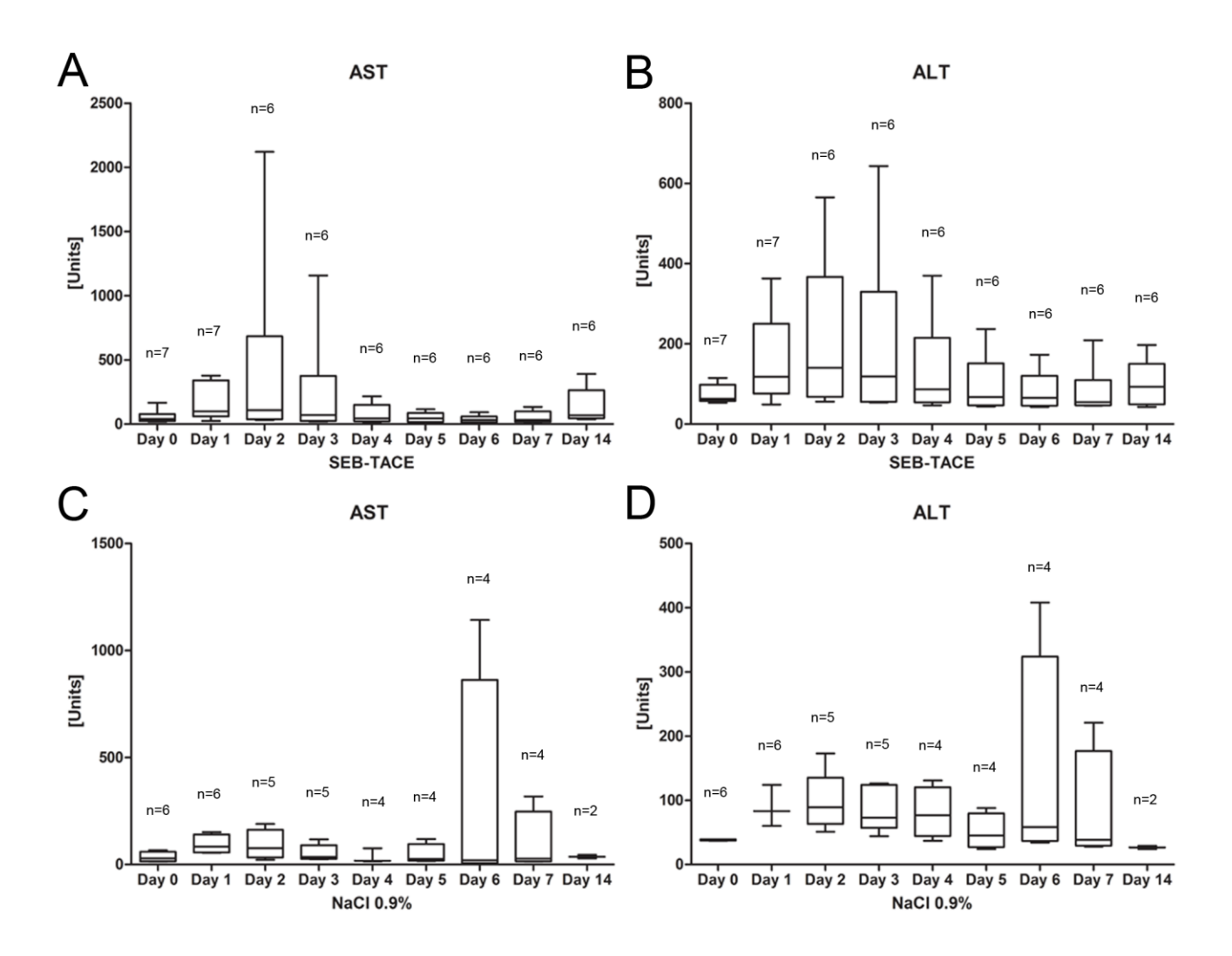


Figure 1. Box plots show, A, mean aspartate aminotransferase (AST) and, B, mean alanine aminotransferase (ALT) levels (in international units per liter) after administration of 0.05 mL of 100-300 μ m SEBs and, C, mean aspartate aminotransferase and, D, mean alanine aminotransferase levels (in international units per liter) after administration of 1 mL of NaCl 0.9%.

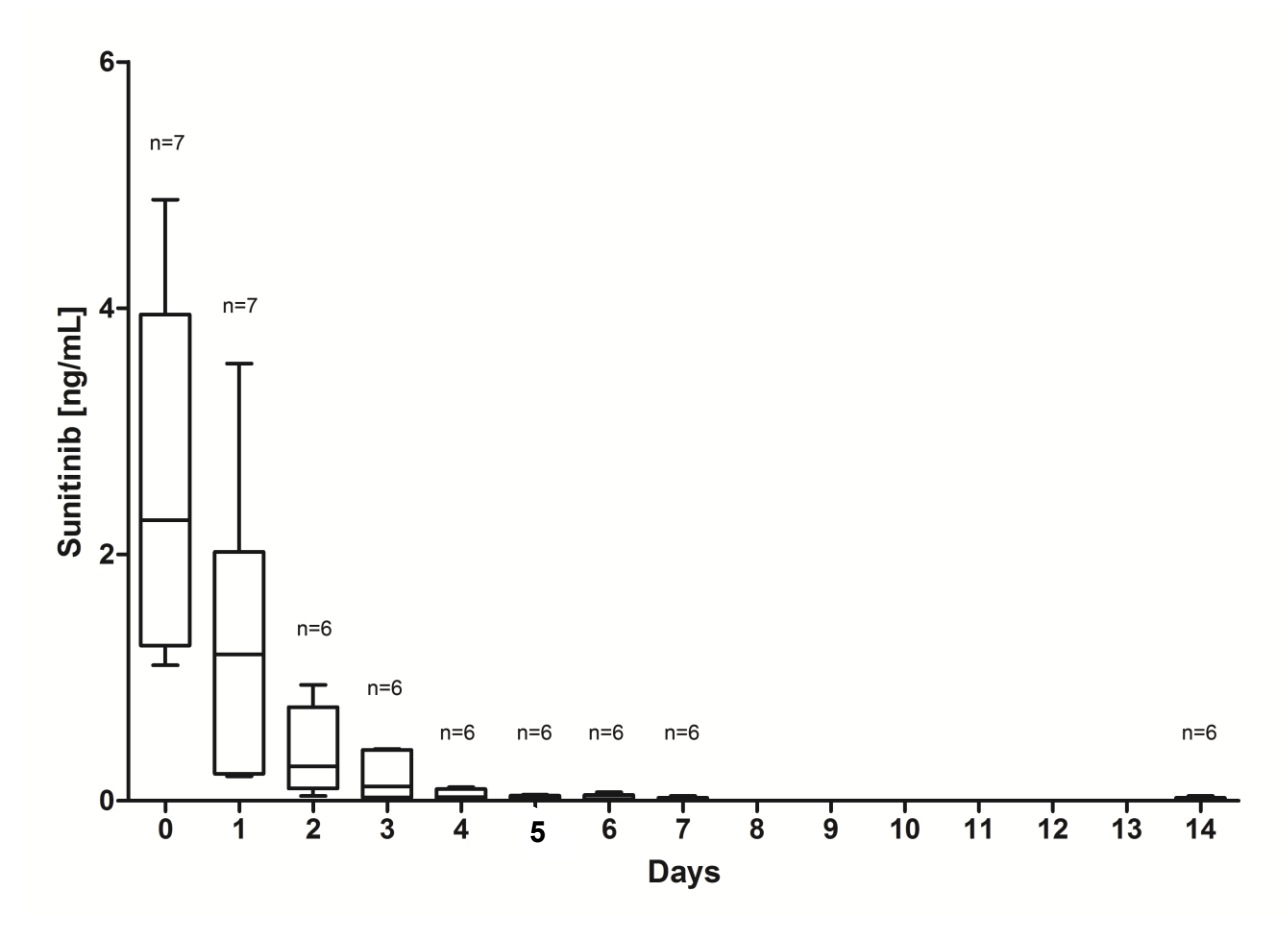


Figure 2. Box plot shows PSCs (in nanograms per milliliter) over time after intra-arterial administration of 0.05 mL of $100-300 \, \mu m$ SEBs (1.5 mg of sunitinib).

Table. Concentration of Sunitinib in the Tumor and in the Right (Untreated) Liver Lobe in the Different SEB-TACE Groups (100-300 μ m and 70-150 μ m) and the Group That Received Oral Sunitinib

| | | Day 1 (μg/g) | Day 14 (μg/g) |
|-----------------|-------------|----------------------|----------------------------------|
| 100-300 µm SEBs | Tumor | 17.8 (<i>n</i> = 1) | 0.16 [0-0.3] (<i>n</i> = 6) |
| | Right liver | 2.3 (n = 1) | Not measurable (n = 6) |
| 70-150 µm SEBs | Tumor | 40.4 (n = 1) | 27.4 [11.8-30] (<i>n</i> = 5) |
| | Right liver | 6.73 (<i>n</i> = 1) | 0.16 [0.03-0.25] (<i>n</i> = 5) |
| Oral sunitinib | Tumor | Not measured | 20.8 [19.1-22.6] (<i>n</i> = 7) |
| | Right liver | Not measured | 35.1 [32.7-35.5] (<i>n</i> = 7) |

Note.—Data in brackets are IQRs.

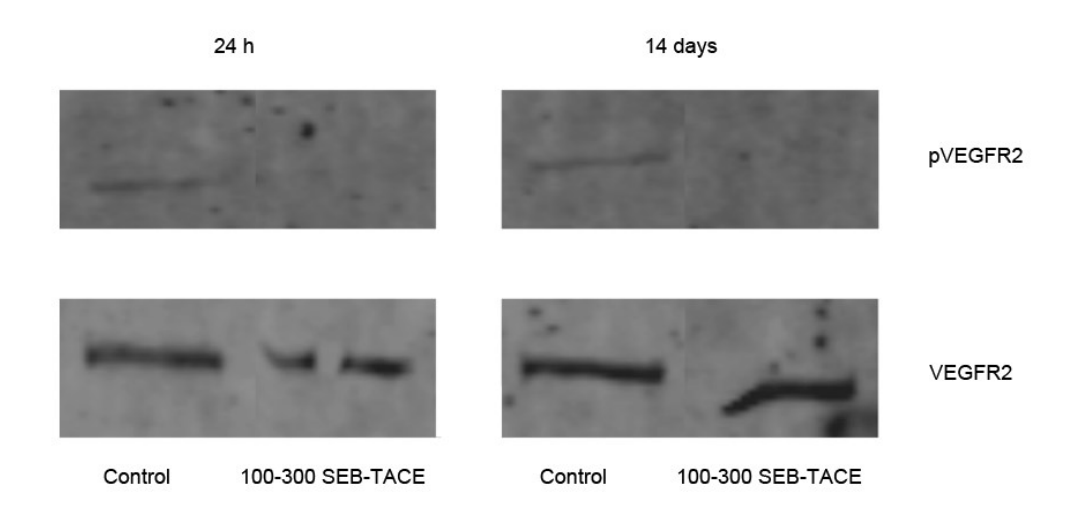


Figure 3. Western blot images of VEGFR2 obtained 24 hours (left column) and 14 days (right column) after intra-arterial administration of NaCl (control) and after 100-300 μ m SEB-TACE. There was no significant difference in the amount of unphosphorylated (inactive) VEGFR2 (lower row) in NaCl and SEB-TACE groups at 24 hours and 14 days. The active or phosphorylated form of VEGFR2 (pVEGFR2, upper row) could only be detected in animals treated with intra-arterial saline injection both at 24 hours and at 14 days but not after SEB-TACE at either 24 hours or 14 days.

3.2 Second Experiment: Comparative Study

One animal died in the 70-150 μ m SEB group 6 hours after the procedure as a result of a ruptured hepatic artery and hemorrhage, and one animal died on day 7 as a result of unknown causes. None of the animals died in the unloaded bead group or the oral sunitinib group.

Tumor volume.—US monitoring of tumor growth in the oral sunitinib group showed that median tumor volume increased from 0.43 cm 3 (IQR, 0.31-0.73 cm 3) on day 0 to 7.97 cm 3 (IQR, 0.73-13.32 cm 3) on day 14 (+1853%; P = .0174 with the Mann-Whitney U test). In the unloaded bead group, the median tumor volume increased from 1.82 cm 3 (IQR, 1.35-2.19 cm 3) on day 0 to 2.58 cm 3 (IQR, 1.47-4.37 cm 3) on day 14 (+42%; P = .12 with the Mann-Whitney U test). Median tumor volume did not change significantly during follow-up (22%) in the 70-150 μm SEB group; it was 0.5 cm 3 (IQR, 0.46-0.6 cm 3) on day 0 and 0.49 cm 3 (IQR, 0.31-1.19 cm 3) on day 14 (P = .93 with the Mann-Whitney U test). The difference in tumor growth was statistically significant between the three groups (P = .044 with the Kruskal-Wallis test). At necropsy, the median tumor volume on day 14 was smaller in the 70-150 μm SEB group than in the unloaded bead group or the oral sunitinib group (0.94, 3.21, and 11.23 cm 3 , respectively; P = .0197 with the Kruskal-Wallis test; Fig 4).

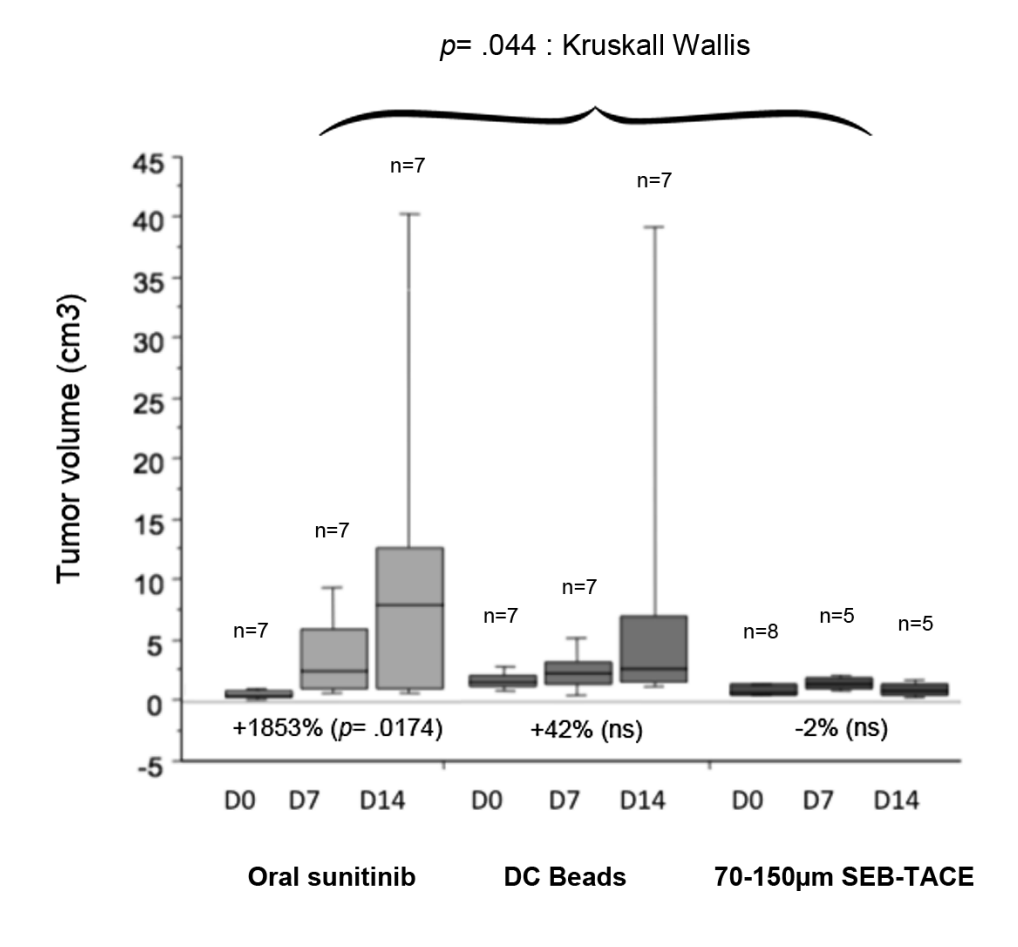


Figure 4. Box plots of tumor volumes as measured with US in the oral sunitinib, unloaded bead (DC Beads), and 70-150 μ m SEB groups at baseline (day 0, *D0*), day 7 (*D7*), and day 14 (*D14*). Tumors in the oral sunitinib group showed the greatest increase in size. The difference in tumor growth was statistically significant between the three groups (P = .044 with the Kruskal-Wallis test). ns = not significant.

Sunitinib concentrations in tumor and liver.—The ITSC in the animal sacrificed on day 1 was 40.4 μ g/g in the 70-150 μ m SEB group. The median ITSC on day 14 was 27.4 μ g/g (IQR, 11.8-30.0 μ g/g) in the 70-150 μ m SEB group and 20.8 μ g/g (IQR, 19.1-22.6 μ g/g) in the oral sunitinib group (P = .43). Sunitinib concentrations in the right liver lobe on day 14 were 0.16 μ g/g (IQR, 0.03-0.25 μ g/g) in the 70-150 μ m SEB group and 35.1 μ g/g (IQR, 32.7-35.5 μ g/g) in the oral sunitinib group (P = .0034, Table).

Inhibition of VEGFR2 phosphorylation.—After a single administration of 70-150 µm SEBs, pVEGFR2 was not detected with Western blot analysis on day 1 or day 14. Fourteen days after treatment with unloaded beads, there was pVEGFR2 overexpression on day 14 in all animals, while in the oral sunitinib group, pVEGFR2 was detectable in three of five animals (Fig 5).

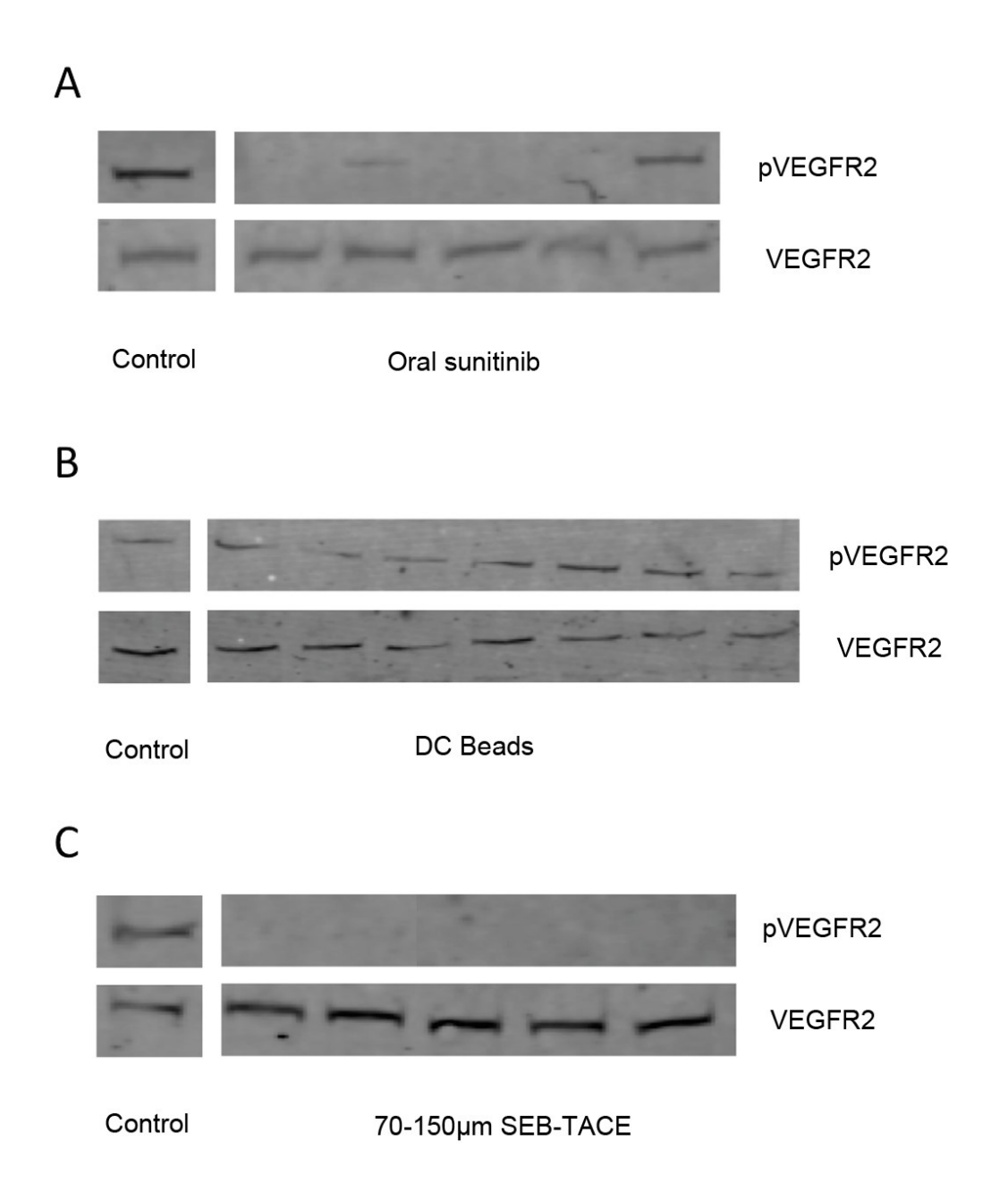


Figure 5. Western blot images obtained 14 days after treatment with, A, oral sunitinib (n = 5; samples from two animals could not be processed for Western blot), B, unloaded beads (DC Beads, n = 7), and, C, 70-150 μm SEB-TACE (n = 5). For each group, the bands in the lower row represent the unphosphorylated (inactive) form of VEGFR2, and the bands in the upper row represent the phosphorylated (active) form of VEGFR2 (pVEGFR2). After daily administration of 6 mg of sunitinib, pVEGFR2 was detectable in three animals (animals 2, 4, and 5). After intra-arterial administration of 0.05 mL of unloaded beads, pVEGFR2 was overexpressed in all animals. After intra-arterial administration of 0.05 mL of 70-150 μm SEBs, no pVEGFR2 was detectable.

Histopathologic analysis.—A total of 79 slides were examined. The median numbers of visible microspheres per slide were 2.6 in the 70-150 μ m SEB group and 3.5 in the unloaded bead group. In the 70-150 μ m SEB group, 39% of the visible microspheres were located inside the tumor or within

2 mm from the tumor margin, and 61% were located in the surrounding liver parenchyma. In the unloaded bead group, 39.5% of the visible microspheres were located inside the tumor or within 2 mm of the tumor margin, and 61.5% were located in the surrounding liver parenchyma. There was no statistically significant difference between the two groups for bead distribution within tissue samples. After treatment, necrotic alterations of tissue were visible around 94.7% of the observed SEBs (Fig 6). Necrotic changes were observed around 25% of unloaded beads (P = .024). Necrotic changes were also observed in the fibrous peritumoral capsule, as well as in an additional rim of normal liver parenchyma surrounding the tumor after SEB-TACE but not after unloaded bead or oral sunitinib administration. Complete response was observed in three of five animals (60%) in the 70-150 µm SEB group and in three of seven animals (42.8%) in the unloaded bead group; no complete response was observed in the oral sunitinib group (P = .02 with the X_2 test). Figure 7 shows the number of complete responses obtained in the three groups. Pairwise post hoc analysis showed a significant difference between the 70-150 μ m SEB group and the oral sunitinib group (P =.016 with the Fisher exact test). There was no difference between the unloaded bead group and the oral sunitinib group (P = .19 with the Fisher exact test) or between the 70-150 μ m SEB group and the unloaded bead group (P = .59 with the Fisher exact test).

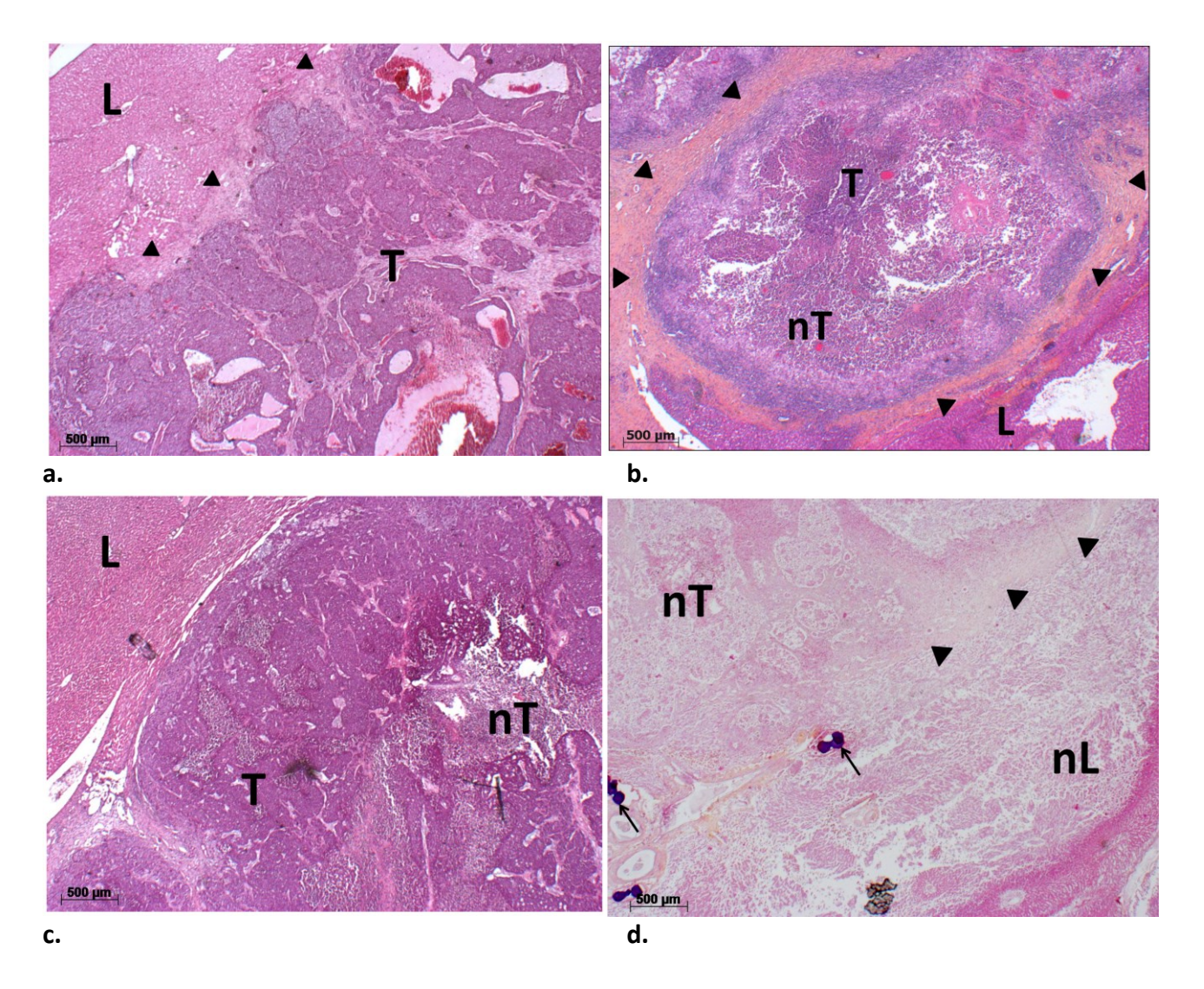


Figure 6. Photomicrographs (hematoxylin-eosin stain; original magnification, x4) of VX2 tumors and surrounding liver tissue in the (a) control (untreated), (b) oral sunitinib, (c) unloaded bead, and (d) 70-150 μ m SEB groups. In the control group (a), the viable tumor (T) is surrounded by a thin and discontinuous fibrous capsule (arrowheads) and normal liver parenchyma (L). In the oral sunitinib group (b), the tumor (T) is surrounded by a thick fibrous capsule (arrowheads). An area of necrotic tissue (nT) is visible in the encapsulated tumor. The surrounding liver tissue (L) appears normal. In the unloaded bead group (c), the tumor is composed of viable tumor tissue (L) and areas of necrotic tissue (L). There is no visible fibrous capsule. In this case, the surrounding liver tissue (L) appears normal. In the 70-150 μ m SEB group (d), SEBs are visible in a small artery (arrows). There is extensive tumor necrosis (L). The fibrous capsule surrounding the tumors is also completely necrotized (arrowheads), as well as a rim of surrounding liver parenchyma (L).

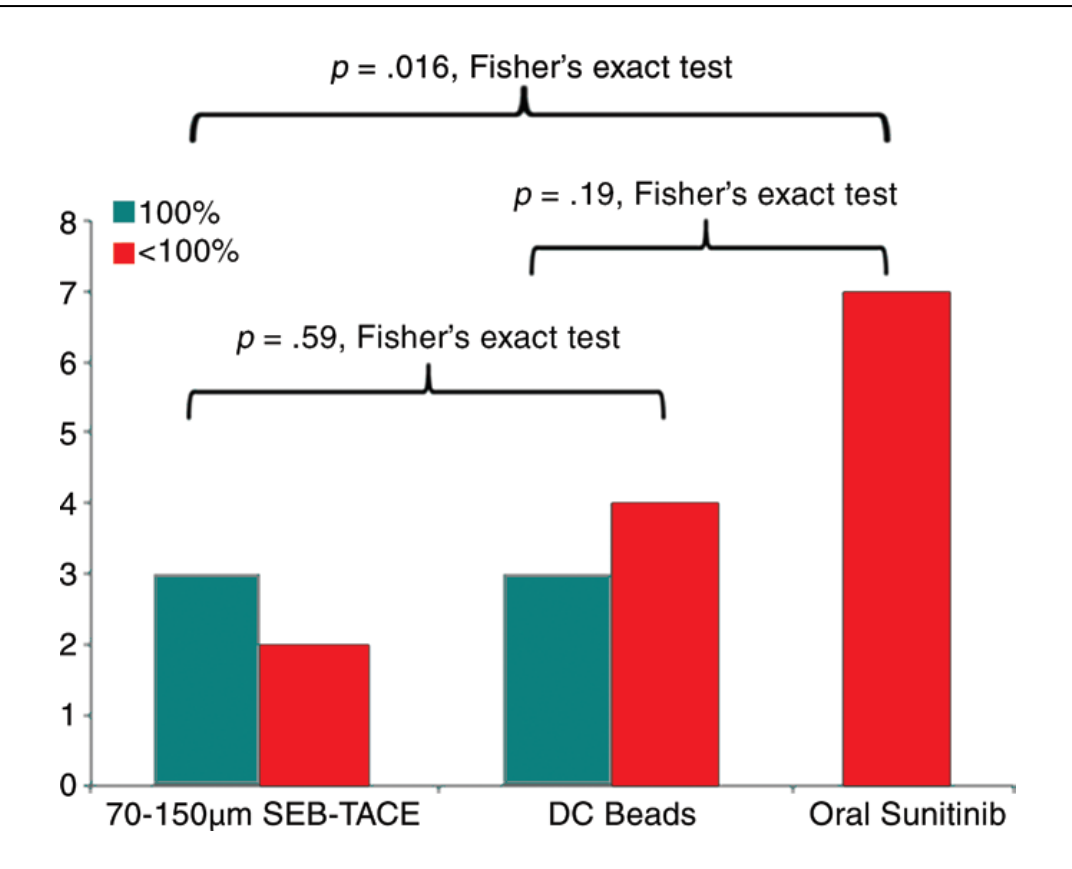


Figure 7. Bar graph shows the number of complete responses (100% tumor necrosis) and partial responses (<10% tumor necrosis) obtained in the three groups. Complete response was observed in three of five animals (60%) in the 70-150 μ m SEB group and in three of seven animals (42.8%) in the unloaded bead (DC Beads) group. No complete response was observed in the oral sunitinib group (P = .02) with the Fisher exact test). The difference between the 70-150 μ m SEB group and the oral sunitinib group was significant (P = .016) with the Fisher exact test). There was no difference between the unloaded bead group and the oral sunitinib group (P = .19) with the Fisher exact test) and between the 70-150 μ m SEB group and the unloaded bead group (P = .59) with the Fisher exact test). Note that all tumors did have a certain percentage of necrosis; we did not observe any absence of response.

4 Discussion

TACE performed by using a cytostatic drug combined with an embolic agent has been shown to be effective for the treatment of intermediate-stage HCC. However, hypoxia caused by embolization induces a cascade of intracellular events that lead to upregulation of the genes involved in angiogenesis (8, 9, 12). Vascular endothelial growth factor overexpression after TACE is closely related to tumor prognosis, the development of metastases, and poor outcomes (12). This was the clinical basis for developing SEBs and for using an antiangiogenic agent to overcome harmful TACE-related molecular events. Although sunitinib seemed to be a promising option for the treatment of patients with advanced HCC because of its antiangiogenic and cytotoxic action on HCC cells, its use was abandoned because of clinically significant systemic toxicity (24). However, we hypothesized

that the effects of sunitinib delivery by drug-eluting beads would be less systemic and more effective locally.

The results of the first experiment confirmed the good biological and pharmacokinetic profile of 100-300 µm SEB-TACE. Indeed, clinical tolerance to 100-300 µm SEB-TACE was excellent because all treated animals survived until the end of the study. Transient postprocedural increase of liver enzymes returned to an expected level and was similar to that in previous publications in which drug-eluting technologies were used (32). No sunitinib-related toxicity (liver failure, dysrhythmia, diarrhea, emesis, or conjunctival irritation) was observed. One animal died from unknown causes during follow-up after administration of 70-150 µm SEB-TACE (6.6% SEB TACE—related mortality). In comparison, the reported mortality of conventional TACE is 4% (33). Our results confirm the low toxicity of SEB-TACE when compared with the reported systemic toxicity of sunitinib (24). Indeed, the use of sunitinib has been the subject of debate since the publication of the results of the phase III trial in which oral sunitinib was compared to oral sorafenib in patients with HCC (34). That study was terminated early because of a lack of benefit of systemic sunitinib when compared with sorafenib and for safety reasons because of more serious adverse events in the sunitinib group (34).

TACE with 100-300 µm SEBs provided high ITSC on day 1, while sunitinib concentrations remained low in the untreated contralateral liver lobe. The latter may be due to systemic exposure from drug recirculation and inadvertent nontarget embolization. Despite a low ITSC on day 14, VEGFR2 phosphorylation was still not detectable at this point. This confirms the sustained and continuous release of sunitinib from SEBs at a time when systemic sunitinib was barely measurable and suggests that low local-regional doses of sunitinib could still cause a clinically significant antiangiogenic effect.

Because of the current trend in using smaller drug-eluting TACE beads (27), we designed a second study by using smaller SEBs to compare the antitumoral effectiveness with that of unloaded beads and oral sunitinib. The results of this comparative trial were encouraging for 70-150 μ m SEBs compared with unloaded beads and oral sunitinib. The use of smaller 70-150 μ m beads resulted in high ITSC on day 1 and, most importantly, on day 14. At the time the animals were sacrificed, the ITSC after administration of a single dose of 70-150 μ m SEBs was similar to that observed after daily oral administration of 6 mg of sunitinib (cumulative dose of 84 mg), highlighting the sustained

release of the drug from SEBs. Both sizes of beads demonstrated similar release profiles *in vitro* (25).

In relation to tumor growth, the antitumor profile of SEBs was clearly better than that of unloaded beads and oral sunitinib (changes in tumor volume, -2%, +42%, and +1853%, respectively, on day 14; P = .044). Although the ITSC of oral sunitinib was similar to that of SEB-TACE, the former did not induce a complete histologic tumor response, while five complete responses were observed in the tumors treated with SEB-TACE, which confirms the added benefit of embolization. In addition, histologic tumor response was not significantly different between oral sunitinib and embolization with unloaded beads. After SEB-TACE, we observed an unusual histopathologic pattern with tumor necrosis, as well as a fibrous peritumoral capsule and surrounding normal tissue. This may be related to the local-regional diffusion of sunitinib. Further studies are ongoing on tissue samples to correlate this peritumoral necrosis phenomenon with local sunitinib concentrations.

Our study has several limitations. We did not compare SEB-TACE to conventional TACE or TACE with doxorubicin-eluting beads. However, our goal was to identify the additive effect of sunitinib-loaded beads in relation to embolization-induced ischemia. We also chose not to test oral sunitinib in association with embolization with unloaded beads because, as shown in previous studies, the systemic toxicity of sunitinib could prevent the clinical use of this combination (24). The small number of animals is another limitation, and animals were treated by groups (ie, one group after the other); thus, randomization was not performed, which explains the difference in tumor volumes. Further analysis of drug distribution around the beads is planned to gain further understanding of this mechanism.

In conclusion, our study showed that SEB-TACE was safe, resulting in high ITSC with minimum systemic levels. Tumor control was better with SEB-TACE than with oral sunitinib, probably because of sustained inhibition of VEGFR2 phosphorylation and subsequent inhibition of postembolization tumor angiogenesis rebound.

5 Acknowledgments

We thank Thierry de Baere, MD, and Florentina Pascale, VMD, for their support with the animal experiments, and we thank Jean-François Knebel, MSc, for the statistical work.

6 References

1. Cho SK, Shin SW, Do YS, et al. Single-bolus regional chemotherapy with doxorubicin versus chemoembolization in a rabbit VX2 tumor model. Diagn Interv Radiol. 2011;17(4):374-380.

- 2. Choi JW, Cho HJ, Park JH, et al. Comparison of drug release and pharmacokinetics after transarterial chemoembolization using diverse lipiodol emulsions and drug-eluting beads. PLoS One. 2014;9(12):e115898.
- 3. Dzodic R, Gomez-Abuin G, Rougier P, et al. Pharmacokinetic advantage of intra-arterial hepatic oxaliplatin administration: comparative results with cisplatin using a rabbit VX2 tumor model. Anticancer Drugs. 2004;15(6):647-650.
- 4. Llovet JM, Bruix J. Systematic review of randomized trials for unresectable hepatocellular carcinoma: Chemoembolization improves survival. Hepatology. 2003;37(2):429-442.
- 5. Sahara S, Kawai N, Sato M, et al. Prospective evaluation of transcatheter arterial chemoembolization (TACE) with multiple anti-cancer drugs (epirubicin, cisplatin, mitomycin c, 5-fluorouracil) compared with TACE with epirubicin for treatment of hepatocellular carcinoma. Cardiovasc Intervent Radiol. 2012;35(6):1363-1371.
- 6. Lammer J, Malagari K, Vogl T, et al. Prospective randomized study of doxorubicin-eluting-bead embolization in the treatment of hepatocellular carcinoma: results of the PRECISION V study. Cardiovasc Intervent Radiol. 2010;33(1):41-52.
- 7. European Association For The Study Of The L, European Organisation For R, Treatment Of C. EASL-EORTC clinical practice guidelines: management of hepatocellular carcinoma. J Hepatol. 2012;56(4):908-943.
- 8. Harris AL. Hypoxia--a key regulatory factor in tumour growth. Nat Rev Cancer. 2002;2(1):38-47.
- 9. von Marschall Z, Cramer T, Hocker M, Finkenzeller G, Wiedenmann B, Rosewicz S. Dual mechanism of vascular endothelial growth factor upregulation by hypoxia in human hepatocellular carcinoma. Gut. 2001;48(1):87-96.

10. Liang B, Zheng CS, Feng GS, et al. Correlation of hypoxia-inducible factor 1alpha with angiogenesis in liver tumors after transcatheter arterial embolization in an animal model. Cardiovasc Intervent Radiol. 2010;33(4):806-812.

- 11. Liao XF, Yi JL, Li XR, Deng W, Yang ZF, Tian G. Angiogenesis in rabbit hepatic tumor after transcatheter arterial embolization. World J Gastroenterol. 2004;10(13):1885-1889.
- 12. Shim JH, Park JW, Kim JH, et al. Association between increment of serum VEGF level and prognosis after transcatheter arterial chemoembolization in hepatocellular carcinoma patients. Cancer Sci. 2008;99(10):2037-2044.
- 13. Llovet JM, Ricci S, Mazzaferro V, et al. Sorafenib in advanced hepatocellular carcinoma. New England Journal of Medicine. 2008;359(4):378-390.
- 14. Cheng AL, Kang YK, Chen Z, et al. Efficacy and safety of sorafenib in patients in the Asia-Pacific region with advanced hepatocellular carcinoma: a phase III randomised, double-blind, placebo-controlled trial. Lancet Oncol. 2009;10(1):25-34.
- 15. Wilhelm SM, Carter C, Tang L, et al. BAY 43-9006 exhibits broad spectrum oral antitumor activity and targets the RAF/MEK/ERK pathway and receptor tyrosine kinases involved in tumor progression and angiogenesis. Cancer Res. 2004;64(19):7099-7109.
- 16. Chung YH, Han G, Yoon JH, et al. Interim analysis of START: Study in Asia of the combination of TACE (transcatheter arterial chemoembolization) with sorafenib in patients with hepatocellular carcinoma trial. Int J Cancer. 2013;132(10):2448-2458.
- 17. Sabri SS, Caldwell SH, Kumer SC, et al. Combined transmesenteric and transhepatic recanalization of chronic portal and mesenteric vein occlusion to treat bleeding duodenal varices. J Vasc Interv Radiol. 2014;25(8):1295-1299.
- 18. Pawlik TM, Reyes DK, Cosgrove D, Kamel IR, Bhagat N, Geschwind JF. Phase II trial of sorafenib combined with concurrent transarterial chemoembolization with drug-eluting beads for hepatocellular carcinoma. J Clin Oncol. 2011;29(30):3960-3967.
- 19. Park JW, Koh YH, Kim HB, et al. Phase II study of concurrent transarterial chemoembolization and sorafenib in patients with unresectable hepatocellular carcinoma. J Hepatol. 2012;56(6):1336-1342.

20. Choi GH, Shim JH, Kim MJ, et al. Sorafenib alone versus sorafenib combined with transarterial chemoembolization for advanced-stage hepatocellular carcinoma: results of propensity score analyses. Radiology. 2013;269(2):603-611.

- 21. Chow LQ, Eckhardt SG. Sunitinib: from rational design to clinical efficacy. J Clin Oncol. 2007;25(7):884-896.
- 22. Christensen JG. A preclinical review of sunitinib, a multitargeted receptor tyrosine kinase inhibitor with anti-angiogenic and antitumour activities. Ann Oncol. 2007;18 Suppl 10:x3-10.
- 23. Blay JY, Reichardt P. Advanced gastrointestinal stromal tumor in Europe: a review of updated treatment recommendations. Expert Rev Anticancer Ther. 2009;9(6):831-838.
- 24. Faivre S, Raymond E, Boucher E, et al. Safety and efficacy of sunitinib in patients with advanced hepatocellular carcinoma: an open-label, multicentre, phase II study. Lancet Oncol. 2009;10(8):794-800.
- 25. Fuchs K, Bize PE, Dormond O, et al. Drug-eluting beads loaded with antiangiogenic agents for chemoembolization: in vitro sunitinib loading and release and in vivo pharmacokinetics in an animal model. J Vasc Interv Radiol. 2014;25(3):379-387 e372.
- 26. Denys A, Bize P, Jordan O, Doelker E, Boulens N. Chemo-embolization composition comprising anti-angiogenic agents. Patent no. WO 2012073188 A1. July 6, 2012.
- 27. Padia SA, Shivaram G, Bastawrous S, et al. Safety and efficacy of drug-eluting bead chemoembolization for hepatocellular carcinoma: comparison of small-versus medium-size particles. J Vasc Interv Radiol 2013;24(3):301-306.
- 28. Verbois S. Pharmacology/toxicology review and evaluation. U.S. Food and Drug Administration. 2006; Available from: http://www.accessdata.fda.gov/drugsatfda_docs/nda/2006/021938_S000_Sutent_PharmR.pdf. Published 2006. Accessed February 3, 2016.
- 29. Rao PP, Pascale F, Seck A, et al. Irinotecan loaded in eluting beads: preclinical assessment in a rabbit VX2 liver tumor model. Cardiovasc Intervent Radiol. 2012;35(6):1448-1459.

30. Haouala A, Zanolari B, Rochat B, et al. Therapeutic Drug Monitoring of the new targeted anticancer agents imatinib, nilotinib, dasatinib, sunitinib, sorafenib and lapatinib by LC tandem mass spectrometry. J Chromatogr B Analyt Technol Biomed Life Sci. 2009;877(22):1982-1996.

- 31. Mendel DB, Schreck RE, West DC, et al. The angiogenesis inhibitor SU5416 has long-lasting effects on vascular endothelial growth factor receptor phosphorylation and function. Clin Cancer Res. 2000;6(12):4848-4858.
- 32. Hong K, Khwaja A, Liapi E, Torbenson MS, Georgiades CS, Geschwind JF. New intra-arterial drug delivery system for the treatment of liver cancer: preclinical assessment in a rabbit model of liver cancer. Clin Cancer Res. 2006;12(8):2563-2567.
- 33. Garwood ER, Fidelman N, Hoch SE, Kerlan RK, Jr., Yao FY. Morbidity and mortality following transarterial liver chemoembolization in patients with hepatocellular carcinoma and synthetic hepatic dysfunction. Liver Transpl. 2013;19(2):164-173.
- 34. Cheng AL, Kang YK, Lin DY, et al. Sunitinib versus sorafenib in advanced hepatocellular cancer: results of a randomized phase III trial. J Clin Oncol. 2013;31(32):4067-4075.